NASA
Contractor Report 195479

Army Research Laboratory
Contractor Report ARL–CR–238

Bell Helicopter Advanced Rotorcraft Transmission (ART) Program

Zachary S. Henry
Bell Helicopter Textron, Inc.
Fort Worth, Texas

June 1995

Prepared for
Lewis Research Center
Under Contract NAS3–25455

National Aeronautics and
Space Administration

U.S. ARMY
RESEARCH LABORATORY

DISCLAIMER NOTICE

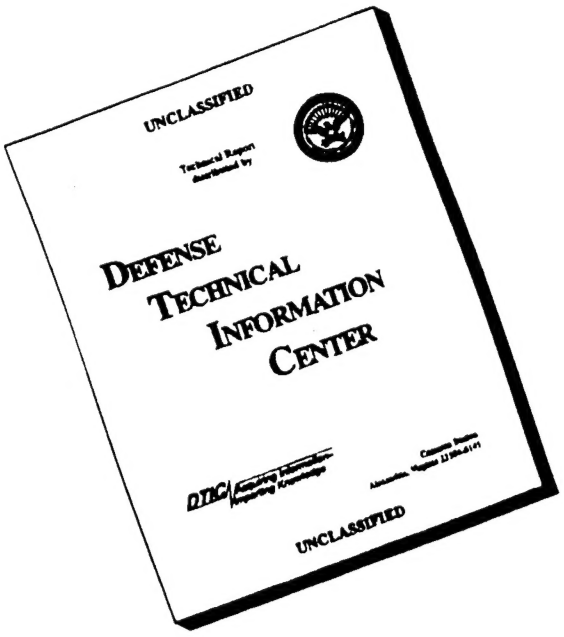

THIS DOCUMENT IS BEST QUALITY AVAILABLE. THE COPY FURNISHED TO DTIC CONTAINED A SIGNIFICANT NUMBER OF PAGES WHICH DO NOT REPRODUCE LEGIBLY.

Bell Helicopter
Advanced Rotorcraft Transmission (ART) Program
Final Report

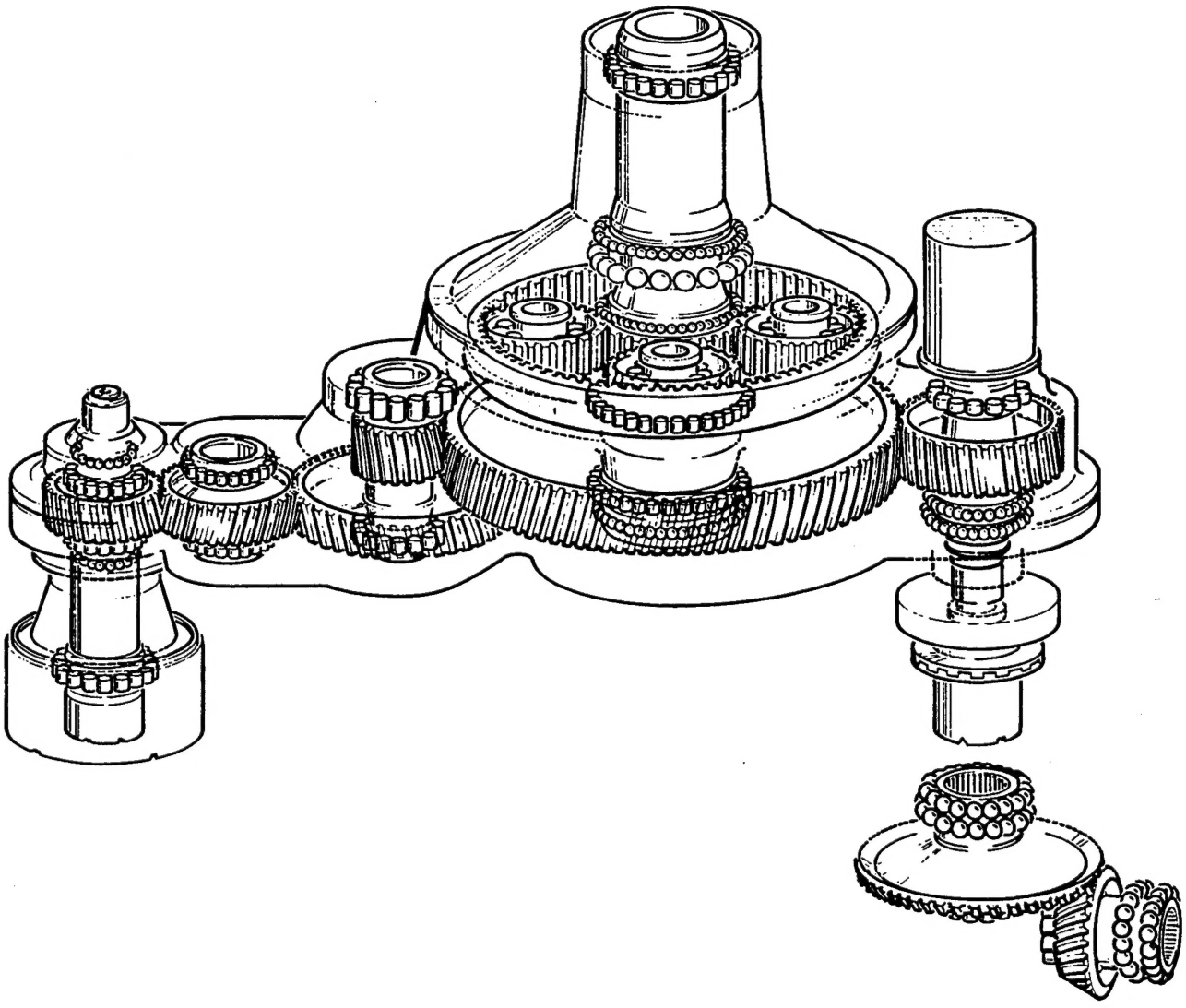

Prepared For:

Army Research Laboratory Vehicle Propulsion Directorate
National Aeronautics and Space Administration
Lewis Research Center
Cleveland, Ohio 44135

TABLE OF CONTENTS

PAGE

1.0 SUMMARY 1

2.0 INTRODUCTION 3

3.0 SELECTION OF EVALUATION PROCEDURES AND ASSUMPTIONS 5

3.1 REFERENCE AIRCRAFT 5

3.1.1 TRANSMISSION RATINGS 5
3.1.2 TAKEOFF WEIGHTS 6
3.1.3 PERFORMANCE 6
3.1.4 MISSION TYPES 6
3.1.5 MISSION PROFILES 6

3.2 STATE-OF-THE-ART TRANSMISSION (SOAT) 7

3.2.1 XV-15 RESIZE GROUND RULES AND ASSUMPTIONS 7

3.2.1.1 INPUT SECTION - DOUBLE HELICAL GEARS 7
3.2.1.2 PLANETARY SECTION AND MAST 11
3.2.1.3 INTERCONNECT DRIVE SECTION 12

3.2.2 SOAT WEIGHT 13
3.2.3 SOAT NOISE ESTIMATE 15
3.2.4 SOAT COST ESTIMATES 15

4.0 PRELIMINARY DESIGN TRADEOFF STUDIES 18

4.1 PLANETARY SELECTION 18

4.1.1 SIMPLE PLANETARY 18
4.1.2 SPLIT POWER PLANETARY 18
4.1.3 SELF-ALIGNING-BEARINGLESS PLANETARY 19
4.1.4 COMPOUND PLANETARY 23
4.1.5 HIGH CONTACT RATIO PLANETARY 23
4.1.6 PLANET BEARING SELECTION 25

4.2 OVERRUNNING CLUTCH SELECTION 25

4.3 INPUT GEAR TRAIN SELECTION 27

4.4. TRANSMISSION CONFIGURATION SELECTION 28

4.4.1 BASELINE CONFIGURATION #1 29
4.4.2 CONFIGURATION #2 29
4.4.3 CONFIGURATION #3 29

TABLE OF CONTENTS (Cont'd)

PAGE

4.4.4 CONFIGURATION #4 34
4.4.5 CONFIGURATION #5 34
4.4.6 FINAL ART DERIVATIONS - CONFIGURATIONS #6 AND #7 36

4.5 LUBE SYSTEM EVALUATION 39

4.5.1 THREE MICRON FILTRATION 39
4.5.2 SUPPLEMENTAL LUBE SYSTEM 39
4.5.3 DESICCANT AIR SUPPLY 39
4.5.4 HOT RUNNING CAPABILITY 39

4.5.4.1 TEMPERATURE RISE ACROSS TRANSMISSION 40
4.5.4.2 OIL-IN TEMPERATURE 40
4.5.4.3 WEIGHT ANALYSIS 40

4.5.4.3.1 WEIGHT REDUCTION 40
4.5.4.3.2 WEIGHT INCREASE 42
4.5.4.3.3 WEIGHT SUMMARY 42

4.6 ACCESSORY GEAR MANUFACTURING METHOD SELECTION 42
4.7 CROSS SHAFTING EVALUATION 44

4.7.1 BEARING SELECTION 44
4.7.2 CRITICAL SPEED EVALUATION 45

4.8 GEAR AND BEARING LIFE PREDICTION METHODOLOGY 49

4.8.1 GEAR TOOTH PITTING LIFE DETERMINATION 49

4.8.1.1 STRESS-LIFE EXPONENT DETERMINATION 49
4.8.1.2 BASIC HERTZ STRESS DETERMINATION 51

4.8.1.2.1 WEIBULL SLOPE DETERMINATION 51
4.8.1.2.2 LOAD DISTRIBUTION AND DYNAMIC FACTORS 52
4.8.1.2.3 BASIC TEST PARAMETERS 53
4.8.1.2.4 BASIC HERTZ STRESS DESIGN POINT 53

4.8.1.3 GEAR TOOTH PITTING LIFE CALCULATION 54
4.8.1.4 GEAR TOOTH PITTING LIFE ADJUSTMENT FACTORS 55

4.8.1.4.1 MATERIAL FACTOR 56
4.8.1.4.2 MATERIAL PROCESSING FACTOR 57
4.8.1.4.3 LUBRICANT FACTOR 57
4.8.1.4.4 OIL FILTER RATING FACTOR 58
4.8.1.4.5 SHOT PEENING FACTOR 60
4.8.1.4.6 SLIDING VELOCITY FACTOR 62
4.8.1.4.7 STRESSED VOLUME FACTOR 63

TABLE OF CONTENTS (Cont'd)

PAGE

4.8.1.5 MTBR DETERMINATION 65

4.8.1.5.1 MTBR CHARACTERISTICS 66
4.8.1.5.2 TOTAL FAILURE RATE DETERMINATION 67

4.8.1.5.2.1 PITTING FAILURE RATE 67
4.8.1.5.2.2 OTHER FAILURES FAILURE RATE 68
4.8.1.5.2.3 TBO FAILURE RATE 68

4.8.1.5.3 MTBR CALCULATION 69

4.8.2 BEARING PITTING LIFE DETERMINATION 70

4.8.2.1 BOUNDARY LUBRICATION REGIMES AND HIGHER 70
4.8.2.2 LUBRICANTS WITH FRICTION MODIFIER ADDITIVE PACKAGES 71
4.8.2.3 PLANET BEARING PITTING LIFE CALCULATION 71
4.8.2.4 OTHER BEARINGS PITTING LIFE CALCULATION 72
4.8.2.5 BEARING PITTING LIFE ADJUSTMENT FACTORS 72

4.8.2.5.1 MATERIAL FACTOR 73
4.8.2.5.2 MATERIAL PROCESSING FACTOR 73
4.8.2.5.3 HEAT TREATMENT FACTOR 73
4.8.2.5.4 LUBRICANT FACTOR 73
4.8.2.5.5 OIL FILTER RATING FACTOR 74
4.8.2.5.6 SHOT PEENING FACTOR 74
4.8.2.5.7 STRESSED VOLUME FACTOR 74

4.9 BEARING MATERIAL SELECTION 75
4.10 FAILSAFE PROPROTOR MAST EVALUATION 77

4.10.1 XV-15 DERIVATIVE STEEL/COMPOSITE PROPROTOR MAST 77

4.10.1.1 MATERIAL PROPERTIES AND LOAD CONDITIONS 77
4.10.1.2 PROPOSED STEEL/COMPOSITE MAST 78
4.10.1.3 FINITE ELEMENT ANALYSIS - ALL STEEL MAST (BASELINE) 80
4.10.1.4 FINITE ELEMENT ANALYSIS - STEEL/COMPOSITE MAST 80

4.10.1.4.1 STEEL ELEMENT STRESSES 81
4.10.1.4.2 COMPOSITE ELEMENT STRESSES AND STRAINS 81

4.10.1.5 FAIL-SAFE ANALYSIS 82
4.10.1.6 EFFECT OF TEMPERATURE ON MAST STRENGTH 83
4.10.1.7 CONCLUSIONS 84

TABLE OF CONTENTS (Cont'd)

PAGE

4.10.2 ART STEEL/COMPOSITE PROPROTOR MAST 84

4.10.2.1 MATERIAL PROPERTIES AND LOAD CONDITIONS 85
4.10.2.2 CLASSICAL STRESS ANALYSIS 85
4.10.2.3 FAIL SAFE ANALYSIS - ART MAST 87
4.10.2.4 CONCLUSIONS 88

4.11 HOUSING MATERIAL SELECTION 88

4.11.1 INVESTMENT CAST HOUSINGS 89

4.11.1.1 FINITE ELEMENT ANALYSIS 89
4.11.1.2 RESULTS 90

4.11.2 SAND CAST MAIN CASE AND OTHER HOUSINGS 91

4.12 GEAR IMPROVEMENT METHODS 91

4.12.1 PRECISION FORGING 91
4.12.2 PLASMA CARBURIZING 93
4.12.3 SPIRAL BEVEL GEARS 96

4.13 SEAL SELECTION 96
4.14 DIAGNOSTICS 96
4.15 INTEGRATED COMPONENTS 97
4.16 NOISE IMPROVEMENT DETERMINATION METHODOLOGY 97

5.0 MISSION ANALYSIS 99

5.1 PREDICTED WEIGHT 99
5.2 PREDICTED NOISE 101
5.3 PREDICTED MTBR 101
5.4 ART BENEFITS 101

6.0 COMPONENT VERIFICATION TESTS 103

6.1 HIGH CONTACT RATIO PLANETARY TESTS 103

6.1.1 PLANETARY NOISE AND VIBRATION MEASUREMENTS 108
6.1.2 PLANETARY EFFICIENCY MEASUREMENTS 126
6.1.3 PLANETARY SCORING TESTS 128
6.1.4 PLANETARY GEAR TOOTH PITTING AND BEARING PITTING TEST 130
6.1.5 PLANETARY GEAR TOOTH BENDING FAILURE MODE & EFFECT TEST 130
6.1.6 PLANETARY LOSS-OF-LUBE TESTS 135
6.1.7 PLANETARY TITANIUM CARRIER COATINGS EVALUATION 138

TABLE OF CONTENTS (Cont'd)

PAGE

6.2 IMPROVED SPIRAL BEVEL GEARS 139

6.2.1 SPIRAL BEVEL GEAR ANALYSIS 141
6.2.2 SPIRAL BEVEL KINEMATIC ERROR TESTS 142
6.2.3 SPIRAL BEVEL LOADED TOOTH CONTACT PATTERN EVALUATION 145
6.2.4 SPIRAL BEVEL NOISE AND VIBRATION TESTS 147
6.2.5 SPIRAL BEVEL DYNAMIC & STATIC TOOTH BENDING STRAIN SURVEY 150
6.2.6 SPIRAL BEVEL GEAR TOOTH PITTING FATIGUE TESTS 156
6.2.7 SPIRAL BEVEL GEAR TOOTH BENDING FATIGUE TESTS 158
6.2.8 SPIRAL BEVEL GEAR TOOTH SCORING TESTS 158
6.2.9 CONFIGURATION #3C MODIFICATION TO ELIMINATE HARDLINE 160

6.3 FLEXURE FATIGUE TESTS 163

6.3.1 MATERIAL AND PROCESS IMPROVEMENTS 163
6.3.2 FLEXURE FATIGUE TEST SPECIMEN 164
6.3.3 FLEXURE FATIGUE TEST PROCEDURE 164
6.3.4 FLEXURE FATIGUE TEST RESULTS 166

6.4 HIGH TEMPERATURE WE43 MAGNESIUM EVALUATION 174

6.4.1 MAGNESIUM FLAT PANEL CORROSION TESTS 174
6.4.2 MAGNESIUM HOUSING CORROSION TESTS 183

7.0 SUMMARY OF RESULTS 198

LIST OF FIGURES

FIGURE		PAGE
1	FAAV REFERENCE AIRCRAFT - TTR IN AIRPLANE MODE	5
2	XV-15 GEAR AND BEARING TRAIN	8
3	SOA GEAR AND BEARING TRAIN (XV-15 RESIZED FOR TTR POWER)	9
4	TWO STAGE SIMPLE PLANETARY - 15.0156:1 REDUCTION RATIO	19
5	SPLIT POWER PLANETARY - 15.0469:1 REDUCTION RATIO	19
6	FOUR SPINDLE SABP - 15.1345:1 REDUCTION RATIO	20
7	SIX SPINDLE SABP - 14.984:1 REDUCTION RATIO	21
8	TTI PROPOSED SABP LAYOUT FOR ART	22
9	COMPOUND PLANETARY SIZING REQUIREMENTS FOR ART	23
10	HIGH CONTACT RATIO, LO-SPEED PLANETARY- 13.8181:1 REDUCTION RATIO	24
11	SPRING OVERRUNNING INPUT CLUTCH	26
12	MULTI-ROW, SPRAG OVERRUNNING INPUT CLUTCH	26
13	ART PRELIMINARY LAYOUT - BASELINE CONFIGURATION #1	30
14	BASELINE CONFIGURATION #1 - BOTH ENGINES OPERATING	31
15	BASELINE CONFIGURATION #1 - OPPOSITE ENGINE DRIVING	32
16	CONFIGURATION #2 - CLUTCH ASSEMBLY LOCATED AT ENGINE INPUT	33
17	CONFIGURATION #3 - ACCESSIBLE CLUTCH ASSEMBLY	34
18	CONFIGURATION #4 - CLUTCH LOCATED IN BULL GEAR	35
19	CONFIGURATION #5 - CLUTCH LOCATED IN 1ST STAGE HELICAL REDUCTION	35
20	CONFIGURATION #6 - TWO STAGE PLANETARY, SINGLE STAGE HELICAL REDUCTION	37
21	CONFIGURATION #7 - TWO STAGE HELICAL REDUCTION, SINGLE STAGE PLANETARY	38
22	SUBCRITICAL INTERCONNECT DRIVESHAFT (ICDS) ASSEMBLY	46
23	SUPERCRITICAL INTERCONNECT DRIVESHAFT (ICDS) ASSEMBLY	46
24	HANGER BEARING ASSEMBLY FOR SUBCRITICAL ICDS ASSEMBLY	47
25	SQUEEZE FILM DAMPER ASSEMBLY FOR SUPERCRITICAL ICDS SYSTEM	47
26	RELATIONSHIP BETWEEN STRESS LIFE EXPONENT AND λ RATIO	50
27	LUBRICANT LIFE ADJUSTMENT FACTOR	58
28	OIL FILTER RATING LIFE ADJUSTMENT FACTOR	59
29	FAILSAFE STEEL/COMPOSITE MAST	79
30	XV-15 MAST	79
31	ART STEEL PROPROTOR MAST	84
32	ART COMPOSITE/STEEL PROPROTOR MAST	84
33	214ST TAILROTOR GEARBOX HOUSING GEOMETRY FOR FINITE ELEMENT MODELING	89
34	VAR 9310 SINGLE TOOTH BENDING DATA - CONVENTIONAL VS. PRECISION FORGED	92
35	HARDNESS PROFILE - PLASMA CARBURIZING	94
36	HARDNESS PROFILE - GAS CARBURIZING	94
37	RATIO OF Rc60 AT ROOT TO Rc50 AT P.D. (FOR 5 HOUR CARB. LOADS)	95

LIST OF FIGURES (Cont'd)

FIGURE		PAGE
38	ADVANCED ROTORCRAFT TRANSMISSION (ART) - PRELIMINARY DESIGN	100
39	ART PLANETARY ASSEMBLY	105
40	ART PLANETARY TEST STAND SCHEMATIC (CROSS SECTION SHOWN IN FIGURE 41)	106
41	ART PLANETARY TEST ASSEMBLY & INSTRUMENTATION	107
42	ART PLANETARY TEST ASSEMBLY FREE-BODY DIAGRAM	108
43	ART HCR PLANETARY STEP 1 VIBRATION DATA - 75% TORQUE, 480 RPM	110
44	ART HCR PLANETARY STEP 2 VIBRATION DATA - 100% TORQUE, 480 RPM	111
45	ART HCR PLANETARY STEP 3 VIBRATION DATA - 125% TORQUE, 480 RPM	112
46	ART HCR PLANETARY STEP 4 VIBRATION DATA - 75% TORQUE, 600 RPM	113
47	ART HCR PLANETARY STEP 5 VIBRATION DATA - 100% TORQUE, 600 RPM	114
48	ART HCR PLANETARY STEP 6 VIBRATION DATA - 125% TORQUE, 600 RPM	115
49	ART HCR PLANETARY GEAR MESH HARMONICS VIBRATION AMPLITUDE SUMMARY	116
50	VIBRATION LEVELS OF ATCI HCR PLANETARY @ 125% TORQUE & 565 RPM	117
51	VIBRATION LEVELS OF ATCI STD PLANETARY @ 125% TORQUE & 565 RPM	117
52	ART HCR PLANETARY STEP 1 NOISE DATA - 75% TORQUE, 480 RPM	119
53	ART HCR PLANETARY STEP 2 NOISE DATA - 100% TORQUE, 480 RPM	120
54	ART HCR PLANETARY STEP 3 NOISE DATA - 125% TORQUE, 480 RPM	121
55	ART HCR PLANETARY STEP 4 NOISE DATA - 75% TORQUE, 600 RPM	122
56	ART HCR PLANETARY STEP 5 NOISE DATA - 100% TORQUE, 600 RPM	123
57	ART HCR PLANETARY STEP 6 NOISE DATA - 125% TORQUE, 600 RPM	124
58	ART HCR SUN/PLANET FUNDAMENTAL FREQUENCY NOISE AMPLITUDE SUMMARY	125
59	NOISE LEVELS OF ART VS. ATCI PLANETARIES (125% TORQUE, HELICOPTER SPEED)	125
60	ART HCR PLANETARY - EFFICIENCY VS. TORQUE	127
61	ART HCR PLANETARY - EFFICIENCY VS. TORQUE (DRAG TORQUE COMPARISON)	128
62	HCR PLANETARY - RESULTS OF FAILURE MODE TEST (LOCKED-UP)	133
63	HCR PLANETARY - RESULTS OF FAILURE MODE TEST (PLANET TEETH WEDGED ON TOP OF RING GEAR TEETH)	134
64	HCR PLANETARY ONE HOUR LOSS-OF-LUBE TEST - RING GEAR BLANK TEMP	136
65	HCR PLANETARY FOUR HOUR LOSS-OF-LUBE TEST - RING GEAR BLANK TEMP	136
66	HCR PLANETARY ONE HOUR LOSS-OF-LUBE TEST - RING GEAR BLANK TEMP (NO EMERGENCY AIR/OIL MIST LUBRICATION)	137
67	HCR PLANETARY TITANIUM CARRIER WEAR & FRETTING PROBLEM LOCATIONS	138
68	CROSS SECTION OF OH-58D MAIN TRANSMISSION	140
69	LTCA PREDICTED SPIRAL BEVEL GEAR MEMBER TOOTH CONTACT PATTERNS	141
70	MOUNTING LOCATION OFFSET TERMINOLOGY FOR KINEMATIC ERROR TESTS	142
71	SCHEMATIC OF SPIRAL BEVEL LOADED TOOTH CONTACT TEST RIG	146
72	GEAR TOOTH CONTACT PATTERNS FROM LOADED TOOTH CONTACT TESTS	146
73	NASA 500 HP TEST STAND WITH OH-58D TRANSMISSION INSTALLED	147
74	SPIRAL BEVEL NOISE TEST - SOUND INTENSITY MEASUREMENT SYSTEM	148

LIST OF FIGURES (Cont'd)

FIGURE		PAGE
75	SPIRAL BEVEL VIBRATION TEST - ACCELEROMETER LOCATIONS	148
76	RESULTS OF SPIRAL BEVEL NOISE MEASUREMENTS	149
77	RESULTS OF SPIRAL BEVEL VIBRATION MEASUREMENTS (ACCELEROMETER #1)	150
78	SPIRAL BEVEL FILLET & ROOT STRAIN GAGE LOCATIONS	151
79	STRAIN GAGE LOCATIONS ON SPIRAL BEVEL PINION AND GEAR	151
80	IMPROVED SPIRAL BEVEL STATIC TOOTH BENDING STRAIN TEST SET-UP	152
81	SPIRAL BEVEL STATIC STRAIN TEST RESULTS AT 125% TORQUE	153
82	MAXIMUM MEASURED STRESS CYCLE AT TOOTH FILLET GAGES - SPIRAL BEVEL STATIC STRAIN SURVEY AT 125% TORQUE	154
83	MODIFIED GOODMAN DIAGRAMS FOR SPIRAL BEVEL GEAR AND PINION	154
84	MEASURED STRESS LEVEL VS. TORQUE LEVEL (SPIRAL BEVEL STATIC STRAIN)	155
85	SCHEMATIC OF SPIRAL BEVEL DYNAMIC TEST RIG	157
86	HARDLINE IN FLANK OF CONF. #3C SPIRAL BEVEL PINION AFTER 180 HR PITTING/BENDING TEST	158
87	COMPARISON OF LTCA PREDICTED SPIRAL BEVEL GEAR TOOTH CONTACT PATTERNS	160
88	RESULTS OF NOISE TEST CONDUCTED ON TOPREM MODIFIED SPIRAL BEVEL PINION	161
89	RESULTS OF VIBRATION TESTS CONDUCTED ON TOPREM MODIFIED SPIRAL BEVEL PINION	161
90	HARDLINE ON FLANK OF TOPREM MODIFIED SPIRAL BEVEL PINION	162
91	NOTCHED FLEXURE FATIGUE SPECIMEN MACHINED FROM BAR STOCK	164
92	NOTCHED FLEXURE FATIGUE SPECIMEN (PRECISION FORGING)	165
93	FLEXURE FATIGUE TEST FIXTURE	165
94	FATIGUE LIFE OF GAS CARBURIZED & STEEL SHOT PEENED, X-53, NOTCHED FLEXURE FATIGUE SPECIMENS MACHINED FROM BAR STOCK (CONF. #1)	170
95	FATIGUE LIFE OF PLASMA CARBURIZED & STEEL SHOT PEENED, X-53, NOTCHED FLEXURE FATIGUE SPECIMENS MACHINED FROM BAR STOCK (CONF. #2)	170
96	FATIGUE LIFE OF PLASMA CARBURIZED & CERAMIC SHOT PEENED, X-53, NOTCHED FLEXURE FATIGUE SPECIMENS MACHINED FROM BAR STOCK (CONF. #3)	171
97	FATIGUE LIFE OF GAS CARB. & STEEL SHOT PEENED, X-53, NOTCHED FLEXURE FATIGUE SPECIMENS - NOTCH PRECISION FORGED PARALLEL (LONGITUDINAL) TO STARTING BAR STOCK GRAIN FLOW (CONF. #4)	171
98	FATIGUE LIFE OF GAS CARB. & STEEL SHOT PEENED, X-53, NOTCHED FLEXURE FATIGUE SPECIMENS - NOTCH PRECISION FORGED PERPENDICULAR (TRANSVERSE) TO STARTING BAR STOCK GRAIN FLOW (CONF. #5)	172
99	FATIGUE LIFE OF PLASMA CARB. & STEEL SHOT PEENED, X-53, NOTCHED FLEXURE FATIGUE SPECIMENS - NOTCH PRECISION FORGED PARALLEL (LONGITUDINAL) TO STARTING BAR STOCK GRAIN FLOW (CONF. #6)	172
100	FATIGUE LIFE OF PLASMA CARB. & STL SHOT PEENED, X-53, NOTCHED FLEXURE FATIGUE SPECIMENS MACHINED FROM BAR STOCK VS. SPECIMENS WITH NOTCH PREC. FORGED PARALLEL (LONGITUDINAL) TO STARTING BAR STOCK GRAIN FLOW (CONF. #2 VS. #6)	173
101	MAGNESIUM CORROSION TEST PANEL ASSEMBLY HARDWARE	175
102	MAGNESIUM FLAT PANELS PRIOR TO CORROSION TESTS	175
103	CORROSION TEST CYCLE	176
104	MAGNESIUM FLAT PANELS AFTER 246 HOUR CORROSION TEST	176
105	MAGNESIUM FLAT PANELS AFTER 246 HOUR CORROSION TEST	177

LIST OF FIGURES (Cont'd)

FIGURE		PAGE
106	TYPICAL SCRIBED DAMAGE - MAGNESIUM PANEL ASSEMBLY B-2	178
107	MAGNESIUM FLAT PANEL AFTER ADDITIONAL 244 HR CORROSION TEST (490 HOURS TOTAL) - SPECIMEN A-6	178
108	MAGNESIUM FLAT PANEL AFTER ADDITIONAL 244 HR CORROSION TEST (490 HOURS TOTAL) - SPECIMEN B-2	179
109	BARE PANELS PRIOR TO CORROSION TEST	181
110	BARE PANELS AFTER 247 HOUR CORROSION TEST	181
111	BARE PANELS AFTER 247 HOUR CORROSION TEST - CORROSION DEBRIS REMOVED	182
112	MAGNESIUM HOUSING CORROSION TEST ASSEMBLY -TOP VIEW	184
113	MAGNESIUM HOUSING CORROSION TEST ASSEMBLY - SIDE VIEW A-A	184
114	MAGNESIUM HOUSING CORROSION TEST ASSY - VIEWS B-B & C-C	185
115	MAGNESIUM HOUSING CORROSION TEST CYCLE	185
116	WE43 MAGNESIUM HOUSING ASSY PRIOR TO CORROSION TESTS - TOP VIEW	188
117	WE43 MAGNESIUM HOUSING ASSY PRIOR TO CORROSION TESTS - BOTTOM VIEW	188
118	WE43 MAGNESIUM HOUSING ASSY PRIOR TO CORROSION TESTS - SIDE VIEW 1	189
119	WE43 MAGNESIUM HOUSING ASSY PRIOR TO CORROSION TESTS - SIDE VIEW 2	189
120	WE43 MAGNESIUM HOUSING ASSY PRIOR TO CORROSION TESTS - SIDE VIEW 3	190
121	WE43 MAGNESIUM HOUSING ASSY PRIOR TO CORROSION TESTS - SIDE VIEW 4	190
122	ZE41 MAGNESIUM HOUSING ASSY AFTER 576 HOUR CORROSION TEST - TOP VIEW	191
123	ZE41 MAGNESIUM HOUSING ASSY AFTER 576 HOUR CORROSION TEST - BOTTOM VIEW	191
124	ZE41 MAGNESIUM HOUSING ASSY AFTER 576 HOUR CORROSION TEST - SIDE VIEW 1	192
125	ZE41 MAGNESIUM HOUSING ASSY AFTER 576 HOUR CORROSION TEST - SIDE VIEW 2	192
126	ZE41 MAGNESIUM HOUSING ASSY AFTER 576 HOUR CORROSION TEST - SIDE VIEW 3	193
127	ZE41 MAGNESIUM HOUSING ASSY AFTER 576 HOUR CORROSION TEST - SIDE VIEW 4	193
128	WE43 MAGNESIUM HOUSING ASSY AFTER 576 HOUR CORROSION TEST - TOP VIEW	194
129	WE43 MAGNESIUM HOUSING ASSY AFTER 576 HOUR CORROSION TEST - BOTTOM VIEW	194
130	WE43 MAGNESIUM HOUSING ASSY AFTER 576 HOUR CORROSION TEST - SIDE VIEW 1	195
131	WE43 MAGNESIUM HOUSING ASSY AFTER 576 HOUR CORROSION TEST - SIDE VIEW 2	195
132	WE43 MAGNESIUM HOUSING ASSY AFTER 576 HOUR CORROSION TEST - SIDE VIEW 3	196
133	WE43 MAGNESIUM HOUSING ASSY AFTER 576 HOUR CORROSION TEST - SIDE VIEW 4	196
134	ZE41 MAGNESIUM HOUSING ASSY - CLOSE-UP OF CORROSION AFTER DISASSEMBLY (SEE FIGURE 125)	197

LIST OF TABLES

TABLE		PAGE
1	COMPONENT WEIGHT INCREASES - XV-15 TO SOAT	14
2	XV-15 GEAR AND BEARING FAILURE RATES BASED ON MTBR	16
3	XV-15 GEAR AND BEARING FAILURE RATES BASED ON L_{10} LIVES	17
4	PLANETARY SELECTION MATRIX	18
5	CLUTCH SELECTION MATRIX	27
6	INPUT GEAR SELECTION MATRIX	28
7	ART CONFIGURATION SELECTION MATRIX	36
8	ACCESSORY GEAR MANUFACTURING METHOD MATRIX	43
9	SUBCRITICAL VS. SUPERCRITICAL WEIGHT COMPARISON	45
10	CROSS-SHAFT SELECTION MATRIX	48
11	BASIC TEST PARAMETERS FOR PLANETARY GEAR TESTING AT BHTI	55
12	STATE-OF-THE-ART LIFE ADJUSTMENT FACTORS FOR GEAR TOOTH PITTING FATIGUE LIFE AT L_2 LEVEL USING TABLE 11 DATA AS BASELINE	56
13	PARAMETERS AND LIFE ADJUSTMENT FACTORS FOR ART BEARINGS @ L_{10} LEVEL	72
14	MAXIMUM STRESS COMPARISON - GLOBAL MODEL VS. LOCAL SUBMODEL(XV-15 MAST)	80
15	STATIC STRENGTH OF XV-15 STEEL MAST	80
16	FATIGUE STRENGTH OF XV-15 STEEL MAST	80
17	MAXIMUM STRESSES IN STEEL COMPONENT OF XV-15 FAILSAFE MAST	81
18	FIBER STRAINS (μIN/IN) IN COMPOSITE PORTION OF XV-15 FAILSAFE MAST	81
19	INTERLAMINAR STRESS (PSI) IN COMPOSITE PORTION OF XV-15 FAILSAFE MAST	82
20	COMPOSITE FIBER STRAIN (μIN/IN) WHEN THE STEEL FAILS (XV-15 FAILSAFE MAST)	82
21	STRESS (PSI) IN THE STEEL WHEN THE COMPOSITE FAILS (XV-15 FAILSAFE MAST)	82
22	THERMAL STRESSES IN XV-15 FAILSAFE MAST- TEMPERATURE CHANGE FROM +260° F TO -65° F	83
23	THERMAL STRESSES IN XV-15 FAILSAFE MAST - TEMPERATURE CHANGE FROM +260° F TO +350° F	83
24	MARGINS OF SAFETY FOR STATIC STRENGTH OF ART STEEL MAST	85
25	STATIC AND FATIGUE STRENGTHS IN SECT D-D AND E-E (ART STEEL MAST)	86
26	STATIC AND FATIGUE STRENGTHS OF STEEL ELEMENT (ART STEEL/COMPOSITE MAST)	86
27	COMPOSITE FIBER STRAINS (μIN/IN) OF LAYER #1 UNDER COMBINED LIMIT LOADS (ART STEEL/COMPOSITE MAST)	87
28	STRESSES AND MARGINS OF SAFETY IN THE STEEL WHEN THE COMPOSITE FAILS (ART STEEL/COMPOSITE MAST)	87
29	COMPOSITE FIBER STRAINS (μIN/IN) WHEN THE STEEL FAILS (ART STEEL/COMPOSITE MAST)	88
30	FIBER STRAINS (μIN/IN) IN SECTION D-D WITH DIFFERENT FIBER ORIENTATIONS (ART STEEL/COMPOSITE MAST)	88
31	214ST TAILROTOR GEARBOX HOUSING WALL THICKNESSES FOR SHELL MODEL INPUT	90
32	MARGINS OF SAFETY FOR CAST HOUSINGS	90
33	MINIMUM MECHANICAL PROPERTIES OF SEVERAL HOUSING ALLOYS AT 75° F	91
34	SUMMARY OF COMPONENT WEIGHTS - SOAT VS. ART COMPONENTS	99
35	REFERENCE AIRCRAFT COST AND WEIGHT COMPARISON	102

LIST OF TABLES (Cont'd)

TABLE		PAGE
36	BASIC DESIGN DATA FOR ART PLANETARY	104
37	HCR PLANETARY NOISE AND VIBRATION TEST SCHEDULE	109
38	HCR PLANETARY NOISE AND VIBRATION TEST SCHEDULE (ADDITIONAL TESTS)	126
39	HCR PLANETARY SCORING TEST SCHEDULE	129
40	HCR PLANETARY GEAR TOOTH BENDING FATIGUE TEST SCHEDULE	131
41	DESIGN DATA FOR ART AND OH-58D SPIRAL BEVEL GEARS	139
42	SUMMARY OF PREDICTED SPIRAL BEVEL MAXIMUM STRESSES & KINEMATIC ERRORS	141
43	TRANSMISSION ERROR SUMMARY FOR CONFIGURATION #1 SPIRAL BEVEL SET (PINION SERIAL NO. A-22, GEAR SERIAL NO. A-15)	143
44	TRANSMISSION ERROR SUMMARY FOR CONFIGURATION #1 SPIRAL BEVEL SET (PINION SERIAL NO. A-30, GEAR SERIAL NO. A-4)	143
45	TRANSMISSION ERROR SUMMARY FOR CONFIGURATION #2 SPIRAL BEVEL SET (PINION SERIAL NO. A-93, GEAR SERIAL NO. A-35)	143
46	TRANSMISSION ERROR SUMMARY FOR CONFIGURATION #2 SPIRAL BEVEL SET (PINION SERIAL NO. A-73, GEAR SERIAL NO. A-33)	144
47	TRANSMISSION ERROR SUMMARY FOR CONFIGURATION #3A SPIRAL BEVEL SET (PINION SERIAL NO. A-111, GEAR SERIAL NO. A-19)	144
48	TRANSMISSION ERROR SUMMARY FOR CONFIGURATION #3B SPIRAL BEVEL SET (PINION SERIAL NO. A-116, GEAR SERIAL NO. A-6)	144
49	TRANSMISSION ERROR SUMMARY FOR CONFIGURATION #3C SPIRAL BEVEL SET (PINION SERIAL NO. A-65, GEAR SERIAL NO. A-45)	145
50	SUMMARY OF PREDICTED SPIRAL BEVEL KINEMATIC ERROR LEVELS VS. MEASURED LEVELS	145
51	COMPARISON OF MEASURED STRESS LEVELS FROM STATIC AND DYNAMIC STRAIN TESTS AT 125% TORQUE	156
52	SPIRAL BEVEL GEAR TOOTH SCORING TEST SCHEDULE	159
53	TRANSMISSION ERROR SUMMARY FOR TOPREM MODIFIED PINION & ORIGINAL CONF. #3C SPIRAL BEVEL GEAR SET	162
54	CONFIGURATION #1 - BASELINE NOTCHED FLEXURE FATIGUE DATA (MACHINED FROM BAR STOCK, GAS CARBURIZED, STEEL SHOT PEENED)	166
55	CONFIGURATION #2 - NOTCHED FLEXURE FATIGUE DATA (MACHINED FROM BAR STOCK, PLASMA CARBURIZED, STEEL SHOT PEENED)	167
56	CONFIGURATION #3 - NOTCHED FLEXURE FATIGUE DATA (MACHINED FROM BAR STOCK, PLASMA CARBURIZED, CERAMIC SHOT PEENED)	168
57	CONFIGURATION #4 - NOTCHED FLEXURE FATIGUE DATA (PREC. FORGED, GAS CARB., STL SHOT PEENED, NOTCH PARALLEL TO GRAIN FLOW OF STARTING BAR STOCK)	168
58	CONFIGURATION #5 - NOTCHED FLEXURE FATIGUE DATA (PREC. FORGED, GAS CARB., STL SHOT PEENED, NOTCH TRANSVERSE TO GRAIN FLOW OF STARTING BAR STOCK)	169
59	CONFIGURATION #6 - NOTCHED FLEXURE FATIGUE DATA (PREC. FORGED, PLASMA CARB., STL SHOT PEENED, NOTCH PARALLEL TO GRAIN FLOW OF STARTING BAR STOCK)	169
61	SUMMARY OF FLEXURE FATIGUE TEST RESULTS	174
61	MAGNESIUM FLAT PANEL SPECIMEN PROTECTION SCHEMES	174
62	MAGNESIUM FLAT PANEL CORROSION TEST RESULTS	180
63	MAG HOUSING ASSY COMPONENTS & HARDWARE MATERIAL & FINISH	187

LIST OF SYMBOLS

A - heat transfer convection area
a - stress life exponent
B - width of contact band when 2 cylinders are pressed together
B_l - bearing piting life at which 1% of the specimens have failed
b - weibull exponent
c - 36,000 psi (fatigue alowable)
d_b - base circle diameter
E - modulus of elasticity
E11 - transverse modulus of elasticity
E12 - modulus of elasticity normal to fiber orientation
F - gear tooth face width
F(t) - probability of faiure prior to time t
Fsu - ultimate shear strength
Fsy - shear yield strength
Ftu - ultimate tensile strength
Fty - tensile yield strength
F_T^{tu} - ultimate tensile stress normal to fiber orientation
F^{isu} - interlaminar shear stress
f_b - gear tooth bending stress
f_c - gear tooth compressive stress
f_M - material factor
f_R - reliability
f_S - size factor
f_{SC} - scatter factor
f_{SF} - surface finish factor
G - modulus of rigidty
G12 - fiber modulus of rigidty
h_{min} - minimum oil film thickness
i - no. of rows of rollers
K - total no. of different gears
L - life, % failure
L_c - composite life
L_2 - time to failure of 2 percent of a certain component
L_{10} - time to failure of 10 percent of a certain component
L_{50} - time to failure of 50 percent of a certain component
$L_{63.2}$ - time to failure of 63.2 percent of a certain component
Lambda - constant failure rate
l_l - effective length of rollers
ℓ - effective involute length
N - no. of teeth on gear
n - total no. of like gears of kind i
Q_a - power loss to air
Q_O - power loss to oil
Q_T - total power loss
R - radius of curvature
S - hertz stress

LIST OF SYMBOLS (Cont'd)

S_{STDY} - mean bending stress
S_{OSC} - oscillatory bending stress
S_E - material endurance limit
T_a - ambient temperature
T_c - transmission housing temperature
t - percent failed of life L
U - heat transfer coefficient
V - rolling velocity
V_s - sliding velocity
v - stressed volume of gear
Vbe - air speed for min power required to fly (best endurance)
Vlrc - air speed to fly 99% of specific range (long range cruise)
Vmcp - air speed at maximum continuous engine power
W_N - normal load
z_o - depth of maximum subsurface shear stress
β - weibull slope
ΔT - change in temperature
λ - lambda ratio
σ - composite surface roughness
μ - absolute filter rating
τ - residual stress
θ_H - degrees of roll at highest point of single tooth contact (HPSTC)
θ_L - degrees of roll at lowest point of single tooth contact (LPSTC)
ν - poisson's ratio
$\nu 12$ - poisson's ratio of fibers
α - coefficient of thermal expansion
$\alpha 11$ - transverse coefficient of thermal expansion
$\alpha 12$ - coefficient of thermal expansion normal to fiber orientation
ε_L^{tu} - ultimate transverse tensile strain
ε_{LT}^{su} - ultimate tensile shear strain
ε_T^{cu} - ultimate compressive strain normal to the fiber orientation
ε_L^{cu} - transverse ultimate compressive strain
ε_T^{tu} - ultimate tensile strain normal to the fiber orientation

LIST OF ACRONYMS

AEO	- all engines operative
AGMA	- American Gear Manufacturers Association
AHIP	- Army Helicopter Improvement Program
AMS	- American Materials Scoiety
ANSYS	- Analysis Systems (finite element analysis software)
ART	- Advanced Rotorcraft Transmission
ASME	- American Society of Mechanical Engineers
ATCI	- Advanced Transmission Components Investigation
AVSCOM	- Aviation Systems Command
BHTI	- Bell Helicopter Textron Inc.
CBN	- cubic boron nitride
CEVM	- consumable electrode vacuum melt
CNC	- computer numerically controlled
C/P	- capacity/load in pounds
dB	- decibels
dBA	- 'A' weighted decibels
D-H	- double helical
DOC	- direct operating cost
EHD	- elastohydrodynamic
FAAV	- Future Attack Air Vehicle
FEA	- finite element analysis
FM	- frequency modulated
FPSTC	- first point of single tooth contact
GAG	- ground-air-ground
GFY	- Government Fiscal Year
GPM	- gallons per minute
HCR	- high contact ratio
HOGE	- hover out of ground effect
HP	- horsepower
HPSTC	- high point of single tooth contact
ICDS	- interconnect driveshaft
IR&D	- independent research and development
IRP	- intermediate rated power
KSI	- thousand pounds per square inch
LAF	- life adjustment factor
LOL	- loss-of-lube
LPSTC	- low point of single tooth contact
LTCA	- loaded tooth contact analysis
MTBF	- mean time between failures
MTBR	- mean-time-between-removal
NASA LeRC	- National Aeronautics and Space Administration, Lewis Research Center
NOE	- nap of the earth
ODA	- offensive deep attack
OEI	- one engine inoperative
PD	- pitch diameter
PEEK	- polyetheretherketone

LIST OF ACRONYMS (Cont'd)

PLANETSYS	- planetary bearing system analysis software
POL	- petroleum, oil, and lubricants
PSI	- pounds per square inch
PV	- pressure-velocity
Rc	- rockwell 'C' scale
RCF	- rolling contact fatigue
RMC	- root mean cubed
RPM	- revolutions per minute
RTM	- Rolls-Royce Turbo Mecca
S-N	- stress level vs. cycles to failure
SABP	- self-aligning-bearingless-planetary
SAWE	- Society of Allied Weight Engineers
SLS	- sea level standard
SOA	- state-of-the-art
SOAT	- state-of-the-art transmission
STD	- standard
TBO	- time between overhaul
TCA	- tooth contact analysis
TDC	- thin dense chrome
TOPREM	- spiral bevel gear flank modification
TTI	- Transmission Technology Inc.
TTR	- Tactical Tiltrotor
VAR	- vacuum arc remelt
VIMVAR	- vacuum induction melt, vacuum arc remelt

1.0 SUMMARY

Future rotorcraft transmissions of the 1990's and beyond the year 2000 require the incorporation of key emerging material and component technologies using advanced and innovative design practices in order to meet the requirements for a reduced weight to power ratio, a decreased noise level, and a substantially increased reliability. The specific goals for the future rotorcraft transmission when compared with a current state-of-the-art transmission (SOAT) are 1) a 25% weight reduction, 2) a 10dB reduction in the transmitted noise level, and 3) a system reliability of 5000 hours mean-time-between-removal (MTBR) for the transmission. This report summarizes the work conducted by Bell Helicopter Textron Inc. to achieve these goals under the Army funded and managed Advanced Rotorcraft Transmission (ART) program contracted by NASA Lewis Research Center (Contract No. NAS3-25455). This effort was conducted from 1988 to 1995.

The program was basically divided into the following sub-tasks:

- Selection of the procedures and ground rule assumptions to be used in conducting the tradeoff studies to accomplish the program goals. These included the selection of a reference aircraft and a reference SOAT.

- Preliminary design of an ART for the reference aircraft including tradeoff studies to optimize the design to meet the program objectives.

- A mission analysis to determine the impact of the ART on the reference aircraft mission, performance, and operating cost.

- Detail design and analysis of the critical components and subsystems of the ART selected for substantiation tests.

- Manufacture and testing of the selected test components.

The reference aircraft selected by BHTI for the ART program was the Tactical Tiltrotor (TTR) a 17,000 lb gross weight aircraft which meets the requirements for the Future Attack Air Vehicle (FAAV). The SOAT selected for comparison with the ART was the left hand side transmission from the XV-15 tiltrotor. To account for the difference between the power levels of the XV-15 and TTR, a paper study was conducted to upgrade the XV-15 transmission to TTR power and speed requirements including the weight, noise, and reliability levels.

The selection process for the ART preliminary configuration was centered upon defining the best gearbox to meet the ART requirements for weight reduction, noise reduction, increased component life, and airframe and control restrictions associated with the reference aircraft. A configuration tradeoff study was conducted to determine the lightest transmission that could fit into the available envelope permitted by the reference airframe and rotor controls. The three major factors contributing to the final configuration selection were the number of reduction stages in the input helical gear train, the number of planetary systems and the location of the overrunning clutch. The ART incorporates a two stage reduction input helical train and a single stage reduction planetary system output to the proprotor. The overrunning clutch is located at the transmission input from the engine. Based on the results of the design tradeoff studies, this transmission meets the three stated goals of the program. The study comparing the SOAT with the ART showed the ART to be 29% lighter, and up to 13 dB quieter than the SOAT. The calculated MTBR for the ART was in excess of 5000 hours as compared to 3845 hours for the SOAT.

The high risk component and material technologies selected for the component testing portion of the ART program include the following:

- Sequential meshing high contact ratio planetary with cantilevered support posts
- Thin dense chrome (TDC) plated M50 NiL double row spherical roller planetary bearings
- Reduced kinematic error and increased bending strength spiral bevel gears
- High temperature WE43 magnesium housing evaluation and coupon corrosion tests
- Flexure fatigue tests of precision forged coupons simulating precision forged gear teeth
- Flexure fatigue tests of plasma carburized coupons simulating plasma carburized gear teeth

The tests conducted on the high contact ratio planetary were highly successful substantiating the integrity of the lightweight design. The planetary demonstrated a gear tooth scoring resistance in excess of 650° F and no gear tooth bending fatigue failures after one million cycles on the planet pinions at 220% load. A four hour loss-of -lube (secondary air/oil mist only) test was successfully run at aircraft operating conditions with no failures of any of the planetary components. A 250 hour pitting endurance test was conducted with no gear or bearing pitting failures.

Tests conducted on the improved spiral bevel gears demonstrated up to an 18 dB noise level reduction provided by the reduced kinematic error geometry and a 50% reduction in the measured vibration levels. Incorporating an increased radius fillet into the gear tooth root produced up to a 24% reduction in the measured gear tooth bending stress. Scoring tests were conducted at 150% load with both DOD-L-85734 and MIL-L-7808 oil at 390° F with no gear tooth scoring observed.

Fatigue tests conducted on carburized, ground and shot peened notched flexure specimen manufactured from precision forged X-53 blanks demonstrated a 20% increase in bending fatigue strength over specimen fully machined from X-53 bar stock. Additional notched flexure fatigue tests showed a slight decrease in the bending fatigue strength of plasma carburized specimen compared to those carburized using the conventional gas carburizing process.

Corrosion tests conducted on ZE41 and WE43 magnesium demonstrated the superior corrosion resistance of the WE43. Its non-galvanic corrosion resistance is similar to A357 aluminum. To prevent galvanic corrosion, a sealing system was developed using DOW 17 and a resin topcoat which effectively insulates the magnesium from galvanic potentials. A 576 hour corrosion test conducted on a fully sealed WE43 magnesium housing produced very little corrosion.

2.0 INTRODUCTION

With the increased performance demands placed on future rotorcraft, it has become essential that an all encompassing design and test program be implemented in order to provide an advanced technology drive system capable of meeting the performance objectives for future rotorcraft. The three areas of greatest concern to improved drive system design are reduced weight and size, reduced noise level, and increased reliability. Bell Helicopter Textron Inc. was contracted by NASA Lewis Research Center (Contract No. NAS3-25455) under Army funding and management to design an Advanced Rotorcraft Transmission for a Future Attack Air Vehicle. The ART was to have a system reliability of 5000 hours mean-time-between-removal, a 25% weight reduction and a 10 dB transmitted noise level reduction when compared to a selected SOA transmission. A smaller, lighter drive system will not only enhance the aerodynamic performance of the aircraft but will also permit the installation of additional advanced avionics and payload packages available for future rotorcraft. A reduction in the noise level produced by a rotorcraft drive system reduces the noise induced fatigue experienced by the pilot thereby improving his performance. A reduction in the vibration level reduces the fatigue damage to local components and sensors. Finally, any increases in the reliability and maintainability of a rotorcraft drive system translate directly into savings in operating costs and a reduction in rotorcraft accidents attributable to drive system failures.

Previous work in the area of drive system design advancement has been limited by funding and/or production schedules. Individual components of existing drive systems were selected for design improvements and qualification tests. The existing design of the drive system and surrounding components of course limited the improvements available to the selected components. The next step in advancing drive system technology was to expand the design improvements from individual components to an entire transmission. The intent of the Advanced Transmission Components Investigation (ATCI) [1], AVSCOM Contract DAAJ02-76-C-0046, from 1976 to 1983 at BHTI was to concentrate the design improvement efforts on the entire transmission of an existing helicopter without the restrictive schedule requirements characteristic of helicopter market demands. Strict schedule requirements for helicopters prevent extended development or significant design iterations which forces the design of the required drive system for the helicopter to be conservative and not optimized for lightweight, quiet, long-life operation. The results of the ATCI (1) program were an 18% reduction in weight, an 85% increase in life, a 2 hour loss-of-lube operating capability at max power, and a 3% reduction in recurring cost and a 25% reduction in operating cost [1]. The ART program takes the ATCI effort a step further by removing the obstacle of improving an existing design and allowing as it were a clean sheet of paper to design a drive system with more room for innovation and risk. This extra flexibility in the design is provided by the component test portion of the ART program which allows individual testing of new and innovative designs that would be considered too risky for incorporation into a complete drive system designed and manufactured for test.

Any realistic approach to designing an advanced drive system to meet the stated goals of the ART program must include an existing drive system for comparison purposes, and an appropriate airframe must be selected to introduce typical design constraints.

This report presents the results of all of the work conducted under this program including conclusions and recommendations. The program was divided into the following 9 subtasks.

TASK I - Selection of Evaluation Procedures and Assumptions. Select the procedures and ground rule assumptions to be used in conducting the tradeoff studies to accomplish the program goals. These included the selection of a reference aircraft and a reference SOA transmission.

TASK II - Preliminary Design and Tradeoff Studies. Prepare a preliminary design of an ART for the reference aircraft including tradeoff studies to optimize the design to meet the program objectives.

TASK III - System Performance Evaluation. Conduct a mission analysis to determine the impact of the ART on the reference aircraft mission, performance, and operating cost.

TASK IV - Detail Design and Analysis of ART Components for Test. Conduct detail design and analysis of the critical components and subsystems of the ART selected for substantiation tests.

TASK V - Development of Component and Subsystem Test Plans. Prepare detailed component test plans defining tests, schedule, and data acquisition requirements for each component and subsystem to be tested.

TASK VI - Preparation of Component Test Rigs. Prepare test rigs as required to conduct component and subsystem tests defined in TASK V.

TASK VII - Fabrication of Component Test Articles. Fabricate components required to conduct tests defined in TASK V.

TASK VIII - Component Verification Testing. Conduct component and subsystem tests defined in TASK V.

TASK IX - Final Report

3.0 SELECTION OF EVALUATION PROCEDURES AND ASSUMPTIONS

3.1 REFERENCE AIRCRAFT

The Tactical Tiltrotor (TTR) aircraft was selected as the reference aircraft for the ART program. This aircraft was designed to meet the FAAV requirements, and the BHTI ART transmission was designed to fit in the TTR airframe. The TTR configuration is different from the originally proposed configuration in that it has tilting engines. An extensive trade-off study at BHTI indicated that although a fixed engine configuration has the possibility of producing the lightest drive train arrangement, the tilting engine configuration results in a lighter aircraft. Furthermore, since there was a better possibility of an airframe availability with the tilting engine arrangement it was decided to choose the TTR as the reference aircraft. An artists conception of the TTR in airplane mode is shown in Figure 1.

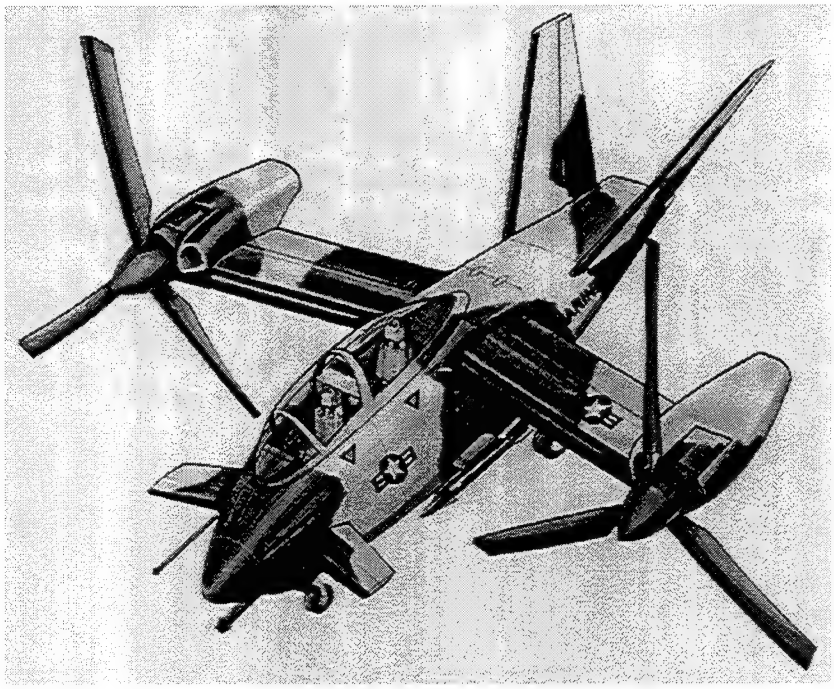

FIGURE 1: FAAV REFERENCE AIRCRAFT - TTR IN AIRPLANE MODE

3.1.1 TRANSMISSION RATINGS

The BHTI ART transmission (for the TTR) was designed for the following requirements:

Engine	RTM 322 (anticipated growth version) or GE CT6-8
Input Power	2522 HP - for all engines operative (AEO) 2777 HP - one engine inoperative (OEI)
Input RPM	20,900 - in helicopter mode 16,720 - in airplane mode

Mast RPM	600	- in helicopter mode
	480	- in airplane mode
Mast power	2444 HP (AEO)	
	2933 HP (1.2 Transient Factor for Sizing Planetary Gears)	

3.1.2 TAKEOFF WEIGHTS

4000 ft/95° F Short Takeoff	27,750 lb
4000 ft/95° F Vertical Takeoff	17,300 lb

3.1.3 PERFORMANCE

4000 ft/95° F Dash Speed	330 -350 knots	
4000 ft/95° F Vertical Rate of Climb	1000 ft/min	
Sea Level Std Maximum Normal Load Factors	Transient	6.0 g
	Sustained	3.0 g

3.1.4 MISSION TYPES

The TTR was designed to provide improved capabilities in several types of missions. These missions as well as the design attributes they suggest are:

MISSION	DESIGN FEATURE
1) Low Level Air-to-Air	Good Maneuverability
2) Close Combat	Good Low Speed Performance (For bob-up and NOE)
3) Offensive Deep Attack	Good Cruise/Long Range

Of these mission types the Offensive Deep Attack (ODA) was critical from an aircraft sizing perspective. Several different ODA type profiles were examined, resulting in the selection of the 4000 ft/95° F Deep Penetration as the design mission. The fallout design was then evaluated in several other types of profiles, including two escort missions to insure multi-mission versatility.

3.1.5 MISSION PROFILES

The following missions were synthesized for the purpose of pre-design and are thought to be representative of FAAV and marine escort requirements.

Deep Penetration (Design Mission) - 4000 ft/95° F

1) 1 min HOGE
2) Cruise 400 km (216 Nmi) @ Vlrc
3) 20 min on-station (10 min NOE + 10 min HOGE)
4) Cruise 400 km (216 Nmi) @ Vlrc
5) Reserve (20 min @ Vbe)

Escort Mission #1 - 3000 ft/91.5° F

1) 10 min idle
2) 1 min HOGE
3) Cruise 200 Nmi @ Vlrc
4) 5 min loiter @ IRP
5) Offload 1/2 Ordnance
6) 10 min loiter @ IRP
7) Cruise 200 Nmi @ Vlrc
8) Reserve (30 min @ Vbe)

Escort Mission #2

1) 10 min idle @ SL/103° F
2) 1 min HOGE @ SL/103° F
3) 40 min Vbe loiter @ SL/103° F
4) Climb to 4000 ft/87.6° F
5) 50 Nmi Vlrc cruise @ 4000 ft/87.6° F
6) 15 min IRP loiter @ 4000 ft/87.6° F
7) Offload 743 lb Ordnance
8) 50 Nmi Vmcp cruise @ 4000 ft/87.6° F
9) Descend to SL/103° F
10) 25 min Vbe loiter @ SL/103° F
11) Climb to 4000 ft/87.6° F
12) 50 Nmi Vmcp cruise @ 4000 ft/87.6° F
13) 5 min IRP loiter @ 4000 ft/87.6° F
14) Offload 743 lb Ordnance
15) 50 Nmi Vlrc cruise @ 4000 ft/87.6° F
16) SL/103° F reserve (30 min @ Vbe)

3.2 STATE-OF-THE-ART TRANSMISSION (SOAT)

The XV-15 left transmission, without the speed-up gearbox, was selected as the SOAT. To account for the rather large difference between the power levels of the XV-15 and TTR aircrafts, a paper study was completed to upgrade the gears and bearings in the XV-15 left transmission to TTR power and speed requirements. Layouts of the present XV-15 left transmission and the transmission resized for TTR power and speed requirements showing all the gears and bearings are shown in Figures 2 and 3.

3.2.1 XV-15 RESIZE GROUND RULES AND ASSUMPTIONS

3.2.1.1 INPUT SECTION - DOUBLE HELICAL GEARS

a) Power level: 2777 HP (OEI condition) engine input at 20,900 RPM

b) The centerline distance between the mast and the input double helical was increased from 17.00 to 24.40 inches to accommodate input from RTM 322 engine. If the original XV-15 transmission had not used an engine speed up gearbox, the center line distance between the mast and the input to the transmission would have been 22.80 inches.

c) A trade-off study was made to optimize the number of idlers between the engine input and collector gear.

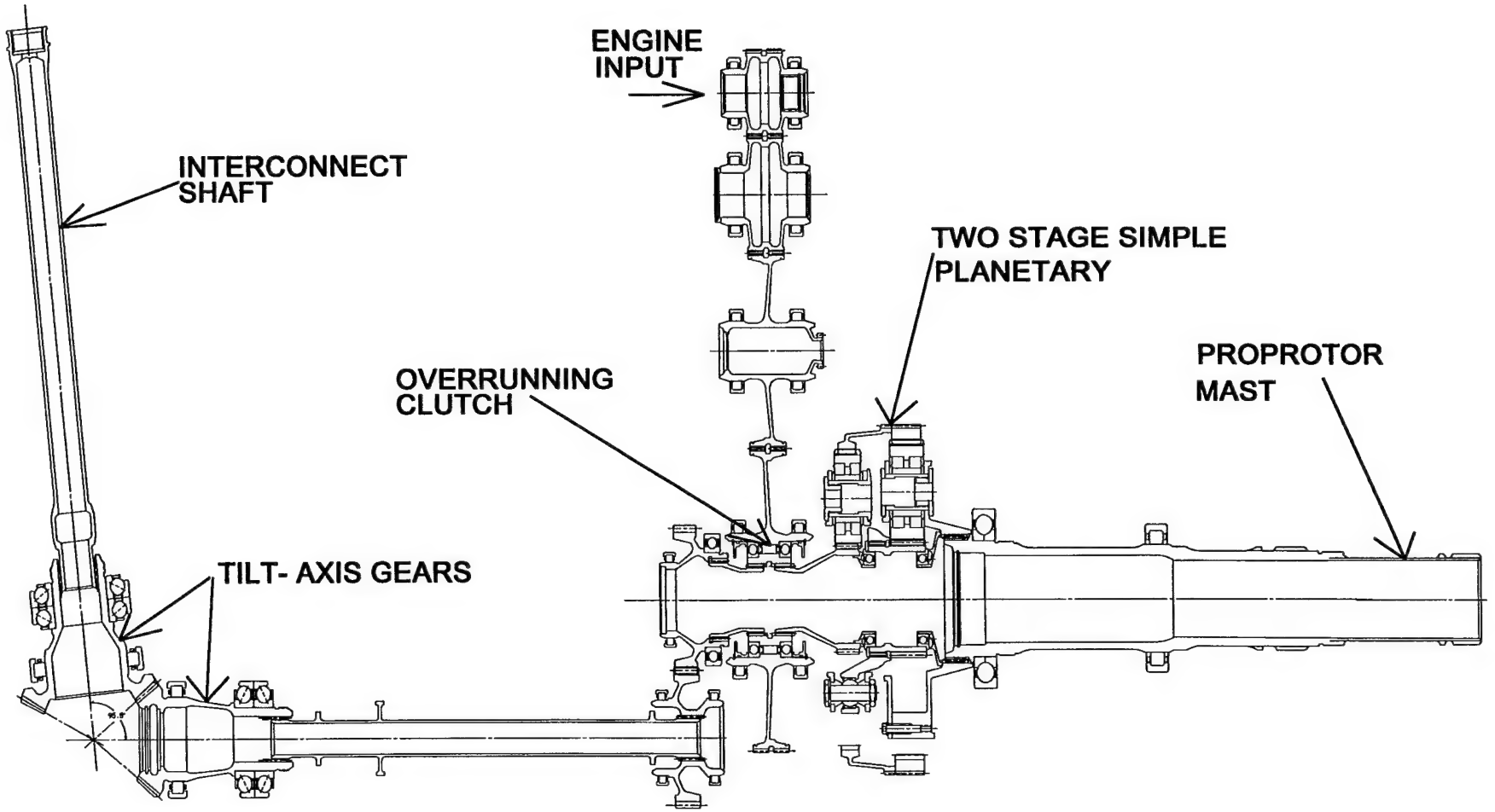

FIGURE 2: XV-15 GEAR AND BEARING TRAIN

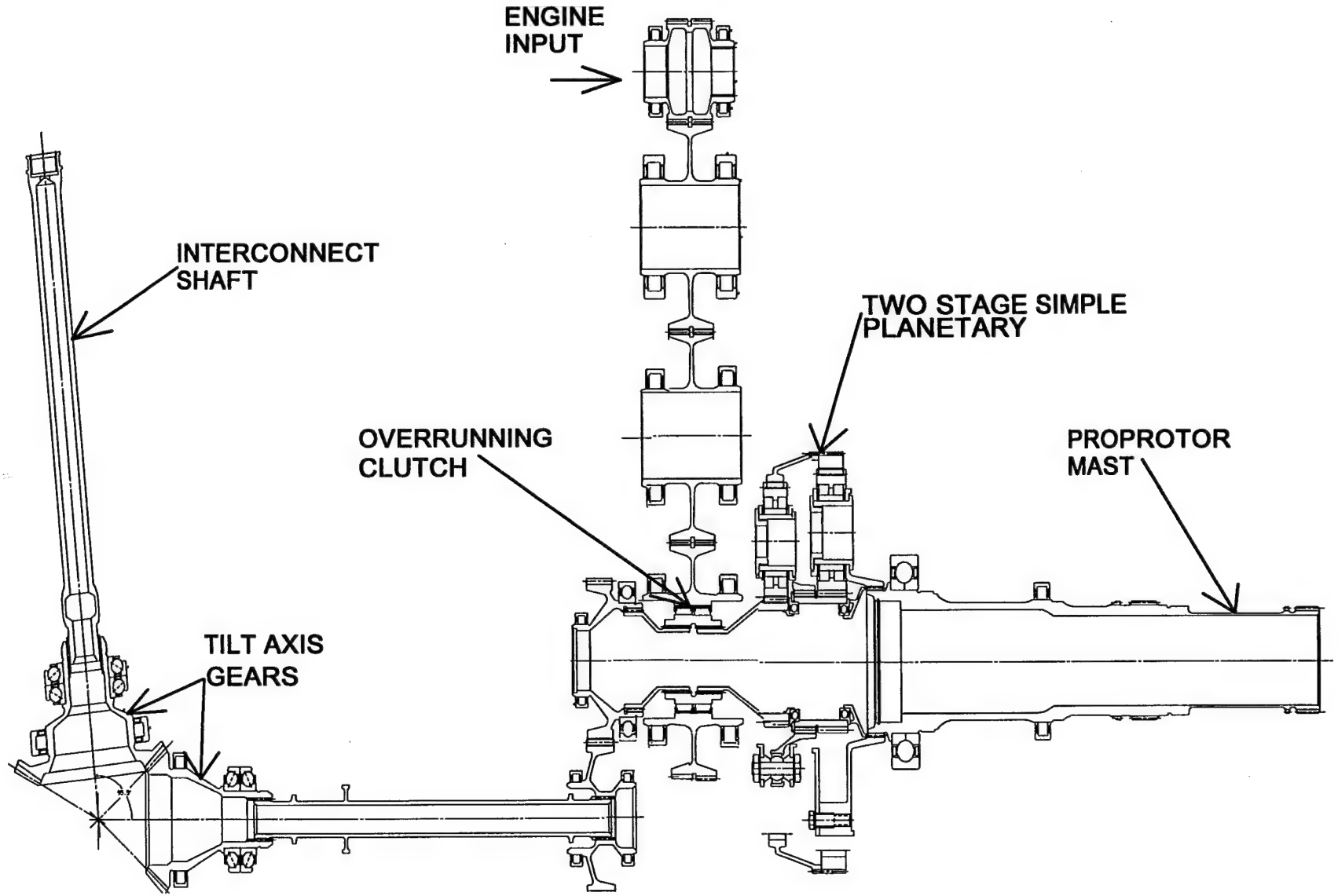

FIGURE 3: SOA GEAR AND BEARING TRAIN (XV-15 RESIZED FOR TTR POWER)

d) The gears were sized for the following allowables:

- Bending stress: 39 KSI max (reversed bending)
- Hertz stress: 117 KSI max
- Scoring temperature: 330° F max (AGMA flash temp. index)

The following rationale was used in developing these allowables:

Bending stress:

The original XV-15 aircraft was designed purely as a research aircraft and therefore the drive system was not designed to meet today's standard 125% overtorque qualification requirement. The XV-15 drive system had a capability for 110% overtorque qualification testing. The SOAT should be designed to pass a 125% overtorque test since the ART transmission would be designed in this way. Therefore, the new operating bending stress allowables for the input section gears were arrived at as follows:

New operating bending stress allowable, f_b was

f_b = Previous max operating bending stress X (1.10/1.25)

The maximum operating reversed bending stress in the input section gears for the XV-15 was 44 KSI at the OEI power of 1650 HP.

Therefore,

$f_b = 44 \times (1.10/1.25) = 38.7$ KSI (rounded off to 39 KSI)

Hertz Stress:

The rationale used for bending stress allowables also applied here. The only difference is that the multiplication factor was $(1.10/1.25)^{1/2}$ instead of (1.10/1.25).

Therefore, new operating Hertz stress allowable, f_c was:

f_c = Previous max Hertz stress allowable X $(1.10/1.25)^{1/2}$

The maximum operating Hertz stress in the input section gears for the XV-15 was 125 KSI at the OEI power of 1650 HP.

Therefore,

$f_c = 125 \times (1.10/1.25)^{1/2} = 117$ KSI

e) The bearings were sized for approximately the same unadjusted life as the present XV-15 bearings.

f) Maximum pitch line velocity was maintained at approximately the same level as the present XV-15.

g) The overrunning clutch for SOAT was sized for the same Hertz and hoop stresses as the present XV-15 clutch at the OEI power of 1650 HP.

3.2.1.2 PLANETARY SECTION AND MAST

a) Power level: 2933 HP at 600 RPM mast output. The 2933 HP figure was derived as follows:

The mast power for ART (TTR) transmission is 2444 HP, under AEO conditions. At BHTI a 1.2 multiplication factor is used for transient loads. Therefore, the power level to be used for design of the planetary, for bending strength, was:

2444 X 1.2 = 2933 HP

b) The planetaries for the resized SOAT are similar to the present XV-15 planetaries in the following areas:

No. of planetaries:	2
Reduction ratio :	3.875 to 1 for each stage
No. of planets - lower:	3
No. of planets - upper:	6

c) The gears were sized for the following allowables:

- Bending stress:	50 KSI max (reversed bending)
- Hertz stress:	170 KSI max
- Scoring temperature:	330° F max (AGMA flash temp. index)

The following rationale was used in developing these allowables:

Bending stress:

The rationale used for resizing the input section also applied here.

New operating bending stress allowable, f_b was:

f_b = Previous max operating bending stress X (1.10/1.25)

The maximum operating reversed bending stress in the planetary gears for the XV-15 was 56.3 KSI at the AEO power of 1460 HP.

Therefore,

$f_b = 56.3 \times (1.10/1.25) = 49.5$ KSI (rounded off to 50 KSI)

Hertz Stress:

The rationale used for bending stress allowables also applied here. The only difference was that the multiplication factor was $(1.10/1.25)^{1/2}$ instead of (1.10/1.25).

Therefore, new operating Hertz stress allowable, f_c was:

f_c = Previous max Hertz stress allowable X $(1.10/1.25)^{1/2}$

The maximum operating Hertz stress in the planetary gears for the XV-15 was 181.4 KSI at the AEO power of 1460 HP.

Therefore,

$f_c = 181.4 \text{ X } (1.10/1.25)^{1/2} = 170 \text{ KSI}$

d) The bearings were sized for approximately the same unadjusted life as the present XV-15 bearings.

e) The mast was sized for TTR gross weight of 17,300 lbs. The bending stresses for the SOAT mast will be comparable to the stresses on present XV-15 mast.

3.2.1.3 INTERCONNECT DRIVE SECTION:

a) Power level: 1542 HP at 9020 RPM under OEI conditions. 1542 HP was an estimated power requirement for the interconnect drive section and was slightly more than half the OEI power of 2777 HP, to account for driving the required accessories under OEI conditions.

b) The interconnect drive section gears were sized for the following allowables:

- Bending stress:
  - Spur gears: 44 KSI max (reversed bending)
  - Spiral bevel gears: 36 KSI max (reversed bending)
- Hertz stress:
  - Spur gears: 161 KSI max
  - Spiral bevel gears: 210 KSI max
- Scoring temperature:
  - Spur gears: 345° F max (AGMA flash temp. index)
  - Spiral bevel gears: 191° F max (AGMA flash temp. index)

The following rationale was used in developing these allowables:

Bending stress:

The rationale used for resizing the input section also applied here.

New operating bending stress allowable, f_b was:

f_b = Previous max operating bending stress X (1.10/1.25)

Spur Gears:

The maximum operating reversed bending stress in the interconnect drive section for the XV-15 was 50 KSI at 825 HP (OEI condition).

Therefore,

$f_{b(spur)} = 50 \text{ X } (1.10/1.25) = 44 \text{ KSI}$

Spiral Bevel Gears:

The maximum operating reversed bending stress in the interconnect drive section for the XV-15 was 40.8 KSI at 825 HP (OEI condition).

Therefore,

$f_{b(bevel)} = 40.8 \text{ X } (1.10/1.25) = 35.9 \text{ KSI (rounded off to 36)}$

Hertz Stress:

The rationale used for bending stress allowables also applied here. The only difference is that the multiplication factor was $(1.10/1.25)^{1/2}$ instead of (1.10/1.25).

Therefore, the new operating Hertz stress allowable, f_c was:

f_c = Previous max Hertz stress allowable X $(1.10/1.25)^{1/2}$

Spur Gears:

The maximum operating Hertz stress in the input section gears for the XV-15 was 172 KSI at 825 HP (OEI condition).

Therefore,

$f_{c(spur)} = 172 \text{ X } (1.10/1.25)^{1/2} = 161 \text{ KSI}$

Spiral Bevel Gears:

The maximum operating Hertz stress in the input section gears for the XV-15 was 224 KSI at 825 HP (OEI condition).

Therefore,

$f_{c(bevel)} = 224 \text{ X } (1.10/1.25)^{1/2} = 210 \text{ KSI}$

c) The bearings were sized for approximately the same unadjusted life as the present XV-15 bearings.

d) Bending stresses for the SOAT interconnect shaft were comparable to the stresses on present XV-15 shaft.

3.2.2 SOAT WEIGHT

The estimated weight of the SOAT was derived using the calculated weights of the gears and bearings shown in Figure 3 and by increasing the weight of the remaining transmission components for the increased horsepower using the following guidelines and assumptions:

1. All case and housing weights were developed using XV-15 case stresses and the following criteria:

   a. Size of new gears, bearings and planetaries.

   b. With increased torque, case walls were thickened to match XV-15 shear stress.

   c. With increased rotor thrust, case walls were thickened to match XV-15 tensile stress.

   d. Weight penalties for bending stresses and frequency placement are considered to be proportional to rotor thrust and are included in item c.

2. Seal, spacer, adapter, retainer, and all other hardware weights were increased by the horsepower ratio per the factors outlined in the Society of Allied Weight Engineers (SAWE) Paper 1120 [2].

3. Planetary weights were ratioed up from XV-15 weights based on the increased horsepower ratio and the weight of the component gears and bearings.

4. Lubrication system weights were increased on the basis of horsepower using the methods of the SAWE Paper 1120 [2]. Oil weight is included.

5. Spindle weights were increased on the basis of constant deflection with increased rotor thrust.

A comparison between the XV-15 transmission and the SOAT is summarized in Table 1 below.

TABLE 1: COMPONENT WEIGHT INCREASES - XV-15 TO SOAT

COMPONENTS	XV-15 WT(LBS)	SOAT WT(LBS)	WEIGHT INCREASE
Cases & Housings	203	427	210%
Bearings	17	33	194%
Seals, Spacers, Retainer	9	18	200%
Gears	45	78	173%
Adapters	1	2	200%
Planetaries	76	106	139%
Lube System	87	163	187%
Freewheeling Unit	5	12	240%
Hardware	17	34	200%
Spindle	34	41	120%
Torque Drive	3	3	-0-
Mast	22	35	159%
Mast Bearings	7	12	171%
TOTAL	526	964	183%

- XV-15 LBS/ENGINE INPUT HP = .329
- SOAT LBS/ENGINE INPUT HP = .347

The design power was increased from 1600 HP to 2777 HP for the input section of the transmission assembly (174% increase) and from 1460 HP to 2933 HP for the mast and planetary section (201% increase).

3.2.3 SOAT NOISE ESTIMATE

The noise estimate for the SOAT was made by the Gear Dynamics and Gear Noise Research Lab of Ohio State University using the XV-15 transmission gear meshes. At 1650 HP the SOAT noise level was estimated to be 102 to 109 dBA. At 2777 HP the noise level was estimated to be 111dBA.

3.2.4 SOAT COST ESTIMATES

The recurring production cost of the SOAT was estimated to be $297,000 projected for 1,000 transmissions. The direct operating cost (DOC) for the SOAT was estimated to be $14.58 per flight hour based on the MTBR of each XV-15 transmission component and $50.64 per flight hour based on the L_{10} life of each of the XV-15 transmission components. Erroneous fleet cost projections may result if adjustments for fleet size and aircraft flying hour programs are not made when using these cost estimates. These costs were derived according to the following ground rules and assumptions for the XV-15:

1. All costs are expressed in Government Fiscal Year (GFY) 1988 dollars.

2. The recurring production cost estimate represents an average cost for 1000 transmissions; cost improvement (90% learning curve) was assumed only for the labor component of recurring production cost.

3. Production cost estimates based on BHTI historical data.

4. Recurring Production Burdens:

   a. Standard Vendor/Raw Material Burden: 1.25

   b. Subcontract Burden: 1.3

   c. Manufacturing Details Labor Rate: $100/hour

5. The DOC includes only costs associated with the left transmission.

6. The DOC includes only parts replacement cost and labor cost for the gear and bearing failures specified in Tables 2 and 3.

7. Each part failure results in the replacement of only the failed part.

8. Replenishment spares are costed at the average of 1000 units; assume spares requirements do not significantly lower the recurring production cost of parts.

9. Each failure results in 1000 hours of labor, equivalent to an XV-15 transmission overhaul.

10. Assumed maintenance labor rate is $11.50/hour, consistent with current Army programs.

11. The DOC based on the MTBRs of the transmission components assumes that failures per flight hour = $(MTBR)^{-1}$.

12. For the DOC based on the L_{10} life of the transmission components, the failure rate is determined by assuming that at the L_{10} life, 10 percent of the components in the transmission have failed.

13. The DOCs are based on the aggregation of fractional numbers of failures for each component specified. These failure rates and resulting DOCs have not been adjusted for specific aircraft flying hour programs or specific fleet sizes.

TABLE 2: XV-15 GEAR & BEARING FAILURE RATES BASED ON MTBR

PART NUMBER	NOMENCLATURE	MTBR(HR)	FAILURE RATE (FAILURES/HR)
300-040-153-003	Upper Pinion	13,703	0.000072977
300-040-155-005	Upper Ring Gear	49,300	0.000020284
300-040-151-003	Upper Sun Gear	49,300	0.000020284
300-040-152-001	Lower Pinion	9,567	0.000104526
300-040-154-003	Lower Ring Gear	17,200	0.000058139
300-040-150-003	Lower Sun Gear	17,200	0.000058139
300-040-210-017	Input Gear	10,542,000	0.000000095
300-040-213-011	Idler Gear	2,975,000	0.000000336
300-040-214-007	Idler Gear	3,878,000	0.000000258
300-040-212-007	Bull Gear	60,300,000	0.000000017
300-040-107-103	Gear	49,050	0.000020387
300-040-108-003	Gear	49,050	0.000020387
300-040-302-001	Gear	49,050	0.000020387
300-040-301-001	Pinion	49,050	0.000020387
300-040-112-003	Bearing	14,200	0.000070423
300-040-113-001	Bearing	215,000	0.000004651
300-040-113-003	Bearing	60,000	0.000016667
300-040-114-001	Bearing	375,000	0.000002667
300-040-181-001	Bearing	27,000,000	0.000000037
300-040-136-009	Bearing	64,000	0.000015625
300-040-167-001	Roller Set	3,583	0.000279096
300-040-725-001	Roller Set	28,333	0.000035295
300-040-116-001	Bearing	41,500	0.000024096
300-040-117-003	Bearing	60,000	0.000016667
300-040-117-003	Bearing	42,000	0.00002381
300-040-405-001	Bearing	11,000	0.000090909
300-040-306-003	Bearing	54,000	0.000018519
300-040-406-003	Bearing	59,000	0.000016949
300-040-405-001	Bearing	14,500	0.000068966

TABLE 3: XV-15 GEAR & BEARING FAILURE RATES BASED ON L_{10} LIVES

PART NUMBER	NOMENCLATURE	QTY	L_{10} LIFE (HR)	FAILURE RATE (FAILURES/HR)
300-040-153-003	Upper Pinion	6	2,485	0.000241449
300-040-155-005	Upper Ring Gear	1	248	0.000403226
300-040-151-003	Upper Sun Gear	1	248	0.000403226
300-040-152-001	Lower Pinion	3	867	0.000346021
300-040-154-003	Lower Ring Gear	1	173	0.000578035
300-040-150-003	Lower Sun Gear	1	173	0.000578035
300-040-210-017	Input Gear	1	637,143	0.000000157
300-040-213-011	Idler Gear	1	248,984	0.000000402
300-040-214-007	Idler Gear	1	250,456	0.000000399
300-040-212-007	Bull Gear	1	2,645,000	0.000000027
300-040-107-103	Gear	1	1,482	0.000067476
300-040-108-003	Gear	1	1,482	0.000067476
300-040-302-001	Gear	1	1,482	0.000067476
300-040-301-001	Pinion	1	1,482	0.000067476
300-040-112-003	Bearing	2	2,840	0.000070423
300-040-113-001	Bearing	2	43,000	0.000004651
300-040-113-003	Bearing	2	12,000	0.000016667
300-040-114-001	Bearing	2	75,000	0.000002667
300-040-181-001	Bearing	1	2,700,000	0.000000037
300-040-136-009	Bearing	1	6,400	0.000015625
300-040-167-001	Roller Set	6	2,150	0.000279071
300-040-725-001	Roller Set	3	8,500	0.000005294
300-040-116-001	Bearing	1	4,150	0.000024096
300-040-117-003	Bearing	1	8,400	0.000011905
300-040-117-003	Bearing	2	6,000	0.000033333
300-040-405-001	Bearing	1	1,450	0.000068966
300-040-306-003	Bearing	1	5,400	0.000018519
300-040-406-003	Bearing	1	5,900	0.000016949
300-040-405-001	Bearing	1	1,100	0.000090909

The component L_{10} lives and MTBRs for the gears and bearings were calculated with a methodology derived by BHTI from empirical data and several technical sources. These life calculations are basically a function of compressive stress, oil film thickness, surface finish, a Weibull distribution derived from empirical data, and several material process and lube system adjustment factors. The specific methodology is presented in Section 4.8 of this report.

4.0 PRELIMINARY DESIGN AND TRADEOFF STUDIES

4.1 PLANETARY SELECTION

Prior to deriving the final preliminary configuration for the ART, a tradeoff study was conducted on several different planetary configurations. It was anticipated that some form of a planetary reduction would be required to meet the required speed reduction from 20,900 RPM engine input speed to 600 RPM mast output speed. All of the planetaries were sized for 2933 HP for gear tooth bending fatigue and scoring limits and 2444 HP for gear tooth pitting fatigue limits. All of the planetary systems except for the single stage high contact ratio planetary were sized for approximately a 15:1 speed reduction ratio.

Each planetary design was limited in overall size by the nacelle and rotor control envelope established for the reference aircraft, and attention was given to the assembly requirements and producibility of the individual components of each planetary configuration.

Table 4 presents a summary of the selection process for the ART planetary in matrix form comparing the planetaries described below. The comparative factors range from 1 for most favorable to 5 for least favorable.

TABLE 4: PLANETARY SELECTION MATRIX

PLANETARY	WEIGHT	NOISE	LIFE	SURVIVA-BILITY	COST	EFFICIENCY	RISK	SPATIAL ENVELOPE	TOTAL
Simple	2	5	4	5	2	3	1	2	24
Split Power	3	5	4	5	3	3	2	2	27
SABP	5	2	1	2	4	2	4	4	24
Compound	4	4	3	3	2	2	1	5	24
HCR	1	3	2	2	3	4	2	1	18

4.1.1 SIMPLE PLANETARY

The baseline planetary for these tradeoff studies is a simple two stage planetary system, shown in Figure 4, which is similar to the SOAT planetary system except the planet bearings are spherical rollers, the carriers are made from titanium, and the planet bearings are mounted on cantilevered posts integral with the carrier. A weight analysis of the simple planetary assembly yielded a total subsystem weight of 144 lb.

4.1.2 SPLIT POWER PLANETARY

One variation of the simple two stage planetary system is the split power planetary which basically contains the same number of components except the planets in the low speed section are fixed and both ring gears rotate. As shown in Figure 5, torque is split from the input sun gear and transmitted to the output carrier along two separate paths, one path through the four planet posts and the other through the 138 tooth output ring gear splined to the output carrier, hence the name split power planetary. As compared to the simple planetary, the split power planetary is 15.0 lb heavier and is configured in such a way that the high speed planets cannot be lubricated with the supplemental air-oil mist nozzles planned for the ART (see Figure 41) since they are completely encased by the output carrier and ring gear assembly.

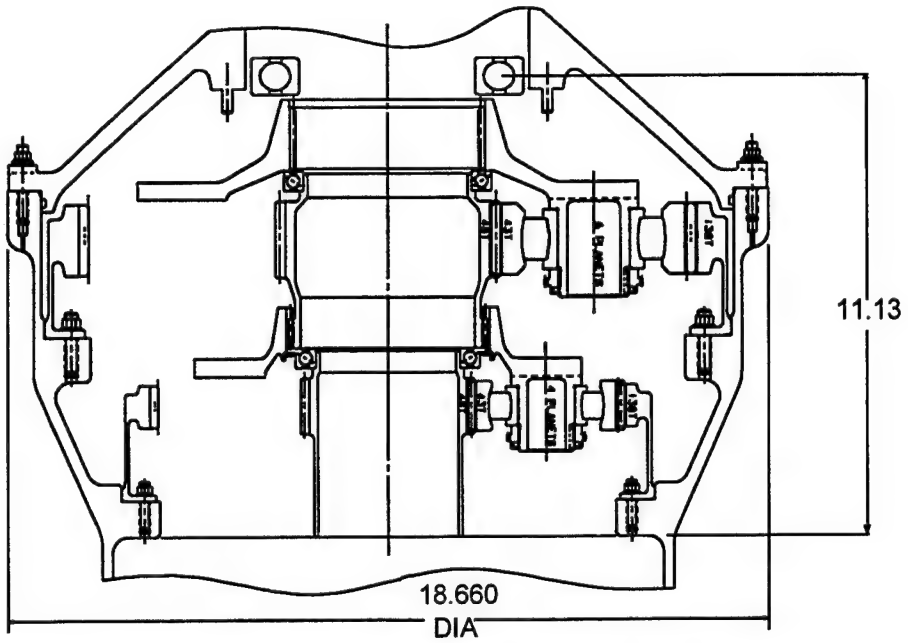

FIGURE 4: TWO STAGE SIMPLE PLANETARY - 15.01561 REDUCTION RATIO

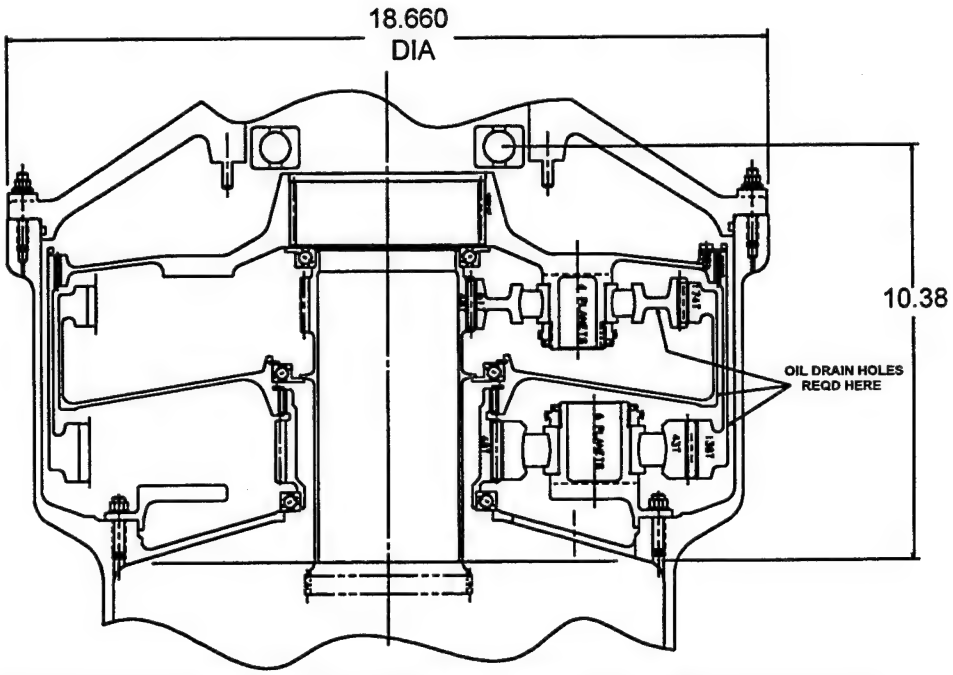

FIGURE 5: SPLIT POWER PLANETARY - 15.0469:1 REDUCTION RATIO

4.1.3 SELF-ALIGNING-BEARINGLESS PLANETARY (SABP)

Both a four (4) and a six (6) planet configuration layout of a SABP were sized for the ART power and speed requirements defined in Section 4.1 and are shown in Figures 6 and 7. The methodology defined in Reference [3] was used to design each SABP. The goal was to limit the overall size of each configuration to

the dimensions established by the nacelle and rotor control requirements for the ART airframe, but it was not possible to meet this with the 15:1 reduction ratio requirement. Therefore, the overall diameter limit was observed and the height limit was exceeded on each configuration. Each of the layouts was sent to Transmission Technology Co. Inc. (TTI) to review BHTI's SABP layouts for technical and manufacturing feasibility and provide comments and recommendations in a summary report.

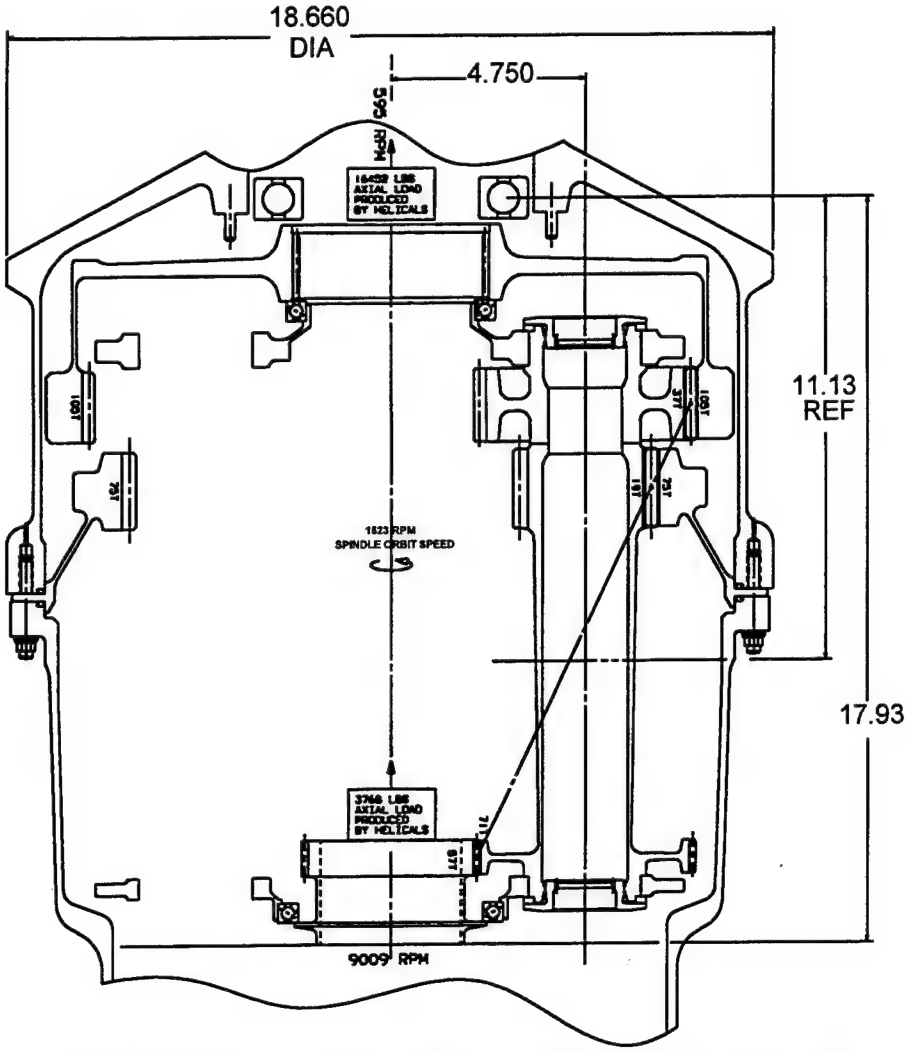

FIGURE 6: FOUR SPINDLE SABP - 15.1345:1 REDUCTION RATIO

TTI's review agreed with the selection of gear tooth pressure angles and helix angles and gear tooth number combinations required for assembly, but recommended that the gear tooth stresses be reduced. TTI also recommended the use of the maximum number of spindles allowed by the overall geometry restrictions. BHTI's layouts showed the six spindle arrangement to be lighter and more compact than the four spindle arrangement.

With regard to the roller ring design requirements, TTI analyzed the system as a conventional roller bearing with the same stress calculations and allowables. The recommended roller ring deflection range was .0004 to .0015. TTI recommended gear tolerances comparable to those required for a compound epicyclic planetary since the alignment and indexing requirements are critical to the successful operation of the SABP. Increased alignment and indexing errors increase the magnitude of nonuniform load distribution. The required

alignment between the three planets on each spindle complicates the manufacturing and inspection process for the spindle, and torsional windup of the three planet spindle must be accounted for with lead correction. Deviation from the design balance line for the SABP will result in non-uniform load distribution and all misalignment and indexing errors will of course increase the magnitude of the dynamic gear tooth loads.

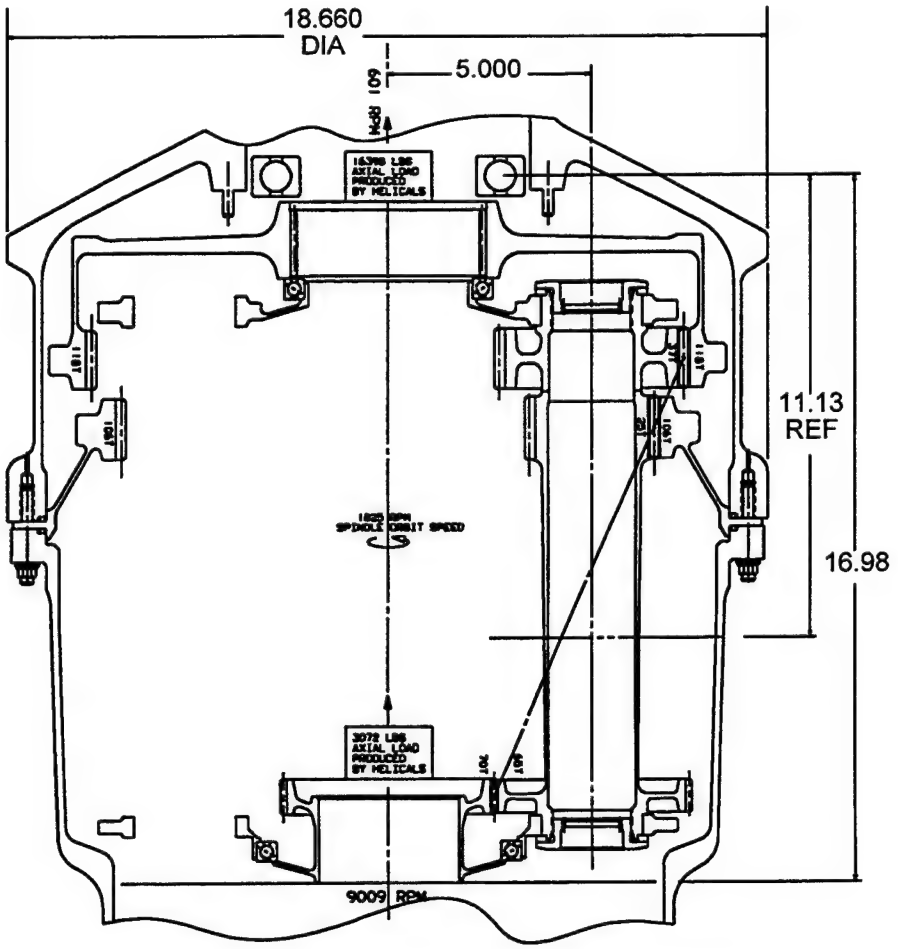

FIGURE 7: SIX SPINDLE SABP - 14.984:1 REDUCTION RATIO

TTI's specific conclusions and recommendations are as follows:

1. The two Bell SABP schematics reviewed were found to have the correct number of teeth to permit assembly and the overall contact ratio was found to be in the desired range.

2. From a gear tooth stress and strength point of view, both schematics were found to have excessive stresses and the gear sizing should be modified to reduce the stress levels and to achieve a better balance between bending and compressive stresses.

3. The design procedure used by TTI, whether for conventional planetaries or SABP's, is an iterative process. The two Bell schematics are considered to represent an excellent starting point. It is recommended that this process be continued as the concept of SABP offers many advantages and benefits not only to the designer and manufacturer but also to the ultimate user. Low weight, reduced number of major components, flexibility of design, lower manufacturing cost and higher reliability are but a few of the beneficial claims made for the SABP.

As stated earlier, the resulting gear tooth stresses for both of the BHTI SABP layouts are within current drive system design allowables at BHTI and are therefore not considered excessive. A decrease in design allowable stresses would of course result in a larger, heavier planetary arrangement. While the SABP may have fewer major components, the reduced weight benefit was not realized in any of the SABP layouts for the ART. BHTI's weight analysis found the six spindle SABP sized for the same power, speed and reduction ratio requirements as a two stage simple planetary was approximately 28% heavier. BHTI's four spindle SABP was approximately 45% heavier than the two stage simple planetary. A weight analysis was also performed on the layout of the SABP recommended by TTI (see Figure 8) for the speed and power requirements of the ART and was approximately 88% heavier than the two stage simple planetary.

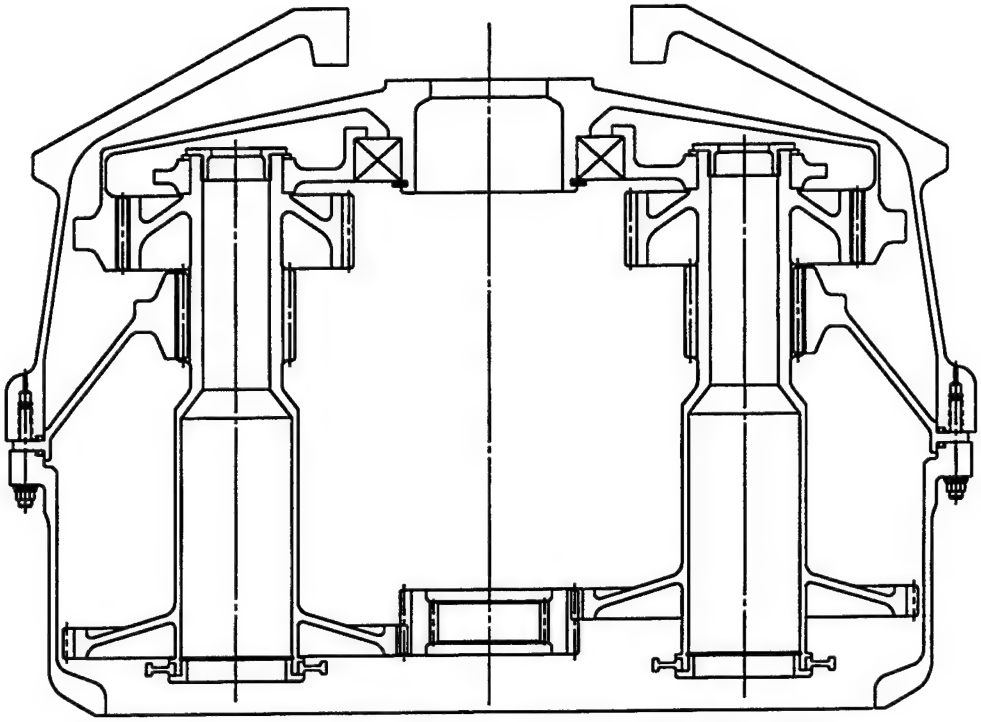

FIGURE 8: TTI PROPOSED SABP LAYOUT FOR ART

The higher reliability claim for the SABP is very subjective since reliability is more than a function of the number of components but also involves component life which affects the overall weight of the system. All other factors being equal, an increase in reliability for a system requires an increase in weight. Therefore, a simple planetary system could be made more reliable by increasing the size of the gears which would decrease the gear tooth stresses and increase the component lives of the gears. Any reduction in manufacturing costs due to reduction in major components for the SABP appear to be offset by the increased manufacturing costs for the three planet spindle. Not only is the alignment procedure costly but an extra set of planet gears must be manufactured.

The SABP would probably run quieter than the simple planetary since it uses helical gears instead of standard spur gears. Another advantage the SABP has over a simple planetary is the elimination of the planet bearings which could extend the operating time in a loss-of-lube situation. However, with the use of the supplemental lube system for enhanced loss-of-lube operation (see Section 4.5.2) in the ART, this advantage is minimized.

4.1.4 COMPOUND PLANETARY

The compound planetary is similar to the simple planetary except that the planet gears are made up of two gears on one shaft with the larger gear meshing with the sun gear and the smaller gear meshing with the fixed ring gear. A preliminary effort was made in sizing a compound planetary to be used in place of the two stage simple planetary shown in Figure 4. Figure 9 shows that the compound planetary does not yield a sufficient reduction ratio for the space allowed by the ART rotor and nacelle and would require a preliminary input reduction to 4897 RPM from the engine input speed of 20,900 RPM to meet the 600 RPM mast output requirement for the ART.

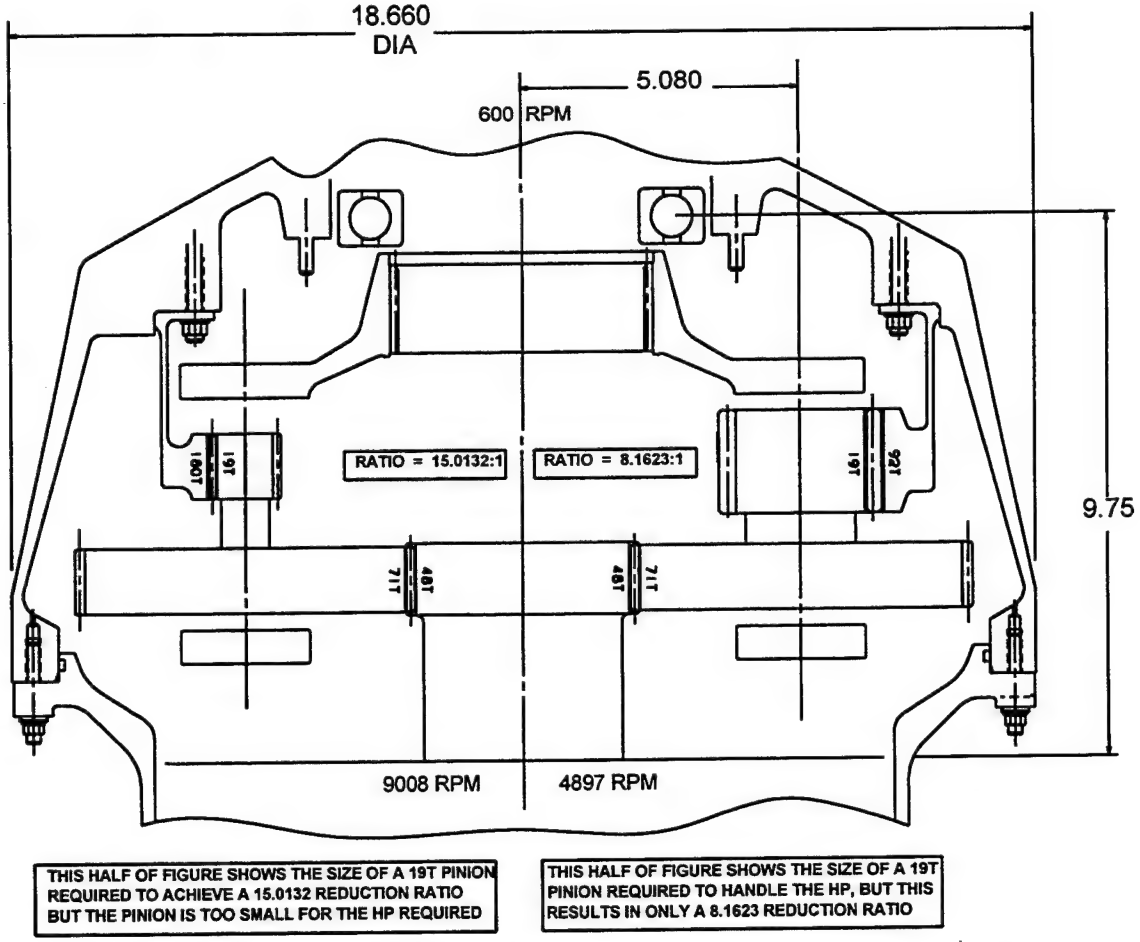

FIGURE 9: COMPOUND PLANETARY SIZING REQUIREMENTS FOR ART

4.1.5 HIGH CONTACT RATIO (HCR) PLANETARY

A high contact ratio (HCR) planetary is a planetary spur gear system with tooth contact ratios in the sun/planet and ring/planet meshes greater than 2, as compared to a simple planetary system with tooth contact ratios less than 2. The higher tooth contact ratio for HCR planetaries results in a quieter running planetary and a reduction in the dynamic loading of the gear teeth. From a survivability standpoint, the tooth contact ratio greater than 2 allows the planetary system to continue to operate even with the loss of a tooth.

One of the disadvantages of a HCR planetary is the increased sliding velocity between meshing teeth due to the increased height of the teeth required to achieve a contact ratio greater than 2. This increased sliding results in higher power losses for the gear meshes and therefore less efficiency and higher surface temperatures (scoring problems) for the meshing gear teeth. The resultant weight savings realized for any HCR planetary must exceed the effective weight increase due to the loss in efficiency and often the increased scoring temperature for a HCR gear mesh forces the gear face widths to be wider than required to meet bending and hertz stress limits.

An initial attempt was made to size a lighter weight two stage HCR planetary with the same reduction ratio and same tooth numbers as a previously sized two stage simple planetary shown in Figure 4. The calculated scoring temperature for the high speed HCR planetary was excessive and the planetary bearings in the low speed HCR planetary did not have enough capacity for the design loads. Letting the bearings size the HCR low speed planetary, i.e. larger diameter bearings, the diametral pitch of the planetary gears was decreased from 11.375 to 11.000 and the number of teeth on each gear was increased. This resulted in a HCR planetary shown in Figure 10 with a slightly lower reduction ratio, 3.818 instead of 3.875, but approximately 8 lbs lighter than the simple planetary. The bending stress on the HCR planet gear is allowed to be 120% higher than that of the simple planet gear because of the reduction of the dynamic load factor for HCR gears as observed in previous HCR planetary testing at BHTI [1].

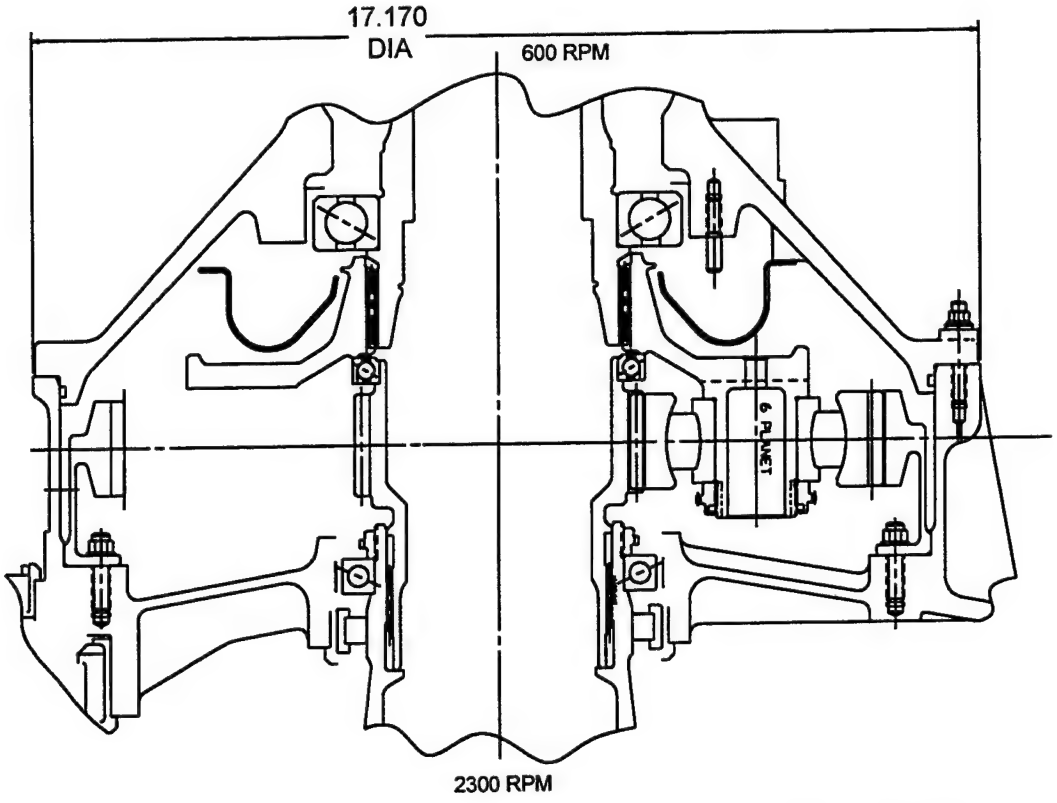

FIGURE 10: HIGH CONTACT RATIO, LO-SPEED PLANETARY- 3.81818:1 REDUCTION RATIO

Since the HCR planetary at the high speed location was heavier than the simple planetary, due to increased face widths required to meet the scoring limit, a transmission configuration eliminating the high speed planetary and incorporating a two stage helical reduction gear train was investigated (see Section 4.4). The

advantage of this type of transmission over a single stage helical reduction and a two stage planetary with a simple high speed planetary is that all of the gear meshes in the transmission would have tooth contact ratios greater than 2. This of course would be a quieter running transmission and more survivable should a tooth failure occur.

4.1.6 PLANET BEARING SELECTION

The planet spherical roller bearings were analyzed using PLANETSYS, a computer program purchased from SKF Aerospace Bearing Co. This program calculates bearing life, hertzian stress, heat loss, and roller contact footprint, based on individual roller loads. These loads are derived from bearing geometry, planet ring stiffness, centrifugal force, static forces and dynamic forces.

Single and double row bearing configurations were investigated for the high contact ratio planetary described in Section 4.1.5. The following table shows the comparison of the results.

	SINGLE ROW BEARING	DOUBLE ROW BEARING
Weight (lbs)	3.939	3.925
PD (in)	2.643	2.7
Life (hrs)*	270	240
Heat Loss (HP)	2.48	1.945
Hertz Stress (ksi)	300	290

* Bearing life is unadjusted, that is, no material, process, or lubrication factors have been included.

Since this evaluation showed the single and double row bearings to be similar in size, weight, and life, both configurations were tested in the high contact ratio planetary component tests.

4.2 OVERRUNNING CLUTCH SELECTION

Two types of overrunning clutches were sized for the input section of the ART, the spring overrunning clutch and the sprag overrunning clutch. Although the 20,900 RPM input speed presents an increased risk to successful operation of either clutch type, the input section was chosen for sizing the clutches because the low torque will provide the lightest overrunning clutch package. Locating the clutch assembly at the input section as shown in Figure 16 allows the interconnect cross-shaft output gear and idler to be driven directly by the bull gear instead of by a separate gear as required in the SOAT (see Figure 3) for proper overrunning capabilities and also allows clutch repair or inspection without major disassembly of the transmission or removal from the aircraft. The weight savings for moving the clutch assembly from the bull gear to the input section is approximately 27 lb for the gears, bearings, and clutch assembly alone.

Figure 11 shows the spring overrunning clutch which was sized using the guidelines from Reference [4]. This clutch assembly was primarily sized for weight comparison with the sprag clutch since the results of the tests in the report indicate much more development work is required for the spring clutch before it can be considered for the ART. The weight analysis found the spring clutch assembly to be 3.4 lb heavier than the sprag clutch assembly.

Figure 12 shows the sprag overrunning clutch which, because of the high input speed, incorporates four rows of sprags as a way to decrease the diameter of the inner race and thereby the PV product which would

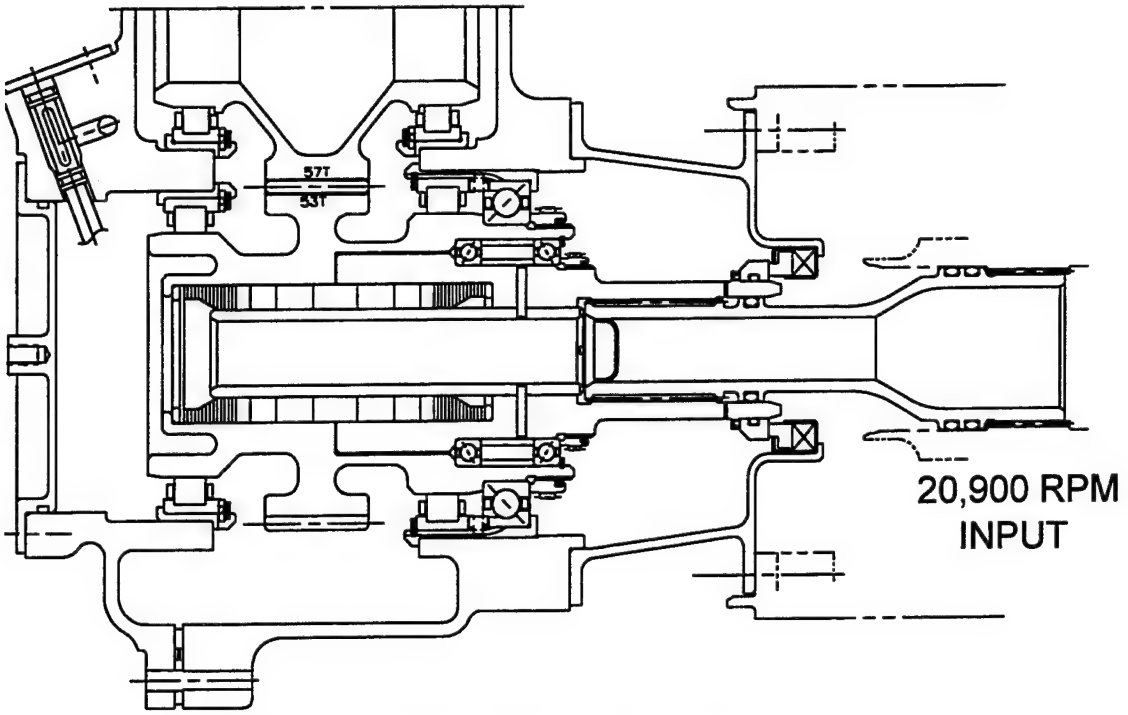

FIGURE 11: SPRING OVERRUNNING INPUT CLUTCH

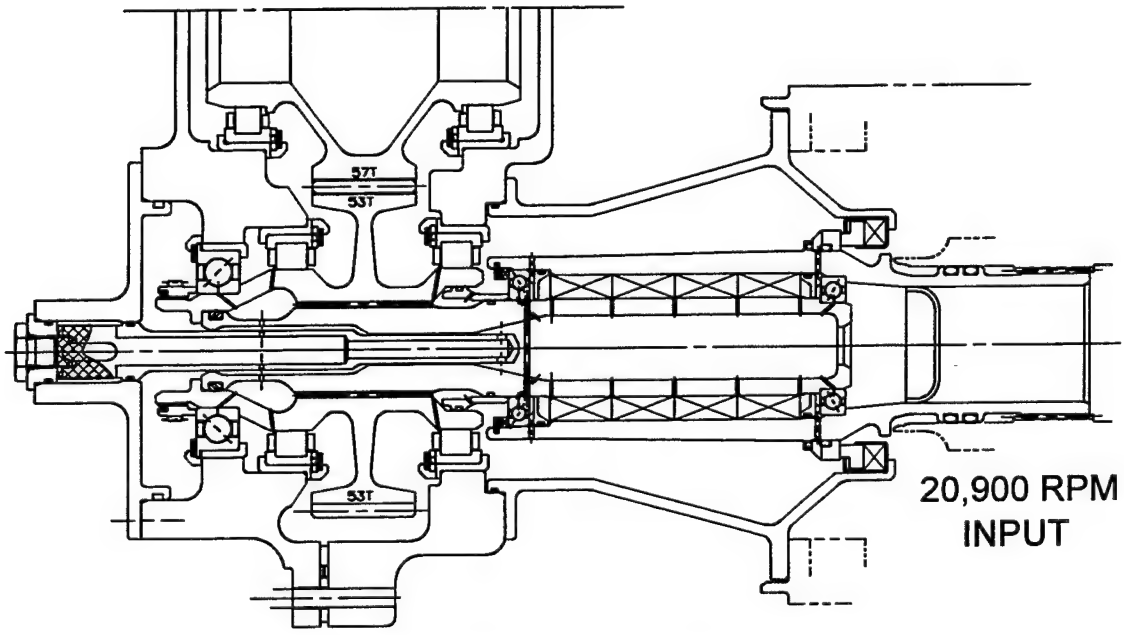

FIGURE 12: MULTI-ROW, SPRAG OVERRUNNING INPUT CLUTCH

otherwise be excessive if only two rows of sprags were used. The PV product is a function of the inner race outside diameter and the overrunning speed of the clutch. Using four rows of sprags instead of two, it was assumed that the maximum load carried by one row of sprags would decrease from 60% to 35%. The outer race outside diameter was tapered to allow the windup of the sprags due to hoop deflections of the outer race to match the torsional windup of the inner race, thereby more evenly distributing the transmitted torque across the four rows of sprags. The sprag design is not without design risks as the use of four rows of sprags is a new approach for helicopter applications and the 20,900 RPM operating speed exceeds those for most sprag clutches in use today.

Realizing that any significant weight reductions in the clutch assembly will only be achieved by locating the clutch on the input shafting, the roller ramp clutch was not investigated because of its maximum speed limitation of approximately 12,000 RPM [3] which forces it into a higher torque location and therefore heavier configuration.

Table 5 presents the selection process matrix for the clutch tradeoff study considering the spring, sprag, and roller ramp clutches and showing the reason for selection of the sprag clutch for the ART. The comparative factors range from 1 for most favorable to 5 for least favorable.

TABLE 5: CLUTCH SELECTION MATRIX

CLUTCH	WEIGHT	LIFE	SURVIVA-BILITY	COST	RISK	SPATIAL ENVELOPE	TOTAL
SPRAG	1	3	2	2	4	2	14
SPRING	2	3	3	4	5	2	19
ROLLER RAMP	5	2	4	3	2	4	20

4.3 INPUT GEAR TRAIN SELECTION

In high speed gear trains, where parallel axis gears are required, either helical or double helical (D-H) gears are usually used because of the smoother running operation provided by the larger tooth contact ratio attainable in these types of gears. When the XV-15 tiltrotor transmissions were designed in the late 1960's, D-H gears were selected for the high speed input gear train where the pitch line velocity is 25,000 fpm. The D-H gears were chosen over single helical gears for the following reasons:

1. The effect of the gear tooth misalignment error is only half that for single helicals because of the ability of the D-H gears to shift axially to equalize the loads on the two rows of teeth.

2. Higher face contact ratios for the same face width are attainable on D-H gears because higher helix angles can be used due to the resultant zero axial thrust load component inherent in a D-H mesh. This cancellation of the axial loads permits thinner webs and smaller bearings and negates the requirement for thrust bearings on the first and last gear in the train.

There are some disadvantages associated with D-H gears when compared with single helical gears:

1. Higher Cost - Making a D-H gear is similar to making two single helical gears.

2. Less Accuracy - Electron beam welding two helical gear halves to produce one D-H gear, as was done to manufacture the D-H gears for the XV-15, introduces some inaccuracies due to distortion. If the D-H gear is machined from a single piece of material, then the necessary gap between the two rows of teeth must be increased to allow even small wheel grinding of both rows of teeth. The accuracy of a small wheel ground gear will probably be less than that of a large wheel ground gear, such as would be possible with single helicals, because the small wheel tends to break down faster because of the reduced grinding surface area of the wheel.

3. Higher Assembled Cost - Because D-H gears are not free to move axially relative to one another, at least one of the members at either end of the gear train must be free to move axially to prevent overloading one row of teeth. This freedom was provided on the XV-15 gear trains by making the splined connection from the input shaft to the input D-H pinion a "working" crowned gear coupling. This was accomplished by building in a 1/2° shaft misalignment. The result is that the coefficient of friction at the shaft-to-pinion connection is kinetic and generally predictable instead of static and unpredictable. The lower kinetic coefficient of friction combined with a 35° helix angle on the D-H gear teeth insures the axial movement of the gear with minimal unbalanced loads on the two rows of the gear teeth.

Since the XV-15 D-H gears were designed, BHTI has designed and put into production several single helical gear applications comparable to D-H gears. This was accomplished by reducing the helix angle from 35° to around 10° and extending the face width to obtain a face contact ratio of about 1.1, where 1.0 is the minimum amount to assure uniform angular motion by helical action alone. The low helix angle of 8° to 12° produces a sufficiently low axial thrust which does not necessitate the use of excessively sturdy gear rims and webs or large thrust bearings.

Based on the reasons discussed above and the factors presented in the comparative matrix, Table 6, where the factors range from 1 for most favorable to 5 for least favorable, the input gears for the ART will be single helical with a helix angle of 10° and a minimum face contact ratio of 1.1. The gear rims and webs will be designed using FEM analysis to insure a lightweight but sturdy gear.

TABLE 6: INPUT GEAR SELECTION MATRIX

GEAR TYPE	WEIGHT	NOISE	LIFE	SURVIV-ABILITY	COST	EFFICIENCY	TOTAL
STD SPUR	3	5	4	5	2	3	22
HIGH CONTACT RATIO	1	3	2	2	3	5	16
SINGLE HELICAL	2	2	1	2	3	2	12
DOUBLE HELICAL	5	1	1	1	5	1	14

4.4 TRANSMISSION CONFIGURATION SELECTION

The following selection process for the ART preliminary configuration was an attempt to derive the best gearbox to meet both the ART requirements for weight reduction, noise reduction, and increased life and airframe and control restrictions associated with the reference aircraft. The layouts depicted in each of the figures presented for configurations 1 thru 5 are right hand gearbox configurations (one input idler eliminated) and provide only enough detail to determine the benefit or detriment of each configuration and are therefore incomplete in some areas.

Figures 20 and 21 are left hand gearboxes derived from configurations 1 thru 5 and are presented more completely for weight analysis purposes.

4.4.1 BASELINE CONFIGURATION #1

The baseline configuration shown in Figure 13 is of course similar to the SOAT except it includes an extra idler gear in the interconnect loop to meet the cross-shafting location requirements for the reference aircraft. Locating the clutch in the bull gear increases the transmission survivability, since the transmission can still be operated through the cross-shafting should any of the input power train fail. Figure 14 shows the power loop for a normally operating gearbox, and Figure 15 shows the power loop for a gearbox with either a failed engine or a failed gear in the input helical train. Locating the clutch in the bull gear, however forces the removal and disassembly of the transmission for any clutch repair or inspection.

4.4.2 CONFIGURATION #2

As shown in Figure 16, the next step to decrease the weight of the ART was to move the clutch to the input location where higher speed (20,900 RPM instead of 9,006 RPM) yields lower torque and a lighter clutch assembly. This relocation allows the interconnect cross-shaft output gear and idler to be driven directly by the bull gear instead of by a separate gear as required in Configuration #1 and also allows clutch repair or inspection without major disassembly of the transmission or removal from the aircraft. Placing the clutch forward of the input pinion is the most desirable location since it would allow clutch repair and inspection without removing the engine. However, this is not possible since the diameter of the drive shaft which would have to extend from the engine drive spline through the clutch inner race to drive the outer race of the clutch assembly would not meet the torque requirements for the ART.

As shown in Figure 16, this configuration is less survivable than Configuration #1 since a failure of any of the input helical gears could result in loss of the bull gear and therefore the entire transmission, i.e. the bull gear is in the power loop when either engine is driving. However, this configuration yields a lighter bull gear with smaller bearings sized by life requirements instead of geometric requirements, a lighter clutch assembly, one less gear, one less splined shaft, two less bearings, and a more compact housing. The weight savings for the gears, bearings, and clutch assembly alone amount to approximately 27 lb. The vibration monitoring portion of the diagnostic system will significantly reduce the chance of a catastrophic failure in the input helical train.

4.4.3 CONFIGURATION #3

Locating the clutch on the input shaft presents a certain amount of risk since most sprag clutches are designed for less than 15,000 RPM. The four row clutch assembly in Figure 16 and as described in Section 4.2 is an untested concept and requires component testing before it can be included in the final ART design. A separate IR&D program was conducted at BHTI which successfully validated the 4-row clutch design.

Configuration #3 as shown in Figure 17 is an attempt to place the clutch assembly in a location with a lower speed. To accomplish this, it was necessary to incorporate a speed reduction in the helical train prior to the bull gear reduction, which also made it possible to eliminate the 1st stage high speed planetary assembly. The clutch was sized for 12,040 RPM and 2777 HP and was located to provide access without removing the transmission from the aircraft. This configuration however does not fit the reference aircraft envelope restrictions since it forces the location of the rotor controls to be extended an additional 5.0 inches.

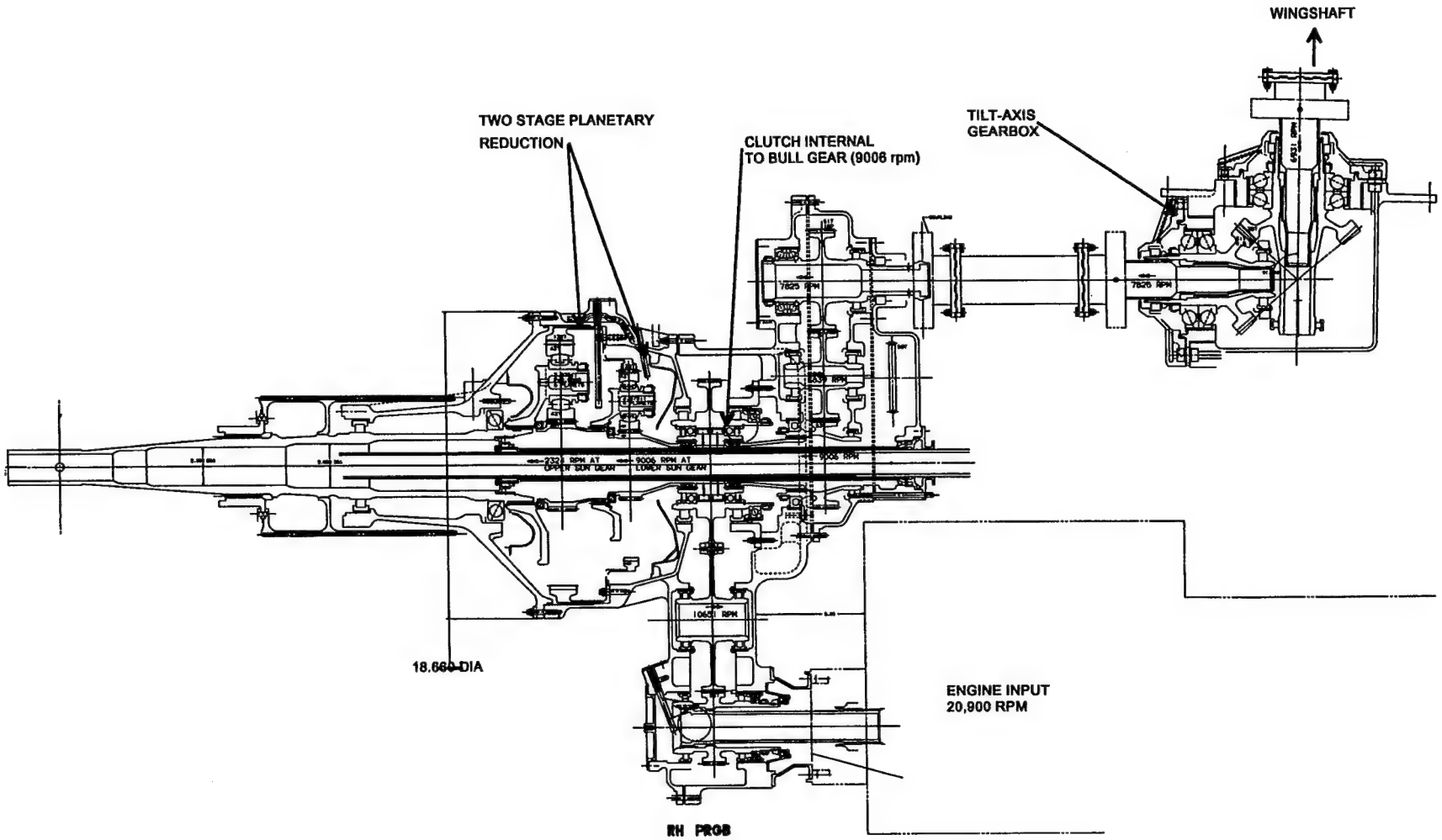

FIGURE 13: ART PRELIMINARY LAYOUT - BASELINE CONFIGURATION #1

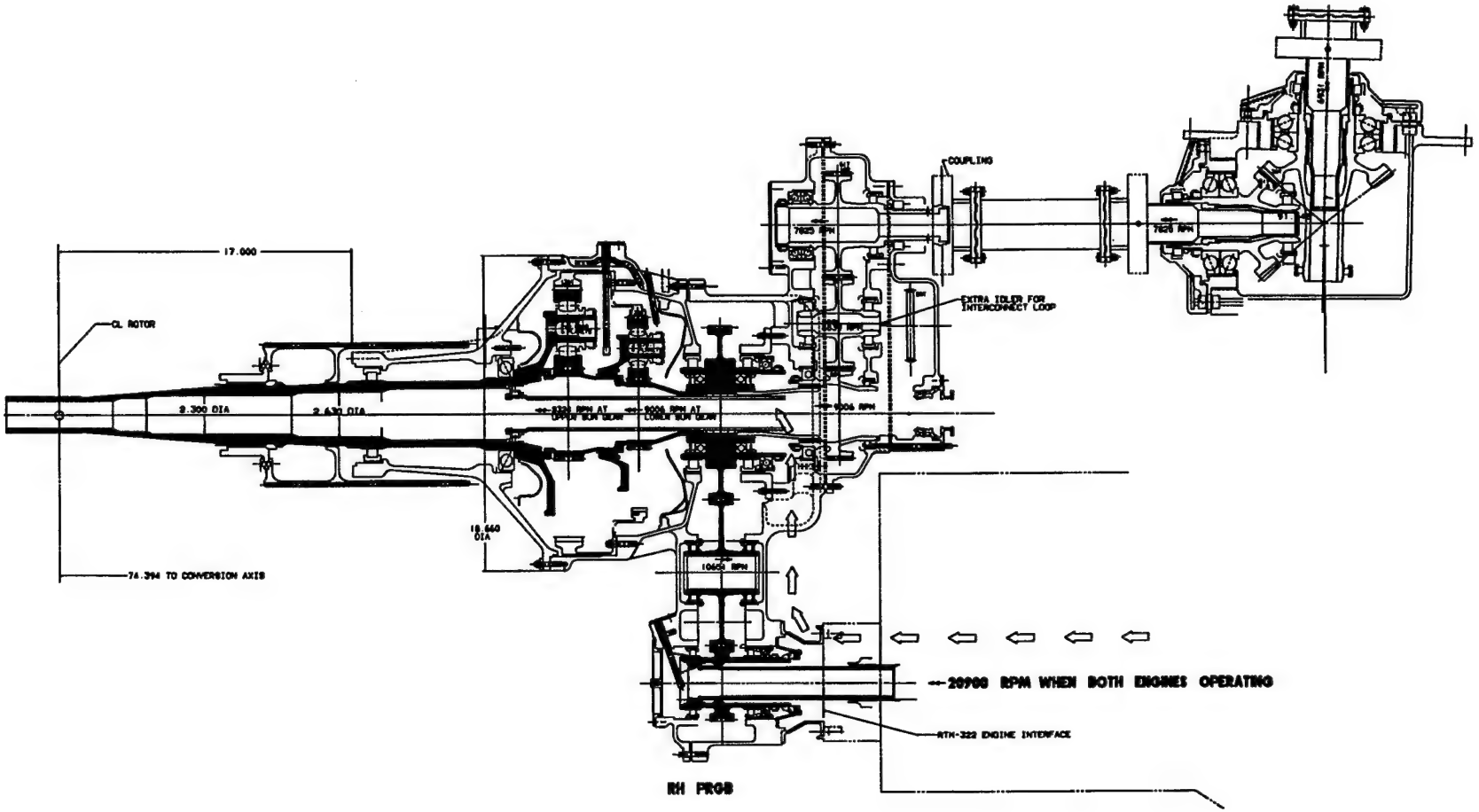

FIGURE 14: BASELINE CONFIGURATION #1, BOTH ENGINES OPERATING

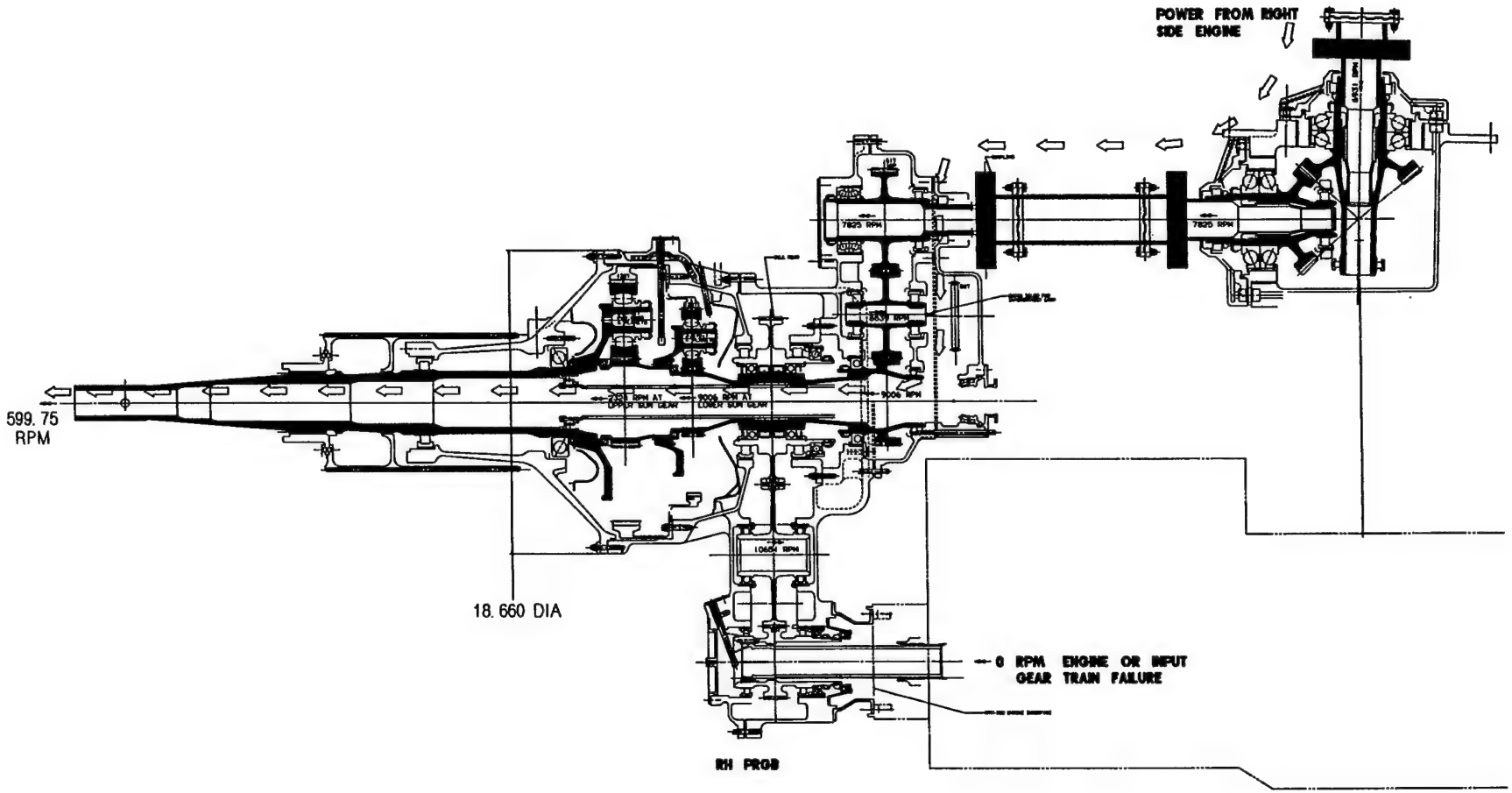

FIGURE 15: BASELINE CONFIGURATION #1, OPPOSITE ENGINE DRIVING

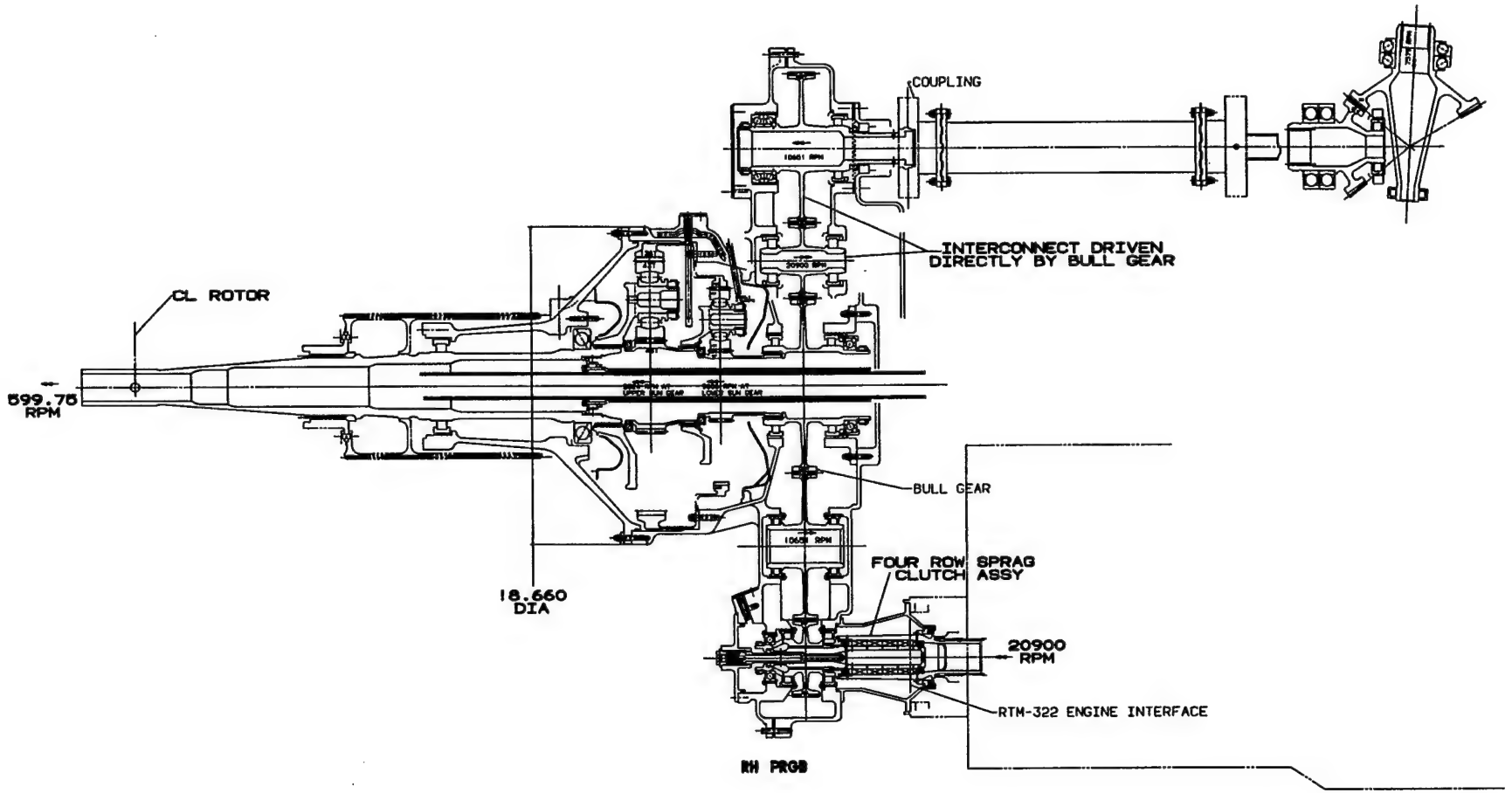

FIGURE 16: CONFIGURATION #2 - CLUTCH ASSEMBLY LOCATED AT ENGINE INPUT

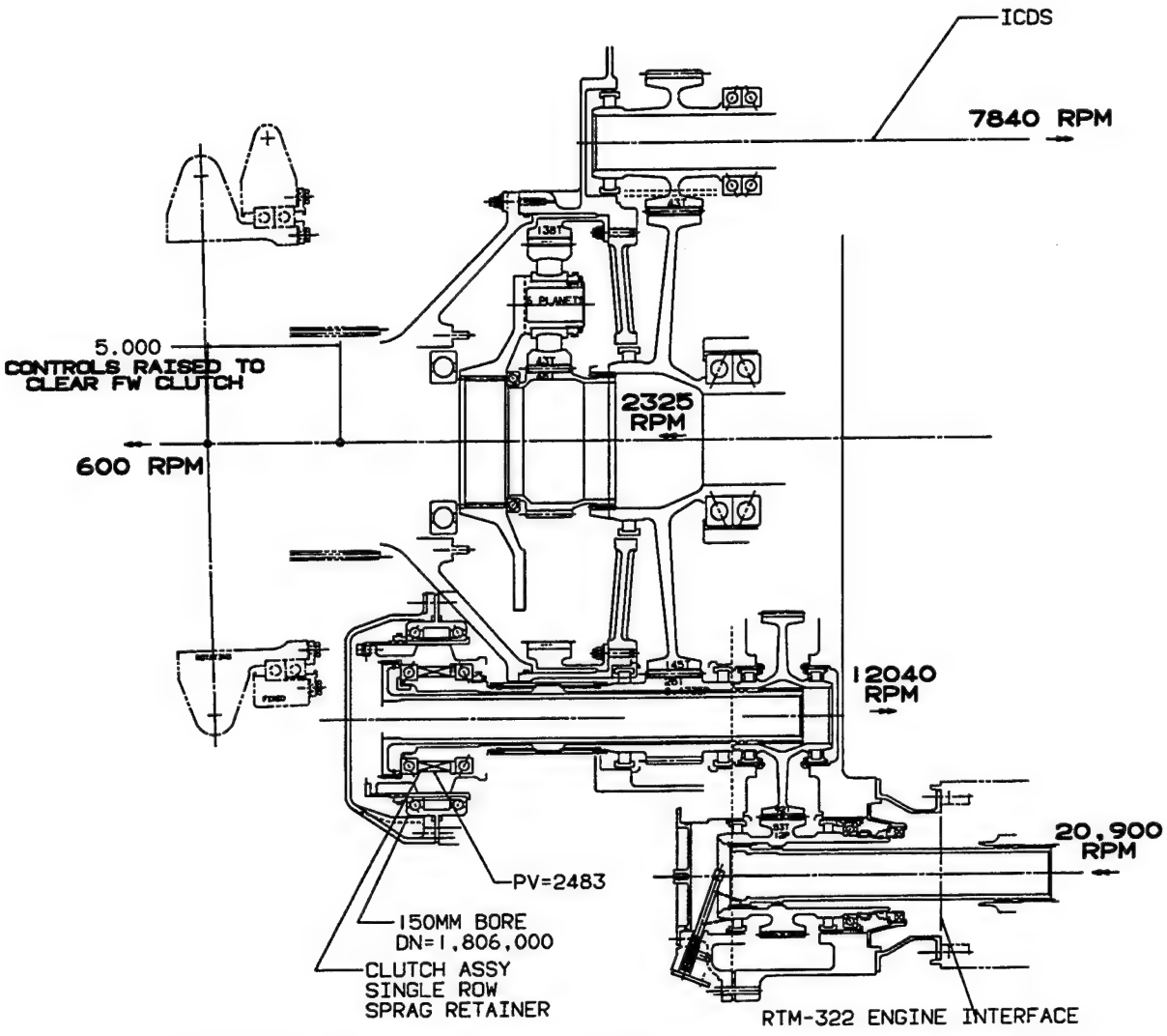

FIGURE 17: CONFIGURATION #3 - ACCESSIBLE CLUTCH ASSEMBLY

4.4.4 CONFIGURATION #4

Configuration #4 shown in Figure 18 depicts the ART with the clutch located in the bull gear. While the envelope restrictions of the reference aircraft are met, the weight penalty with the addition of the splined shaft and separate drive gear for the interconnect cross-shafting remains unattractive as explained in section 4.4.2.

4.4.5 CONFIGURATION #5

Configuration #5, shown in Figure 19, shows the clutch assembly integrated into the input cluster gear envelope. Separating the cluster gear into two separate gears forces the addition of three extra bearings, two rollers and a ball bearing, to carry the thrust load of the helical gear. With the clutch assembly now subjected to an axial thrust load, except for the input pinion, the interchangeability of all of the helical gears between the right and left hand gearboxes is eliminated because the helix angle must be reversed to maintain the same axial load direction on the clutch assembly. This configuration does not fit the reference aircraft envelope restrictions since it forces the location of the rotor controls to be extended an additional 1.5 inches.

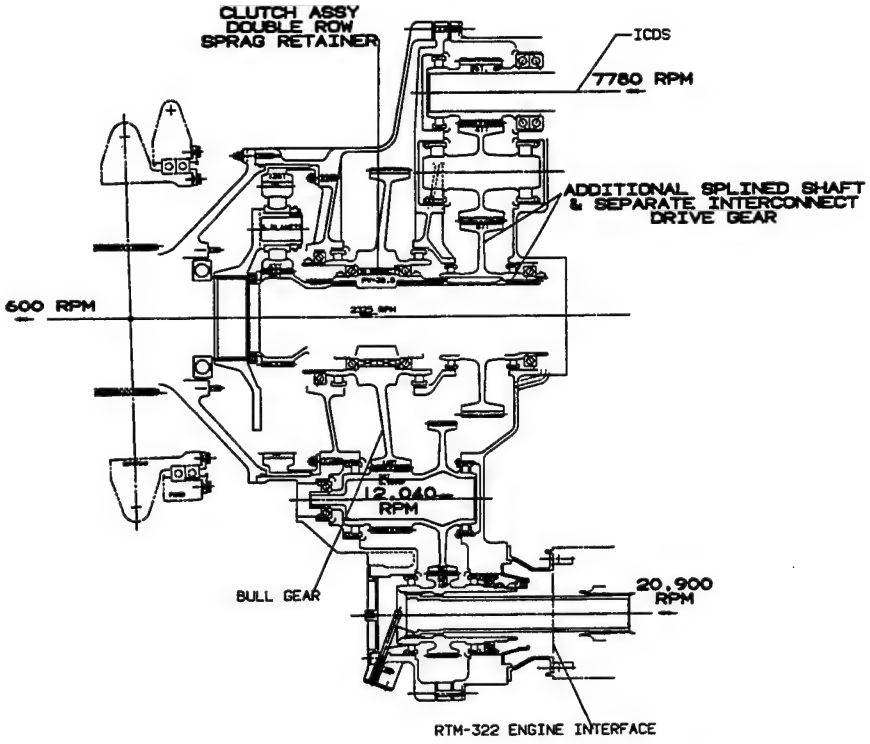

FIGURE 18: CONFIGURATION #4 - CLUTCH LOCATED IN BULL GEAR

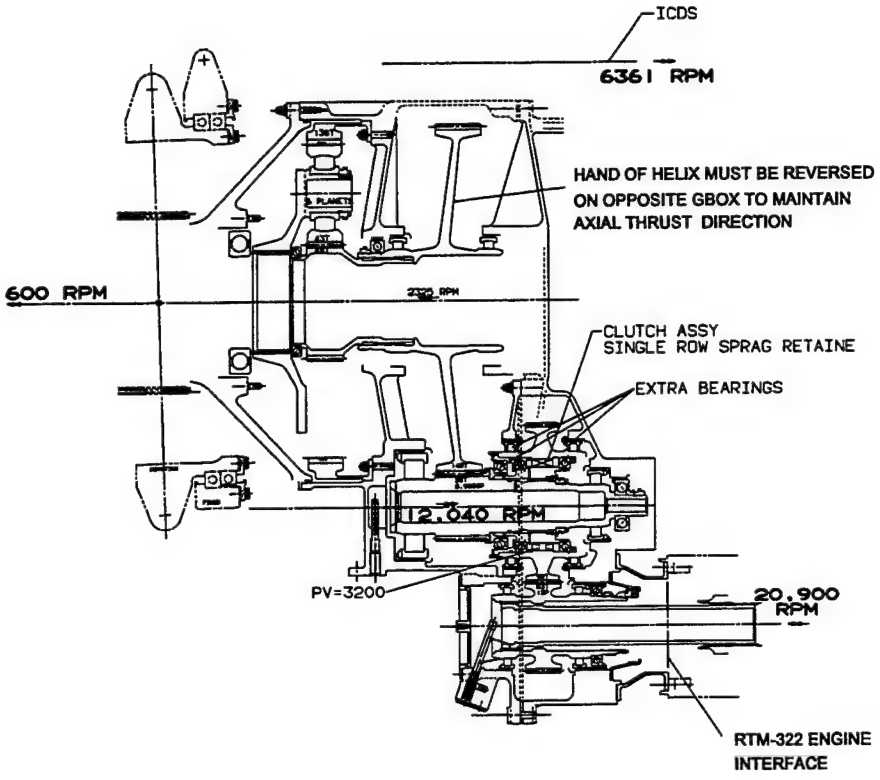

FIGURE 19: CONFIGURATION #5 - CLUTCH LOCATED IN 1ST STAGE HELICAL REDUCTION

4.4.6 FINAL ART DERIVATIONS - CONFIGURATIONS #6 AND #7

Configurations #6 and #7 shown in Figures 20 and 21 present the lightest combinations of configurations 1 thru 5. Figure 20 depicts the layout of the left hand ART with a single stage reduction input helical train and a two stage planetary reduction. Figure 21 depicts the layout of the left hand ART with a two stage reduction input helical train and a single stage planetary reduction.

A detailed layout and weight analysis was prepared for each of these configurations, #6 and #7, to determine which would be proposed for the ART preliminary layout. Configuration #7 was selected because it is lighter weight and has fewer gear meshes and fewer bearings. It also fits into a more compact housing, and has no gears with a tooth contact ratio less than 2.

Table 7 presents a summary of the selection process for the ART configuration in matrix form comparing the configurations described above. The comparative factors range from 1 for most favorable to 5 for least favorable. Configuration #2 is not included in the matrix since it is a right hand version of configuration #6.

TABLE 7: ART CONFIGURATION SELECTION MATRIX

CONFIGURATION	WEIGHT	NOISE	LIFE	SURVIV-ABILITY	COST	EFFICIENCY	RISK	SPATIAL ENVELOPE	TOTAL
#1- BASELINE	5	4	5	5	4	4	1	3	31
#3- ACCESSIBLE CLUTCH	4	2	2	2	3	2	3	4	22
#4- BULL GEAR CLUTCH	4	2	3	2	4	3	3	3	24
#5- 1ST STAGE CLUTCH	3	2	2	2	4	2	4	4	23
#6- TWO STAGE PLANETARY	2	4	4	3	3	4	4	2	26
#7- TWO STAGE HELICAL	1	2	2	2	2	2	5	1	17

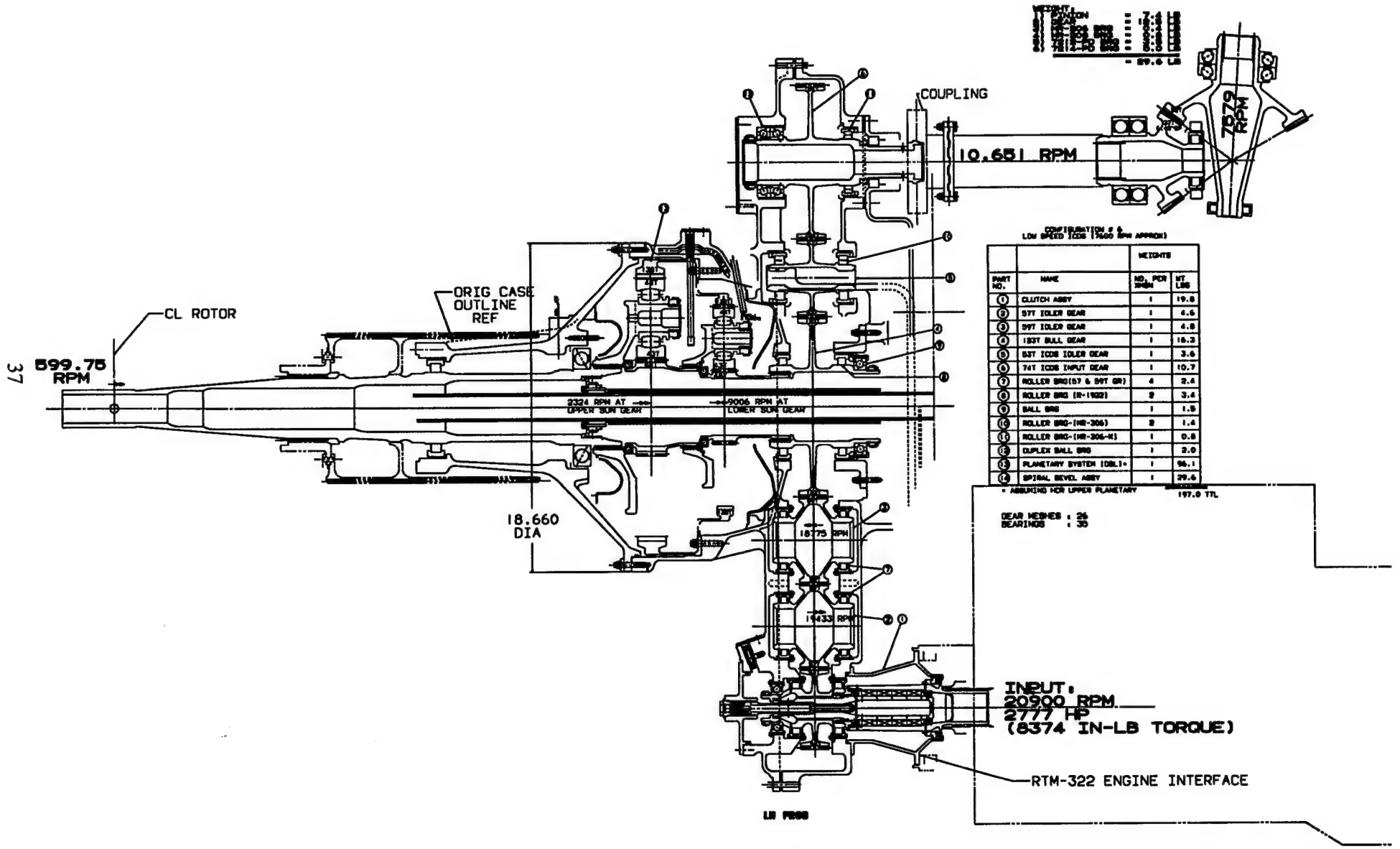

PART NO.	NAME	WEIGHTS NO. PER ENGN	WT LBS
A	CLUTCH ASSY	1	19.8
B	57T IDLER GEAR	1	4.6
C	59T IDLER GEAR	1	4.8
D	183T BULL GEAR	1	18.3
E	63T ICDS IDLER GEAR	1	3.6
F	74T ICDS INPUT GEAR	1	10.7
G	ROLLER BRG(57 & 59T GR)	4	2.4
H	ROLLER BRG (R-1922)	2	3.4
I	BALL BRG	1	1.5
J	ROLLER BRG-(NU-306)	2	1.4
K	ROLLER BRG-(NU-306-K)	1	0.8
L	DUPLEX BALL BRG	1	2.0
M	PLANETARY SYSTEM (DBL)*	1	96.1
N	SPIRAL BEVEL ASSY	1	29.6

* ASSUMING NOR UPPER PLANETARY

FIGURE 20: CONFIGURATION #6 - TWO STAGE PLANETARY, SINGLE STAGE HELICAL REDUCTION

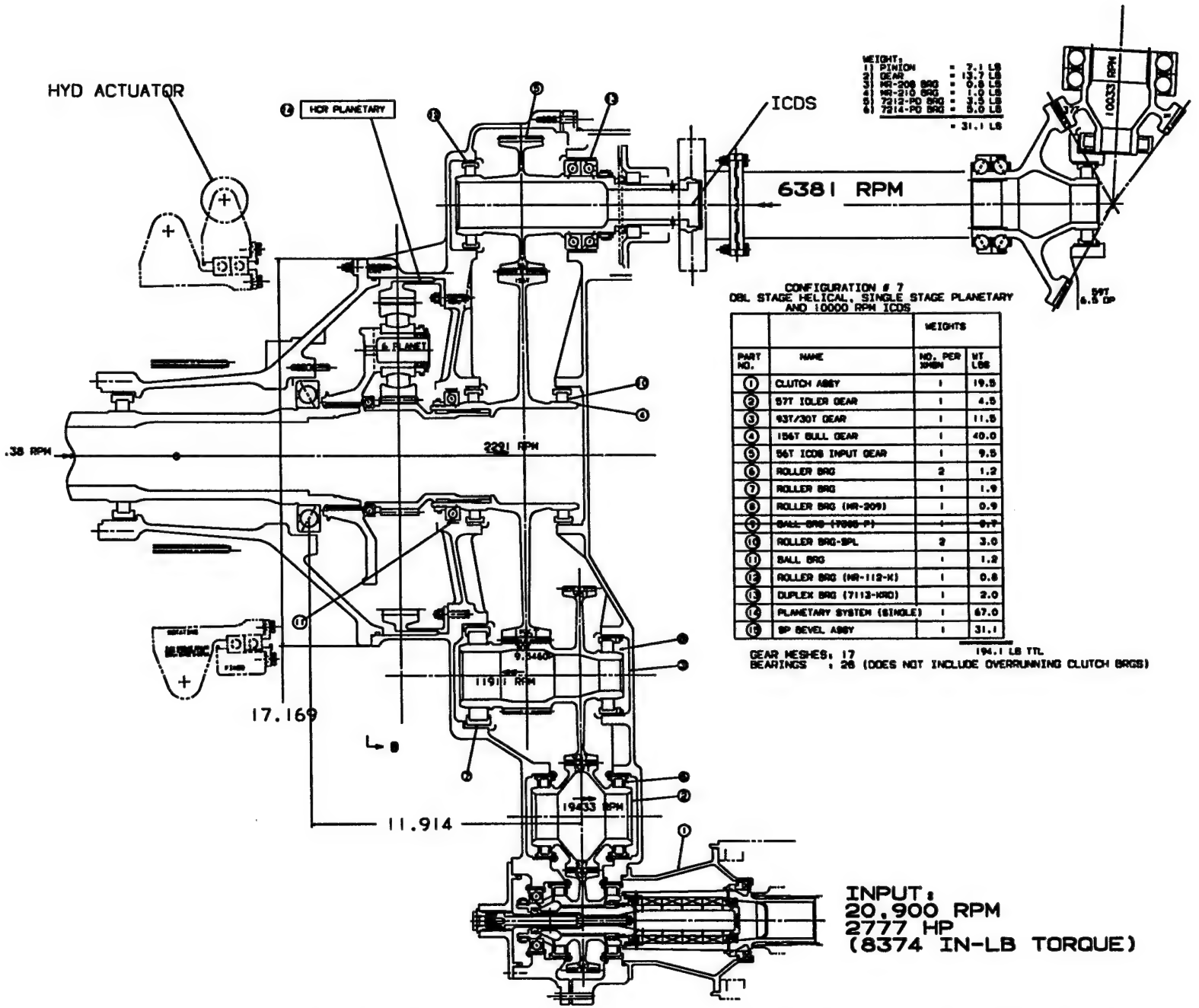

FIGURE 21: CONFIGURATION #7 - TWO STAGE HELICAL REDUCTION, SINGLE STAGE PLANETARY

4.5 LUBE SYSTEM EVALUATION

The lube system for the ART incorporates many low risk, available technology items. The only advanced technology concept added to the lube system that will entail any risk for the ART is a hot running capability. The lube system is sized by analyzing the lubrication and cooling requirements for each bearing and gear mesh in the transmission. The oil cooler in the nacelle is located as close to the transmission as the nacelle arrangement will allow so that the external oil lines can be kept to a minimum. The cooler is sized by the analytical transmission heat rejection requirements. The air supply for the oil cooler will be provided by the nacelle blower. This blower will not only provide air flow through the cooler but will also provide air circulation through the nacelle. Air circulation will aid transmission cooling due to convection through the cases by continually removing the heated air from inside the nacelle.

4.5.1 THREE MICRON FILTRATION

Three micron filtration will improve the reliability and service life of the dynamic components by removing the larger physical contaminants that are flushed and suspended in the lubricant. The cleaner lubricant results in longer life characteristics for the gears and bearings as described in sections 4.8.1.4.4 and 4.8.2.5.5.

4.5.2 SUPPLEMENTAL LUBE SYSTEM

The continuous operation supplemental air-oil mist lube system (see Figure 41) enhances operation of high contact ratio spur gears, spiral bevel gears, and other dynamic components during loss-of-lube operation of the transmission. The transmission cases will have several side-by-side cored passages; one for the lubricant and one for the air. Small nozzles will be placed at selected locations along the cored passages throughout the gearbox. Air from the air pump blowing through the nozzles will create a venturi effect that sucks the lube out of the cored passage to create an air-oil mist. In a loss-of-lube condition, the air-oil mist will extend operating time by keeping the dynamic components wetted with the oil mist which will retard heat generation due to friction. This is essential especially for the high contact ratio planetary spur gears that will be used in the ART. High contact ratio spur gears, although being lighter, quieter, and having longer service life than standard spur gears, do not operate as long in a loss-of-lube condition due to faster heat generation by the longer teeth. This system was demonstrated in the high contact ratio planetary component test described in Section 6.1.

4.5.3 DESICCANT AIR SUPPLY

Air will be injected into the transmission by an air pump which supplies air to the supplemental air-oil mist lube system. The air will provide a positive pressure inside the transmission to keep contaminants in the outside air from entering. A desiccant air supply is used for the air supply so that any moisture in the air is removed prior to its injection into the transmission. Moisture in a transmission interacts to form acids that are detrimental to the transmission components service life. Removal of the moisture prior to the air entering the transmission will help retard corrosion formation inside the transmission. Failure due to corrosion is one of the major causes of component replacement at overhaul of rotorcraft transmissions.

4.5.4 HOT RUNNING CAPABILITY

A hot running capability tradeoff study was conducted for the ART to determine the weight savings. The baseline for this weight saving study was the standard conditions for the lube system design that was in use at BHTI during the time period the XV-15 tiltrotor drive system was designed. This tradeoff study revealed a potential 40 lb weight saving.

The hot running capability concept involves operating the transmission at elevated temperatures so that a lighter lube system can be used. The current standard maximum oil-in operating temperature for a transmission is 230° F. For the hot running transmission this would be increased to 284° F. By running at the higher temperature, the difference between the oil-in and oil-out temperatures will be smaller because more heat is lost through convection. With the smaller temperature delta, less oil flow is needed to carry the heat away from the transmission. This results in a lighter lube system by reducing the amount of oil, the size of the reservoir, the size of the pump, and the size of the cooler. The hot running capability of the transmission is made possible by the use of DOD-L-85734 oil, gears and bearings made from high hot hardness steels, and housings made from WE43 magnesium which has properties similar to A356 aluminum at elevated temperatures. The hot running capability was successfully demonstrated during the planetary component tests and the spiral bevel scoring tests with a WE43 housing (see Section 6.2.8).

4.5.4.1 TEMPERATURE RISE ACROSS TRANSMISSION

The temperature rise across the baseline transmission was approximately 10° F at maximum continuous power. With a maximum oil-in temperature of 230° F this 10° F rise results in an oil-out temperature of 240° F. The ART will have a maximum oil-in temperature of 284° F and an oil-out temperature of 334° F for a 50° F temperature rise. The greater temperature rise is the direct result of reducing the capacity of oil in the transmission. This 50° F plus the 54° F increase in the allowable maximum oil-in temperature provide the beneficial condition for maximum heat rejection through the case walls.

4.5.4.2 OIL-IN TEMPERATURE

As noted above, the ART will have a maximum oil-in temperature of 284° F. This temperature level was selected as being sufficiently high to allow a significant increase in potential weight savings but not high enough to present a scoring problem or a coking problem for the DOD-L-85734 oil.

4. 5.4.3 WEIGHT ANALYSIS

It is known that the weight of the FAAV transmission can be reduced by using a higher oil-out temperature, but it is also known at the same time that the life of the transmission will be reduced because of the thinner oil film in the lubricated contacts as a result of the higher temperatures. The following procedure shows how the final 40 lb weight saving was determined.

4.5.4.3.1 WEIGHT REDUCTION

The following equations are assumed to be valid for the FAAV transmission for an oil-out temperature of 230° F:

$$Q_T = Q_o + Q_a \qquad \text{Equation (4.5.0)}$$

$$Q_o = 2/3\ Q_T \qquad \text{Equation (4.5.1)}$$

$$Q_a = 1/3\ Q_T \qquad \text{Equation (4.5.2)}$$

Where Q_T = total power loss
Q_o = power loss to oil
Q_a = power loss to air

The observation that 1/3 of the total power loss is convected/radiated was made during the 1960's on the UH-1 transmission. For this analysis, it is assumed that the nacelle blower and the arrangement of the transmission inside the nacelle are effective in providing a "gentle breeze" across the transmission housings, i.e., there are no significant dead air spaces.

Assuming also that (1) the average temperature of the housing walls is equal to the oil-out temperature, (2) the baseline oil-out temperature is 230° F, (3) the FAAV transmission oil-out temperature is 334° F, and (4) the ambient temperature is 125° F, then it can be shown that there is a 100% increase in the amount of heat rejected to the air:

$$\Delta T_1 = T_{c1} - T_a = 230° \text{ F} - 125° \text{ F} = 105° \text{ F}$$

$$\Delta T_2 = T_{c2} - T_a = 334° \text{ F} - 125° \text{ F} = 209° \text{ F}$$

Using the following standard heat transfer equation

$$Qa = UA\Delta T \qquad \text{Equation (4.5.3)}$$

and noting that Q_a is proportional to ΔT for a constant overall heat transfer coefficient (U) and a constant area (A) then

$$Qa = \frac{\Delta T_2}{\Delta T_1} = \frac{209°F}{105°F} = 1.99 \approx 2 \textit{ or a } 100\% \textit{ increase}$$

Since the total heat rejection has not changed and the heat rejected to the air has doubled, then the heat rejected to the oil is less:

$Q_O = Q_T - 2Q_a$, from Eq. (4.5.0) for a 100% increase in Q_a

$Q_O = Q_T - 2(1/3)Q_T$, from Eq. (4.5.2)

$$Q_O = Q_T - 2/3\ Q_T = 1/3\ Q_T \qquad \text{Equation (4.5.4)}$$

The specific weight of a standard lube system at BHTI is approximately 4 lb per 100 HP transmitted. Applying this factor to the FAAV transmission, its lube system weighs

(4 lb/100 HP) x (2522 HP) = 101 lb

The factor of 4 lb per 100 HP is based on Eq. (4.5.1),

$Q_O = 2/3\ Q_T$,

but now

$Q_O = 1/3\ Q_T$, Eq. (4.5.4).

Therefore,

101 lb/X lb = $(2/3\ Q_T)/(1/3\ Q_T)$

X = 101/2 = 50.5 lb, weight of FAAV lube system with 100% increase in Q_a.

This represents a potential weight savings of 101 - 50.5 = 50.5 ≈ 50 lb for the hot running FAAV transmission. This value is based on reducing all of the components in the lube system proportionally which is a reasonable assumption for the first 50 lb weight savings.

4.5.4.3.2 WEIGHT INCREASE

The weight increase due to the higher operating temperature of the FAAV transmission was determined by translating the loss in gear tooth pitting life into the increase in weight required to negate that loss in life. The low speed planetary sun-planet mesh on the XV-15 tiltrotor was used to make this determination. The life of the low speed sun gear was calculated at two oil-out temperatures: 230° F and 334° F. It was assumed that the oil in the tooth contacts was at these oil out temperatures. The change in temperature affects only two variables in the gear tooth pitting life equation: lubricant viscosity and the lubricant pressure viscosity coefficient. The life calculations at the 230° F and 334° F temperature showed a 26% decrease in life at the hotter temperature.

Recalculating the pitting life at the 334° F temperature while varying the face width of the planets until the 26% decrease in life was negated showed that the planet face width increased from 1.501 inches to 1.660 inches. This translates into 1.484 lb total for the 6 planets. Based upon the 1.484 lb increase for the planets, it is assumed that there would be a total increase in weight of the FAAV transmission of 10 lb to gain back the 26% decrease in life.

4.5.4.3.3 WEIGHT SUMMARY

Based upon the above analysis and assumptions, there is a potential weight savings of 50 - 10 = 40 lb in the FAAV transmission when designed to operate at an oil-out temperature of 334° F instead of 230° F.

4.6 ACCESSORY GEAR MANUFACTURING METHOD SELECTION

In the original proposal for the ART, a method for manufacturing accessory gears was outlined which would reduce the cost of accessory gears previously manufactured with the same process required for power gears. The method was as follows:

- Hob gear teeth.
- Green grind gear teeth using CBN grinding.
- Nitride gear teeth using normal techniques.
- Remove nitride white layer by chemical means (instead of grinding)
- Hone gear teeth to improve surface finish after chemical etching.

Since that time, several other processes have been considered and are presented in Table 8 for comparison. Summing the risk/cost factors assigned to each option it can be seen that Option 6 is the most attractive. Option 6 is also less expensive than the process outlined above since the honing operation is eliminated. For accessory gears not requiring integral roller races and having ball bearing journals only, as do the accessory gears presented in the ART configuration (Figure 38), induction hardening would not be required resulting in even less expensive accessory gears.

For the ART accessory gears the following rationale should be used for design and manufacture. For bending stresses up to 35 KSI in reverse bending and 50 KSI in unidirectional bending the gears should be made from VAR 300M alloy steel per AMS 6417 thru hardened to Rc 52-55. If there are integral roller races, the raceways should be induction hardened to Rc 56 minimum. The gears should be processed as follows:

- Hob gear teeth.
- Thru harden to Rc 52-55.
- Finish grind gear teeth (CBN).
- Induction harden raceways (if applicable).
- Finish grind bearing raceways and/or journals.

For bending stresses below 25 KSI reverse bending or 35 KSI unidirectional bending it is felt that shot peening the gear teeth is not necessary. For stresses above these levels, the gear teeth should be shot peened after finish grinding.

TABLE 8: ACCESSORY GEAR MANUFACTURING METHOD MATRIX

OPTION	MATL	METHOD OF MFG	HEAT TREAT			CVN CORE (FT-LB)	POSITIVE FEATURES	NEGATIVE FEATURES	TESTS REQD	1 = LOW 5 = HIGH	
			CORE (RC)	TEETH (RC)	RACES (RC)					RISK	COST
1	4340 Aly Stl	-Hob -CBN Grind -Tuftride	34-38	50 min	50 min	50-60	Operating History . Good Core Properties.	No Experience on Roller Races. Expensive Process.	RCF Tests	4	3-
2	4340 Aly Stl	-Hob -CBN Grind -Melonize	34-38	50 min	50 min	50-60	Cheaper Than Option 1. Good Core Properties.	No Experience on Roller Races. Expensive Process.	RCF Tests	4	2
3	300M Aly Stl	-Hob -Heat Treat -CBN Grind	52-55	52-55	52-55	15-20	Operating History. Cheaper Than Options 1 & 2	No Experience on Roller Races. Poor Core Properties.	RCF Tests	4	1
4	Nitr-alloy-N	-Hob -Nitride -CBN Grind	38-42	60 min	60 min	10-15	Operating History. No Problems With Roller Races.	Heat Treat Cost More Than Options 1 Thru 3. Poor Core Properties. CBN Grinding of Nitrided Steel an Unknown.	CBN Grinding Qual. Metallurgical & Residual Stress.	2	3+
5	4340 Aly Stl	-Hob -Induction Harden GearTeeth & Brg Races -CBN Grind	32-26	56 min	56 min	50-60	No Problems With Roller Races.	Risk of Induction Hardened Gear Teeth.	Tooth Bending Tests.	5	4
6	300M Aly Stl	-Hob -Heat Treat -Induction Harden Brg Races -CBN Grind	52-55	52-55	52-55	15-20	Operating History. No Problems With Roller Races.	Cost More Than Option 3. Poor Core Properties.	None	2	2
7	300M Aly Stl	-Hob -Heat Treat -CBN Grind -Ni Plate Brg Races	52-55	52-55	60 min	15-20	Operating History.	Poor Core Properties. Durability of Ni Plate Unknown.	RCF Tests	5	1+
8	9310 Aly Stl	-Hob -Carburize -CBN Grind (.010 Max Stock Rem.)	33-41	60 min	60 min	80-100	Operating History. No Problems With Roller Races. Best Core Properties.	Cost More Than Most Options.	None	1	4

4.7 CROSS SHAFTING EVALUATION

Tiltrotor aircraft require interconnect shafting between the left and right hand proprotor gearboxes to provide proprotor synchronization and single engine operating capabilities. Because of this requirement it is advantageous to run the cross-shafting at high speeds to yield lower torque and therefore lighter drive system components; drive shafts, bearings, spiral bevel gears in the tilt axis gearbox etc. A tradeoff study was conducted to evaluate the feasibility of a high speed interconnect drive shaft system, examining the availability of hanger bearings and the incorporation of a supercritical shafting configuration. The main benefit to the ART is the lighter spiral bevel set in the tilt axis gearbox which is possible if high speed hanger bearings are available. Whether the shafting is supercritical or subcritical does not affect the allowable speed. A relatively low speed shaft system can be made supercritical simply by making the shaft segments longer. The benefit of making a shaft system supercritical is the weight saving due to the elimination of hanger bearings which was compared to the weight and number of dampers required for the supercritical system.

The tradeoff study was constrained by survivability requirements and airframe requirements for the reference aircraft; wing angle, wing length, attainable output speed from the proprotor gearbox, etc. as listed below:

1. Shaft Diameter > 4.500 X .064 min wall thickness (composite tube) - survivability requirement

2. Hanger Bearing Bore = 65mm minimum - survivability requirement

3. 25,000 fpm spiral bevel gear pitch line velocity - design limit

4. 3.50° nominal driveshaft misalignment from centerline of airframe to tilt axis output - airframe requirement

5. Maximum driveshaft length = 130.0 inches - airframe restriction

6. 1542 HP - maximum power during single engine operation

7. 6381 RPM input speed to tilt axis gearbox- maximum attainable due to ART configuration

8. 10,175 RPM tilt axis gearbox output speed to interconnect shafting. This was derived during the configuration tradeoff study, Section 4.4.6. A faster output speed would require a larger, heavier spiral bevel gear. Also, it was felt that speeds greater than 10,000 RPM presented too great a risk since the current maximum shaft speed for hanger bearing supported shafts longer than 36.0 inches on BHTI designs is less than 7,000 RPM.

4.7.1 BEARING SELECTION

Usually, the limiting factor on the speed of the shaft design is the speed limitation of the grease packed hanger bearings. The interconnect shaft bearing design criteria specifies that the bearings shall be able to operate at 10,175 RPM with a 10 pound axial load, a 12 pound radial load, and a 165 in-lb moment (V-22 interconnect shaft bearing loads). The bearings are to be grease lubricated. Both ceramic hybrid and steel bearing designs were evaluated. Ceramic hybrid bearings have steel races and ceramic balls. They can be press fitted to a shaft just as a steel bearing. The ball loads due to centrifugal force are much less with ceramic balls than steel balls, due to the 60% lighter weight. However, ceramic hybrid bearings have a significant disadvantage in applications involving oscillatory loading; they suffer catastrophic failure and are primarily suited for applications at high RPM with no oscillatory loads. Eventhough the L_{10} calculated life for

the ceramic bearing was twice that of a comparable steel bearing, the ceramic hybrid bearing was considered inappropriate for this application since the interconnect driveshaft system is subject to oscillatory loading, potentially detrimental to ceramic bearings.

Steel bearings made of M-50-NiL carburized steel races and M-50 steel balls, are the most suited for the cross shafting bearing application. Carburized and heat treated M-50-NiL steel produces a bearing with case hardness for increased rolling contact fatigue life and at the same time a core with lower hardness for improved fracture toughness. The globular and uniform distribution of the carbides in M-50 NiL apparently overcomes the problem of irregular carbides inherent with M-50 alloy.

At the loads described above, the steel bearing was modeled in a bearing computer program written by A. B. Jones (High -Speed Ball & Radial Roller Bearing Analysis Program, 1983). The results of the computer run are as follows:

Unadjusted Bearing Life ---------- 12,400 Hrs
Max. Inner Race Hertz Stress ----- 176,000 PSI
Max. Spin/Roll Ratio---------- 0.227
Max. Contact Load ---------- 25.1 Lbs

4.7.2 CRITICAL SPEED EVALUATION

Two separate interconnect driveshaft systems were sized using the guidelines outlined, one operating below the critical speed of the system (subcritical) and the other operating above the 2nd critical speed of the system (supercritical). Figure 22 shows the configuration and the critical speeds of the subcritical system, and Figure 23 shows the configuration and critical speeds of the supercritical system. To make the subcritical system supercritical, two hanger bearing assemblies (see Figure 24) were removed to replace the three shaft segments spanning the 130 inch maximum gap with one single driveshaft. A squeeze film damper assembly (see Figure 25) required to safely traverse the first two critical speeds of the system was installed in place of one hanger bearing assembly at the end of the 130 inch long driveshaft. Reducing the number of hanger bearing assemblies also reduces the number of couplings needed to span the 3.50° wing angle. The two remaining couplings on the supercritical system must now operate at a larger misalignment angle (increased size and weight) than the four couplings on the subcritical system. A weight comparison of both systems is presented in Table 9 below.

TABLE 9: SUBCRITICAL VS. SUPERCRITICAL WEIGHT COMPARISON

DESCRIPTION	SUBCRITICAL		SUPERCRITICAL	
	QTY	WEIGHT (LB)	QTY	WEIGHT (LB)
Shaft Assembly	3	9.6	1	8.8
Hanger Assembly	4	27.2	1	6.8
Damper Assembly	-	—	1	15.3
2.25° Coupling	-	—	2	22
1.25° Coupling	4	17.2	-	—
Hanger Bearing Support Assembly	4	12.7	2	8.3
TOTAL		66.7		61.2

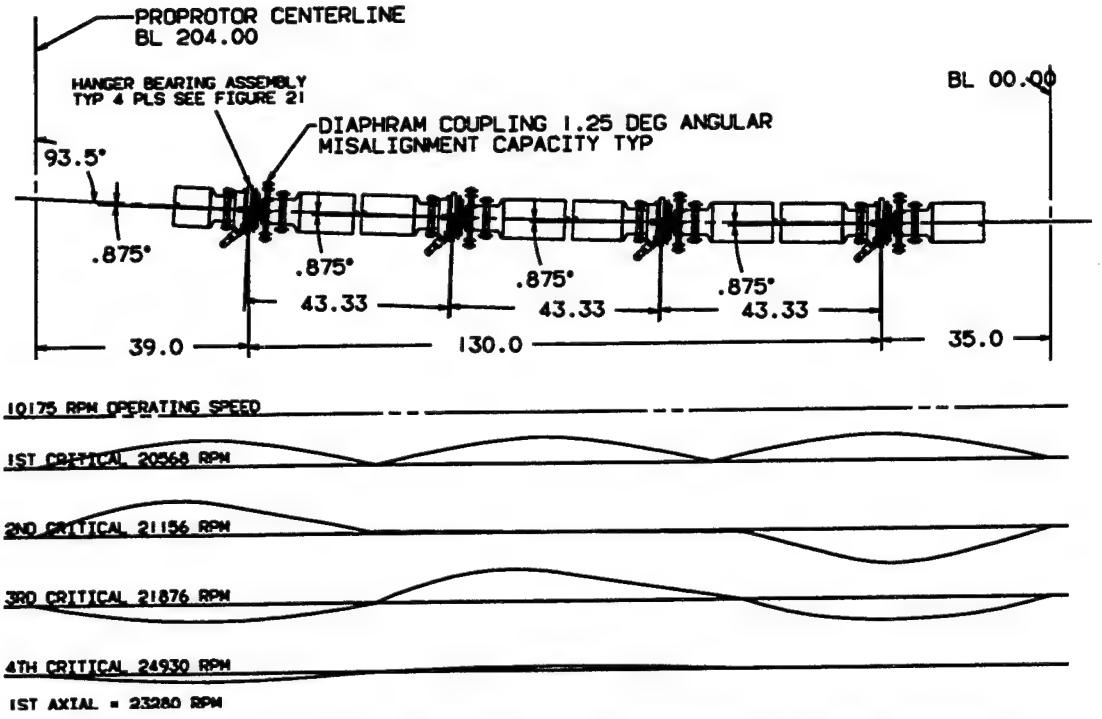

FIGURE 22: SUBCRITICAL INTERCONNECT DRIVESHAFT (ICDS) ASSEMBLY

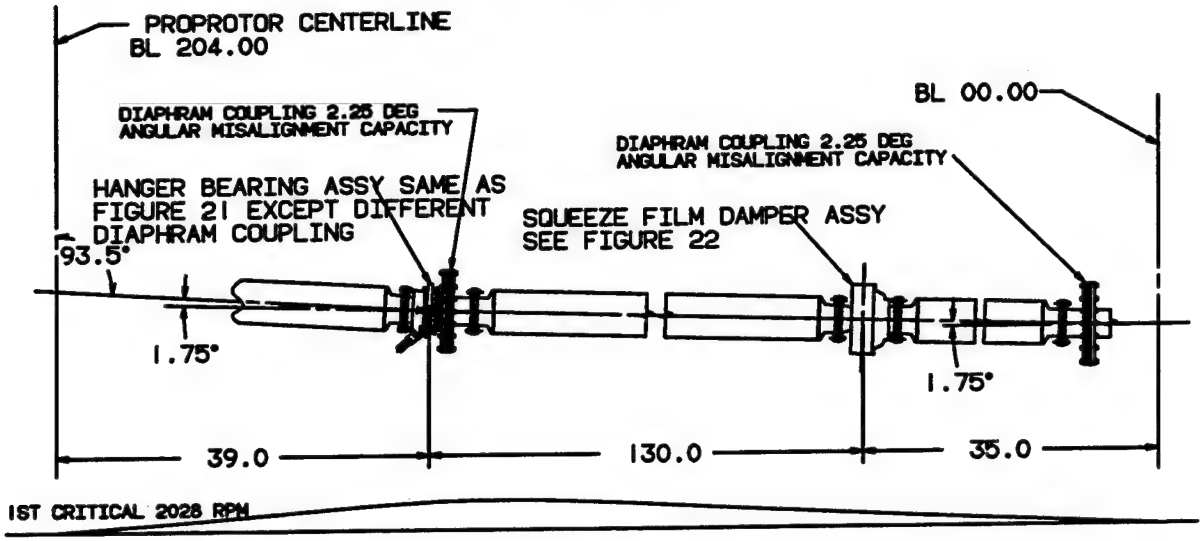

FIGURE 23: SUPERCRITICAL INTERCONNECT DRIVESHAFT (ICDS) ASSEMBLY

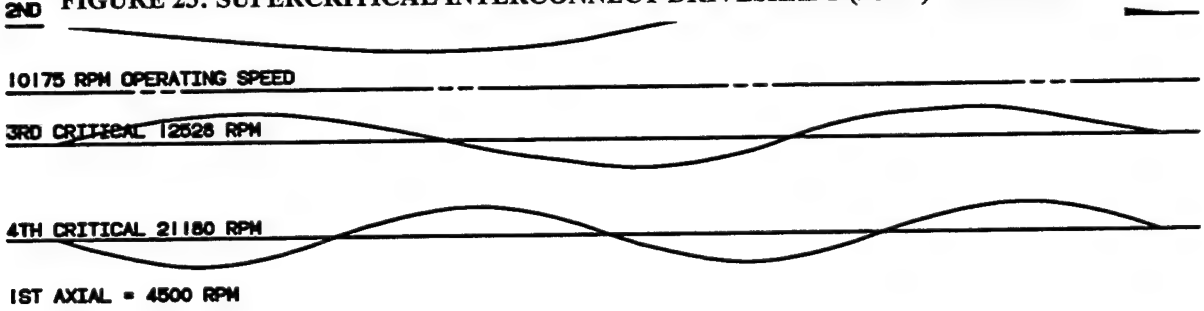

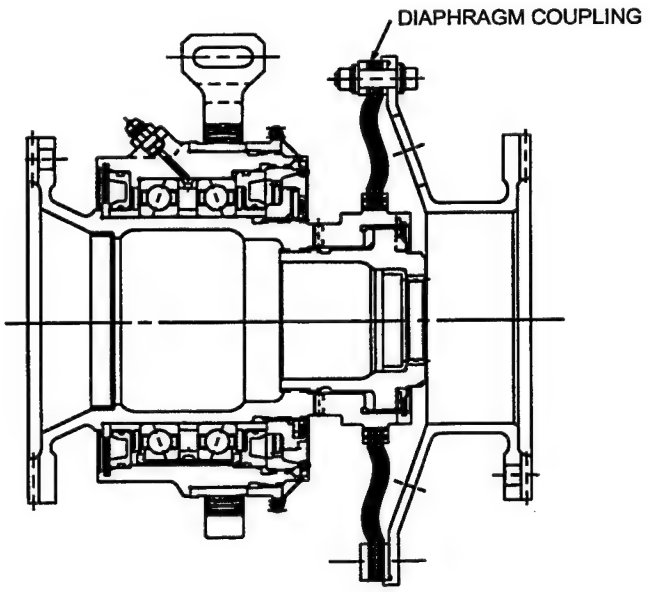

FIGURE 24: HANGER BEARING ASSEMBLY FOR SUBCRITICAL ICDS SYSTEM

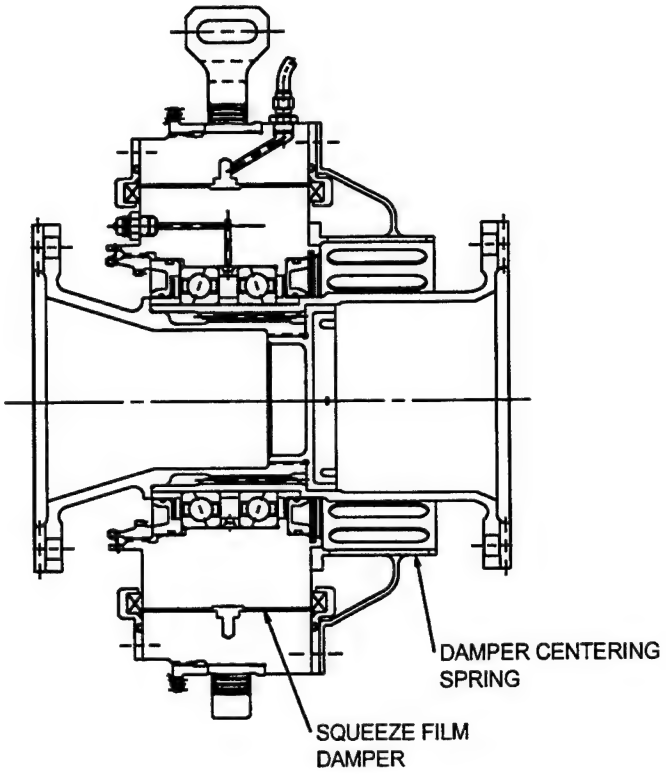

FIGURE 25: SQUEEZE FILM DAMPER ASSEMBLY FOR SUPERCRITICAL ICDS SYSTEM

The supercritical system is only 5.5 lb lighter than the subcritical system because of the weight penalty for the damper assembly, the 2.25° couplings, and the heavier support assemblies required for the more heavily loaded remaining hanger bearing and damper assembly.

Some of the difficulties presented by a supercritical system include:

1. The squeeze film damper usually requires significant test time to develop a workable assembly tailored to the system.

2. The maintenance requirements for a squeeze film damper are much more stringent than for a hanger bearing assembly. If the damper does not function properly, considerable damage could be incurred by the whirling driveshaft.

3. High precision balancing is required for supercritical driveshafts which is more costly than the standard balancing procedure for subcritical driveshafts.

4. The effect of gyroscopic moments on the natural frequencies of supercritical shafts is significant, especially when they are attached to large inertial discs such as diaphragm couplings.

5. High angle operating flexible couplings are less reliable.

Because of the small weight saving, when compared to the risks and difficulties listed above, the supercritical system is not an attractive system for the ART drive system. If the subcritical system had needed more than four hanger bearing assemblies, then the resultant weight savings for the supercritical system would have warranted its implementation despite the increased risk. Table 10 below presents a summary in matrix form of the evaluation process for the ART interconnect cross-shafting. The comparative factors range from 1 for most favorable to 5 for least favorable.

TABLE 10: CROSS-SHAFT SELECTION MATRIX

SYSTEM	WEIGHT	LIFE	SURVIVABILITY	COST	RISK	TOTAL
Subcritical	3	1	2	3	2	11
Supercritical	2	2	4	2	4	14

4.8 GEAR AND BEARING LIFE PREDICTION METHODOLOGY

The following presents the basic method developed by BHTI for the ART MTBR analysis. Since rigorous verification of the methods presented would require years of research, it should be recognized that these methods are felt to be the most logical using the available data presented. Therefore, the methods presented are subject to change as more pertinent test data becomes available.

4.8.1 GEAR TOOTH PITTING LIFE DETERMINATION

A basic S-N curve for the life limiting mode of failure of gear tooth pitting is required to calculate the unadjusted life of a gear of a new design. On log-log paper this S-N curve is usually a straight line and all that is required to define the straight line is its slope (stress life exponent) and the hertz stress at any point on the curve. Thus, the S-N curve may be described by the hertz stress at N cycles and the stress-life exponent corresponding to the percent-failed life (L_{50}, L_{10}, L_2 etc.) associated with N cycles. Also, if there is a range of stress or cycles peculiar to a curve it must be noted.

The following discussion shows how the basic stress-life exponent and the basic hertz stress point are derived and how the unadjusted tooth pitting life of a gear is calculated.

4.8.1.1 STRESS-LIFE EXPONENT DETERMINATION

Since gear tooth pitting life is inversely proportional to the hertz stress raised to some power **'a'** the following basic equation is used to calculate the pitting life of gears:

$$L_x = L_y(S_y/S_x)^a \qquad \text{Equation (4.8.0)}$$

Where L = life, % failure level
S = hertz stress
x,y = new design and baseline data respectively
a = slope of straight line curve on S-N diagram (log-log), the stress life exponent

The point determined by the intersection of L_x and S_x on an S-N diagram is often shown in literature, but less often discussed is the nature of the exponent **'a'**. Bowen [6] points out the high risk involved in using any particular "standard" life curve without considering the tribological states associated with the curve and the new design. Dudley [7] goes further and suggests some discrete values for the exponent **'a'**, one for each of the three regimes of lubrication.

BHTI uses an approach similar to that of Dudley except the exponent **'a'** is represented by a continuous curve instead of discrete values (see Figure 26). The stress-life exponent **'a'** is shown as a function of Lambda (λ) for the three experimental curves and the one design curve shown. The equation for the design curve, **D,** is

$$\mathbf{a} = 10/3(\lambda) + 6 \qquad \text{Equation (4.8.1)}$$

Where $\lambda = h_{min}/\sigma$, Lambda ratio
h_{min} = minimum oil film thickness, microinch
σ = composite surface roughness, AA

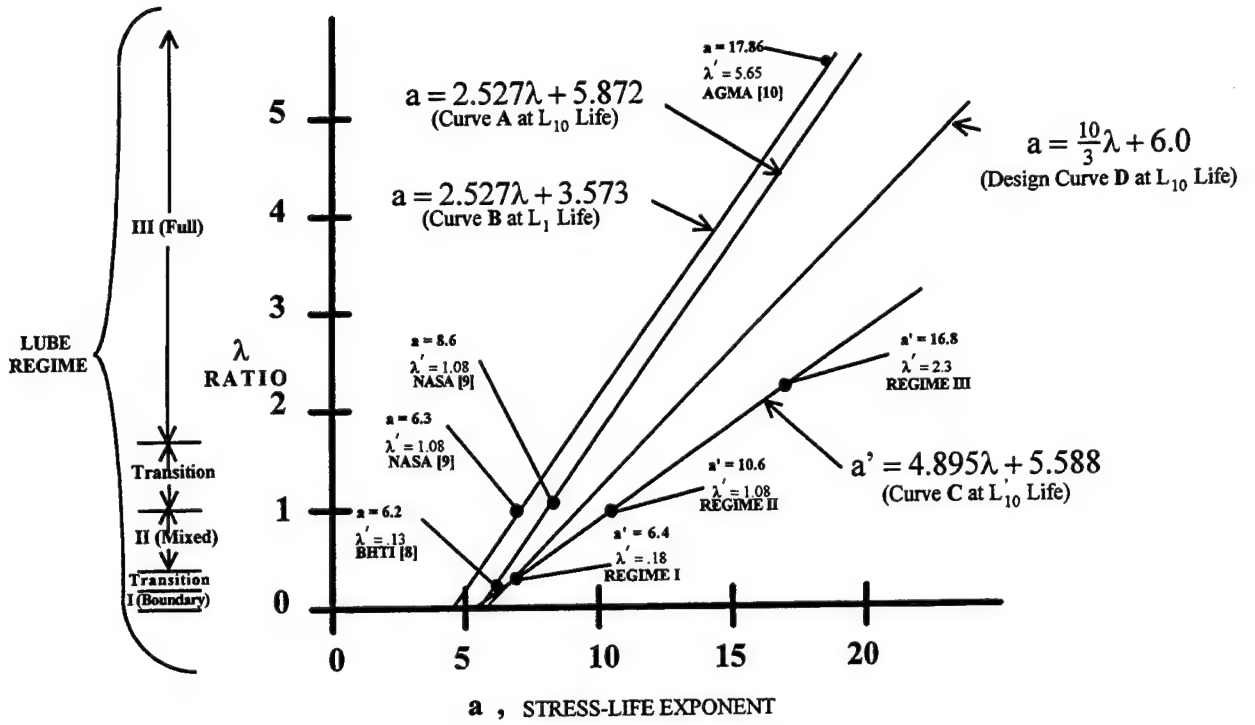

λ' = VALUE OF λ RATIO CORRESPONDING TO A GIVEN **a** OR **a'** LOCATED ON THE CURVE SHOWN

FIGURE 26: RELATIONSHIP BETWEEN STRESS LIFE EXPONENT AND λ RATIO

This design curve was developed as follows. Two test points and the assumption that the curve is a straight line were used to define curve **A**. The lower point came from planetary gear testing at BHTI and gear failures from the same planetary from field service, both reported by Bowen [8]. The higher point on curve **A** came from test rig work performed at NASA Lewis by Townsend et al [9].

The elastohydrodynamic (EHD) film thickness equation used to determine the Lambda ratio for the two test points on curve **A** is the Dowson equation used by Lynwander [11]. The after run-in surface roughness value was used and the value used for both BHTI's gears and NASA's gears was 15AA.

Curve **B** in Figure 26 is an attempt to show where AGMA's gear tooth pitting data might fit in. Since AGMA's data is given at the L_1 level, curve **B** was set up to be compatible with L_1 life data by using Townsend's [9] stress-life exponent of 6.3 which corresponds to the L_1 level of his test data. The slope of curve **B** is essentially equal to that of curve **A** for small changes in hertz stress. Using AGMA's stress-life exponent of 17.86 [10] results in a λ ratio of 5.65. This value is in the range of λ ratios found in drive system test stand gearboxes at BHTI, thus lending some credibility to curve **B** and the relationship of AGMA data to specific test data.

Curve **C** in Figure 26 is constructed from data obtained from Dudley [7: Figure 3.46 and page 2.22]. The slope of the curve and its position was determined by placing the stress-life exponent 6.4 in the boundary lubrication regime (lube regime I) and then locating the 10.6 value at the upper limit of the mixed lubrication

regime (lube regime II) in order to make it parallel to curve **A** as close as possible. Maintaining the straight line concept on this graph, the stress-life exponent 16.8 falls into place on curve **C** in the full lubrication regime (lube regime III).

The position of these lubrication regimes and transition zones along the λ ratio axis are taken from Dudley [7:Figure 3.46] for a composite (effective) surface roughness of 15AA. Using a similar value of 10AA would show little change in the lubrication regime positions.

Curve **D** in Figure 26 is arbitrarily selected to be midway between curves **A** and **C**. This is the curve that should be used for design of new gears. In the low λ regions curve **D** is a reasonable estimate of both curves **A** and **C**. In the higher λ regions it is not. However, the gear tooth pitting lives associated with high λ values are usually of such great length that the effects of any error in the location of curve **D** is significantly reduced. For this same reason the extrapolation of curve **D** is acceptable since it projects the gear into the endurance limit area (near infinite life) associated with high λ ratios.

Thus, curve **D** in Figure 26 defines the stress-life exponent for a given λ ratio. This curve has not been rigorously established herein, but it is logical in shape and position. It is in agreement with the relative short lives of gears operating in thin film applications and also in agreement with the fact that some gears never seem to pit in thick film applications. It agrees with some bearing manufacturers who are beginning to say that rolling contact bearings operating in thick film applications may have an endurance limit. If a roller bearing were designed using curve **D** in Figure 26, and the λ ratio was 4.2, the load-life exponent would be 10 (20/2) instead of the usual 10/3. This would increase the life of a roller bearing with a C/P value of 5 by a factor of 45,688. For a bearing with an L_{10} life of 5000 hours calculated using the load-life exponent 10/3, the L_{10} life determined by using 10 instead of 10/3 would be 228,439,000 hours. Practically speaking this bearing has an endurance limit.

4.8.1.2 BASIC HERTZ STRESS DETERMINATION

As noted in Section 4.8.1.1, the point determined by the intersection of life and hertz stress on an S-N diagram is often shown in literature. Also, every company involved in the design of gearboxes probably has their own design points. AGMA[10] shows an allowable hertz stress of 225,000 PSI at 10^7 L_1 cycles for aircraft quality carburized and hardened gears. For similar gears, BHTI uses 225,000 PSI at 10^7 L_{50} cycles and Townsend [9] shows 222,000 PSI at 6.38×10^7 L_{50} cycles. Before these values and others like them can be compared and normalized to a basic common design point, many factors have to be considered. Some of these affect the stress of the gear, others affect the strength and reliability of the gear.

4.8.1.2.1 WEIBULL SLOPE DETERMINATION

One factor, which is rather obvious from the hertz stress comparisons shown above, is the Weibull slope (dispersion exponent) which is required to compare different test data as they are reported. Townsend [9] reported an average Weibull slope of 1.9 with his stress-life data shown above. BHTI uses an average Weibull slope of 4 with its stress-life data, in the absence of specific test data. Bowen [6] reported on some of the same data which was generated at BHTI under his guidance. He reported Weibull slopes which varied from 2.7 to 10.

Another but smaller Weibull slope value is required when adjusting the L level at or near the operating root-mean-cubed (RMC) load level, an average power level over the life of the transmission. This is discussed in Section 4.8.1.3.

4.8.1.2.2 LOAD DISTRIBUTION AND DYNAMIC FACTORS

There are 3 factors which should be applied to the gear tooth load prior to calculating the hertz stress. These are two load distribution factors and the dynamic load factor. The load distribution factors are the gear tooth misalignment factor and the end loading factor. These two factors differ in that the misalignment factor deals with the lengthwise mismatch of the gear teeth whereas the end loading factor treats the "digging in" condition produced by mating teeth of unequal length regardless of whether or not misalignment error is present. Harris [12] refers to this condition as edge loading when describing essentially the same effect caused by a cylindrical roller bearing, uncrowned and not end relieved, mating with its longer inner or outer race. Also, Harris [12, Table 14.12] shows an increase in the basic dynamic capacity of a cylindrical roller bearing with modified line contact (end relieved) versus line contact (not end relieved) by the ratio .61/.45=1.36 in the bearing life equation. For a constant life and stress-life exponent, the load varies inversely with the basic dynamic capacity. Thus the load will be increased by the factor of 1.36 when using cylindrical rollers with line contact instead of modified line contact.

Because of the similarity between gear teeth and roller bearings relative to compressive stress profiles, the load distribution factor of 1.36 for end loading will be used for all spur and helical gears having teeth without having the ends relieved. Even though it is very common for mating gears to have equal face widths, it is highly unlikely that any will perfectly match at each end of the teeth and prevent the "digging in" process from occurring because of the tolerances on face widths, end chamfers (usually produced by hand), and running position. This end load factor of 1.36 which translates into an end stress factor of 1.17 is considerably less than the approximate stress value of 2.5 determined by Walker [13] by measuring the footprints of a cylinder pressed against a rack tooth. Walker's test was performed to determine the buttressing effect of unused tooth length on the hertz stress profile.

The difference between the two stress factors, 1.17 and 2.5, is very significant. For example, using a stress-life exponent of 5.10, the 1.17 factor shows a life 50 times greater than that for the 2.5 factor. The 2.5 stress factor appears to be realistic but for some reason it does not seem to translate into a contact stress or a subsurface shear stress that is as harmful as its magnitude suggests. The baseline planetary testing performed by BHTI on the UH-1 planetary gears at 1400 HP did not indicate the presence of a hertz stress 2.5 times the calculated unfactored hertz stress of 172,836 PSI on the low speed sun-planet mesh. That value would be 2.5 x 172,836 = 432,090 PSI. This does not include an estimated misalignment load distribution factor of 1.36 which would raise the working hertz stress to $1.36^{1/2}$ x 432,090 = 503,899 PSI, and this mesh is truly a buttressed mesh because the length of the sun teeth are 1.540 inches compared to 1.333 inches for the planet teeth. The estimated L_{50} life of this low speed sun gear at 503,899 PSI hertz stress is 309,965 cycles whereas the actual L_{50} life was 4.72×10^7 cycles, 152 times longer. This is the reason why it is believed that the 2.5 stress factor determined by Walker [13] is not all that effective.

When S-N curves are made from test data, the working hertz stress is used because that is the actual stress in the part. Then, when these S-N curves are used as allowable hertz stress curves, they will be compatible with the design working hertz stress values which include load distribution and dynamic factors of identical or similar values. AGMA assigns unity to the misalignment and dynamic factors in its reported allowable hertz stress of 225,000 PSI at 10^7 L_1 cycles. AGMA [10, Section 13.1 item (8)] makes mention of "tooth crowning and end relief" as an influence on load distribution but discusses the subject no further.

BHTI and Townsend [9] do not assign unity to the misalignment and dynamic factors in their allowable hertz stress values of 225,000 PSI and 222,000 PSI, respectively. The intended use of those values is for similar applications where the derating factors are similar. Thus, these two values will have to be adjusted upward by

the effects of the misalignment, end loading, and dynamic factors involved in the tests before these values can be considered as true allowable working stresses.

Also, the AGMA value of 225,000 PSI should be adjusted upward by the effect of the end loading factor since it is most likely that the data base on which the 225,000 PSI was built was developed and reported from gear tests and field usage on gears that were not crowned (end relieved).

4.8.1.2.3 BASIC TEST PARAMETERS

The other factors involved in normalizing the reported hertz stress values to a basic common design point are called life adjustment factors. These are multiplicative factors applied to the basic gear tooth pitting life to make the basic life agree with the actual life observed in tests or in field service. These factors are discussed in Section 4.8.1.4, however, the ones that are applicable must be "backed out" of the reported allowable hertz stress values in order to reach a common basic design point.

This leads to establishing the basic condition or environment associated with the finalized basic common design point, the condition in which all life adjustment factors are equal to one. The basic condition will be based on BHTI's experience in testing the low speed UH-1 planetary. This work is summarized by Bowen [6].

The basic condition can best be described in terms of the life adjustment factors involved. Table 11 in Section 4.8.1.4 shows the life adjustment factor (LAF) category, the specific item described for the basic test, and the assigned LAF. This applies to gears that are case hardened and exhibit AGMA class 13 or similar tolerances.

4.8.1.2.4 BASIC HERTZ STRESS DESIGN POINT

In order to adjust the hertz stress value of 225,000 PSI at 10^7 L_{50} cycles used by BHTI for the effects of the load distribution and dynamic factors, a single test sample point from the 9 used to establish BHTI's S-N curve will be used. This point will be the UH-1 upper planetary sun-planet mesh with the sun driving the planet. This point was selected because it was developed on tests where the environmental conditions are more exact, it contains the most specimens (9) of those tested, and it was operating in the normal mode (sun driving). Bowen [6] identifies this point as HI LO S1P.

The calculated hertz stress with no load distribution factors or dynamic factor is 172,836 PSI at 4.72×10^7 L_{50} cycles at the first point of single tooth contact on the sun gear with the sun gear driving. Since the pitch line velocity of the sun gear relative to the planet is only 1188 fpm the dynamic factor is taken as unity. The load distribution factor is based upon an estimated operating misalignment of .0006 in/in. This gives a multiplicative load factor of 1.47 per Dudley [7]. This increases the unfactored hertz stress of 172,836 PSI to 209,553 PSI at 4.72×10^7 L_{50} cycles. The load distribution end loading factor is taken as 1.36 (see Section 4.8.1.2.2) since these gears were not crowned (end relieved). This further increases the hertz stress to $1.36^{1/2} \times 209,553 = 244,378$ PSI at $4.72 \times 10^7 L_{50}$ cycles.

Two operations must now be made to change this value to a hertz stress at 10^7 L_{10} cycles. The L_{50} cycles must be adjusted to L_{10} cycles and the hertz stress must be adjusted to 10^7 L_{10} cycles. The former requires the Weibull slope and the latter requires the stress-life exponent.

The Weibull slope will be that which was obtained from the plot of the failures which was used to define the single test sample noted above. That Weibull slope is 2.31, as determined by the least squares curve fit

method. The stress-life exponent will be that which was developed at BHTI by Bowen [8] and used to establish the lowest point on the curve in Figure 26: **a** = 6.20.

The final hertz stress design point can now be calculated. In order to move the Weibull slope line down from the L_{50} point to the L_{10} point, the following equation may be used:

$$LOG\, t_1 = [LOG\, LOG(\tfrac{1}{1-F(t_1)}) - LOG\, LOG(\tfrac{1}{1-F(t_2)})]/\beta + LOG\, t_2 \qquad \text{Equation (4.8.2)}$$

Where **t** = percent failed life **L**
F(t) = probability of failure prior to time **t**
ß = Weibull slope
If **t** = $\mathbf{L_{50}}$ life, then **F(t)**=**F**($\mathbf{L_{50}}$) = .50

For **ß**=2.31, the 4.72 x 10^7 L_{50} cycles becomes 2.09 x 10^7 L_{10} cycles.

In order to adjust the 244,378 PSI hertz stress at 2.09 x 10^7 cycles to a hertz stress at 10^7 L_{10} cycles, Eq. 4.8.0 is rearranged as follows and the calculation made:

$$S_y = S_x (L_x/L_y)^{1/a} \qquad \text{Equation (4.8.3)}$$

$$S_y = 244{,}378\ ((2.09 \times 10^7\ L_{10}\ cy)/(10^7\ L_{10}\ cy))^{1/6.20}$$

$$S_y = 275{,}193\ PSI \approx 275{,}000\ PSI \text{ at } 10^7\ L_{10} \text{ cycles}$$

This value of 275,000 PSI hertz stress at 10^7 L_{10} cycles is BHTI's basic design point for allowable working hertz stress on gear teeth with all life adjustment factors equal to 1 as shown in Table 11.

4.8.1.3 GEAR TOOTH PITTING LIFE CALCULATION

After the gearbox designer has adjusted the gear mesh load by the appropriate load distribution factors (misalignment and end loading) and the dynamic factor, the hertz stress at the first point of single tooth contact is calculated.

Using BHTI's basic design point of 275,000 PSI at 10^7 L_{10} cycles Eq. (4.8.0) yields

$$L_x = 10^7(275{,}000/S_x)^a,\ L_{10} \text{ cycles} \qquad \text{Equation (4.8.4)}$$

Where **a** = stress-life exponent at L_{10} reliability taken from Figure 26, curve **D** (design curve)

If the result in L_2 cycles (or other reliability) is desired, use Eq. (4.8.2). The value for **ß** should be selected carefully. Others parameters being equal, **ß** is known to decrease with stress level [9]. The value of 2.31 used above was the result of testing gears at the hertz stress level of 244,378 PSI. Where the hertz stress requirement dictates the size of a gear, the working hertz stress at the RMC load used at BHTI is approximately 200,000 PSI. Thus, this is the hertz stress level for which the Weibull slope is desired. Townsend et al [9] showed a one point drop in **ß** over a stress level drop of 50,000 PSI (all K-factors = 1). Adjusting this stress upward by the probable effect of the load distribution factors and dynamic factor to about 62,500 PSI, and assuming that **ß** varies directly with stress level, then the 2.31 value is reduced to 1.61 as follows:

$$(244{,}378 - 200{,}000)/62{,}500 \times 1 = .70\ \Delta\beta$$

$$\beta = 2.31 - .70 = 1.61$$

Since this value of 1.61 is close to the value of 1.5 used by the bearing industry to define the life adjustment factors [shown in Table 14.17 in ref. 12] for bearing life reliabilities other than that associated with the usual L_{10} failure level, it is recommended that the β value of 1.5 be used for gears also.

4.8.1.4 GEAR TOOTH PITTING LIFE ADJUSTMENT FACTORS

Life adjustment factors are required to adjust the basic pitting life of a gear to predict the actual life of the gear operating in its prescribed environment. Table 11 shows the LAF categories associated with the basic planetary gear testing at BHTI and Table 12 shows the LAF's developed as described in the following sections for the ART. These same categories will be considered herein and are repeated as follows:

- Material
- Material Processing
- Lubricant
- Oil Filter Rating
- Shot Peening
- Sliding Velocity
- Stressed Volume

TABLE 11: BASIC TEST PARAMETERS FOR PLANETARY GEAR TESTING AT BHTI

CATEGORY	BASIC TEST PARAMETER	LAF
Material	AMS6260 ALY STL	1
Material Processing	VAR	1
Lubricant	MIL-L-7808E	1
Lubricant Additives	None	1
Oil Filter Rating	25 Micron Absolute[(a)]	1
Shot Peening	None	1
Sliding Velocity Index	0.718544	1
Stressed Volume, in^3	0.045	1

(a)This cannot be established with absolute certainty, however the baseline planetary testing was done during the time frame that this size filter was in use on the UH-1 series helicopter which uses the baseline planetary The usual custom when testing helicopter parts is to simulate the helicopter conditions as much as possible.

Other potential categories such as gearbox operating temperature, lubricant properties at that temperature, gear speed, and gear tooth surface roughness are accounted for in the λ ratio calculation, which is the ratio of the minimum oil film thickness to the composite surface roughness of the meshing gear teeth.

Each of the above 7 LAF categories will be treated separately in the discussion that follows. The intent is to show the independence of each and the effects of each on the pitting life of a gear. The end result is to show the difference in the life as measured during the basic planetary testing at BHTI in the mid-sixties and the predicted life today using the LAF's described herein.

TABLE 12: STATE-OF-THE-ART LIFE ADJUSTMENT FACTORS FOR GEAR TOOTH PITTING FATIGUE LIFE AT L_2 LEVEL USING TABLE 11 DATA AS BASELINE

CATEGORY	PARAMETER	LAF
MATERIAL	X-53	2
MATERIAL PROCESSING	VIMVAR	2.5
LUBRICANT	DOD-L-85734	SEE FIG. 24
OIL FILTER RATING	3 MICRON ABSOLUTE	SEE FIG. 25
SHOT PEENED	SHOT PEENED	1.5 OR EQ. (4.8.12)
SLIDING VELOCITY INDEX	SLIDING VELOCITY	EQ. (4.8.16)
STRESSED VOLUME, IN^3	STRESSED VOLUME	EQ. (4.8.24)

4.8.1.4.1 MATERIAL FACTOR

When BHTI designed the original UH-1 series helicopter in the mid 1950's, the gear steel selected for the sun gear and planets in both the high speed and low speed planetaries was AMS6260 air melt steel. During the mid 1960's when the baseline planetary testing was performed, the same AMS6260 type of steel was used although the process was changed from air melt to vacuum arc remelt (VAR). Thus, the LAF for material for the baseline testing is 1 as shown in Table 11.

During the early 1970's, in the search for a high hot hardness carburizing gear steel to increase the gearbox loss-of-lube running time, Carpenter Steel Co. developed what is now called Carpenter Pyrowear 53 (X-53). BHTI took this steel and pioneered the carburizing process to where it has comparable case properties, at a 450° F temper, to AMS6260 tempered at 300° F. Manufacturing and testing development work under the Advanced Transmission Components Investigation (ATCI) program for the U.S. Army[1] during the 1976 to 1984 time frame on sun gears, planets, ring gears and bevel gears made of X-53, and subsequent optimizing of the carburizing process led to the design decision to make all of the power gears (except planetary ring gears) in the V-22 tiltrotor gearboxes out of X-53.

Parallel with the design work on the V-22 gears, additional gear specimens made from X-53 were tested for bending strength and pitting life in direct comparison with specimens made of AMS6260. Both steels were manufactured by the same process, vacuum induction melt followed by vacuum arc remelt (VIM VAR). BHTI manufactured the gears. The gear tooth pitting tests were conducted at the NASA Lewis Research Center (NASALeRC), Cleveland, Ohio, on their gear tooth pitting fatigue test rig. The results showed a 2.68 L_2 life (50% confidence level) increase for gears made of VIM VAR X-53 over gears made of VIM VAR AMS6260. Thus, the LAF for using X-53 steel instead of AMS6260 is conservatively estimated to be 2 at the L_2 level.

4.8.1.4.2 MATERIAL PROCESSING FACTOR

As noted in section 4.8.1.4.1, the baseline planetary testing was performed on sun gears and planets made of AMS6260 vacuum arc remelted (VAR) steel. For this reason the LAF shown in Table 11 for the material processing factor is 1.

Most of BHTI's state-of-the-art power gears are made of VIM VAR steels. Thus a LAF for VIM VAR steels is required. The testing work has already been accomplished at NASA LeRC on their gear tooth pitting fatigue test rig. The testing of the VAR AMS6260 gears is reported as consumable electrode vacuum melted AISI 9310 using oil **'F'**. (These two steels and their processing are virtually identical.) The L_2 life is 8.56 million cycles. The testing of the VIM VAR AMS6260 gears [14] showed an L_2 life of 25 million cycles. (Both of these cycle values are 50% confidence numbers). This shows a 2.94 L_2 life increase for gears made from VIMVAR AMS6260 over gears made from VAR AMS6260. Thus, the LAF for material processing is conservatively estimated to be 2.5 at the L_2 level for VIM VAR gear steel. This assumes the independence of the material and the processing of the material relative to the gear tooth pitting life.

4.8.1.4.3 LUBRICANT FACTOR

Starting in the mid 1950's with the turbine powered UH-1 series helicopter, BHTI began using the MIL-L-7808 type oil in transmissions and gearboxes. In particular, MIL-L-7808E was used in the baseline planetary testing during the mid 1960's. The higher viscosity turbine engine oil MIL-L-23699 was introduced at BHTI during the 1960's, however the MIL-L-7808 type was retained for cold weather operation. Then, in the early 1980's a significant departure from custom occurred. A lubricating oil specifically formulated for gearboxes was introduced into service in BHTI's Model 222B helicopter. This oil is basically a MIL-L-23699 type with the addition of a friction modifier additive package. It started out as Aeroshell 555, later became Royco 555, and is now covered by DOD-L-85734. This oil is now recommended for use in practically all BHTI helicopter and tiltrotor gearboxes.

Since MIL-L-7808E was used in the baseline planetary testing it is shown in Table 11 with a LAF of 1. It is also shown in Figure 27 with a LAF of 1 as a non-varying function of the λ ratio. The other curve in Figure 27 is for DOD-L-85734 oil. It is established by two data points **'A'** and **'B'**. Point **'A'** was determined by Townsend [15] during the evaluation of the effect of five lubricants on the gear tooth pitting life of VAR AISI 9310 spur gears at NASA LeRC. The test specimens were 8 pitch, 20° pressure angle, 28 tooth, carburized, hardened, and ground spur gears operating at 10,000 RPM with a hertz stress of 248 KSI (all derating factors = 1). Two of the five lubricants were Aeroshell 500 oil meeting MIL-L-23699 specifications and Aeroshell 555 oil meeting DOD-L-85734 specifications. The failure index (number of failures out of number of tests) was 20 out of 20 with a Weibull slope of 1.1 for the 500 oil and 18 out of 18 with a Weibull slope of 4.5 for the 555 oil. The results of the tests showed the L_2 life of the gears operating in the 555 oil to be 16 times greater than the L_2 life of the gears operating in the 500 oil, the confidence level being 50%.

The other data point in Figure 27, point **'B'**, is not a test data point. It is located along the x-axis at the position LAF=1 by definition as noted above. The location of point **'B'** along the y-axis at the position λ ratio = 3 was made with the intent to place this point in the full lubrication regime where it is assumed that the effect of friction modifiers in the oil on the gear tooth pitting life is negligible or nonexistent.

The extension of the curve down to point **'C'** is purely arbitrary but probably true to nature. The location of point **'C'** along the y-axis is at λ ratio=.11 which is the value for the data point provided by BHTI from the result of planetary testing.

The friction modifiers in the DOD-L-85734 oil are credited with the large increase in pitting life in the boundary and mixed lubrication regimes. These modifiers tend to reduce the stress near the surface of the teeth which allows early surface initiated fatigue failures to become more like classical subsurface initiated fatigue failures. Also, the conjunction temperature is probably reduced due to less friction in the gear mesh. This should increase the oil viscosity, which promotes longer life. The dependence of the lubricant factor on the λ ratio only is assumed.

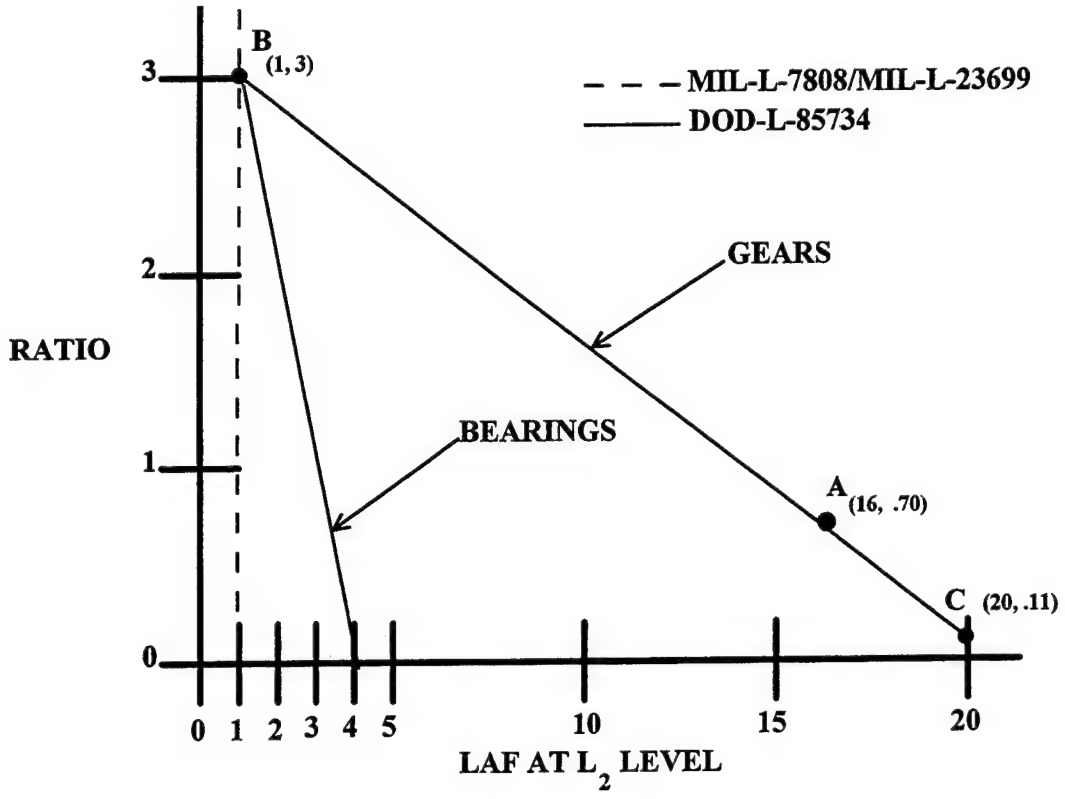

FIGURE 27: LUBRICANT LIFE ADJUSTMENT FACTOR

4.8.1.4.4 OIL FILTER RATING FACTOR

The UH-1 series helicopter of the mid 1950's used an 80 micron absolute oil filtration for the transmission lube system. This can be interpreted to mean that no spherical particle larger than 80 micrometers in diameter will pass through the filter. In the pursuit of longer times between oil changes and increased times between overhauls (TBO), a porous medium oil filter with an absolute rating of 25 microns was introduced in the early 1960's. Finally, during the early 1980's all new designs at BHTI began using 3 micron absolute oil filters as the evidence became quite clear [16] that longer mean times between failure (MTBF) were assured with finer filtration. A quantitative relationship between bearing pitting lives and oil filter ratings has been provided by Sayles and McPherson [17]. Since the concern is about damage to the contacting surfaces, their work is assumed to apply to gears also. This relationship is:

$$L \propto \mu^{2/3} \qquad \text{Equation (4.8.5)}$$

Where L = life at L_{10} level
μ = absolute filter rating

There also seems to be a relationship between filter rating and the λ ratio just as there is between lubricant factor and the λ ratio as discussed in Section 4.8.1.4.3. This is because the thicker the oil film the larger the hard particles can be without causing damage to the contacting surfaces. These two relationships are shown combined in Figure 28. Since the 25 micron oil filter was used in the baseline planetary testing, it is shown in Table 11 with a LAF of 1. It is also shown in Figure 28 with a LAF of 1 as a non-varying function of the λ ratio.

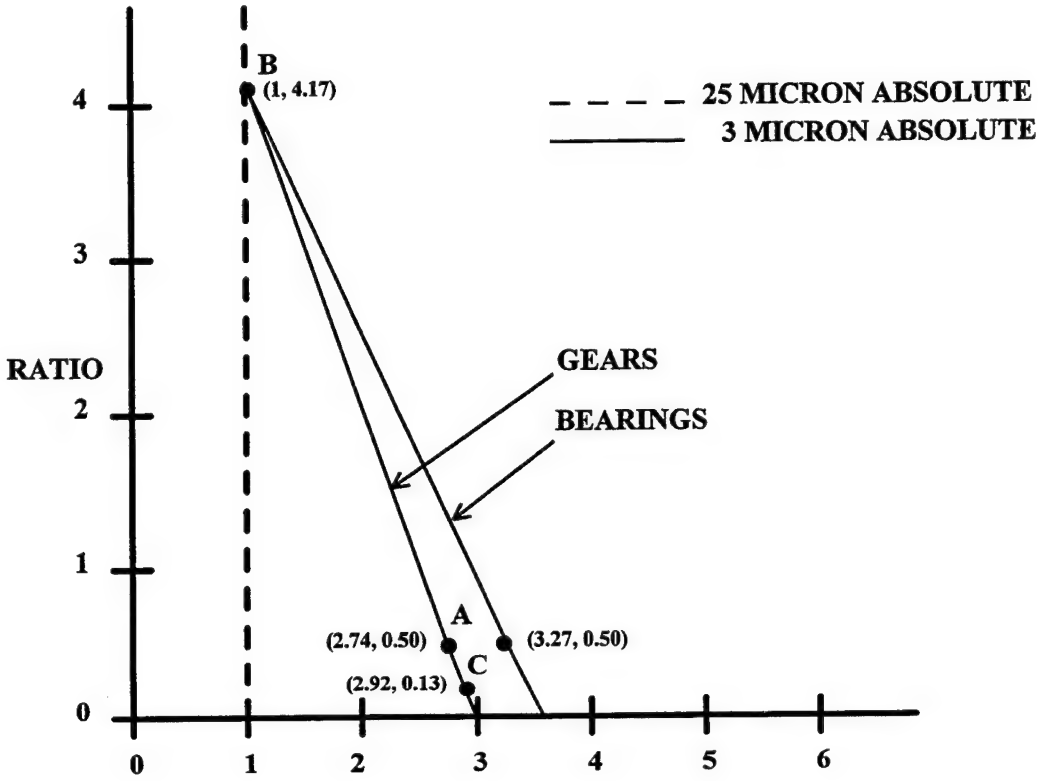

FIGURE 28: OIL FILTER RATING LIFE ADJUSTMENT FACTOR

Figure 28 is set up similar to Figure 27 and some of the rationale for its construction is used. The curve for the 3 micron filter is established by two data points '**A**' and '**B**'. Point '**A**' was derived from test conditions and test results contained in reference [17]. The test bearings were standard 25-mm bore, extra-light series, single-row cylindrical roller bearings. Actual gear tooth pitting fatigue debris was fed into the bearing fatigue machine and bearing lives were measured in terms of absolute filter ratings. In fitting the test results for point '**A**' to Figure 28, the Lambda ratio was recalculated in accordance with reference [9] and the L_{10} lives were transformed to L_2 lives using the given Weibull slopes.

Data point **'B'** is not a test data point. Its location along the x-axis at the position LAF=1 is by definition from Table 11. Its location along the y-axis is at λ ratio = 4.167. This value is based on the following assumed relationship and rationale:

$$\lambda_B/\lambda_A = \mu_B/\mu_A$$

Where μ = absolute filter rating
'A' and **'B'** = discrete points in Figure 28

Using the test results from reference[17] and the λ ratio calculation method from ref. [9],

$$\lambda_B = \lambda_A(\mu_B/\mu_A) = 0.50(25/3) = 4.167$$

This relationship is based on the observation that if the 3 micron filter removed particles harmful to contacting surfaces operating in the boundary lubrication regime with the λ ratio equal to 0.50, then a 25 micron filter should perform similarly with a proportionate increase in the λ ratio. The assumption that the 3 micron filter removed all of the harmful particles is based on Figure 7 in ref. [17] which shows little increase in life in going to finer than 3 micron absolute filtration. The fact the gap (minimum film thickness) between the two contacting surfaces is calculated to be only 0.155 micrometers and the passage of 3 micrometer hard particles through the contact zone without causing any apparent harmful damage could possibly be due to the beneficial effect of work hardening the contacting surfaces instead of damaging them if the ratio of particle size to film thickness is not too great.

Point **'C'** in Figure 28 represents the intersection of the λ ratio of the baseline planetary testing on the 3 micron absolute line for a LAF value of 2.92. This of course assumes the line connecting points **'A'** and **'B'** is straight and the extension of the line is valid.

The effect that the finer filter rating has on gear tooth pitting life is that it provides for less chance for failure initiation as a result of cleaner oil. This effect is similar to that of VIM VAR steel over VAR steel but is considered to be independent.

4.8.1.4.5 SHOT PEENING FACTOR

Shot peening has been used at BHTI since the early 1960's to increase the bending fatigue strength of spur gear teeth. The shot peening operation was applied to protuberance hobbed gear tooth roots prior to grinding the involute profiles. In the late 1960's the shot peening operation using smaller shot was applied to full form ground roots and involute profiles followed by a honing operation on the involute profiles. At about this same time, BHTI began shot peening bevel gear tooth roots with no attempt to mask the working profiles. Some of the grinding ridges were beaten down by the shot but the surface roughness was changed minimally. The inherent sliding action of spiral bevel gear teeth is beneficial in improving the surface roughness during green-run.

It was not until the early 1970's, in the drive system of the XV-15 tiltrotor that a spur gear was shot peened on the working profiles of the gear teeth without the benefit of honing afterward. The successful operation of that spur gear set led to the desire to determine the effects of shot peening on the gear tooth pitting life. The reasoning was that if the residual compressive stress produced by the shot peening (in addition to that introduced by carburizing) improved the bending fatigue strength of gear teeth, which it does, then the same

residual stress should improve the pitting life, especially when operating in the boundary lubrication regime where most pitting failures are surface initiated.

Thus, a program was initiated with NASA LeRC whereby NASA would furnish the test gears, BHTI would shot peen them, and NASA would test them. The results were reported by Townsend [18] which showed a 1.6 times longer pitting fatigue life at the L_{10} reliability level for the shot peened gears relative to the unpeened gears. The test gears were 8 pitch, 20° pressure angle spur gears made of carburized and hardened consumable electrode vacuum melted AISI 9310 steel. The peening was done with SAE No. 070 cast steel shot to an intensity of .007A-.009A inch almen strip height, 200% coverage on the tooth profiles and roots only.

For a shot peening life adjustment factor, the 1.6 factor above is reduced to 1.5 at the L_{10} level. If the shot peening process differs significantly from that noted above for the test gears, then the shot peening LAF may be determined by the method described in Ref. [18] and shown below:

1. Calculate the depth of maximum shear stress on the gear tooth.

2. By X-ray diffraction determine the magnitude of the residual compressive stress at the depth of the maximum shear stress (from item 1 above) on the shot peened gear and the non-peened gear, both gears being carburized, hardened and finish ground.

3. The LAF can now be calculated:

$$(LAF)_P = L_P/L_S = [(\tau max)_{rS}/(\tau max)_{rP}]^a \qquad \text{Equation (4.8.6)}$$

Where L = fatigue life, L_1, L_2, L_{10}, L_{50}, etc.
τ = shear stress
P = peened
S = standard (nonpeened)
r = residual
a = inverse stress-life exponent (This value must correspond with the particular fatigue life reliability level such as L_1, L_2, L_{10}, L_{50}, etc.)

$$(\tau max)_r = -1.575 \times 10^6 [W_N(R_1+R_2)/(F\ S\ R_1\ R_2)]-1/2\ S_{ry} \qquad \text{Equation (4.8.7)}$$

Where W_N = normal load, lb
R_1, R_2 = radii of curvature of the 2 gears at the first point of single tooth contact (FPSTC),in.
F = tooth face width or length, in.
S = hertz stress at FPSTC, PSI
S_{ry} = residual stress in y-direction (rolling direction), value obtained in item 2 above, PSI

The stress-life exponent '**a**' is given the value 9 in Ref. [18]. This is for a pure rolling condition.

As noted above the LAF for shot peening may be taken as 1.5 at the L_{10} reliability of fatigue life. This is based on '**a** = 9'. For other reliability levels of fatigue life, the following equation may be used. It is derived from test data in Ref. [18].

$$(LAF)_P = L_P/L_S = (1.0443)^a \qquad \text{Equation (4.8.8)}$$

4.8.1.4.6 SLIDING VELOCITY FACTOR

Bhattacharyya, et. al. [19], have determined a relationship of sliding velocity with pitting fatigue life using geared roller testing at IIT Research Institute during the early 1970's. Some of the test rollers were similar to gears in that they were carburized, hardened, and ground consumable vacuum melted 8620 gear steel rollers tested in MIL-L-23699 oil at slide-to-roll (slip) ratios from 3.3% to 30%. The relationship is given as:

$$L \propto (|V_1^{1/2} - V_2^{1/2}|)^{-1.25} \qquad \text{Equation (4.8.9)}$$

Where L = fatigue life
V = rolling velocity

The sliding velocity index equation breaks down at the pitch diameter. It is valid only between slip ratios of 3.3% and 30% [19] where:

Slip Ratio = $(V_1 - V_2)/(V_1$ or $V_2)$ (Divide by whichever velocity belongs to the surface being evaluated)

For the planetary gear testing that was used to establish BHTI's basic design hertz stress point, the slip ratio for the low speed sun-planet mesh at the first point of single tooth contact (FPSTC), where the pitting usually starts, is:

$(V_1 - V_2)/V_1 = (80 \text{ ips} - 105 \text{ ips})/80 \text{ ips} = -31\%$ on the sun

and

$(V_1 - V_2)/V_2 = (105 \text{ ips} - 80 \text{ ips})/105 \text{ ips} = 24\%$ on the planet

Where V_1 = rolling velocity of the sun at the FPSTC, ips
V_2 = rolling velocity of the planet at the FPSTC, ips
ips = inches per second

Both of these slip ratios are close to or within the 3.3% to 30% band.

Expanding Eq.4.8.9 above, the life ratio can be determined for sliding velocity:

$$(LAF)_{Vs} = L_x/L_y = (|V_{1x}^{.5} - V_{2x}^{.5}|/|V_{1y}^{.5} - V_{2y}^{.5}|)^{-1.25} \qquad \text{Equation (4.8.10)}$$

Where 1,2 = the two gears in a mesh
x,y = new design and baseline data respectively
V = rolling velocity at FPSTC
V_s = sliding velocity

Using BHTI's low speed sun-planet mesh as the baseline

$$(LAF)_{Vs} = (|V_{1x}^{.5} - V_{2x}^{.5}|/|80^{.5} - 105^{.5}|)^{-1.25}$$

$$(LAF)_{Vs} = (|V_{1x}^{.5} - V_{2x}^{.5}|)^{-1.25}/.718544$$

Rearranging,

$$(LAF)_{V_s} = 1.391703\ (|V_{1x}^{.5} - V_{2x}^{.5}|)^{-1.25} \qquad \text{Equation (4.8.11)}$$

Where V = rolling velocity at FPSTC, ips

4.8.1.4.7 STRESSED VOLUME FACTOR

If the stressed volume in a gear mesh is twice that of the baseline gear mesh, it appears logical to assume that the condition would be the same as running 2 gears instead of 1. Thus, this equation should be valid:

$$1/L_v = [v_x/v_y(1/L)^b]^{1/b} \qquad \text{Equation (4.8.12)}$$

Where L = life to be adjusted
L_v = life adjusted for stressed volume
b = Weibull exponent = 1.5 at RMC power
v_x = stressed volume of new design gear
v_y = stressed volume of baseline gear

Equation (4.8.12) is based on the following familiar Palmgren equation [20] adapted to gears:

$$1/L_e = [\sum_{i=1}^{K} n_i(1/L_i)^b]^{1/b} \qquad \text{Equation (4.8.13)}$$

Where L_e = composite life
K = total no. of different gears
n = total no. of like gears of kind i

Equation (4.8.12) may be rearranged as follows and used in the life adjustment equation as an operative factor:

$$L_v = [v_x/v_y(1/L)^b]^{-1/b} \qquad \text{Equation (4.8.14)}$$

What is required now is a definition of the stressed volume and its numerical value for the baseline gear set. The stressed volume can be defined as:

$$v = N(F\ell z_o) \qquad \text{Equation (4.8.15)}$$

Where v = stressed volume, in^3
N = no. of teeth on gear
F = effective face width, in.
ℓ = effective involute length, in
z_o = depth of maximum subsurface shear stress, in.

The effective involute length is taken as the length of the involute surface on the gear between the lowest point of single tooth contact (LPSTC) and highest point of single tooth contact (HPSTC) since the maximum load is applied to this area.

The following equation was derived by Coy, et. al. [21] for calculating the effective involute length:

$$\ell = (d_b/4)(\theta_H^2 - \theta_L^2), \text{ in} \qquad \text{Equation (4.8.16)}$$

Where d_b = base circle diameter, in.
θ_H = degrees roll at HPSTC, radians
θ_L = degrees roll at LPSTC, radians

The effective involute length for the baseline gear can now be calculated given the following data from the 8.5 pitch, 22° pressure angle, 57 tooth sun gear driving a 31 tooth planet.

d_b = 6.217586 in.
θ_H = .427005 rad
θ_L = .364258 rad

Thus,

$$\ell = (6.217586/4)(.427005^2 - .364258^2) = .077175 \text{ in.}$$

The depth of maximum subsurface shear stress can be determined as follows using Dudley's approach [7]:

$$Z_O = .393\ B, \text{ in} \qquad \text{Equation (4.8.17)}$$

Where B = width of band of contact when two cylinders are pressed together, in

$$B = (4W_N)/(FS_c), \text{ in,} \qquad \text{Equation (4.8.18)}$$

Where W_N = normal tooth load, lb
F = effective face width, in.
S_c = hertz stress, PSI

The normal tooth load and the hertz stress for use in equation (4.8.18) are those values calculated with the two load distribution factors equal to 1 because the end loading factor is effective only near the ends of the teeth, and the misalignment factor is effective in full force at one end only and then tapers down to zero at mid-length. The dynamic load factor is effective on the full effective length of the tooth. Thus its value is included in the normal tooth load and hertz stress calculations.

The depth of maximum subsurface shear for the baseline gear is:

W_N = 3546 lb
F = 1.333 in
S_c = 172,836 PSI @ 10^7 L_1 cycles, basic design point
B = (4 x 3546)/(1.333 x 172,836) = .019597 in
Z_O = .393(.019597) = .007702 in

The stressed volume for the baseline gear can now be calculated:

N = 57 teeth
F = 1.333 in
ℓ = .077175 in
Z_o = .007702 in

Using equation (4.8.15) above,

$$v_y = 57(1.333)(.077175)(.007702) = .045160 \text{ in}^3 \approx .045 \text{ in}^3$$

If the stressed volume in a newly designed gear is calculated in a similar manner and the dimensions are in inches then equation (4.8.14) can be used in the following form to adjust the life of a newly designed gear based on the life of the baseline gear:

$$L_v = [(v_x/.045 \text{ in}^3)(1/L)^b]^{-1/b} \quad \text{see NOTE below} \qquad \text{Equation (4.8.19)}$$

Equation (4.8.12) breaks down for a profile contact ratio of 2 because the effective involute length is zero, thereby making the stressed volume equal to zero. Also as the stress volume approaches zero, the adjusted life approaches infinity which indicates that the gear has an endurance limit, i.e., it will never fail from the pitting mode of failure. This is not too unreasonable since some gears never seem to fail if the hertz stress is kept sufficiently low as would probably be the case if the profile contact ratio were greater than 2 on a gear designed and loaded for a profile contact ratio less than 2.

NOTE:

Due to the uncertainty of the loading conditions on a gear set with a profile contact ratio close to 2, the use of equation (4.8.19) is restricted to gears with a profile contact ratio equal to or less than 1.90; or, if the design profile contact ratio is greater than 1.90, equation (4.8.19) may be used providing the outside diameter of the driving member of the gear set is reduced (theoretically only) to obtain a profile contact ratio of 1.90 for the sole purpose of calculating the effective involute length shown in equation (4.8.15).

4.8.1.5 MTBR DETERMINATION

Assuming all of the known failure modes, except the life limiting mode of failure of pitting on bearings and gear teeth, have been designed and developed out of a gearbox, the customer is ultimately concerned with the mean-time-between-removal (MTBR) of the gearbox. If he has a choice of different manufacturer's gearboxes and other things such as weight, noise level, and initial cost being equal, the customer will choose the gearbox with the longest MTBR time. Since reliability testing for the bearing and gear tooth pitting mode of failure is usually limited in scope due to the time and cost involved, the gearbox designer must have the analytical tools and test data to predict the MTBR of the gearbox with reasonable accuracy. The following discussion develops and presents the rationale for an MTBR calculation method which is effective for a gearbox with insignificant infant mortality and a known useful life.

4.8.1.5.1 MTBR CHARACTERISTICS

The term MTBR applies to the condition that the gear box is removed and disassembled for one of two reasons: a part in the gearbox has failed or the time between overhaul (TBO) has expired. Since either event causes the removal of the gearbox, the TBO event is treated as a failure. Thus, in this context the following relationship exists:

$$MTBR = MTBF \qquad \text{Equation (4.8.20)}$$

The MTBF is a measure of the time until a gearbox fails. It can be measured from test data by adding up the total operating time of all gearboxes tested and dividing by the number of gearboxes that failed.

By definition the constant failure rate, Lambda, is equal to the inverse of the MTBF:

$$Lambda = 1/MTBF \qquad \text{Equation (4.8.21)}$$

Thus, the MTBF may be estimated from the failure rate which is readily obtained as follows:

$$Lambda = \text{no. of failures expected/operating time} \qquad \text{Equation (4.8.22)}$$

For example, relative to gears and bearings,

$$Lambda = .10/L_{10} \text{ life or } .02/L_{2} \text{ life or } .01/L_{1} \text{ life or } .50/L_{50} \text{ life etc.}$$

This means that for a bearing or a gear with an L_{10} life of 5000 hours, the failure rate is:

$$Lambda = .10/5000 = .000020 \text{ failures/hour}$$

or, for 100 bearings or gears each with an L_{10} life of 5000 hours the same failure rate exists:

$$Lambda = .10(100)/5000(100) = 10 \text{ failures}/500{,}000 \text{ hours} = .000020 \text{ failures/hour}$$

Also, by definition, the following is implied when the number of MTBR (or MTBF) hours is specified:

1. The failure rate of the gearbox is constant.

2. The MTBF is the Weibull mean for a constant failure rate, i.e., it is the characteristic life of the gearbox, i.e., it is the $L_{63.2}$ life.

3. The gearbox has only a 36.8% chance of making it to the MTBF time.

Finally the total failure rate of the gearbox is the sum of the individual gear and bearing failure rates plus additional values representing overhauls and other components with known and unknown failure rates. Since it was shown above that MTBR = MTBF, and the failure rate is equal to the inverse of MTBF, then

$$MTBR = 1/Lambda_T \qquad \text{Equation (4.8.23)}$$

Where $Lambda_T$ = total failure rate, failures/hour

Item 1 above is true only if the components in the gearbox have constant failure rates. For a gear or a bearing to have a constant failure rate, its Weibull slope (dispersion exponent) must equal 1. Eventhough the Weibull slope for most of the gears and bearings tested at BHTI are greater than 2 with some gears as high as 10, it was shown in Section 4.8.1.3 that a Weibull slope of 1.5 is probably realistic in the lower stress regime of RMC power operation encountered in service.

Thus, the assumption is made that the failure rate of a gear or a bearing from zero time up to the L_2 point for gears and the L_{10} point for bearings is constant. Little is known about the distribution of pitting failures up to and around the L_2 point, however, Johnson [22] states that there is more scatter in early failures than those around the mean life. This would indicate that a Weibull slope of 1 (constant failure rate) exists around the L_2 point. In any event, assuming a constant failure rate over a long period of time which allows only 2% failures during that time would appear to be wholly satisfactory since it leaves little room for any surprises.

The same cannot be said for assuming a constant failure rate up to the L_{10} point for bearings. However, since the pitting failure of bearings is usually more benign than that of gears and the Weibull slopes of bearings are generally closer to 1 than that of gears, the L_{10} point will be used for bearings.

Whether the L_{10} point or L_2 point is used as a cut-off point for a constant failure rate for bearings is critical to the weight of a gearbox. If a gearbox is to have a constant failure rate and no scheduled overhauls, then the L_{10} life of each bearing (and the L_2 life of each gear) should be equal to or greater than the useful life of the gearbox. The difference in weight between bearings designed for the same life where one is in L_2 hours and the other in L_{10} hours can be significant.

A gearbox should have a constant failure rate. A one hour reliability value at the 10,000 hour point should be the same as that at the 10 hour point. This requirement is essentially met with the L_{10} life of bearings and the L_2 life of gears equal to or greater than the useful life of the gearbox.

4.8.1.5.2 TOTAL FAILURE RATE DETERMINATION

When considering the failure rate of a gearbox (or its components), it is assumed that the failure rate is constant as mentioned in section 4.8.1.5.1, i.e., the infant mortality failures have been developed out of the gearbox and the gearbox will be retired at the end of its useful life (the beginning of the wearout life).

For a properly designed gearbox the life limiting mode of failure is bearing pitting and gear tooth pitting. The other failures to be considered are those from known and unknown origins and the 'failure' caused by removal for overhaul. Thus, the total failure rate is defined as follows:

$$\text{Lambda}_T = \text{Lambda}_P + \text{Lambda}_O + \text{Lambda}_{TBO}, \text{ failures/hour} \qquad \text{Equation (4.8.24)}$$

Where Lambda_P = pitting failure rate, failures/hour
Lambda_O = other failures failure rate, failures/hour
Lambda_{TBO} = no. of overhauls in useful life period, failures/hour

4. 8.1.5.2.1 PITTING FAILURE RATE

The pitting failure rates of gears and bearings is obtained from their L_2 and L_{10} lives respectively,

For Gears: $\text{Lambda} = .02/L_2$, failures/hour

For Bearings: Lambda = $.10/L_{10}$, failures/hour

The summation of all of these failure rates yields the pitting failure rate of the gearbox, $Lambda_P$.

4.8.1.5.2.2 OTHER FAILURES FAILURE RATE

Bowen et. al.[22] reported that 34 premature removals were required from a random group of 173 UH-1 helicopter transmissions surveyed at overhaul circa 1970. Of these 34 removals, 32 were due to bearing or gear failures. The remaining 2 removals were due to other component failures. Thus, the failure rate for other components for the UH-1 transmission is taken as

$$Lambda_O \text{ UH-1} = (2/34)Lambda_T \text{ UH-1}$$

Where $Lambda_T$ UH-1 = 34 failures/172,431 total hrs on the 173 transmissions surveyed
= .000197 failures/hour

$$Lambda_O \text{ UH-1} = (2/34)(.000197) = .000012 \text{ failures/hour} \qquad \text{Equation (4.8.25)}$$

This method was used in establishing the MTBR time on BHTI's ATCI transmission [1] except the 0.000012 failures/hour value was divided by 2 to account for the ATCI transmission having approximately half as many fretting interfaces as the UH-1. Then, to account for unknown failure modes which may occur in an extended life transmission or gearbox, that reduced value was multiplied by 3 and then added to the reduced value of .000006 failures/hour to get .000024 failures/hour for the failure rate of failures from other known and unknown origins.

This has the effect of doubling the .000012 failures/hour value determined by the survey of the 173 UH-1 transmissions. This approach may be wholly satisfactory for certain applications, however, for a reasonably debugged transmission or gearbox such as the UH-1 transmission the original .000012 failures/hour may be more applicable.

Thus, for the general application in transmissions and gearboxes, the failure rate for other failures of both known and unknown origins is 0.000012 failures/hour.

4.8.1.5.2.3 TBO FAILURE RATE

Since the advent of on-condition maintenance in the early 1970's, scheduled overhauls on new designs have been on the decline. However, they may never be completely eliminated in situations where gearbox weight is critical. For example, a 10,000 hour gearbox with a TBO of 5000 hours can use smaller bearings if they are scheduled to be replaced at the 5000 hour mark instead of having to operate at the same reliability level for 10,000 hours.

If for any reason an overhaul is scheduled for a gearbox, the TBO failure rate is simply as shown in equation (4.8.24) and restated here:

$$Lambda_{TBO} = \text{no. of overhauls/useful life of gearbox, failures/hr} \qquad \text{Equation (4.8.26)}$$

For a 10,000 hour gearbox with a TBO of 5000 hours the TBO failure rate is

$$Lambda_{TBO} = 1/10{,}000 = .000100 \text{ failures/hour}$$

To show the adverse effect of an overhaul on the MTBR, the ART requirement of 5000 hours MTBR time is used. Rearranging equation (4.8.23):

$$Lambda_T = 1/MTBR$$

$$Lambda_T = 1/5000 = .000200 \text{ failures/hour}$$

This shows that the TBO failure rate uses 50% of the allowable failure rate. Thus, a scheduled overhaul is not compatible with the ART requirement of 5000 hours MTBR time unless the gearbox contains very few parts.

4.8.1.5.3 MTBR CALCULATION

MTBR calculations are made from the failure rate data using equation (4.8.23):

$$MTBR = 1/Lambda_T$$

Prior to this the gearbox designer needs the following information before he can begin sizing the gears and bearings in his gearbox:

1. Useful life of gearbox
2. Minimum MTBR time for the gearbox
3. Number of scheduled overhauls for the gearbox

The requirement for each gearbox on the Bell-Boeing V-22 Osprey tilt-rotor aircraft is 10,000 hours useful life, 3000 hours minimum MTBR time as a goal with 1500 hours minimum required, and no scheduled overhauls.

The requirement for each gearbox in BHTI's FAAV drive system will be 10,000 hours useful life, 5000 hours minimum MTBR time, and no scheduled overhauls. The designer will first size the gears and bearings such that each gear will have 10,000 hours minimum L_2 life and each bearing will have 10,000 hours minimum L_{10} life, all at RMC power. He will then calculate the failure rates and the MTBR time, which, if equal to or greater than 5000 hours meets the design requirement. If the calculated MTBR time is less than 5000 hours, the gears and/or bearings must be larger or their quantity reduced by a change in concept.

Just as the number of gears and bearings in a gearbox has its effect on the MTBR of the gearbox, the number of gearboxes on an aircraft has its effect on the MTBR of the total drive system. If the FAAV drive system is made up of 5 gearboxes, each with an MTBR of 5000 hours, then the MTBR of the total drive system is 1000 hours as shown:

$$Lambda_T = 1/MTBR1 + 1/MTBR2 + 1/MTBR3 + 1/MTBR4 + 1/MTBR5$$

$$Lambda_T = 5(1/5000) = .001 \text{ failures/hour}$$

$$MTBR = 1/Lambda_T = 1/.001 = 1000 \text{ hours/failure for the total drive system}$$

If the requirement were 5000 hours MTBR for a total drive system consisting of 5 gearboxes, then the average MTBR of the 5 gearboxes must be:

$$Lambda_T = 1/MTBR_{total} = 1/5000 = .0002 \text{ failures/hour}$$

$$Lambda_T = 5(1/MTBR_{average}) = .0002 \text{ failures/hour}$$

$$MTBR_{average} = 5/.0002 = 25000 \text{ hours/failure}$$

4.8.2 BEARING PITTING LIFE DETERMINATION

Bearing pitting lives are calculated using the basic fatigue life equation and adjusting the results with the appropriate life adjustment factors. This method is described by Bamberger et.al. [24] in the ASME engineering design guide titled "Life Adjustment Factors for Ball and Roller Bearings" which was published in 1971. Since that time several technological advancements have been made and tests conducted that indicate additional conditions/factors/methods should be addressed especially in the boundary lubrication regimes. Some of these conditions/factors/methods are:

1. Boundary lubrication regimes where Lambda < 0.6
2. Lubricants with friction modifier additive packages
3. Bearings may have an endurance limit (infinite life) below certain hertz stress levels.
4. In the basic fatigue life equation the exponent for the C/P term may be defined as being dependent on Lambda rather than defined as the customary 3 for ball bearings and 10/3 for roller bearings.
5. New and improved life adjustment factors

The following discussion examines the above items in detail, however their effects on the lives of bearings will be constrained by the following conditions:

Max Hertz Stress = 300,000 PSI hertz stress at 100% load
L_{10} unadjusted life = 200 hr min at 100% load with C/P exponent equal to 3 for ball bearings and 10/3 for roller bearings

The five items above will have the greatest effect on bearing lives associated with thin film applications and the requirement for long MTBR times.

4.8.2.1 BOUNDARY LUBRICATION REGIMES AND HIGHER

The pitting lives of both bearings and gears suffer in the boundary lubrication regimes. This is due primarily to failures being of the surface initiated type at low λ ratios instead of the subsurface initiated type at higher λ ratios. Rather than use an undefined lube factor [ref. 24 makes no provision for a lube factor for $\lambda <$ 0.6] design curve 'D' in Figure 26 will be used to define the C/P exponent (inverse load-life exponent) as a function of λ for bearings in the same manner that it is used to define the inverse stress-life exponent for calculating gear tooth pitting lives. The load-life exponent is taken as the stress-life exponent ('a') divided by

2. When this is done, as λ approaches zero, 'a' approaches 6 and a/2 approaches 3 which is not much less than the customary 10/3. When λ=.6, then a=8 and a/2=4, a value often used as the roller bearing load-life exponent instead of 10/3. Going higher in Figure 26, when λ=1.2, a=10 and a/2=5, a value when applied to C/P values greater than 2 is approximately equivalent to applying a life adjustment factor of 10 to the L_{10} life obtained using the customary 10/3 load-life exponent. Going even higher in Figure 26, when λ=3, a=16 and a/2=8, a value if applied to a C/P value greater than about 5 will send most bearings out into the infinite life region without the need for any life adjustment factors greater than one. This load-life exponent of a/2=8 for λ=3 is almost equal to the value of 9 usually used for bearings under pure rolling conditions.

4.8.2.2 LUBRICANTS WITH FRICTION MODIFIER ADDITIVE PACKAGES

Most rotorcraft gearboxes being developed today are using lubricants with friction modifier additive packages. The advantage over lubricants without the additive packages in terms of pitting fatigue life has been demonstrated for gears and discussed in Section 4.8.1.4.3. The manner in which bearing pitting lives are affected by the additive packages is discussed in Section 4.8.2.5.4.

4.8.2.3 PLANET BEARING PITTING LIFE CALCULATION

According to Zwirlein and Schlicht [25], material becomes fatigued only if plastic deformation occurs and that happens in point contacts on ball bearings above contact pressures of 370,000 PSI. Their investigations at S=370,000 PSI on angular contact ball bearings tested at 12,000 RPM (λ= 3 to 4) indicated an expected endurance limit of 334,000 PSI for ball bearings for classical subsurface initiated pitting failures. For cylindrical roller bearings they stated that for line contact operating at S < 290,000 PSI, classic fatigue is not possible. They make no mention of modified line contact, however they probably mean just that when saying line contact since, at least at BHTI, all heavily loaded roller bearings are crowned (end relieved).

This however does not address the condition for bearings operating in thin film applications. During the ATCI planetary gear tooth pitting tests [1], 12 planets were tested simultaneously each supported by a double row cylindrical roller bearing. During the gear tooth pitting test, 2 of the 12 planet bearing inner races failed. The L_{10} life was 510 hours with a Weibull slope of 4.5.

The bearings were made of VAR 52100 bearing steel and operating in MIL-L-23699 oil. The calculated Lambda ratio was .261 using the method shown in ref. [24]. According to PLANETSYS the maximum hertz stress was 347,000 PSI and the unadjusted L_{10} life was 22 hours. Because of the large difference between the 510 hours and 22 hours, another method was sought to determine the L_{10} of planet bearing inner races operating in thin film applications. The method selected is similar to that used to determine the pitting lives of gears:

$L_x/L_y=(S_y/S_x)^a$ in L_{10} load cycles for bearings

During the test the stationary (relative to the load) inner race was subjected to 4.3×10^8 load cycles at a hertz stress of 347,000 PSI. Thus, the working form of the above equation is

$$L_x = 4.3 \times 10^8 (347{,}000/S_x)^a, \; L_{10} \text{ load cycles}$$

Where L_x = new design L_{10} life, unadjusted
S_x = new design hertz stress
a = stress life exponent from Figure 26, curve D

Note that the possible failure of the rollers or the outer race was not considered. The stationary inner race makes it unlikely that a roller or the outer race will fail unless defective as verified by tests conducted at BHTI. During the 1112 hours of 1400 HP planetary testing performed at BHTI and reported by Bowen [6], 16 planet bearings similar to those described above for the ATCI test were tested simultaneously. The results: 10 inner races failed, 1 outer race failed, and no rollers failed.

4.8.2.4 OTHER BEARINGS PITTING LIFE CALCULATION

The discussion in Section 4.8.2.1 about the relationship of the λ ratio and the stress-life exponent throughout the 3 lubrication regimes provides the rationale for suggesting that all of the bearings in the FAAV gearboxes except planet bearings have their unadjusted lives determined by using the stress-life exponent given by curve D in Figure 26 divided by 2 as the load-life exponent to be used with the familiar C/P term.

The life adjustment factors defined in Section 4.8.2.5 are applicable for all bearings in the FAAV gearboxes unless otherwise noted. As stated in Section 4.8.2, the following constraints must be adhered to in evaluating the lives of the bearings in the FAAV gearboxes:

Max Hertz Stress = 300,000 PSI hertz stress at 100% load
L_{10} unadjusted life = 200 hr min at 100% load with C/P exponent equal to 3 for ball bearings and 10/3 for roller bearings

4.8.2.5 BEARING PITTING LIFE ADJUSTMENT FACTORS

Since a baseline hertz stress has been established for calculating the pitting life of planet bearing inner races, the life adjustment factors (LAF's) must be established relative to the baseline. Table 13 shows the basic test parameters of the planet bearing test and the current state-of-the-art design parameters and their LAF's. The LAF's in Table 13 are applicable to any rolling bearing providing the basic test parameter data are applicable and the unadjusted L_{10} life is known or calculable.

The following discussion provides the rationale for the selection of each LAF shown in Table 13.

TABLE 13: PARAMETERS & LIFE ADJUSTMENT FACTORS FOR ART BEARINGS @ L_{10} LEVEL

CATEGORY	[a]BASIC TEST PARAMETER	SOAT DESIGN PARAMETER	LAF
MATERIAL	52100 PER AMS6444	M50 NiL	2
MATERIAL PROCESSING	CEVM	VIMVAR	2.5
HEAT TREATMENT	THRU HARDENED	CARBURIZED	[b]2.5
LUBRICANT	MIL-L-23699	DOD-L-85734	SEE FIG. 24
OIL FILTER RATING	25 MICRON ABSOLUTE	3 MICRON ABSOLUTE	SEE FIG. 25
[d]SHOT PEENING	NOT SHOT PEENED	SHOT PEENED	[c]1.5
[e]STRESSED VOLUME	.0149 IN^3	--	EQ. (4.8.28)

[a] LAF for basic test parameters = 1.0
[b] Based on zero residual stress in 52100 and 27,000 PSI compressive residual stress in M50 NiL at depth of maximum shear stress
[c] Same value as developed for gears
[d] Applicable to inner races only, non-rotating and rotating
[e] For use with planet bearing inner races only

4.8.2.5.1 MATERIAL FACTOR

M50 NiL bearing steel is shown to have a LAF of 2.0 over 52100 bearing steel in Table 13. This value of 2.0 comes from the comparison of X-53 and 9310 gear steels discussed in Section 4.8.1.4.1 where the gear tooth pitting lives of gears made from X-53 and 9310 and tested at NASALeRC on their gear tooth pitting test rig showed a 2.68 L_2 life increase for gears made of X-53 over 9310. This factor of 2.68 was conservatively reduced to 2.0 for use of X-53 over 9310 (AMS 6260) as shown in Tables 11 and 12.

The reason for choosing the same factor of 2.0 for the bearing pitting lives of M50 NiL over 52100 lies in the hot-hardness similarities of the gear and bearing steels. Both the 9310 gears and 52100 bearings are usually tempered at 300° F whereas X-53 gears and M50 NiL bearings are tempered at 450° F and 975° F respectively. The credibility of this LAF of 2.0 is based on the hot-hardness characteristic being the difference between the pitting resistance of the two gear steels.

4.8.2.5.2 MATERIAL PROCESSING FACTOR

Table 13 shows the material processing parameter of VIM-VAR to have a LAF of 2.5 over CEVM. This factor of 2.5 is the same value selected for the material processing for gears (see Section 4.8.1.4.2) utilizing the same material processing parameters of VIM-VAR and CEVM. This selection for gears was based on testing performed at NASA LeRC on gears made of AISI 9310 gear steel. These gear tooth pitting tests showed a 2.94 L_2 life increase for gears made of VIM-VAR 9310 over gears made of CEVM 9310. The 2.94 factor was conservatively reduced to 2.5.

4.8.2.5.3 HEAT TREATMENT FACTOR

The heat treatment factor for carburizing over through hardening is shown in Table 13 as a conditional 2.5. Carburized M50 NiL is given a determinable LAF over the through hardened 52100 based on the assumption that the latter contains no residual stress and the former's residual stress at the point of maximum shear stress is known. The factor of 2.5 is based on the condition of zero residual stress in the through hardened 52100 steel and 27,000 PSI compressive residual stress in the carburized M50 NiL at the depth of maximum shear stress.

Equations (4.8.6) and (4.8.7) in Section 4.8.1.4.5 for gears can be readily adapted to work for bearings in determining the effects of residual stress on bearing life.

4.8.2.5.4 LUBRICANT FACTOR

The lubricant factor (not to be confused with the lubrication factor F described in ref. [24]) for bearings is shown in Figure 27 on the same graph as that shown for gears, both curves being functions of the λ ratio. The curve for gears is based on published test data [15] and engineering experience whereas the curve for bearings is gleaned from unpublished data [26] and mixed with engineering experience. FAG [26] apparently has done some work concerning the effects of lubricant additives on bearing lives. Figure 1 in ref [26] shows a composite LAF as a function of the λ ratio and lubricants with and without additives. The λ ratio is shown to vary from less than .1 to greater than 5.0. Assuming that the additive package in DOD-L-85734 oil is as effective as the additive package used in the FAG tests, then the curve in Figure 27 for bearings is logical. FAG's work [26] indicates an approximate 5-fold increase in life in the low λ ratio region if an oil additive is used. This is approximately 25% of the value shown for gears in Figure 27 operating in DOD-L-85734 oil when compared to MIL-L-23699 oil.

Thus a straight line curve has been added to Figure 27 to be used for bearings operating in DOD-L-85734 lubricants. The curve begins at LAF=5 and λ ratio=0. It is shown to end at LAF=1 and λ ratio=3 since in thick film applications it is estimated that additive packages containing friction modifiers will have less effect on pitting life.

4.8.2.5.5 OIL FILTER RATING FACTOR

The oil filter rating LAF for bearings is shown in Figure 28 with the LAF factor for gears. In fact, Figure 28 and the rationale behind it are based upon bearing tests performed by Sayles and Macpherson [17], and not gear tests. For a comprehensive explanation of Figure 28 see Section 4.8.1.4.4. The straight line curves for gears and bearings in Figure 28 would be just one curve if both were at the L_{10} level or the L_2 level.

4.8.2.5.6 SHOT PEENING FACTOR

Gear tooth pitting tests conducted by Townsend [18] on gears with and without shot peened working profiles showed a 1.6 increase in the L_{10} life of peened over unpeened. It was shown that this increase in life was due to the increase in residual compressive stress as the result of shot peening the already compressively stressed carburized material. Since bearing pitting life is also a function of the residual stress, bearings may also be shot peened for increased life. The method of calculating this increase in life is mentioned in Section 4. 8.2.5.3 and discussed in detail in Section 4.8.1.4.5.

Table 13 shows a LAF of 1.5 which may be used if the residual stress increase caused by peening of the bearing is unknown. The 1.5 factor was reduced from 1.6 which was determined both by test and x-ray diffraction measurements on gears [18].

Although all of the elements of a bearing may be shot peened, the process is usually limited to inner races because quite often the inner race is integral with an expensive gear where a pitting failure is least desirable or the inner race is a planet bearing inner race which is usually the weakest link in a simple planetary.

4.8.2.5.7 STRESSED VOLUME FACTOR

If the life of planet bearing inner races is calculated by the method shown in Section 4.8.2.3 where the stressed volume is not considered, then a LAF for stressed volume must be developed as it was for gears. The method used will be identical to that described for gears in Section 4.8.1.4.7. The life adjustment equation, which is to be used as an operative factor, is Eq. 4.8.14 repeated below:

$$[(v_x/v_y)(1/L)^b]^{-1/b} \qquad \text{Equation (4.8.14)}$$

Where v_x = stressed volume of new design race
v_y = stressed volume of baseline race
L = life to be adjusted
b = 1.5 = Weibull exponent

The stressed volume is derived as follows;

$$v = (i/2)(\pi d l_i Z_o)\text{, in}^3\text{, stressed volume} \qquad \text{Equation (4.8.27)}$$

Where i = no. of rows of rollers

d = diameter of raceway, in.
l_l = effective length of rollers, in.
Z_o = depth of maximum subsurface shear stress, in.

Since Eq. (4.8.14) involves a ratio of volumes, the stressed volume calculated in Eq. (4.8.27) is simplified as shown by assuming the depth of maximum subsurface shear stress is constant over half of the circumference of the raceway instead of varying from maximum to zero. The depth of maximum subsurface shear stress can be determined from PLANETSYS or other computer programs.

The stressed volume of the baseline planetary bearing inner races (discussed in Section 4.8.2.3) under the conditions at which they were tested is:

$$v_y = (i/2)(\pi d l_l Z_o)\ in^3$$

Where i = 2 rows
d = 1.8300 in
l_l = .4410 in
Z_o = .0059 in

$$v_y = 2/2(\pi 1.8300(.4410)(.0059)) = .0149\ in^3$$

If the stressed volume in a new design planet bearing inner race is calculated in a similar manner and the dimensions are in inches, then Eq. (4.8.14) can be used in the following form to adjust the life of a new design inner race based on the life of the baseline inner race:

$$L_v = [(v_x/.0149\ in^3)(1/L)^b]^{-1/b} \qquad \text{Equation (4.8.28)}$$

The Weibull slope 'ß' can be taken as 1.5 for normal operating loads. See Section 4.8.1.2.4 for rationale.

4.9 BEARING MATERIAL SELECTION

Three candidate materials were considered for manufacturing the components of the ART bearings; VIM-VAR 52100 alloy, VIM-VAR M-50 alloy, and carburized VIM-VAR M-50 NiL alloy for the races and rolling elements and polyetheretherketone (PEEK) for the bearing cages in place of standard bearing cage materials.

VIM-VAR 52100 is a bearing steel that is widely used at BHTI and throughout the industry in current production rotorcraft drive systems. This steel contains spherical carbides and accepts a fine surface finish. Tests performed at BHTI show that the planet bearings of VIM-VAR 52100 exhibited better life than similar bearings made of VIM-VAR M-50. This was attributed to the poorer surface finish on the M-50. The only limitation of VIM-VAR 52100 for helicopter bearing applications of the future is its relatively low temperature capability, about 300° F.

M-50 is probably the most commonly used bearing material in the aircraft industry today. Its big advantage is its higher temperature capability over 52100, which makes it a better choice for helicopter bearing applications for improved loss-of-lube performance and for a hot running transmission as described in Section 4.5.4. Its major disadvantage is the irregular carbides inherent with this material which make it impossible to attain the same fine surface finish as is possible with 52100. This makes M-50 less desirable in

slow speed applications where bearings operate under boundary lubrications as is the case with the ART mast bearings and the HCR planet bearings sized in Section 4.1.6.

M-50 NiL is a low carbon modification of VIM-VAR M-50 steel alloy that contains nickel to provide ferrite control and stability, added toughness, and improved fabricability. By carburizing and heat treating the M-50 NiL it is possible to produce a case hardness for rolling contact fatigue life and a core with a lower hardness for improved fracture toughness. Since the higher carbon at the surface is attained by carburizing, the carbides in M-50 NiL are small, globular, and uniformly distributed. This overcomes the irregular carbide problem and surface finish limitations inherent with M-50 alloy. At the same time, since the basic composition is similar to M-50, M-50 NiL retains the higher operating temperature capability. In this manner, this grade has the potential of combining the advantages of 52100 and M-50 while dramatically improving the toughness. One other advantage that M-50 NiL has over the other two candidate materials is that the carburizing and heat treatment process produces beneficial compressive stresses in the case material which significantly improve the fatigue life of the bearing as described in Section 4.8.2.5.3.

Polyetheretherketone (PEEK) is a high temperature, high strength plastic that can out perform steel as a bearing cage material in some applications where race misalignment occurs. PEEK is approximately 5 times lighter than steel. Misalignment between the races forces the ball contact angle to change continuously as the ball revolves around the race. As a result, balls at different locations around the race are traveling at different speeds. The primary function of the cage is to maintain the bearing element spacing. This means the cage will encounter inertia forces due to the acceleration and deceleration of the bearing elements. Since inertia is a function of acceleration and mass, the inertia force on PEEK will be approximately 5 times less than steel by virtue of its lighter weight. The cage deflection caused by the bearing elements being forced out of the contact zone, also stresses the cage material. The stress in the cage due to this deflection is directly proportional to the modulus of elasticity for the cage material. The modulus of elasticity for PEEK is approximately 25 times less than steel, therefore the stress in a steel cage will be 25 times higher than for PEEK. In terms of design allowable stress, the steel is subjected to 5 times the stress that the PEEK cage would see.

One of the major concerns with the use of PEEK for the ART bearings is its operating temperature capabilities. It is reported to have a continuous operating capability at 500° F and a softening temperature of 630° F. Its continuous operating capability at 500° F makes it a suitable material for the hot running transmission described in Section 4.5.4, but its softening temperature of 630° F presents some risk to its loss-of- lube operating capabilities. However, the supplemental air-oil mist system to be used in the ART should permit loss-of-lube operation for a sufficient time period at temperatures below 630° F.

Because of its high operating temperature capability and life improvement characteristics, M-50 NiL alloy steel shall be used as the race and rolling element material for all of the life limited bearings in the ART. This includes the mast bearings and the planet bearings where the improved pitting life will provide a definite improvement over the bearings in the SOAT. Standard M-50 bearings shall be used for the overrunning clutch bearings, the planetary support bearing, the accessory bearings, and the mast preload bearing, all of which have virtually unlimited life.

Because of the significant weight savings attainable, PEEK cages shall be used in all of the ART bearings in place of the standard steel or bronze, except for the mast bearings and the planet spherical roller bearings because of the high load and low speed characteristics of these bearings. Using PEEK in these locations instead of steel presents an unnecessary risk to the ART.

4.10 FAILSAFE PROPROTOR MAST EVALUATION

Tradeoff studies were completed on two separate mast configurations examining the composite/steel failsafe concept for the XV-15 proprotor mast and the proposed ART proprotor mast. The failsafe mast is a tubular steel mast reinforced internally with a cobonded graphite epoxy composite as shown in Figure 29. The steel mast for this failsafe concept was reduced in wall thickness such that it was suited for limited life at limit load only. The composite tube cobonded inside the steel mast was sized such that the stress level in the steel was held at an acceptable level for fatigue. Also, the laminate was sized such that should the steel fail, limit load could also be carried by the composite portion of the mast. The mast is considered failsafe because a failure in either element will not propagate catastrophically to the other element.

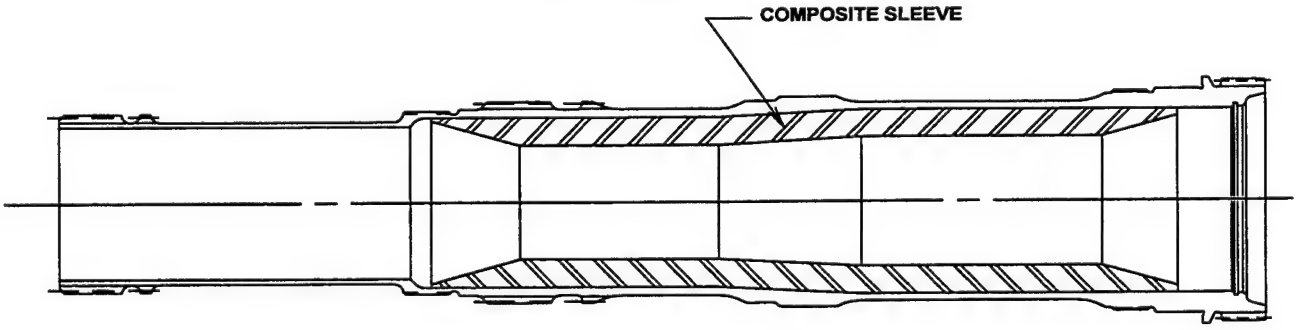

FIGURE 29: FAILSAFE STEEL/COMPOSITE MAST

4.10.1 XV-15 DERIVATIVE STEEL/COMPOSITE PROPROTOR MAST

A failsafe composite/steel mast was designed to match the load carrying capabilities of the XV-15 steel mast. Figure 30 shows a cross section of the XV-15 mast and Figure 29 shows a cross section of the failsafe mast which has the same outside dimensions as the XV-15 mast but has been modified on the internal diameter to include a graphite epoxy sleeve. A weight analysis of both masts found the XV-15 mast to weigh 21.9 lb and the failsafe mast to weigh 18.7 lb.

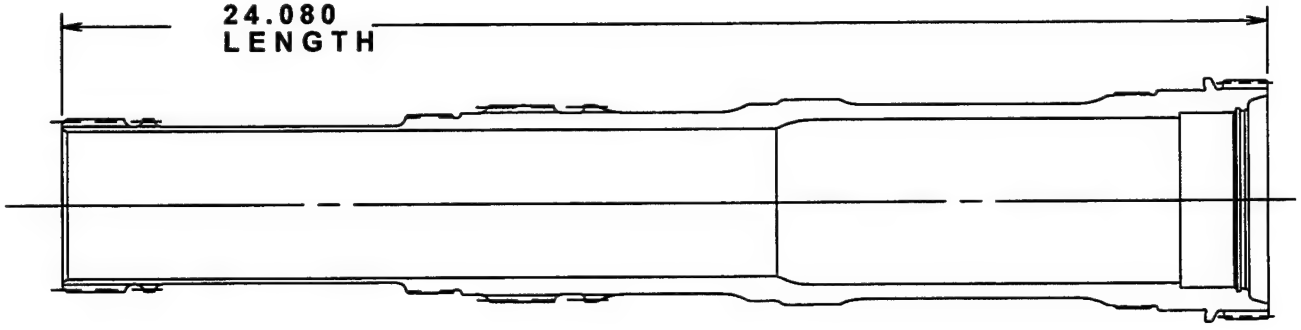

FIGURE 30: XV-15 MAST

Both masts were modeled with the ANSYS computer stress analysis program and were found to have roughly the same stress patterns and static and fatigue strengths in the steel and the same torsional stiffness. The stresses in the composite portion of the failsafe mast are relatively low with a maximum fiber strain of less than 0.2%. Because of the 350° F cure temperature required for the composite portion of the failsafe mast and because the coefficient of thermal expansion of steel is higher than the composite the stress

between the composite and steel will always be compressive precluding any separation of the composite from the steel. From a failsafe point of view, when a failure occurs in the steel portion of the failsafe mast the maximum composite fiber strain is approximately 0.5% which is well within the stress capabilities of the composite material. If a failure occurs in the composite portion of the failsafe mast, the steel portion is strong enough to carry the maximum loads but with a fatigue life of only 30 minutes.

The following sections provide a detailed accounting of the tradeoff study completed on the XV-15 proprotor mast.

4.10.1.1 MATERIAL PROPERTIES AND LOAD CONDITIONS

The material properties of the XV-15 mast, AISI 9310 Alloy Steel, Rc 33, at 230° F are:

E = 30 X 10^6 PSI
G = 12 X 10^6 PSI
v = 0.29
Density = 0.28 lb/in^3
α = 6 X 10^{-6} in/in/°F
Ftu = 145,000 PSI
Fty = 121,900 PSI
Fsu = 86,100 PSI
Fsy = 67,000 PSI
c = 36,000 PSI (Fatigue allowable)

The material properties of IM6/3501 Graphite/Epoxy tape (composite) at room temperature are:

E11 = 21 X 10^6 PSI
E22 = 1.35 x 10^6 PSI
G12 = 0.95 X 10^6 PSI
v12 = 0.34 Density = 0.055 lb/in^3
α11 = 0.2 X 10^{-6} in/in/°F
α22 = 15.2 X 10^{-6} in/in/°F
ε_L^{tu} = 9,280 μ in/in
F_T^{tu} = 4,500 PSI
F^{isu} = 9,800 PSI
ε_{LT}^{su} = 9,500 μ in/in
ε_T^{cu} = 18,300 μ in/in
ε_L^{cu} = 8,300 μ in/in
ε_T^{tu} = 3,430 μ in/in

The load conditions for the tradeoff study are:

Static Loads:

Torque	= 162,800 in-lb
Thrust	= 9,100 lb
Hub Shear	= 1,120 lb

Fatigue Loads:

1. Unlimited Cycles

Torque	= 162,800 ± 16,280 in-lb
Thrust	= 9,100 ± 910 lb
Hub Shear	= ± 1,120 lb

2. Ground-Air-Ground (GAG) (40,000 Cycles)

Torque	= 0 ⇔ 195,360 in-lb
Thrust	= 0 ⇔ 18,200 lb
Hub Shear	= -1120 ⇔ + 1120 lb

4.10.1.2 PROPOSED COMPOSITE/STEEL MAST

The steel/composite mast was created from the XV-15 steel mast by reducing the wall thickness on the I.D. and having a composite tube cobonded onto it. The proposed geometrical configuration is shown in Figure 29.

The steel portion of the mast is the same as the XV-15 mast geometry except that material was removed from the internal surface to reduce the wall thickness to roughly one-half of the original thickness in thin areas. The minimum wall thickness is 0.14 inches. The geometrical configuration on the O.D. was kept unchanged.

The composite portion of the mast is made up of alternating layers of ±45° plies which have a total thickness of 0.54 inches. The angle plies should be interspersed so there are never more than two plies of any orientation together because thick layers are more vulnerable to microcracking, but due to the limitation of finite element computer modeling, six plies of graphite/epoxy tape with the same orientation were used for one layer. The actual lay-ups of the mast would be accomplished with fewer plies of the same orientation for each layer. This will not invalidate the results of this finite element analysis on the composite mast since these results of this FEA will be more conservative. Also, a few plies, say 10%, of graphite/epoxy tapes with 15° orientation will be added in the mast to improve the axial stiffness.

The effective material properties of this composite lay-up are:

$E11 = 3.27 \times 10^6$ PSI
$E22 = 3.27 \times 10^6$ PSI
$G12 = 5.40 \times 10^6$ PSI
$v12 = 0.72$
$\alpha 11 = 1.37 \times 10^{-6}$ in/in/°F
$\alpha 22 = 1.37 \times 10^{-6}$ in/in/°F
$\alpha 12 = 0$

4.10.1.3 FINITE ELEMENT ANALYSIS - ALL STEEL MAST (BASELINE)

A finite element model of the XV-15 steel mast was built using the ANSYS (Swanson Analysis Systems Inc., 1992) finite element program . This model served as a baseline to compare with the subsequent analysis for the steel/composite mast.

A refined submodel was also built to calculate the peak stress in the radius adjacent to the upper spline where the highest stresses are located. The maximum stresses for both models are listed in Table 14 below.

TABLE 14: MAXIMUM STRESS COMPARISON - GLOBAL MODEL VS. LOCAL SUBMODEL (XV-15 MAST)

	MAXIMUM STRESS IN GLOBAL MODEL	MAXIMUM STRESS IN LOCAL SUBMODEL	DIFFERENCE
VON MISES	73,111 PSI	76,593 PSI	4.8%
MAX SHEAR	41,602 PSI	44,165 PSI	6.2%

The margins of safety (M.S.) using the stresses calculated by the submodel are summarized in Tables 15 and 16.

TABLE 15: STATIC STRENGTH OF XV-15 STEEL MAST

	STRESS	M.S. YIELD	M.S. ULTIMATE
VON MISES	76,593 PSI	0.27	0.01
MAX SHEAR	44,165 PSI	0.21	0.04

TABLE 16: FATIGUE STRENGTH OF XV-15 STEEL MAST

	STEADY STRESS	OSCILLATORY STRESS	M.S.
UNLIMITED CYCLES	75,314 PSI	8,939 PSI	0.15
GAG CYCLES (40,000)	43,794 PSI	44,690 PSI	-0.009

The fatigue margin of safety was calculated based on the allowable of 36,000 PSI and unlimited cycles. All of the stresses for static and fatigue evaluations are the results of refined finite element analysis using a local submodel. In order to reduce the computer run time, subsequent stress analyses of the steel/composite mast were conducted on the global models which include the whole mast. The results of these global models were then compared with those of the steel mast global model. It is assumed that they have the same strength if their stresses are similar.

4.10.1.4 FINITE ELEMENT ANALYSIS - STEEL/COMPOSITE MAST

ANSYS was the finite element code used to analyze the steel/composite mast with two types of elements being used. They are 3-D isoparametric elements for steel and 3-D anisotropic elements for composite.

The following assumptions were made for the finite element model:

1. No slippage of the bond between the steel and composite.

2. Linear elasticity of the steel and composite.
3. Constant material properties.
4. Zero initial stress and strain.

Boundary conditions and load conditions are the same as those for the steel mast model.

4.10.1.4.1 STEEL ELEMENT STRESSES

The maximum stresses for the combined loads, 162,800 in-lb torque + 9,100 lb thrust + 1,120 lb hub shear, are listed in Table 17 in comparison with those of the all-steel mast. It is seen that the stress levels in these two masts are about the same. Consequently, it is assumed the steel part of the steel/composite mast would have the same strength as the all-steel mast.

TABLE 17: MAXIMUM STRESSES IN STEEL COMPONENT OF VX-15 FAILSAFE MAST

	MAXIMUM STRESS IN ALL STEEL MAST	MAXIMUM STRESS IN STEEL/COMPOSITE MAST
VON MISES	73,111 PSI	73,620 PSI
MAX SHEAR	41,602 PSI	42,458 PSI

4.10.1.4.2 COMPOSITE ELEMENT STRESSES AND STRAINS

There are a total of twelve layers of graphite/epoxy stack-ups for the composite element. Within each layer, the fibers have the same orientation and are treated as an orthotropic material. The constituitive equations are defined by inputting the material matrices into ANSYS.

The composite layers are numbered from 1 through 12 starting from the outmost layer bonding onto the steel part. The stress and strain are found to be highest in the outer layers and decreasing toward the inner layers. This is mainly due to the load redistribution from the steel part into the composite part.

Tables 18 and 19 show the fiber strains and interlaminar stresses in the first two layers. Strains and stresses in the rest of the layers are significantly lower.

TABLE 18:FIBER STRAINS (μ IN/IN) IN COMPOSITE PORTION OF XV-15 FAILSAFE MAST

	LONGITUDINAL		TRANSVERSE		
	MAX TENSILE	MAX COMPRESSIVE	MAX TENSILE	MAX COMPRESSIVE	SHEAR
LAYER #1	1,314	------	137	1,361	639
LAYER #2	65	1,117	1,374	109	522
MARGIN OF SAFETY	2.14	2.3	0.11	4.98	5.61

$$\text{Margin of Safety} = \frac{\text{(Allowable Fiber Strain)}}{1.5 \times 1.5 \times \text{(Fiber Strain)}} - 1$$

TABLE 19: INTERLAMINAR STRESSES (PSI) IN COMPOSITE PORTION OF XV-15 FAILSAFE MAST

INTERFACE	TENSILE	SHEAR VECTOR SUM
STEEL AND LAYER #1	839	5,092
LAYER #1 AND LAYER #2	639	3,974
MARGIN OF SAFETY	1.38	-0.14

$$\text{Margin of Safety} = \frac{(\text{Allowable Stress})}{1.5 \times 1.5 \times (\text{Stress})} - 1$$

The maximum interlaminar shear stress is located at the lower end of the composite tube adjacent to the steel part. The high stresses are due to the load concentration caused by the torque transmitted through the steel/composite interface. The actual mast design will include a tapered surface at both ends of the composite tube as shown in Figure 29 rather than a uniform thickness composite tube as analyzed for the FEA model. The tapered surfaces will reduce the local stiffness and therefore spread out the load.

4.10.1.5 FAILSAFE ANALYSIS

The primary purpose of the steel/composite mast design is to provide failsafe operation with weight reduction as an added benefit. The failsafe mast will not fail catastrophically if either the steel or the composite fails. The loss of mast stiffness due to the failure of either element will show up as a mast overtorque on the cockpit instrumentation prompting the pilot to make an emergency landing. Meanwhile the other element will be strong enough to assume the loads for at least a certain amount of time. The following tables show the strains and stresses when either element of the steel/composite mast fails.

TABLE 20: COMPOSITE FIBER STRAINS (μ IN/IN) WHEN THE STEEL FAILS (XV-15 FAILSAFE MAST)

	LONGITUDINAL (ALOWABLE)	TRANSVERSE (ALLOWABLE)	SHEAR (ALLOWABLE)
LAYER #1 (+45°)	4,700 (9,280)	-7,850 (-18,300)	2,810 (9,500)
LAYER #2 (-45°)	-3,520 (9,280)	3,380 (3,430)	1,920 (9,500)

TABLE 21: STRESSES (PSI) IN THE STEEL WHEN THE COMPOSITE FAILS (XV-15 FAILSAFE MAST)

	MAXIMUM SHEAR	VON MISES
STRESS	74,950	129,900
M.S. - ULTIMATE	0.15	0.12

The steel portion of the mast must have a certain amount of fatigue life when the composite fails. This fatigue life is estimated as follows:

S_{STDY} = 126,108 PSI
S_{OSC} = 18,158 PSI
S_E = 69,500 PSI (Material endurance limit)

$S'_E = f_M\, f_{SF}\, f_S\, f_R\, f_{SC}\, S_E$

Where

$f_M = 1-(126,108/145,000)^2 = 0.244$ (mean stress factor)
$f_{SF} = 0.85$ for 63AA (surface finish factor)
$f_S = 0.77$ (size factor)
$f_R = 0.897$ for 90% reliability
$f_{SC} = 0.75$ for 25% scatter factor
$S'_E = 7,460$ PSI

R = Failure Stress/Endurance Limit = 18,158/7,460 = 2.43

Cycles of life = 18,000

Assuming a 1/Rev oscillatory stress condition and the rotating speed of 600 RPM, the approximate fatigue life of the mast after the composite element fails is about 30 minutes.

4.10.1.6 EFFECT OF TEMPERATURE ON MAST STRENGTH

The steel/composite mast must demonstrate adequate strength for a -65° F to +350° F thermal cycle. The focus of the thermal stress analysis is the strength of the steel/composite bonding.

It is assumed that the composite will be cured at 260° F at a zero-stress state. Table 22 shows the thermal stresses without mechanical loads when the temperature changes from +260° F to -65° F. Table 23 shows the stresses for the temperature change from +260° F to 350° F.

TABLE 22: THERMAL STRESSES IN XV-15 FAILSAFE MAST- TEMPERATURE CHANGE FROM +260°F TO -65°F

MAX VON MISES STRESS IN STEEL	= 22,641 PSI
MAX LONGITUDINAL FIBER STRESS	= -28,128 PSI
STEEL/COMPOSITE BOND NORMAL STRESS	= -7,644 TO -116 PSI
STEEL/COMPOSITE BOND SHEAR STRESS	= 6,962 PSI

TABLE 23: THERMAL STRESSES IN XV-15 FAILSAFE MAST- TEMPERATURE CHANGE FROM +260°F TO +350°F

MAX VON MISES STRESS IN STEEL	= 6,270 PSI
MAX LONGITUDINAL FIBER STRESS	= 7,789 PSI
STEEL/COMPOSITE BOND NORMAL STRESS	= 32 TO 2,122 PSI
STEEL/COMPOSITE BOND SHEAR STRESS	= 1,928 PSI

The bonding normal stresses between the steel and composite were found to be essentially compressive except for the 2,122 PSI tensile stress when the temperature goes up from +260° F to +350° F.

4.10.1.7 CONCLUSIONS

This steel/composite mast has the same static and fatigue strengths as those of its counterpart, the XV-15 all-steel mast. It is also a failsafe mast with a weight reduction of about 15%.

4.10.2 ART STEEL/COMPOSITE PROPROTOR MAST

Based on the positive results of the tradeoff study for the XV-15 steel/composite mast, a theoretical analysis was conducted to study the feasibility of designing a failsafe steel/composite mast based on the proposed all-steel mast for the ART as shown in Figure 31. As in the design of the XV-15 failsafe mast, the purpose of this design is to replace some steel material on the internal diameter of the mast with composite material and still maintain the same static and fatigue strengths. A composite tube will be cobonded onto the steel between the upper spline and the lower bearing as shown in Figure 32. Failsafe operation, which prevents catastrophic failure, is the primary goal of this design in which failure of either element will not propagate catastrophically to the other element.

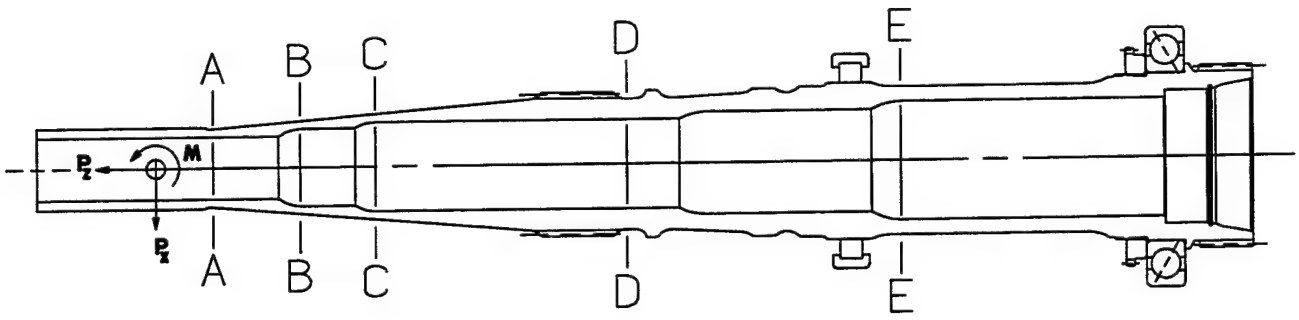

FIGURE 31: ART STEEL PROPROTOR MAST

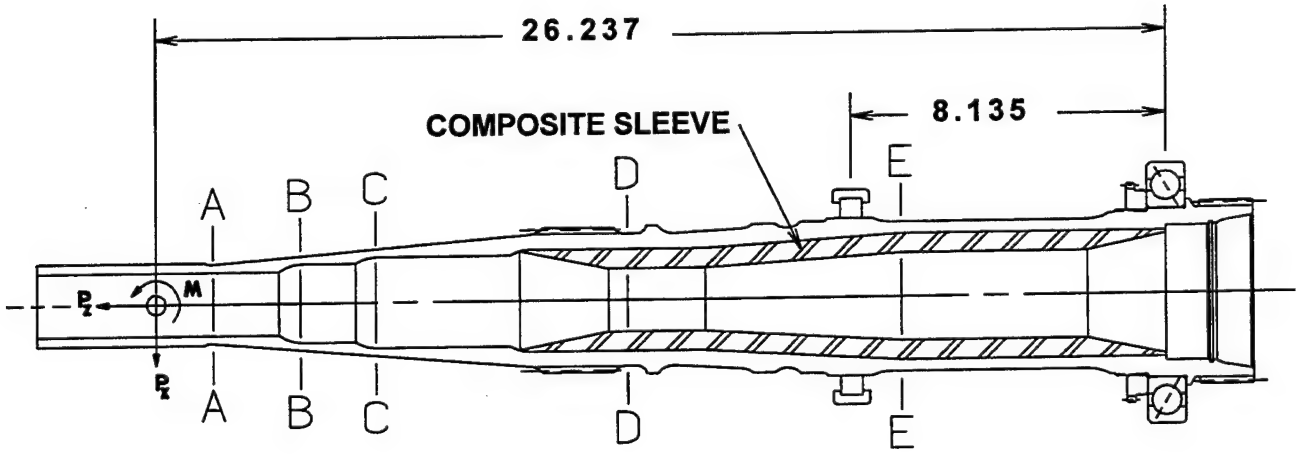

FIGURE 32: ART COMPOSITE /STEEL PROPROTOR MAST

4.10.2.1 MATERIAL PROPERTIES AND LOAD CONDITIONS

The material properties for the steel and composite components of the failsafe mast are the same as those listed in Section 4.10.1.1.

The load conditions for the tradeoff study are:

Static Loads:

Torque	= 385,083 in-lb	(Limit)
Hub Moment	= 35,100 in-lb	(Limit)
Thrust	= 15,650 lb	(Limit)
Hub Shear	= 3,520 lb	(Limit)

Fatigue Loads:

1. Unlimited Cycles

Torque	= 256,722 ± 25,672 in-lb
Hub Moment	= ± 17,550 lb
Thrust	= 7,825 ± 782 lb
Hub Shear	= ± 886 lb

2. Ground-Air-Ground (GAG) (40,000 Cycles)

Torque	= 0 ⇔ 308,066 in-lb
Hub Moment	= -17,550 ⇔ +17,550 in-lb
Thrust	= 0 ⇔ 10,955 lb
Hub Shear	= -886 ⇔ +886 lb

4.10.2.2 CLASSICAL STRESS ANALYSIS

Classical stress analysis was conducted to calculate the stresses in Section D-D and Section E-E to evaluate the designs of the steel and steel/composite masts. Since the proposed steel/composite mast will only have the composite element cobonded between the upper spline and the lower bearing, the strengths in Sections A-A, B-B, and C-C will not be affected by the modification.

The static strengths expressed by margins of safety are listed in Table 24 for Sections A-A, B-B, and C-C.

TABLE 24: MARGINS OF SAFETY FOR STATIC STRENGTH OF ART STEEL MAST

	TENSILE YIELD	TENSILE ULTIMATE	SHEAR YIELD	SHEAR ULTIMATE
SEC. A-A	0.3	-0.01	0.42	0.18
SEC. B-B	0.53	0.16	0.68	0.39
SEC. C-C	0.85	0.4	1.03	0.68

No fatigue calculations were performed because the hub moment for these sections has not been defined.

Detailed stress calculations were performed for both the steel mast and the steel/composite mast. The steel/composite mast was designed to have the same torsional stiffness as the steel mast. To calculate the stresses of the steel/composite mast, the loads were distributed between the steel element and the composite element according to their relative torsional stiffness and flexural rigidity. Effective material properties of the composite element were first calculated by using BHTI's in-house computer program SCAV17 and then treated as an orthotropic material. After the stresses were determined for the orthotropic material, they were transformed into composite fiber directions to calculate the fiber strains.

Table 25 shows the dimensions, loads, and static strengths of sections D-D and E-E of the steel mast under combined limit loads. Fatigue strengths are also listed.

TABLE 25: STATIC AND FATIGUE STRENGTHS IN SECT D-D AND E-E (ART STEEL MAST)

	SECTION D-D	SECTION E-E
OUTSIDE DIAMETER	3.380 IN	3.810 IN
INSIDE DIAMETER	2.300 IN	2.900 IN
TORQUE, IN-LB (LIMIT)	385,083	385,083
THRUST, IN-LB (LIMIT)	15,650	15,650
MOMENT, IN-LB (LIMIT)	77,868	83,052
SHEAR, LB (LIMIT)	3,520	12,149
M.S. TENSILE YIELD	0.011	0.021
M.S. TENSILE ULTIMATE	-0.16	-0.04
M.S. SHEAR YIELD	0.06	0.17
M.S. SHEAR ULTIMATE	-0.12	0
M.S. FATIGUE UNLIMITED CYCLES	0.09	0.2
M.S. FATIGUE GAG CYCLES	-0.04	0.07

For the steel/composite mast, the proposed dimensions, and the static and fatigue margins of safety of the steel element are summarized in Table 26.

TABLE 26: STATIC AND FATIGUE STRENGTHS OF STEEL ELEMENT (ART STEEL/COMPOSITE MAST)

	SECTION D-D	SECTION E-E
OUTSIDE DIAMETER	3.380 IN	3.810 IN
INSIDE DIAMETER	2.597 IN	3.226 IN
M.S. TENSILE YIELD	0.09	0.18
M.S. TENSILE ULTIMATE	-0.17	-0.07
M.S. SHEAR YIELD	0.05	0.14
M.S. SHEAR ULTIMATE	-0.13	-0.03
M.S. FATIGUE UNLIMITED CYCLES	0.05	0.13
M.S. FATIGUE GAG CYCLES	-0.05	0.05

The proposed dimensions and fiber strains of the composite element are listed in Table 27.

TABLE 27: COMPOSITE FIBER STRAINS (μ IN/IN) OF LAYER #1 UNDER COMBINED LIMIT LOADS (ART STEEL/COMPOSITE MAST)

	SECTION D-D	SECTION E-E
OUTSIDE DIAMETER	2.597 IN	3.226 IN
INSIDE DIAMETER	1.600 IN	2.229 IN
LONGITUDINAL (MARGIN OF SAFETY)	2,204 (1.81)	2,050 (2.02)
TRANSVERSE (MARGIN OF SAFETY)	-1,952 (5.25)	-1,753 (5.96)
SHEAR (MARGIN OF SAFETY)	1,545 (3.10)	1,216 (4.21)

All of the loads used for analysis of steel/composite mast are limit loads as shown in Table 25. The margins of safety for fiber are calculated by:

$$\text{Margin of Safety} = \frac{\text{(Allowable Fiber Strain)}}{1.5\times\text{(Fiber Strain)}} - 1$$

Interlaminar stresses are not available from classical hand calculations and are not presented in this report. Numerical analysis or finite element analysis would be required to determine those stresses for evaluation of the bond strength.

4.10.2.3 FAILSAFE ANALYSIS - ART MAST

The primary goal of steel/composite mast design is to provide a fail-safe feature which would prevent catastrophic failure of the mast. To do this, either element of the steel/composite mast will have to assume full loads when the other element fails.

1. If the Composite Element Fails,

   Table 28 lists the stresses under combined maximum loads and the margins of safety in Sections D-D and E-E.

TABLE 28: STRESSES AND MARGINS OF SAFETY IN THE STEEL WHEN THE COMPOSITE FAILS (ART STEEL/COMPOSITE MAST)

	SECTION D-D		SECTION E-E	
	MAXIMUM SHEAR	VON MISES	MAXIMUM SHEAR	VON MISES
STRESSES (PSI)	53,947	94,197	52,566	91,849
M.S. - ULTIMATE	0.65	0.57	0.64	0.58

The estimated fatigue lives of the steel element for sections D-D and E-E after the composite element fails are 5 and 4 hours respectively.

2. If the Steel Element Fails,

Table 29 lists the composite fiber strains under combined maximum loads in sections D-D and E-E when the steel element fails.

TABLE 29: COMPOSITE FIBER STRAINS (μ IN/IN) WHEN THE STEEL FAILS (ART STEEL/COMPOSITE MAST)

	SECTION D-D	SECTION E-E	LOWEST M.S.
LONGITUDINAL (ALLOWABLE)	9,747 (9,280)	5,882 (9,280)	-0.05
TRANSVERSE (ALLOWABLE)	-6,468 (-18,300)	-3,810 (-18,300)	1.83
SHEAR (ALLOWABLE)	20,139 (9,500)	12,728 (9,500)	-0.53

It is found from Table 29 that the fiber shear strain is too high in Section D-D. Several different fiber orientations were also tried to reduce the shear strain. The resultant composite fiber strains in section D-D when the steel element fails are listed in Table 30.

TABLE 30: FIBER STRAINS (μ IN/IN) IN SECTION D-D WITH DIFFERENT FIBER ORIENTATIONS (ART STEEL/COMPOSITE MAST)

ORIENTATION	LONGITUDINAL	TRANSVERSE	SHEAR
± 45 °	9,747	-6,468	20,139
± 38 °	10,208	-10,129	11,152
± 30 °	10,891	-12,227	779

Table 30 indicates that the composite element with the lay-ups of ±38° has the fiber strain levels closer to the allowables, but still too high. A detailed finite element analysis would be necessary to obtain more accurate strain values.

4.10.2.4 CONCLUSIONS

The steel/composite mast has the same static and fatigue strengths as those of the all-steel mast. However, it does not pass the fail-safe test based on the hand calculations of stress and strain. This mast has a much higher moment load than the XV-15 mast while its outside diameters are generally smaller. Moreover, the inside diameter of this mast must be larger than 1.600 inches to allow for instrumentation which must pass through the center of the mast on the reference aircraft. All of these factors make the design of a fail-safe steel/composite mast for the ART more difficult. However, the fiber strains when the steel element fails obtained by hand calculations do not excessively exceed the allowables, and it is probable that with a more thorough investigation a failsafe steel/composite mast could be designed for the ART.

4.11 HOUSING MATERIAL SELECTION

The housings for the ART can be separated into two different categories; those that can be investment cast and those which must be sand cast. Simple housings like the ART top case can be investment cast whereas complex housings as will be required for the ART main case must be sand cast.

4.11.1 INVESTMENT CAST HOUSINGS

Because of the tighter dimensional control afforded by the investment casting process an investment casting can be made lighter than a sand casting of the same part. Several materials were investigated to determine the candidate investment casting material for the ART.

A tradeoff study was conducted comparing investment cast A357 aluminum alloy and 6Al-4V titanium alloy, with a current AZ91C magnesium alloy, sand cast, top case for BHTI's 214ST helicopter tailrotor gearbox to determine which material would yield the lightest top case. The simple structure of the top case lends itself to investment cast applications as will some of the castings required for the ART.

4.11.1.1 FINITE ELEMENT ANALYSIS

A finite element model was first built using isoparametric shell elements with mid-side nodes. Figure 33 shows the geometrical configuration and the breakdown of wall thicknesses listed in Table 31 for finite element computer modeling. This model can be easily modified for different wall thicknesses and materials. The maximum stress was found to be 1,300 PSI in the flange radius of the sleeve using magnesium alloy AZ91C.

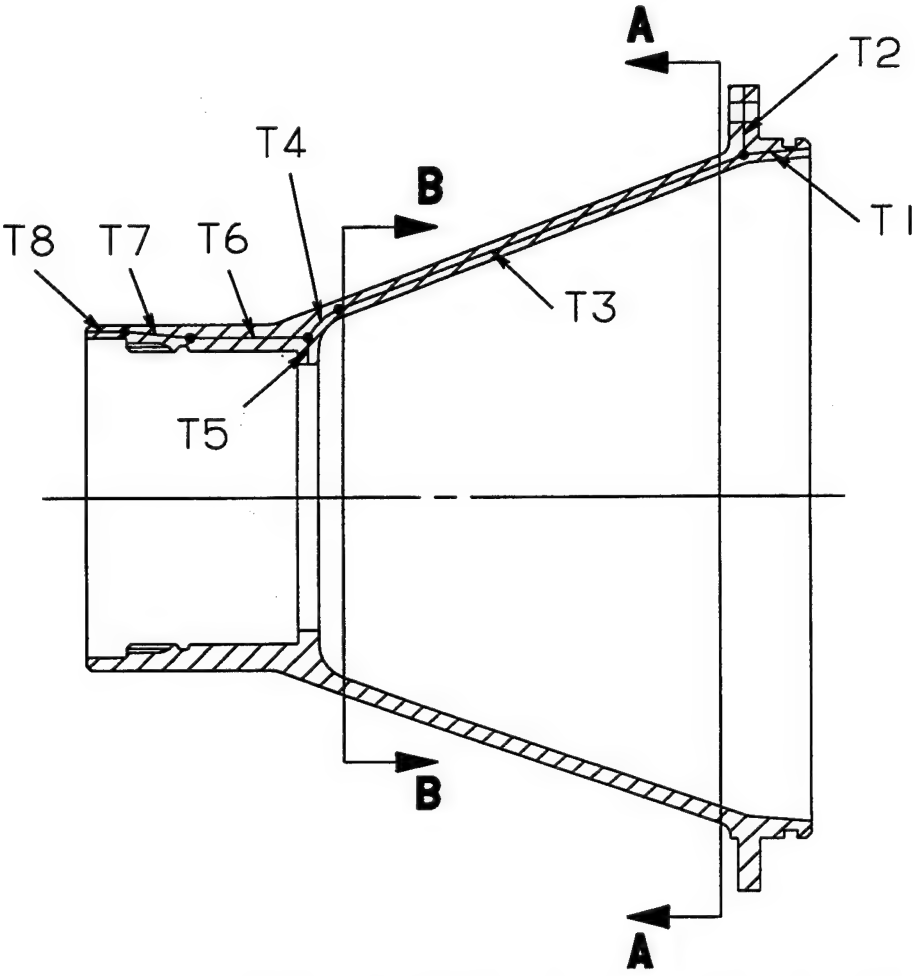

FIGURE 33: 214ST TAILROTOR GEARBOX HOUSING GEOMETRYAND SHELL THICKNESSES FOR FINITE ELEMENT MODELING

TABLE 31: 214ST TAILROTOR GEARBOX HOUSING WALL THICKNESSES FOR SHELL MODEL INPUT

MATERIAL	T1	T2	T3	T4	T5	T6	T7	T8	WEIGHT
AZ91C MAG ALLOY (BASELINE)	0.250	0.312	0.235	0.350	0.293	0.465	0.343	0.135	4.69 LB
A357 AL ALLOY	0.200	0.260	0.140	0.350	0.293	0.250	0.180	0.140	4.67 LB
6AL-4V TI ALLOY	0.100	0.100	0.050	0.150	0.120	0.120	0.080	0.040	3.11 LB

A local submodel was also constructed to represent the local area containing a bolt hole. The flange radius is well defined in this submodel. The displacement solutions of the global model were then extracted and applied on the cut boundaries of the submodel as boundary conditions. Results of the solid submodel were used to verify the shell model. Excluding the local effect due to bolt loads around the bolt hole, the maximum stress in the radius is approximately 1,200 PSI which is consistent with the stress in the shell model.

Stress results of each computer run were checked against static strength and fatigue strength of the materials. Margins of safety were calculated and summarized in Table 32 for Section A-A and Section B-B.

TABLE 32: MARGINS OF SAFETY FOR CAST HOUSINGS

MATERIAL	WEIGHT (REDUCTION)	STATIC STRENGTH (M.S.)				FATIGUE STRENGTH (M.S.)	
		SECTION A-A		SECTION B-B			
		YIELD	ULTIMATE	YIELD	ULTIMATE	SEC A-A	SEC B-B
AZ91C MAG (BASELINE)	4.69 (---)	5.7	5.3	12.8	12	1.86	4.8
A357 AL	4.67 (0.4%)	9.1	8.1	15.5	13.9	1.6	3.7
6AL-4V TI	3.11 (34%)	10.5	7.3	19	13.4	2.35	6.42

4.11.1.2 RESULTS

Table 32 shows that the top case using aluminum alloy A357 has much higher static strength but lower fatigue strength compared to magnesium alloy AZ91-C because A357 has about 130% higher tensile strength but only a 30% higher fatigue allowable. Meanwhile, A357 is 40% heavier than AZ91-C, therefore the weight savings for aluminum is insignificant. For the titanium top case, eventhough the resultant fatigue strength margin of safety is greater than that for the magnesium, the wall thickness for the titanium top case is at its minimum for investment cast applications, i.e. an even greater weight reduction than the 34% for this particular case could be realized for an application with higher loads.

The results of this tradeoff study also eliminate SiC/A357-T6 from consideration as an investment casting material for the ART. Eventhough it was not specifically included in this analysis, its properties are in the range of those for A357-T6 Al alloy and likewise significantly less than those for 6Al-4V Ti.

Based on the results of this tradeoff study it appears that for components that could be investment cast, titanium would yield parts at least 1/3 lighter than investment cast aluminum parts.

4.11.2 SAND CAST MAIN CASE AND OTHER HOUSINGS

It was originally proposed to use WE54-T6 magnesium alloy for the main case and other housings in the ART which do not lend themselves to the investment casting process. Since that time it has been discovered that WE54-T6 suffers a significant reduction in strength after long term exposure to high temperatures. As a replacement, Magnesium Elektron Inc., the company that developed WE54-T6, has developed another magnesium alloy which does not lose its original strength after long term exposure to temperatures up to 575° F. The new alloy has been designated WE43-T6 and possesses the minimum properties at 75° F as shown in Table 33.

TABLE 33: MINIMUM MECHANICAL PROPERTIES OF SEVERAL HOUSING ALLOYS AT 75° F

ALLOY	TENSILE STRENGTH (KSI)	0.2% YIELD STRENGTH (KSI)	ELONGATION (%)
WE43-T6 MAG	36.3	23.5	2
ZE41A-T5 MAG	26.7	18.8	9.5
A356-T6 AL	41.7	26.7	14.7

Although the mechanical properties for WE43-T6 are less than those for A356-T6 at room temperature, they are reported to be the same at 200° F and actually exceed those for A356 at temperatures higher than 200° F. The corrosion resistance of the WE43 magnesium was evaluated and the results are presented in Section 6.4.

Because of its strength retention at elevated temperatures, which makes it an excellent housing material for the hot running transmission described in Section 4.5.4, and because it is 40% lighter than A356, WE43-T6 will be used as the housing material for all of the housings on the ART which must be sand cast.

4.12 GEAR IMPROVEMENT METHODS

In order to meet the weight, noise, and MTBR requirements for the ART, significant improvements had to be made in the gear members. The following sections describe the efforts to make these necessary improvements in each of the different gear types selected for the ART.

4.12.1 PRECISION FORGING

Recent advances in forging equipment, materials and techniques make precision gear forging a potential production process. Precision gear forging differs from the conventional gear forging method commonly used throughout the industry today and is a new approach for the manufacture of highly loaded aircraft gears.

Normal forgings used for making aircraft gears are closed die or rolled ring forgings. Each forging has to undergo extensive machining prior to cutting, generating, or green grinding of the gear teeth. In the near net shape or precision forging method, the gear blank is forged with integral gear teeth. The use of such forgings in the ART has the following two advantages:

- Significantly reduced machining requirement for reduced acquisition costs.

- Improvement in the bending fatigue strength of the gear teeth for reduced weight.

Precision forgings require significantly fewer machining hours than conventional closed die or rolled ring forgings. An added benefit here is the reduced material cost since a smaller percentage of material will go to waste as machining chips. Even with the precision forging technology available today, it is felt that the cutting or generating of gear teeth prior to case hardening cannot be completely eliminated. The amount of material to be removed prior to case hardening will be in the range of .010 to .020 in. This will still leave the conformal grain flow in the root of each tooth which is the reason for the second advantage listed above.

Several attempts have been made to quantify the benefits of precision forging in the area of increased bending strength, but unfortunately most such programs addressed air-melt starting materials. Conformal grain flow in the roots of gear teeth has obvious advantages when using air-melt material because it will minimize the chances of alignment of inclusions in the area of maximum bending stresses. The question to be answered is - Does the advantage of conformal grain flow exist even in "cleaner" starting materials, like VAR and VIM-VAR?

Sikorsky Aircraft conducted a study to evaluate this phenomenon in 1969, under a U.S. Army contract [27]. This work consisted of evaluating the bending fatigue strength of four batches of 8.000 diametral pitch spur gears: baseline and precision forged gears from three different vendors (A, B, and C). All gears were made from the same 2.125 inch diameter bar of VAR 9310 steel. The three precision forging vendors used totally different forging techniques to produce the same final product. The forged teeth had a stock removal allowance of 0.010 to 0.014 per side: approximately 0.003 - 0.005 for green grind and 0.007 to 0.009 for finish grinding. All test gears were carburized and heat treated in one lot to produce 0.035 - 0.045 effective Rc 50 case depth.

The results of the single tooth bending tests conducted on these four batches of gears are summarized in Figure 34. The stress values were calculated using BHTI's computer program and the gear geometry and test loads given in the report.

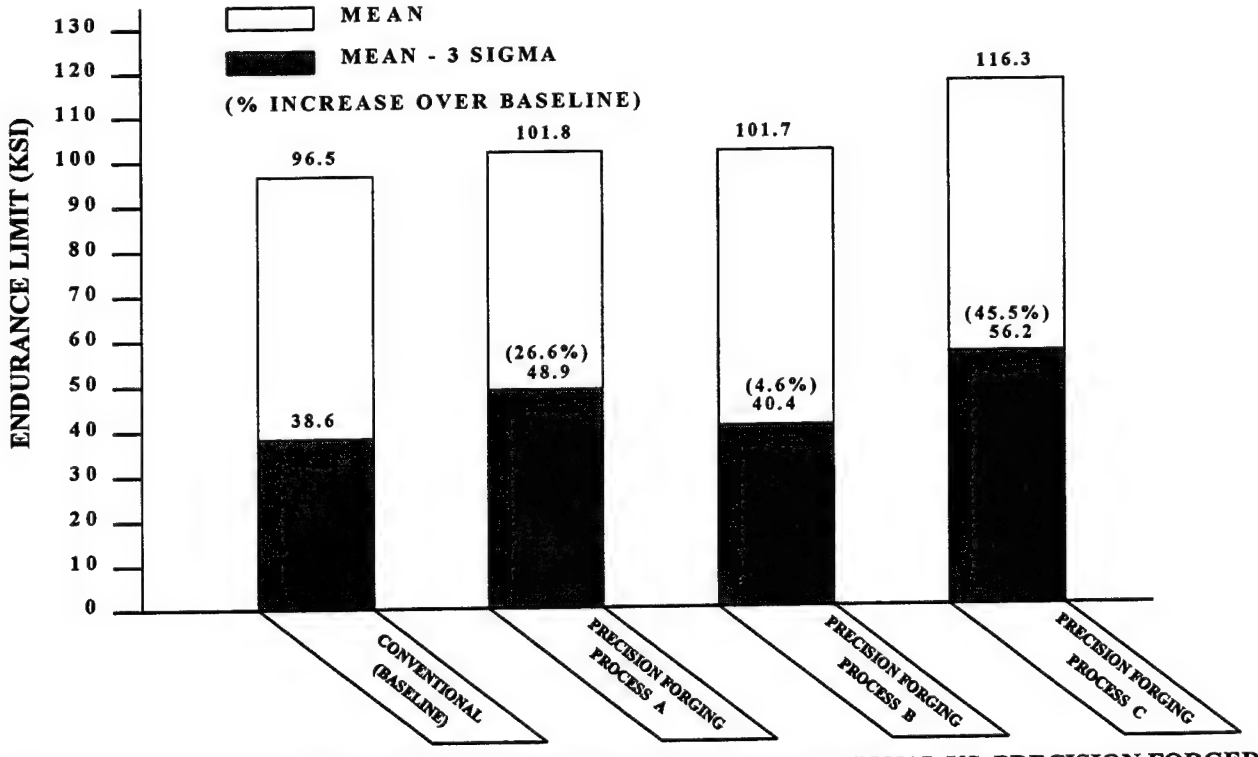

FIGURE 34: VAR 9310 SINGLE TOOTH BENDING DATA - CONVENTIONAL VS. PRECISION FORGED

The results show a 4 to 45% improvement in bending fatigue strength when compared to the baseline gears, at the mean-3sigma level. The variation seen between the products of the 3 precision forging vendors points to the fact that the process of making power gears from precision forgings is dependent upon a number of variables and will require close process control to assure repeatability. To quantify the benefits of precision forging on VIM-VAR starting material, tests were conducted on precision forged flexure fatigue specimens and the results presented in Section 6.3.

4.12.2 PLASMA CARBURIZING

The power gears for the ART which are to be case hardened by carburizing shall be plasma carburized. Plasma carburizing is conducted in a partial vacuum and is a technological step beyond carburizing. It offers the following advantages over the present conventional gas carburizing method:

- The entire process is microprocessor controlled, eliminating the need for periodic atmospheric monitoring with shims. The present practice at BHTI requires an hourly analysis of shims during the entire carburizing cycle to assure the uniformity of process from load to load. The furnace operator is required to make adjustments on an hourly basis depending on the results of the shim analysis. With plasma carburizing, once the cycle is started with predetermined settings, no operator assistance or adjustment is required. The obvious advantage here is consistency from load to load.

- The plasma carburizing process has the potential of yielding a much more uniform case along the profiles and roots of the gear teeth when compared with conventional carburizing. The case depth requirement for gear teeth are generally dictated by the diametral pitch of the gear - coarser pitch gears can stand a deeper case than finer pitch gears. For finer pitch gears (diametral pitch of greater than 12), a relatively shallow case depth in the roots of gear teeth is inherent because in conventional carburizing there is a noticeable difference in case depths obtained at the profiles and at the roots. If the case depth in the roots of finer pitch gears can be increased, then the amount of finish grinding stock removal allowed can also be increased thereby reducing the manufacturing costs.

- Plasma carburizing is inherently less expensive since the amount of gas used for carburizing is a fraction of that required in the conventional process and since the overall processing time for equivalent case depths is shorter. Moreover, since parts come out of the plasma carburizing cycle without any scale or oxide, the need for the labor intensive blast-cleaning process now required after conventional carburizing is eliminated.

BHTI has had one test load plasma carburized, by Abar Ipsen Industries, using gear specimens furnished by BHTI. The material was AISI 9310 and the gear geometry was a 7.8 pitch spur gear. The resulting hardness profiles obtained at the approximate pitch diameter and the root center are shown in Figure 35. Figure 36 shows the hardness profiles at the pitch diameter and root center for the same gear geometry using the conventional carburizing method at BHTI. (The normal effective case depth requirement for this pitch gear at BHTI is 0.034 - 0.042. Abar Ipsen was, however, asked to carburize to a shallower case depth of 0.030 - 0.032 since a shallower case depth will tend to show more of a difference in case depths at the profiles and in the roots.) In spite of the shallower overall case depth in the sample that was plasma carburized, a comparison of Figures 35 and 36 clearly show that the root hardness profile for the plasma carburized sample, especially in the high hardness region, is closer to the hardness profile at the pitch diameter.

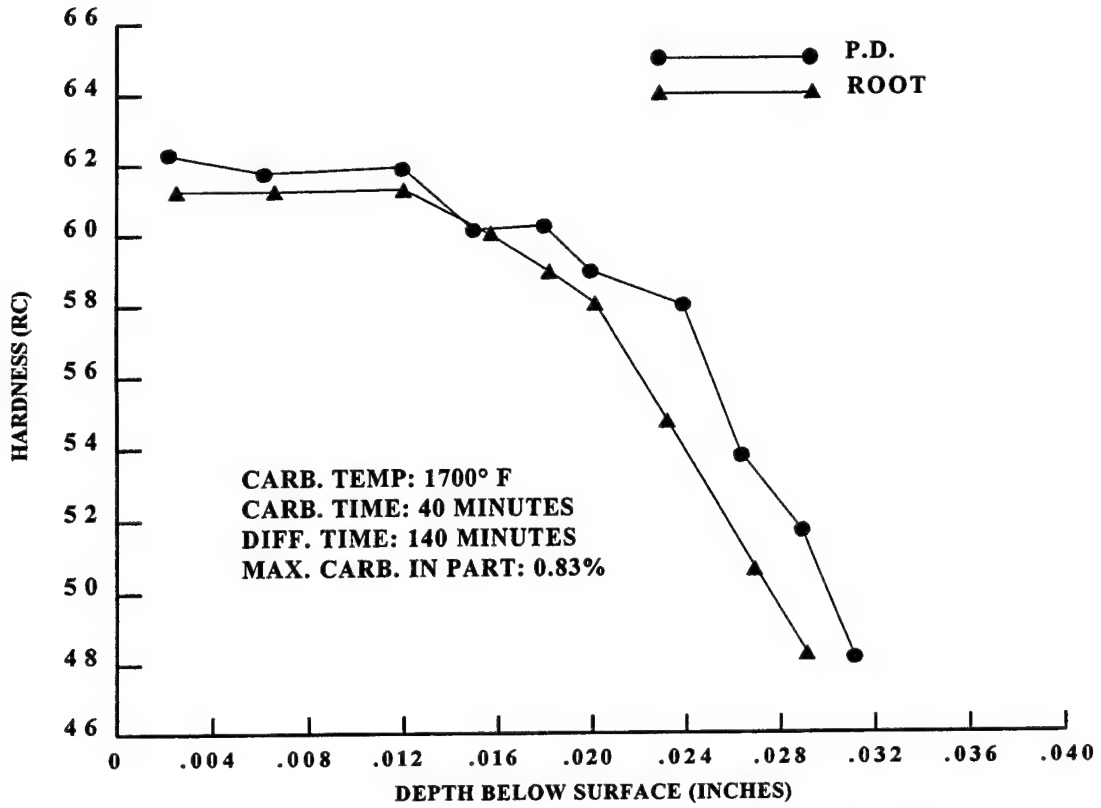

FIGURE 35: HARDNESS PROFILE - PLASMA CARBURIZING

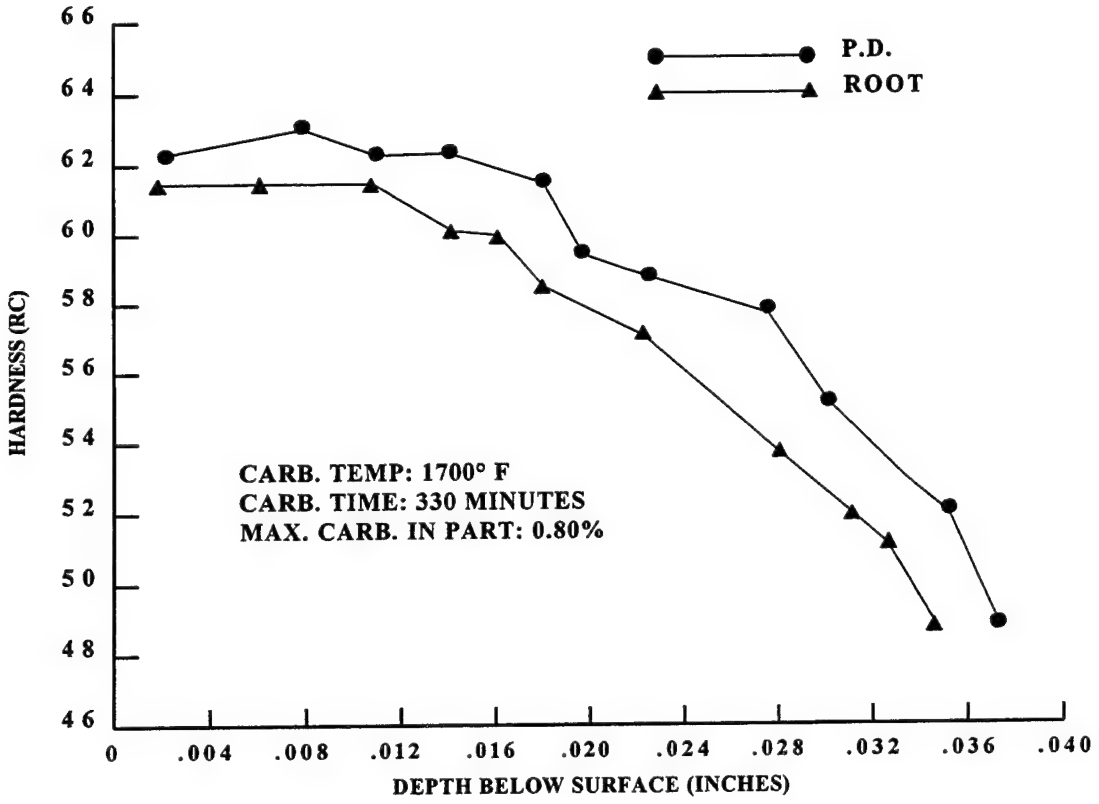

FIGURE 36: HARDNESS PROFILE - GAS CARBURIZING

One of the areas of significance is the Rc60 depth obtained in the root for a certain Rc50 depth at the pitch diameter. Based on BHTI experience, for an effective case depth range of 0.030 - 0.038 at the pitch diameter (which equates to a carburizing time of 5 hours at 1700° F), the average ratio of Rc60 in the root to Rc50 at the pitch diameter is 0.35 with a standard deviation of 0.059. This is based on a total of 144 carburize loads. A calculated normal distribution for this ratio is shown in Figure 37. For the one plasma carburized load processed by BHTI to date, this ratio is 0.52 and is also shown in Figure 37 as a vertical line. Recognizing that this is only one data point, it is still a rather dramatic improvement over conventional carburizing when it is considered that the test load was processed with only a reasonable guess at the required cycle. It is felt that the plasma carburize cycle can probably be adjusted to improve the case properties even more.

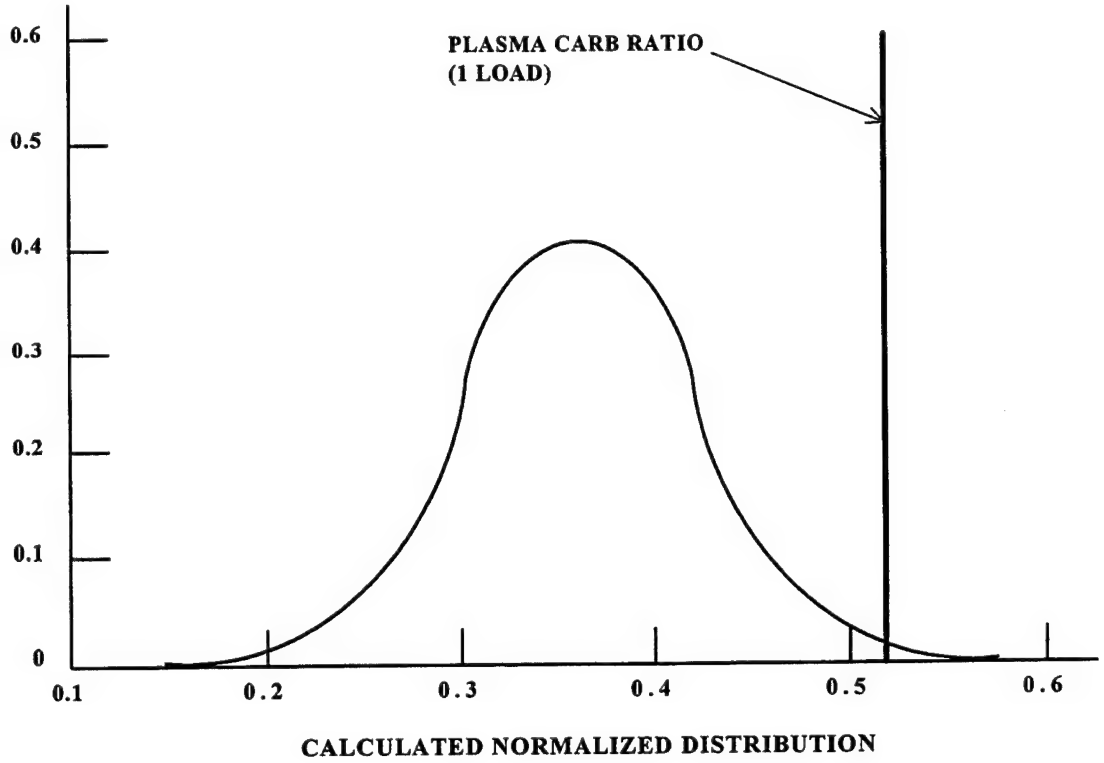

FIGURE 37: RATIO OF Rc60 AT ROOT TO Rc50 AT P.D. (FOR 5 HOUR CARB LOADS)

Additionally, it must be mentioned that the added Rc60 depth in the root was obtained with approximately the same carbon level as obtained on the production conventional carburized loads. The ability to obtain a "better" case in the roots of gear teeth along with its expected residual stress distribution should increase the gear tooth bending fatigue strength. This, of course, will result in some weight reduction of the drive system. To determine the extent of bending strength improvement with this process and to subsequently use plasma carburizing in the FAAV transmission, flexure fatigue tests were conducted with notched coupons. The tests were conducted in conjunction with the precision forging tests and are described in Section 6.3.

4.12.3 SPIRAL BEVEL GEARS

The method of manufacture in conjunction with lightweight aircraft applications has somewhat restricted any appreciable improvements in the noise level and tooth bending fatigue strength of spiral bevel gears. Improvements in these two areas of noise level and strength were achieved by implementing the reduced kinematical error concept [28] and the CNC spiral bevel gear grinder [29] to manufacture spiral bevel gears. The reduced kinematical error concept was used to program the Gleason grinder to grind optimum tooth profiles for increased conjugate action and the CNC Gleason grinder was capable of grinding increased radius tooth roots for increased bending strength.

One of the risks of the zero kinematical error concept is the ability of the gear set to operate under full load in a lightweight nonrigid housing. The deflections of the housing may cause the contact patterns to run-off the teeth heavily.

Three configurations of spiral bevel gear sets were made and tested:

- The baseline OH-58D transmission spiral bevel gear set
- One test configuration identical to the baseline set except with an increased fillet radius
- One test configuration identical to the baseline set except with increased fillet radius and the optimum profile grind derived by Dr. Faydor Litvin of the University of Illinois at Chicago.

These three gear set configurations were tested in an OH-58D transmission to evaluate tooth scoring, pitting, and bending improvements and noise/vibration reductions. Section 6.2 presents the results of the analyses and tests conducted on each spiral bevel set

4.13 SEAL SELECTION

The ART will be designed so that two different types of seals may be used at all seal locations. The two types of seals are spring loaded carbon face seals and magnetic carbon face seals. Seal reliability should be improved because the two seal types selected have an advantage over lip seals due to their ability to function satisfactorily at higher temperatures and at higher operating speeds. Experience at BHTI has shown that seal reliability may decrease in applications where there is marginal lubrication on the seal contact surfaces. To further enhance the service life of the seals, a jet of oil will be directed at each seal to provide positive lubrication of the seal contact surfaces. This is available technology that is used on the V-22 program and should entail virtually no risk to the ART program.

4.14 DIAGNOSTICS

The ART will have diagnostics that will monitor vibration levels and the ferrous debris content of the lubricant for early failure detection. Changes in the vibration signature or in the lubricant debris content will provide indications of an early failure. Provisions will be made during the design of the transmission for the mounting of strategically placed accelerometers to monitor the vibration signature. The transmission will contain magnetic chip detectors of the fuzz-burner type to monitor the lubricant for ferrous debris. In addition the lube system will include a full flow quantitative debris monitor (QDM). This debris monitor keeps track of the number and size of the ferrous particles which interrupt its magnetic flux field and since the full lubricant flow is directed through the monitor, it provides a total picture of the amount and size of ferrous debris being generated in the transmission. As experience is gained, limits will be set for maintenance action or inspection.

4.15 INTEGRATED COMPONENTS

At BHTI, integrated components have been used since the late 1940's on the Model 47 and subsequent transmission designs where the inner raceway of cylindrical roller bearings is integral with the gearshaft. Integration of components reduces the number of parts, reduces the weight, and improves reliability by eliminating the press-fitted surfaces which are a major source of fretting in the transmission. While the initial cost of the integrated components may be higher, the savings on life cycle cost due to fewer replacements for fretting during green run, field maintenance, or overhaul will be far greater.

Unlike roller bearings, integral raceways for ball bearings have not been used at BHTI for contemporary transmission designs. Although not in production, this concept was investigated at BHTI with favorable results on components designed and tested during the Army ATCI program [1].

In the ART, the spiral bevel gears in the tilt axis gearbox and the interconnect output gear shall have ball bearing inner races integral with the gearshafts as shown in Figure 38 in Section 5.0. All gearshafts running on roller bearings shall also have integral roller races. The integral bearing raceways will be double carburized for a deeper case depth so that the gearshaft has the potential to be refurbished if one of the bearings pit out before the gear teeth. By eliminating the clamp-up nut required for the duplex ball bearings and eliminating the press-fitted interface between the bearings and the gearshaft, significant weight improvement will be achieved. MTBR will also be improved due to the elimination of interfaces subject to fretting.

One other item that shall be considered as an integrated component is the integral sun/bull gear shown in Figure 38 in Section 5.0 which eliminates the common splined joint between the sun gear and its mating drive source.

4.16. NOISE IMPROVEMENT DETERMINATION METHODOLOGY

The two primary means to reduce the overall noise generated by a rotorcraft transmission due to the gearmesh generated source noise, are:

1. Change the types of gears used in the transmission. For example replace standard spur gears with high contact ratio spur gears.

2. Modify the gear involute profiles to minimize the gear transmission error of the individual meshes.

As shown in the HCR planetary study in Section 4.1.5, neither of these methods are necessarily detrimental to a lightweight transmission as are some of the other noise reduction techniques such as damping.

The noise level for the SOAT defined in Section 3.2.3 was estimated to be 111 A-wtd. dBA @ 3m and 104 A-wtd. dBA @ 4m based upon the types of gears in the transmission and the maximum input power. These estimates were based on empirical data developed by Opitz et.al. [30]. The major contributors to the noise level are the planetaries which operate in the mesh frequencies most sensitive to the human ear, approximately 1000-2000 hz.

The gear types in the SOAT are standard spur gears (contact ratio less than 2.0), double helical, and spiral bevel. The spur gears in the two planetary assemblies have calculated transmission errors in the 200-400 micro-inch range whereas the double helicals have a maximum transmission error less than 60 micro-inches; transmission error being a strong indicator of relative noise output.

To achieve the 10 dB noise reduction for the ART it was evident that the noise level produced primarily by the planetary assemblies and the spiral bevel mesh had to be reduced. To reduce the noise produced by the planetary, the gears were changed to high contact ratio (contact ratio greater than 2.0) and only one planetary reduction was used instead of two as in the SOAT. A transmission error analysis of a high contact ratio planetary designed for the same power and speed requirements as the SOAT low speed planetary found the transmission error to be 125 micro-inches maximum, substantially less than the 260-360 micro-inches calculated for the SOAT low speed planetary. Also, noise data from Reference [1] indicate that a noise reduction of 10 dB is possible going from a standard spur gear planetary to a high contact ratio planetary. Actual noise levels for the ART high contact ratio planetary were measured during the planetary component tests described in Section 6.1.1.

The remaining gears in the ART are the input helicals and the tilt axis spiral bevel set of which the spiral bevels will be the major noise contributors. The design tooth contact ratio for spiral bevel gears is between 3 and 4. However, for most aircraft type spiral bevel gears, since the transmission housings are lightweight and not very rigid, the loaded gears deflect out of optimum running position and the gear tooth wear patterns run off the edges of the teeth causing undue stress at the edges which are most vulnerable to scoring. For this reason, the gear tooth profiles are modified in a manner similar to spur and helical gears: tooth tip modification and tooth end reliefs. When this is done to spiral bevel gears, the area of the zone of action outside the resultant contact pattern is taken out of action. Thus, the contact ratio of most aircraft spiral bevel gears is less than 3. The calculated modified contact ratio for the OH-58D transmission spiral bevel gears is 2.605.

Vibration surveys on the OH-58A transmission show that the spiral bevel gears run much rougher than the planetary standard spur gears which have a 1.4 contact ratio at the sun-planet mesh. This would indicate that the contact ratio of the spiral bevel gears may be even less than 1.0. However, what is probably happening is that gear tooth conjugate action is not taking place on the spiral bevel gears. Kinematical errors plus gear and housing deflections are being introduced to cause the lack of conjugate action. The reduced kinematical error spiral bevel gears described in Section 4.12.3 will eliminate this problem.

As demonstrated in the tests described in Section 6.2.4 the reduced kinematical error spiral bevel gears yield up to an 18 dB noise level reduction.

Using the same criteria and assumptions as for the SOAT noise estimate, the noise estimate for the preliminary ART shown in Figure 38 in Section 5.0 was 107dBA @ 3m and 104 dBA @ 4m, a 4 dBA overall noise level decrease from the SOAT estimates. It should be noted that these are very broad based estimates and noise level reductions of at least 6 dBA and up to 10 dBA can be expected due to the improvements in the planetary (HCR) and the spiral bevel gear set, the elimination of gears with contact ratios less than 2.0., and because of the reduced number of gear meshes in the ART, 17 instead of 25.

5.0 MISSION ANALYSIS

A study was completed comparing the SOAT with the preliminary ART to determine the impact on mission effectiveness, aerodynamic performance, and operating cost of the lighter, quieter, and increased life ART. Both the SOAT and the ART were analyzed using the same methodology to determine the predicted values of weight, noise, and MTBR.

Based on the results of these analyses and previous tradeoff studies, the proposed Advanced Rotorcraft Transmission (ART), shown in Figure 38 will meet the Army requirements of:

- 25% weight reduction relative to SOAT
- 5000 hour MTBR
- 10 dB noise level reduction relative to SOAT

5.1 PREDICTED WEIGHT

The estimated weight for each transmission was determined from the calculated weights of the gears, the mast, and the bearings sized for each assembly and using the methods of SAWE Paper 1120 [2]. The weight of the ART transmission was reduced for the benefits of a hot running transmission and both transmission weights included only that portion of the mast assembly below the top support case. A breakdown of the component weights for each transmission are listed in Table 34. The substantial weight decrease of the ART cases and housings from the SOAT amount is mainly due to the substitution of WE43 magnesium alloy for the A357 aluminum alloy used for the SOAT cases and housings.

TABLE 34: SUMMARY OF COMPONENT WEIGHTS - SOAT VS. ART COMPONENTS

COMPONENTS	SOAT WT (LBS)	ART WT (LB)	WEIGHT DECREASE
Cases & Housings	427	251	41%
Bearings	33	11	67%
Seals, Spacers, Retainer	18	14	22%
Gears	78	98	-26%
Adapters	2	2	0%
Planetaries	106	63	41%
Lube System	163	123	25%
Freewheeling Unit	12	20	-67%
Hardware	34	25	26%
Spindle	41	41	0%
Torque Drive	3	3	0%
Mast *	21	19	10%
Mast Bearings	12	9	25%
TOTAL	950	679	29%

* Portion of mast weight charged to transmission only.

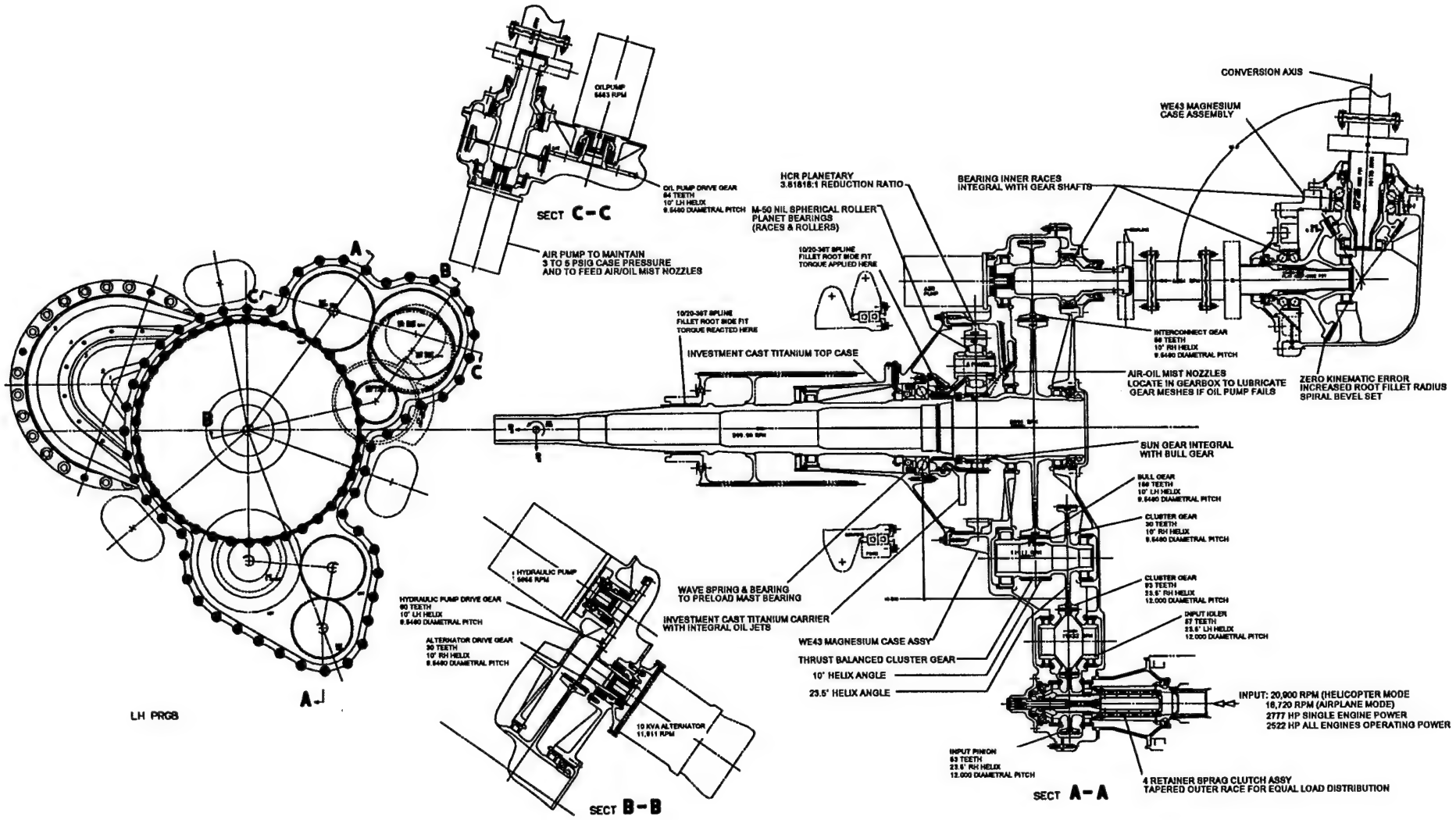

FIGURE 38: ADVANCED ROTORCRAFT TRANSMISSION (ART) - PRELIMINARY DESIGN

5.2 PREDICTED NOISE

Noise estimates for both transmissions were provided based on the gear types utilized (helical, double helical, high contact ratio etc.) and the power requirements. For comparison purposes at 1650 HP the SOAT noise level was estimated to be 102 to 109 dBA and the ART noise level was estimated to be 96 to 104 dBA. Neither of these estimates were factored into any impact on mission effectiveness, aerodynamic performance, or operating cost for the FAAV.

5.3 PREDICTED MTBR

The mean-time-between-removal (MTBR) for both transmissions was calculated using the methodology described in Section 4.8. Unadjusted gear and bearing lives for each transmission were calculated on the basis of the hertz stress and oil film thickness. The oil film thickness was calculated for each gear mesh and bearing at RMC power (approximately 66% power) using MIL-L-23699 oil in the SOAT and DOD-L-85734 oil in the ART. These lives were further adjusted with life adjustment factors as applicable and as explained in the life prediction methodology. The RMC power level is an average power level over the life of the transmission which, if not 100% accurate, is at least sufficient for MTBR comparison.

For the SOAT, the MTBR was calculated for each bearing and gear mesh assuming operation 30% of the time in helicopter mode and 70% of the time in airplane mode with standard lubricant cooling provisions (176° F oil-in temp. in helicopter mode and 154° F oil-in temp. in airplane mode) and a 25 micron oil system filtration. The bearings were analyzed as thru-hardened CEVM 52100 steel and the gears modeled after the same material and manufacturing processes used for the gears in the XV-15 transmission. The double helical input gears, planetary ring gears, and planetary sun gears were made from Nitralloy N alloy steel and nitrided, the planetary pinions were made from 9310 alloy steel and carburized. The MTBR analysis yielded a pitting failure rate for the gears and bearings of 2.4808×10^{-4} failures per hour which when added to the "other failures" failure rate of $.12 \times 10^{-4}$ failures per hour yields a total MTBR of 3845 hours. The major factor contributing to this low MTBR was the low speed sun/planet mesh which because of thin oil film thickness and unhoned sun gear teeth resulted in a combined MTBR for the low speed sun gear and six planets of only 5035 hours.

The MTBR for the ART was also calculated assuming operation 30% of the time in helicopter mode and 70% of the time in airplane mode. However, the gearbox was considered to be a "hot running" transmission with a 211° F oil-in temperature in helicopter mode and 183° F oil-in temperature in airplane mode with a 3 micron oil system filtration. These increased oil-in temperatures of course resulted in thinner oil film thicknesses in the gear and bearing meshes and a subsequent reduction in calculated pitting life. The bearings were analyzed as carburized and hardened VIM VAR M-50 NiL inner races (or X-53 for gears with integral roller races) and the gears as carburized, hardened, shot peened, and honed VIM VAR X-53. The MTBR analysis yielded a pitting failure rate for the gears and bearings of 0.011286×10^{-4} failures per hour which when added to the "other failures" failure rate of $.12 \times 10^{-4}$ failures per hour yields a total MTBR of 76,170 hours. While this figure appears to be excessive when compared with the MTBR calculated for the SOAT, it was derived using the same methodology and is the result of sizing the gears for L_2 useful lives of 10,000 hours and the bearings for L_{10} useful lives of 10,000 hours. It should be noted that the MTBR figure represents the $L_{63.2}$ life of the transmission

5.4 ART BENEFITS

The direct benefits of a lighter more reliable rotorcraft drive system include improved mission effectiveness and aerodynamic performance capabilities and reduced operating and life cycle costs for the transmission

and the aircraft. The improvements of the ART over the SOAT are summarized in Table 35. The cost figures listed in Table 35 were derived using the following ground rules and assumptions:

1. All costs are expressed in government fiscal year (GFY) 1988 dollars.
2. Costs are projected based on the purchase of 600 aircraft with 85% of the aircraft operated.
3. Variance in the development cost is assumed to be minimal between alternatives.
4. Transmission costs were parametrically estimated based on cost relationships with the V-22.
5. Investment costs are based on previous BHTI experience.
6. Direct operating cost (DOC) is estimated on a per aircraft basis.
7. Operating and support costs are based on 420 flight hours per year and 25 years of utilization.
8. Maintainability is assumed unchanged between alternatives.
9. Variance in the military support and indirect support operations costs is assumed minimal between alternatives.
10. Replenishment spares and depot maintenance costs were projected from previous estimates based on changes in production costs and failure rates.
11. Petroleum, oil, and lubricants (POL) were estimated based on JP-4 fuel costs of $1.14 per gal. and weight of 6.5 lbs per gallon.

The column in Table 35 titled "Baseline FAAV" represents the reference aircraft with the baseline SOAT installed. The "ART Improved FAAV" column in Table 35 represents the reference airframe with the ART installed. This aircraft will fly the same mission requirements as the Baseline FAAV and because of its resultant lighter gross weight will also have an increased vertical rate of climb. The last column in Table 35, "Downsize FAAV With ART" represents the full benefits of a cascaded weight reduction for the airframe and drive system due to the lighter ART. This aircraft will also fly the same mission requirements as the baseline FAAV and because the engine power requirements were also "cascaded" to a lower amount, it will also have the same vertical rate of climb as the baseline FAAV. A weight reduction cascade results from the fact that a lighter smaller drive system requires less airframe support structure and the resultant reduction in the total aircraft weight allows an even smaller sized drive system (including engine).

TABLE 35: REFERENCE AIRCRAFT COST AND WEIGHT COMPARISON

	BASELINE FAAV	ART IMPROVED FAAV	DOWNSIZE FAAV WITH ART
TRANSMISSION WT (LB)	950	679	655
A/C EMPTY WT (LB)	11,174	10,672	10,472
A/C GROSS WT (LB)	17,303	16,765	16,499
TRANSMISSION ACQUISITION COST ($ PER UNIT)	381	289	279
A/C ACQUISITION COST ($ PER UNIT)	11,246	11,014	10,844
TRANSMISSION DIRECT OPERATING COST ($ PER FLIGHT HOUR PER UNIT)	0.139	0.116	0.113
A/C DIRECT OPERATING COST ($ PER FLIGHT HOUR PER UNIT)	0.599	0.588	0.582
TRANSMISSION FLEET LIFE CYCLE COST (TOTAL $)	883,581	698,015	678,415
A/C FLEET LIFE CYCLE COST (TOTAL $)	13,847,110	13,649,539	13,514,494

* DOLLARS IN THOUSANDS

6.0 COMPONENT VERIFICATION TESTS

Several high risk technologies were selected from the ART preliminary design for design verification and development tests. These tests included the following component and coupon tests:

- Sequential meshing high contact ratio planetary with cantilevered support posts
- Thin dense chrome plated M50-NiL double and single row spherical roller planetary bearings
- Reduced kinematic error and increased bending strength spiral bevel gears
- Flexure fatigue tests of precision forged coupons simulating precision forged gear teeth
- Flexure fatigue tests of plasma carburized coupons simulating plasma carburized gear teeth
- High temperature WE43 magnesium housing and coupon corrosion tests

The tests conducted and the results are described in the following sections.

6.1 HIGH CONTACT RATIO PLANETARY TESTS

A single stage planetary system was chosen for the ART as shown in Figure 38. This is a simple epicyclic planetary utilizing the following technology:

- High Contact Ratio (HCR) Spur Gears

- X-53 Gear Steel for Sun Gear and Planets

- Nitralloy-N Gear Steel for Ring Gear

- Positive Oiling to Sun/Planet Meshes and Planet Bearings

- Supplemental Air-Oil Mist Lubrication for Loss-of-Lube Operation

- Spherical Roller Planet Bearings; Double or Single Row

- Carburized M50-NiL Planet Bearing Inner Races and Rollers

- Thin Dense Chrome (TDC) Plated Planet Bearing Inner and Outer Races

- Oil-in Temperature of 284° F Maximum

- Oil per DOD-L-85734

- Advanced Surface Coatings to Eliminate Fretting and Galling on the Titanium Carrier

The ART planetary is a dropped-tooth design. Two teeth are dropped from the planet pinions and the original overall dimension of the ring gear remains unchanged. This procedure allows 6 planets to fit within an envelope where normally only five 5 would fit providing an additional load path for increased tooth scoring resistance. The overall planetary ratio remains the same since the planet pinions are idlers and the ring/planet meshes become full recess action. The designed reduction ratio is 3.818181 to 1.

The planetary is also a sequential mesh design whereas the state-of-the-art planetaries were a simultaneous mesh design. If the number of teeth in the sun gear divided by the number of planets is an integer, then the

mesh is simultaneous, and each sun/planet mesh is occurring at the same point in each mesh at the same time; i.e. if one sun/planet mesh is at the highest point of single tooth contact (for a planetary with a tooth contact ratio less than 2) then all of the sun/planet meshes are at the highest point of single tooth contact. If the number of teeth in the sun gear divided by the number of planets is not an integer, then the mesh is sequential as is the case for the ART planetary with 55 teeth on the sun gear and 6 planets (55/6 = 9.1667).

The ART planetary is a fully phased sequential mesh with each sun/planet mesh 1/6th out of phase with the adjacent mesh. The sequential mesh planetary is less likely to generate harmful vibrations because the load impulses on the sun gear are reduced since the teeth on each planet engage the sun teeth at different times instead of simultaneously. For this same reason it can be argued that the sequential mesh planetary will produce lower noise levels than the simultaneous design. Also, the sun gear tooth meshing frequency is increased by a multiplicative factor equal to the number of planets. This may or may not be beneficial depending on the natural frequencies of the surrounding mechanisms.

Figure 39 shows a cross section of the ART planetary and Table 36 lists the basic design data. The planetary is rated at 2444 HP (100% power) at 600 rpm output for continuous operation with the capability of 1.2 X 2444 = 2933 HP for transient load conditions.

TABLE 36: BASIC DESIGN DATA FOR ART PLANETARY

	SUN	PLANET-SUN	PLANET-RING	RING
NUMBER OF TEETH	55	48		155
DIAMETRAL PITCH, IN^{-1}	11.000000	11.000000	11.427185	11.427185
PRESSURE ANGLE, DEG	20.0000	20.0000	12.5292	12.5292
PITCH DIA, IN	5.0000	4.3636	4.2005	13.5641
OD or ID, IN	5.241	4.609		13.560
ROOT DIA, IN	4.695	4.062		14.033
FACE WIDTH, IN	1.690	1.57O		1.570
TOP LAND WIDTH, IN	0.036	0.036		0.081
TOOTH THICKNESS, IN	0.1359	0.1397		0.1922 (space width)
CENTER DISTANCE, IN	4.6818			
CONTACT RATIO	2.28			
NUMBER OF PLANETS	6			

The ART planetary is lubricated via oil pressure passages and integral oil jets in the planet carrier. The oil is fed to the carrier at 80 PSI from the main housing through an annular passage sealed by two hydraulic rings as shown in Figure 39. Twelve .018" diameter oil jet holes provide a total of approximately .70 gpm of oil to the gear meshes. These jet orifices are oriented to provide the maximum impingement depth into the sun gear tooth spaces. An additional twelve .021" diameter holes provide a total of approximately 1.0 gpm of oil to the single row spherical roller planet bearings. For the double row spherical bearings, six .028" diameter holes provide a total of approximately 0.9 gpm of oil. The supplemental air/oil mist lubrication system shown in Figure 41 not only provides lubrication during loss-of-lube operation but operates continuously along with the primary lube system during normal operation.

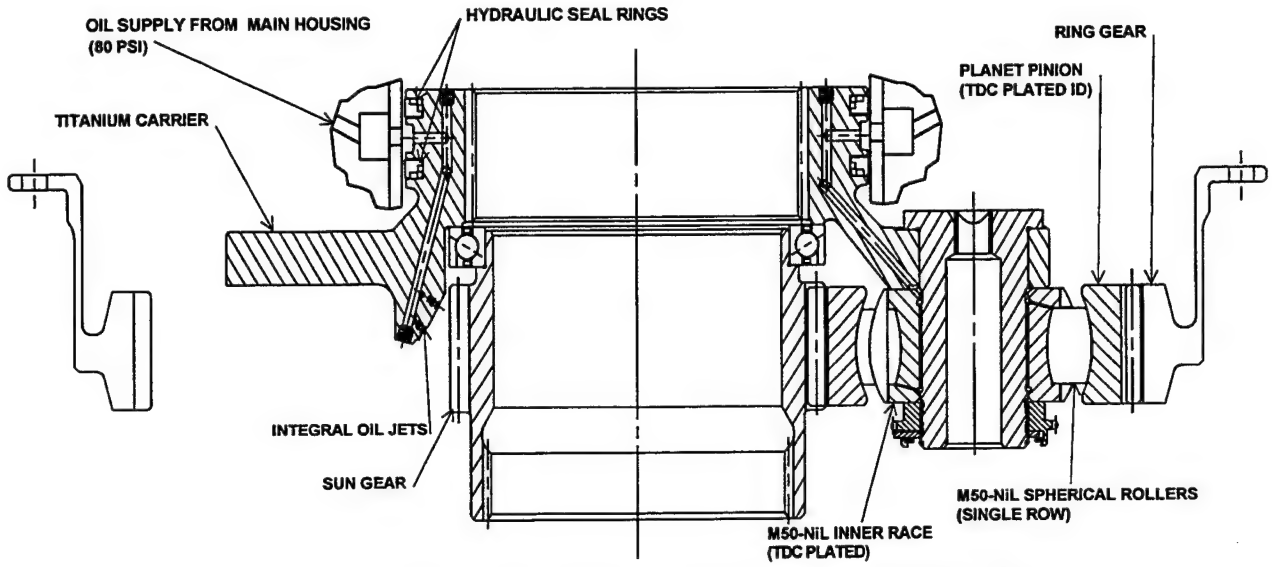

a) PLANETARY ASSEMBLY WITH SINGLE ROW SPHERICAL ROLLER PLANET BEARINGS

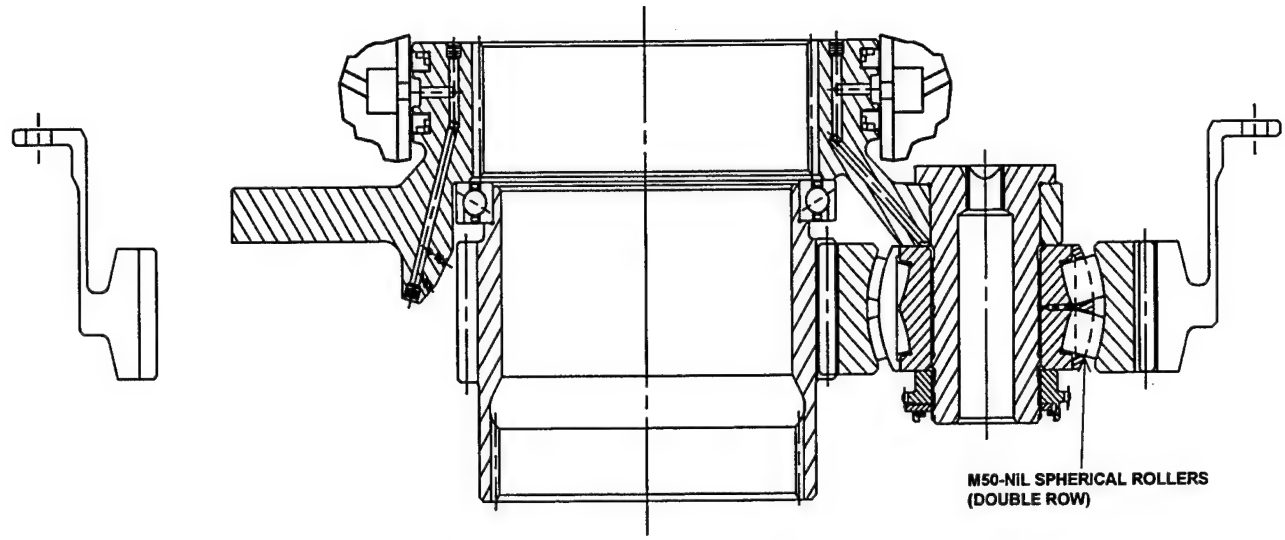

b) PLANETARY ASSEMBLY WITH DOUBLE ROW SPHERICAL ROLLER PLANET BEARINGS

FIGURE 39: ART PLANETARY ASSEMBLY

All of the planetary tests were conducted in the planetary test stand shown in Figures 40 and 41. The stand is an existing back-to-back regenerative rig which was modified to test the ART planetary up to 750,418 in-lb of torque at 600 rpm of the carrier (7144 HP). The test assembly is loaded by hydraulically rotating the two ring gears relative to each other via loading plates. The planetary in the slave (lower) section, although operating upside down, is loaded on the proper sides of the teeth but the direction of rotation is opposite that of the planetary in the test (upper section). A free body diagram of the test assembly is shown in Figure 42.

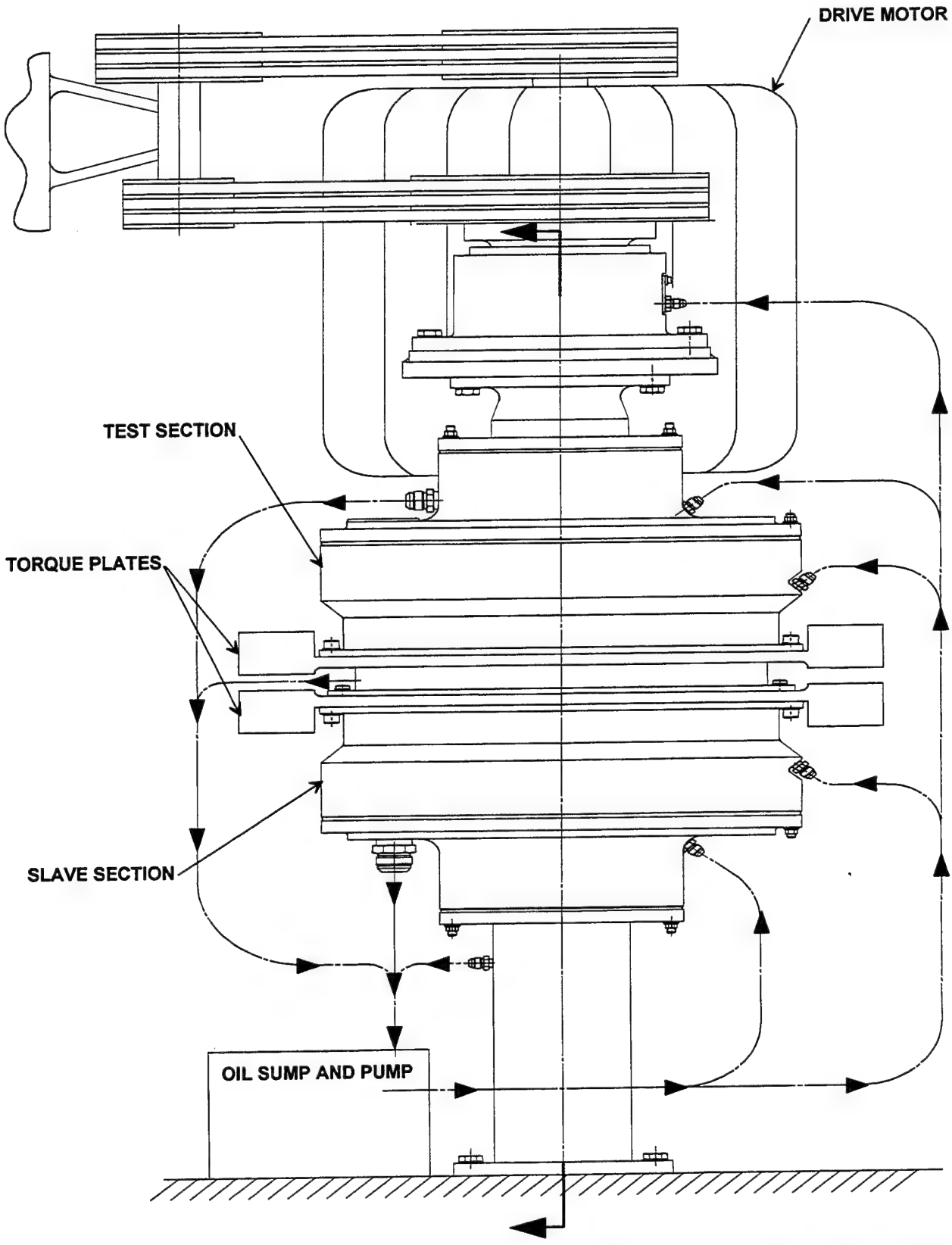

FIGURE 40: ART PLANETARY TEST STAND SCHEMATIC (CROSS SECTION SHOWN IN FIGURE 41)

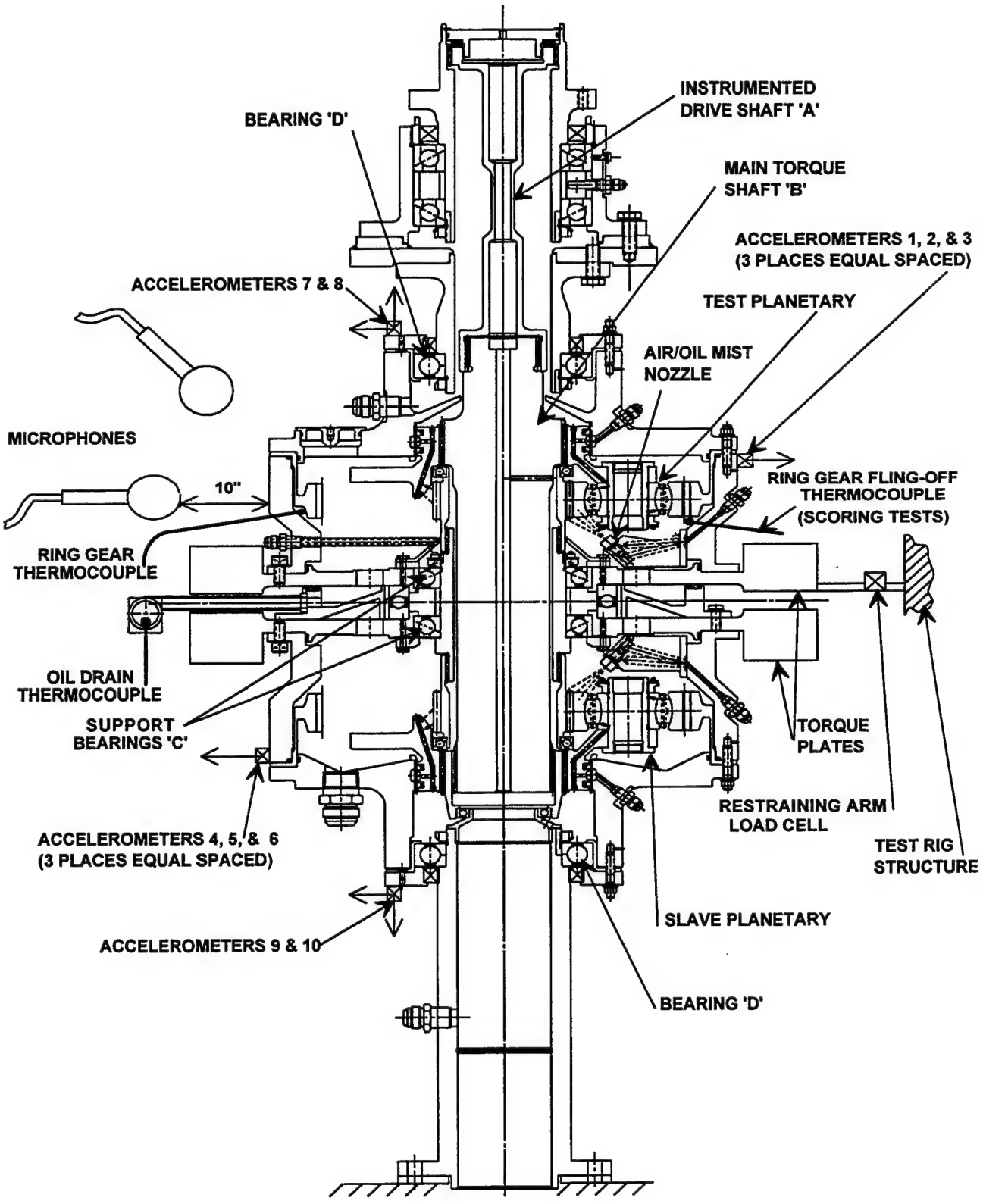

FIGURE 41: ART PLANETARY TEST ASSEMBLY & INSTRUMENTATION

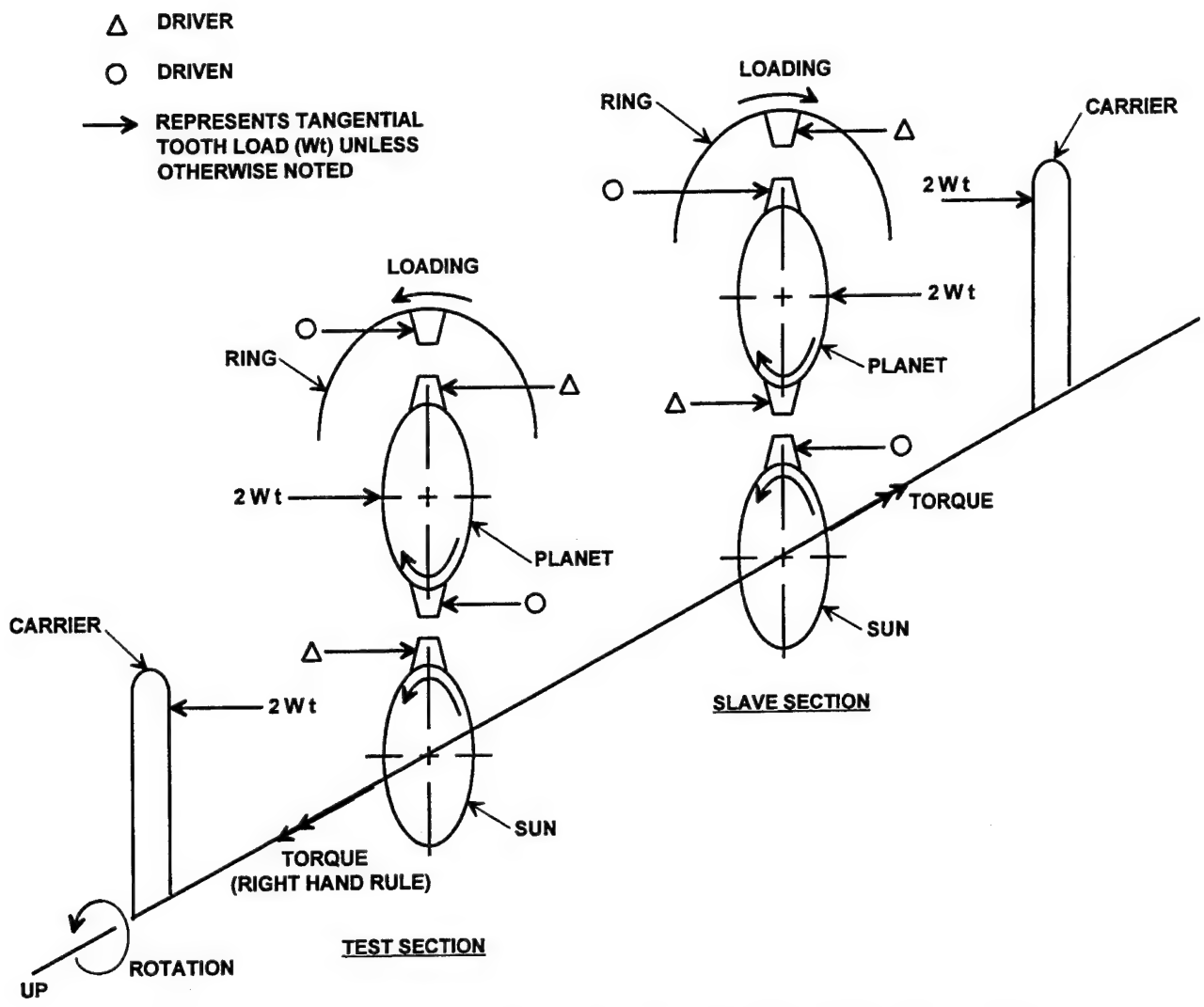

FIGURE 42: ART PLANETARY TEST ASSEMBLY FREE-BODY DIAGRAM

6.1.1 PLANETARY NOISE AND VIBRATION MEASUREMENTS

The first test conducted on the ART planetary was a noise and vibration survey. The objective of this test was to measure and record the sound pressure and vibration levels produced by the planetary operating at 480 and 600 rpm output speed at 3 torque levels, 75%, 100% and 125%. The data was collected for comparison with the noise and vibration data measured for the XV-15 planetary which was tested in the Advanced Transmission Components Investigation [1]. The primary differences between the two planetaries are tooth contact ratio and type of mesh:

	ART	XV-15
Tooth Contact Ratio	2.28 (HCR)	1.49 (STD)
Type of Mesh	Sequential	Simultaneous

The ART planetary was expected to run quieter and with lower vibration levels than the XV-15 planetary because of the higher tooth contact ratio and because it is a sequential design.

The noise and vibration measurements were made on separate tape recorders, direct record for the noise measurements and FM for the vibration measurements. A common sound data channel was recorded on each tape recorder to allow synchronization between the noise and vibration data recorded. For the noise measurements, two microphones were located near the test section of the planetary test rig as shown in Figure 41, one in plane and one 45° out of plane. The microphone positioned in the horizontal plane is similar to the location of the microphone used during the XV-15 planetary noise measurements. The vibration data was recorded with the eight radial and two axial accelerometers located as shown in Figure 41.

The noise and vibration test steps for the HCR planetary were conducted in the order listed in Table 37. Figures 43 thru 48 are plots of the vibration levels at each test step measured with a radial accelerometer attached to the test section of the housing as shown in Figure 41. The plots labeled (a) are data recorded within 10 minutes after the beginning of each step, and the plots labeled (b) are data recorded within 10 minutes before the end of each step. Figure 49 presents a summary of the changes in vibration amplitude from step to step for the 1st 6 gear mesh harmonics of the sun/planet gear mesh. The fundamental frequency is 1240 Hz for steps 1 thru 3 and 1550 Hz for steps 4 thru 6.

TABLE 37: HCR PLANETARY NOISE AND VIBRATION TEST SCHEDULE

STEP	PERCENT LOAD	INPUT SPEED (RPM)	INPUT TORQUE (IN-LB)	POWER (HP) REF	RUN TIME (HR)
1	75	480	192,531	1,466	1.0
2	100	480	256,709	1,955	1.0
3	125	480	320,895	2,443	1.0
4	75	600	192,531	1,833	1.0
5	100	600	256,709	2,444	1.0
6	125	600	320,895	3,055	1.0

Figures 50 and 51 are plots of the measured vibration levels at 125% torque for the ATCI HCR planetary and standard planetary respectively, tested under the ATCI program [1]. The ATCI planetary was designed to transmit 1460 HP at 565 RPM in helicopter mode, and the fundamental frequency of the sun/planet meshes is 1300 Hz for both planetaries.

The vibration levels in the 0 to 5000 Hz frequency range for the ART planetary shown in Figure 48 compare favorably to the vibration levels for the ATCI HCR planetary (Figure 50) especially when considering that the ART planetary is transmitting 67% more power than the ATCI planetary. As compared to the ATCI standard planetary (Figure 51) the ART planetary vibration levels are significantly lower as expected.

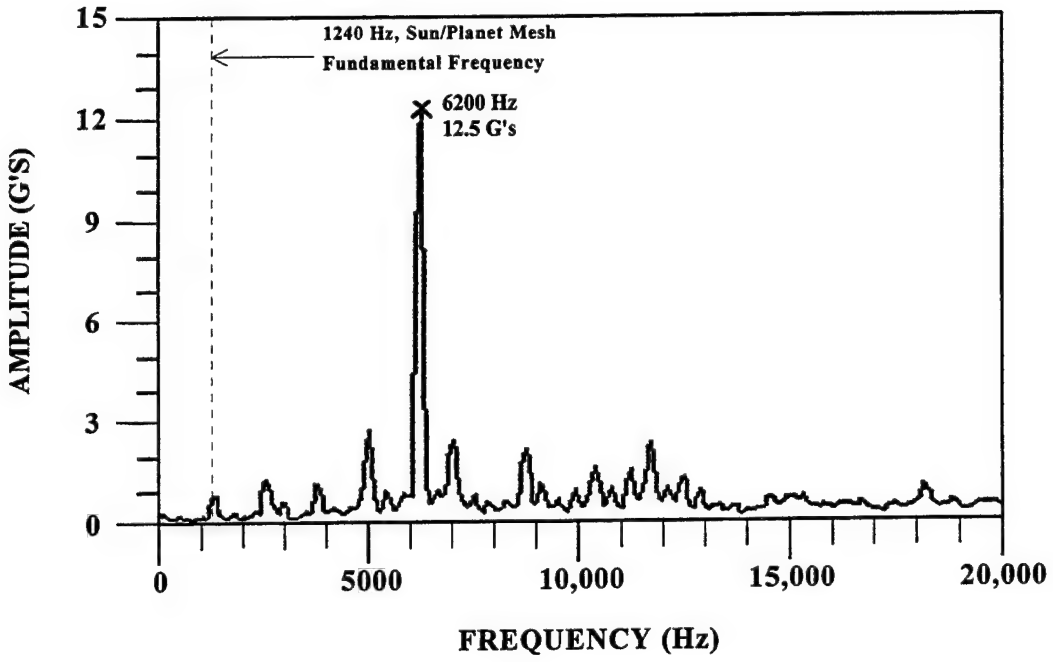

(a) Recorded approx. 10 min after start of step

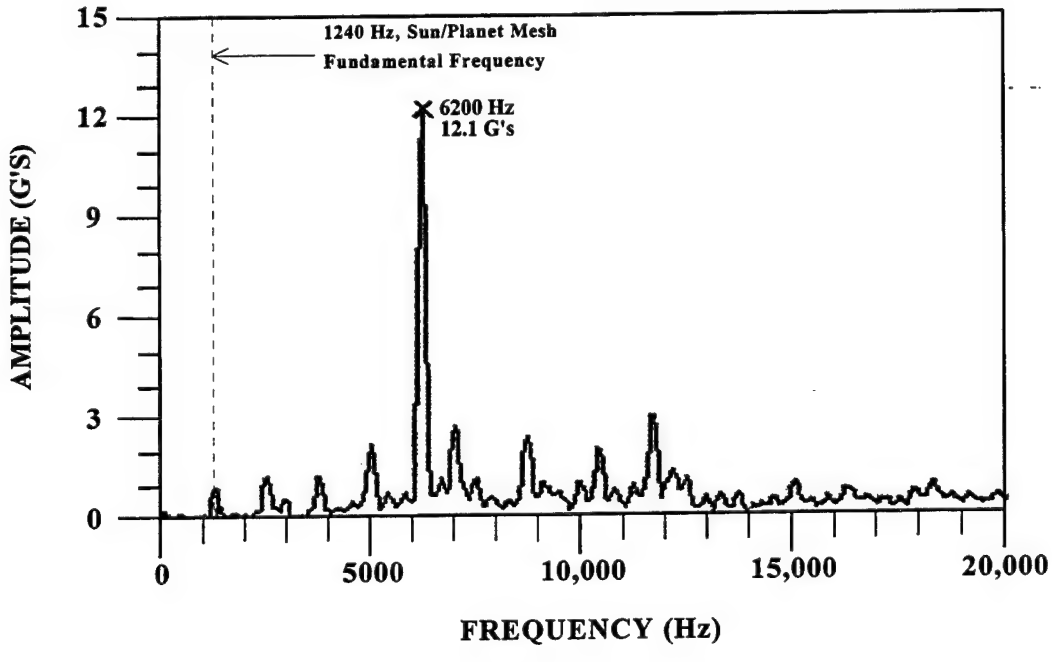

(b) Recorded approx. 10 min before end of step

FIGURE 43: ART HCR PLANETARY STEP 1 VIBRATION DATA - 75% TORQUE, 480 RPM

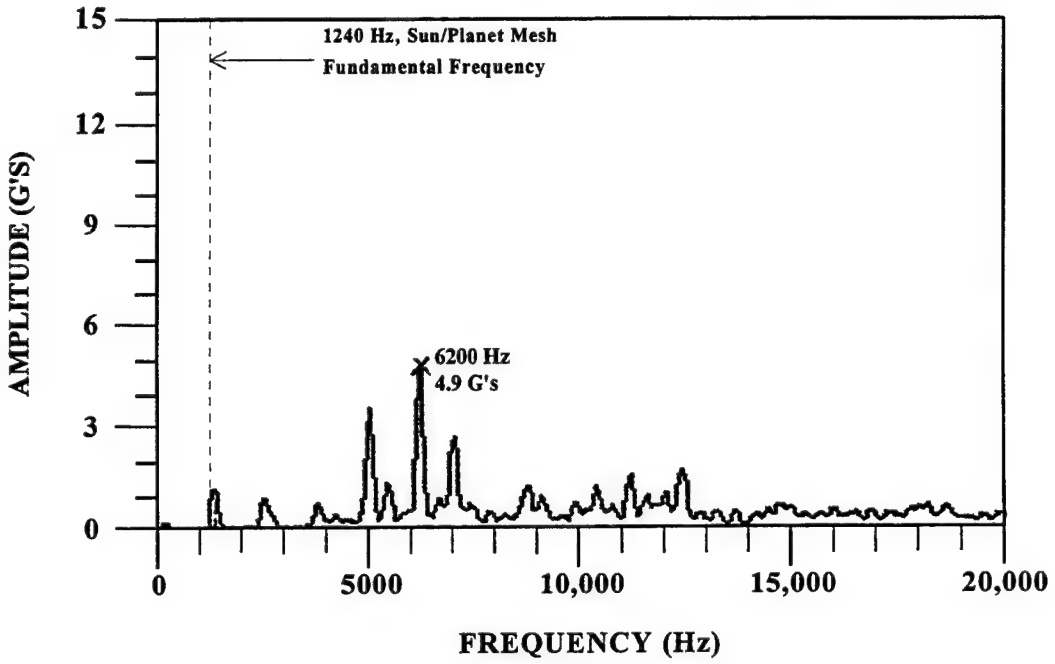

(a) Recorded approx. 10 min after start of step

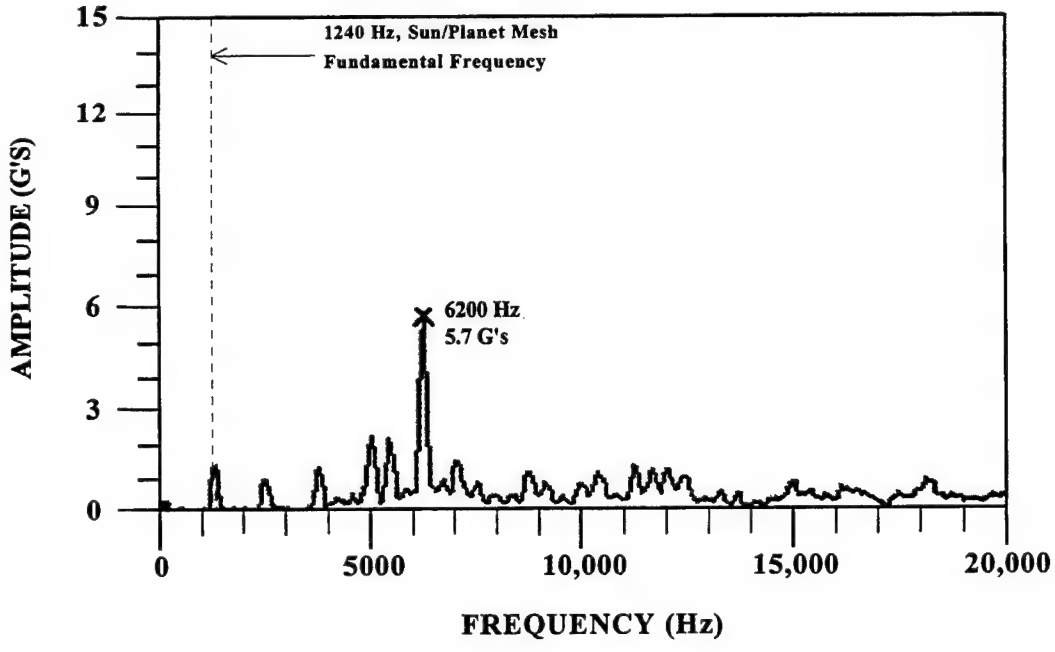

(b) Recorded approx. 10 min before end of step

FIGURE 44: ART HCR PLANETARY STEP 2 VIBRATION DATA - 100% TORQUE, 480 RPM

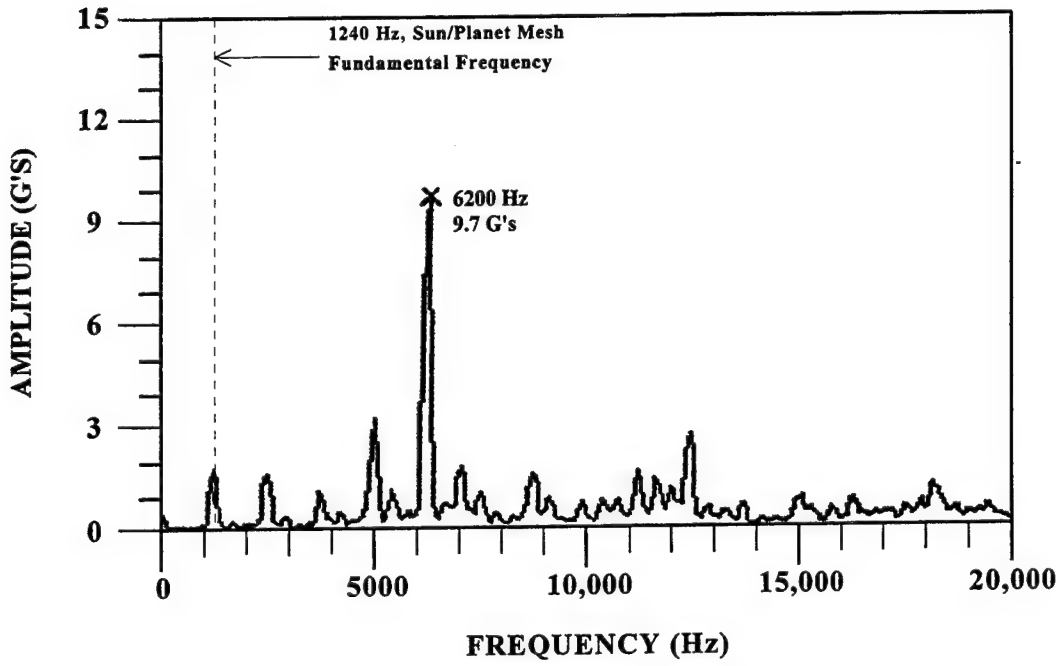

(a) Recorded approx. 10 min after start of step

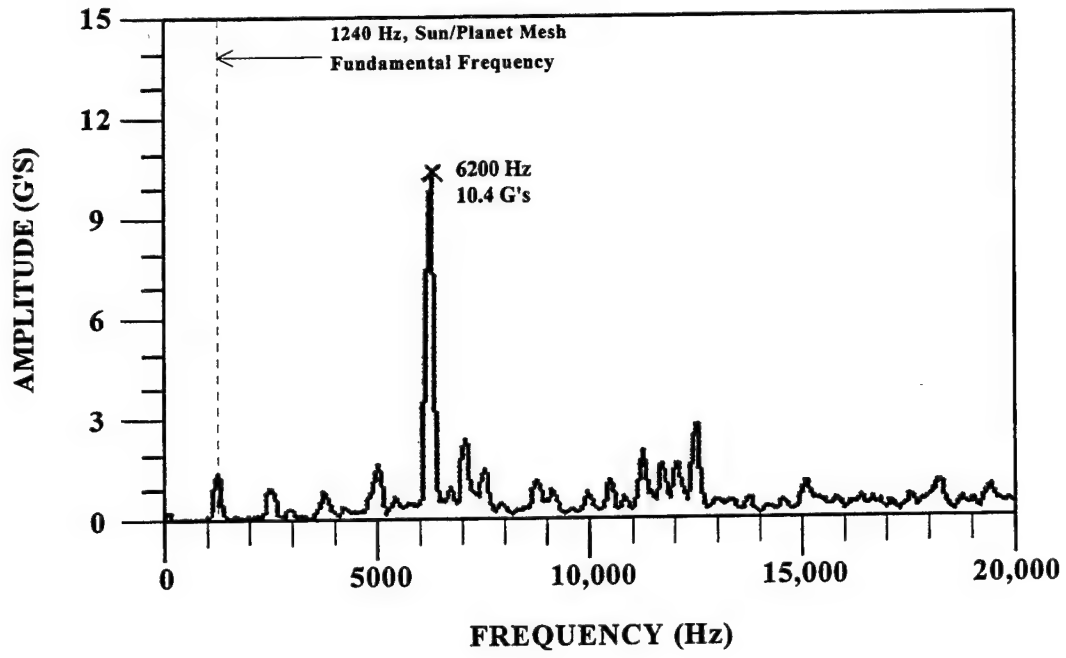

(b) Recorded approx. 10 min before end of step

FIGURE 45: ART HCR PLANETARY STEP 3 VIBRATION DATA - 125% TORQUE, 480 RPM

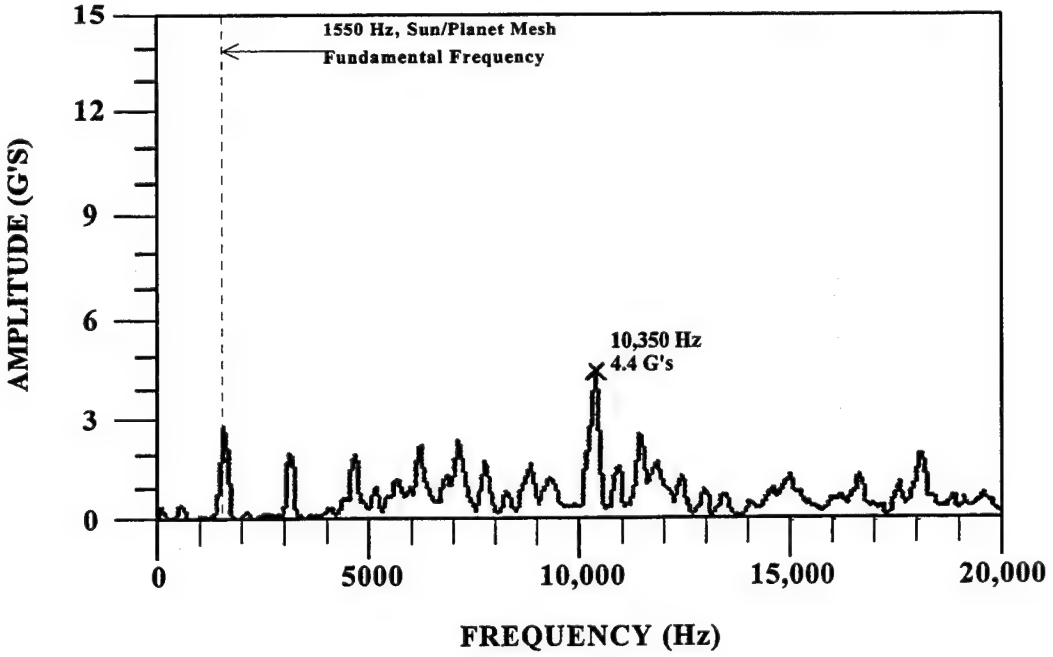

(a) Recorded approx. 10 min after start of step

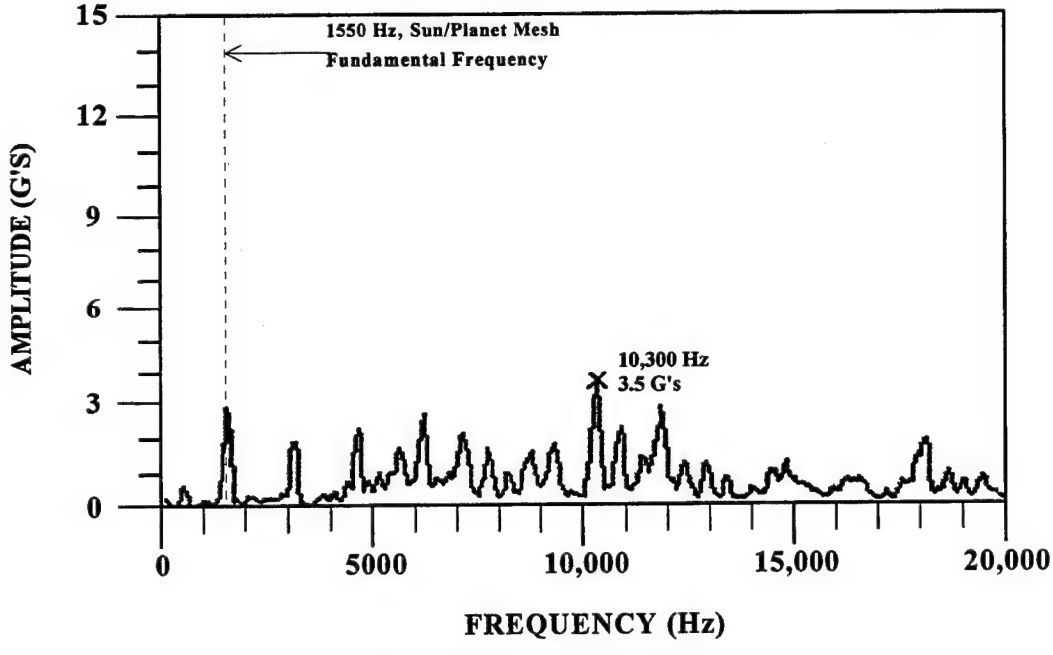

(b) Recorded approx. 10 min before end of step

FIGURE 46: ART HCR PLANETARY STEP 4 VIBRATION DATA - 75% TORQUE, 600 RPM

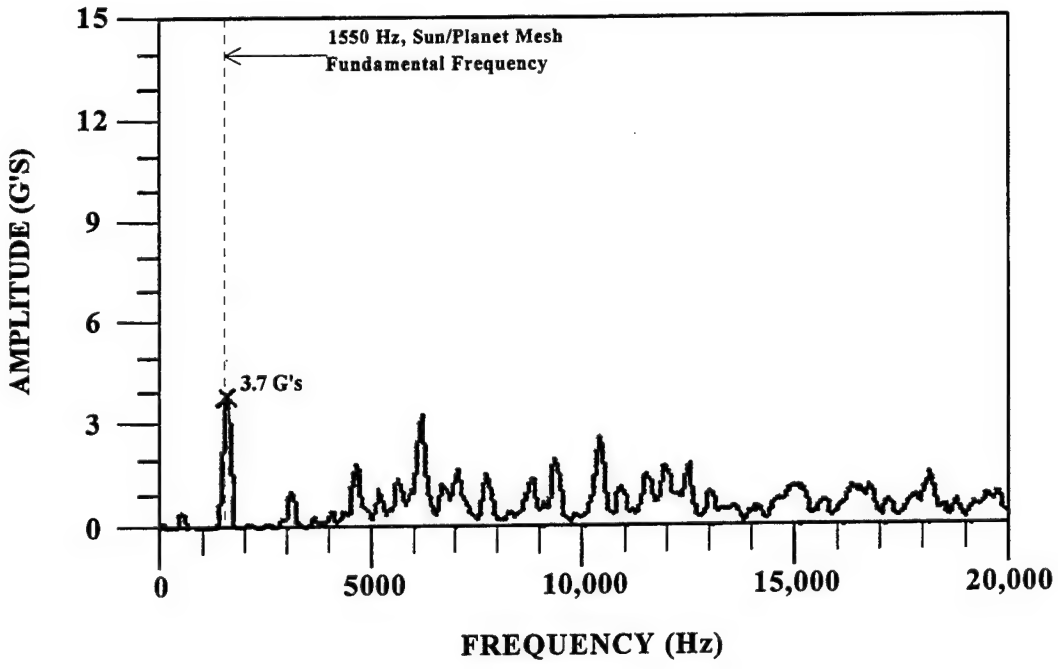

(a) Recorded approx. 10 min after start of step

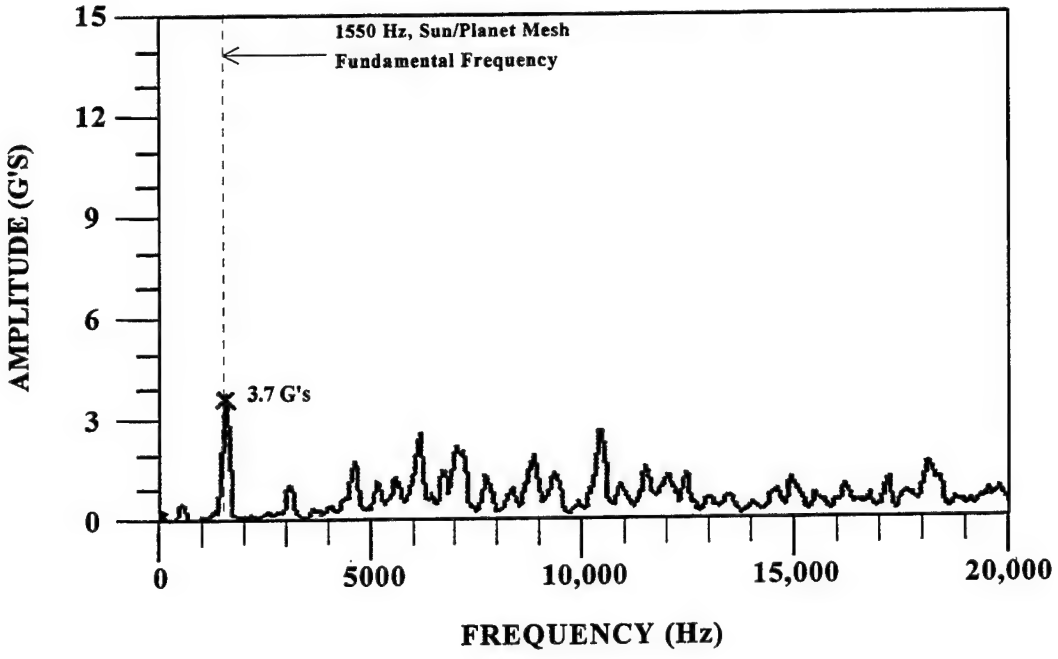

(b) Recorded approx. 10 min before end of step

FIGURE 47: ART HCR PLANETARY STEP 5 VIBRATION DATA - 100% TORQUE, 600 RPM

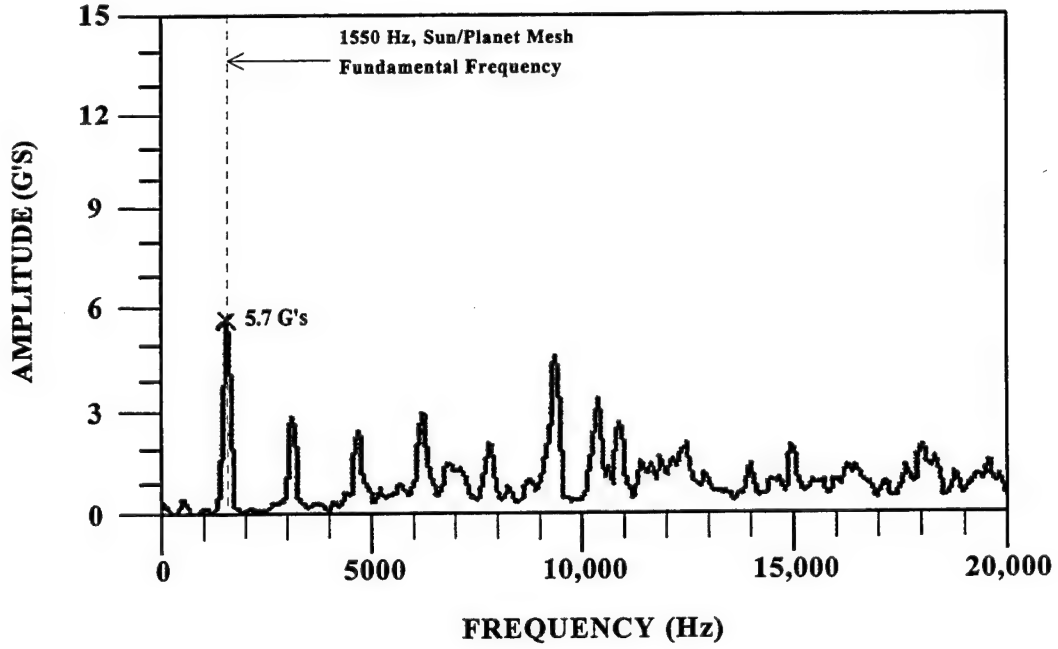

(a) Recorded approx. 10 min after start of step

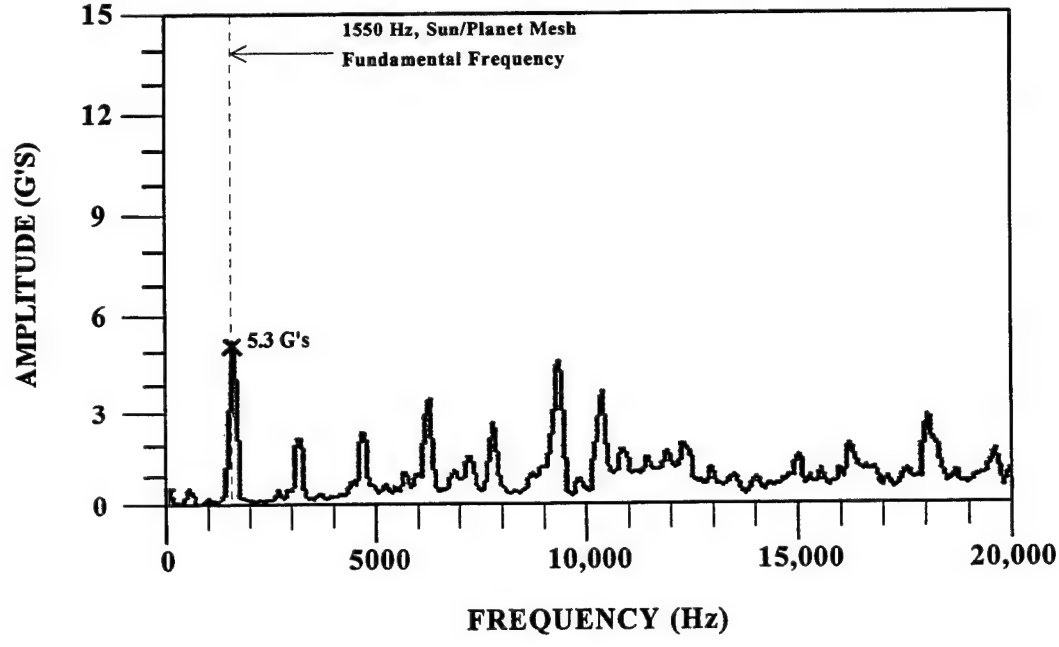

(b) Recorded approx. 10 min before end of step

FIGURE 48: ART HCR PLANETARY STEP 6 VIBRATION DATA - 125% TORQUE, 600 RPM

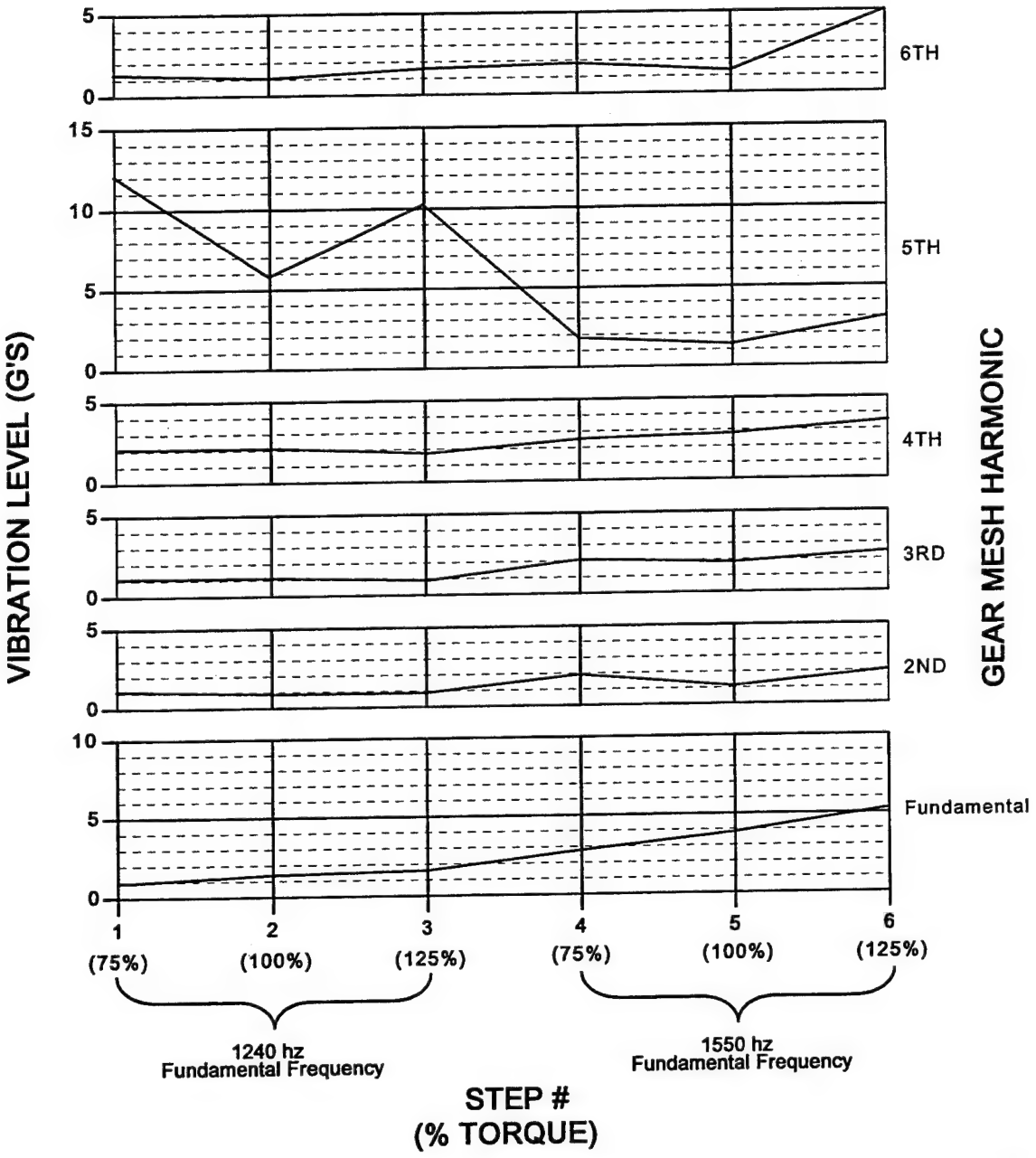

FIGURE 49: ART HCR SUN/PLANET GEAR MESH HARMONICS VIBRATION AMPLITUDE SUMMARY

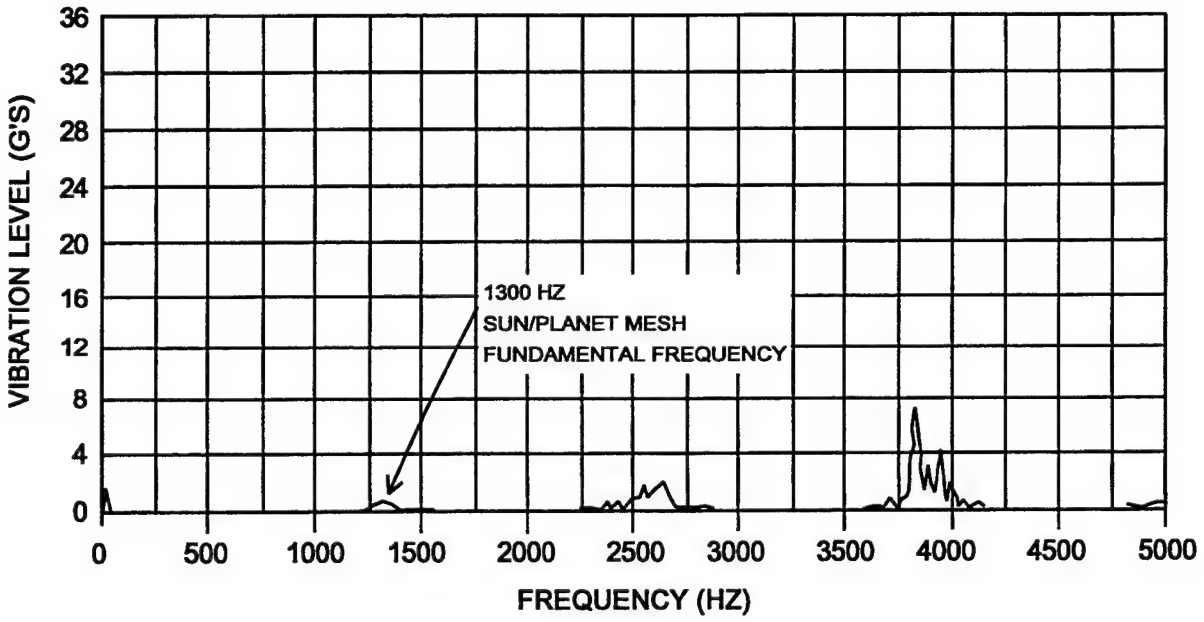

FIGURE 50: VIBRATION LEVELS OF ATCI HCR PLANETARY @ 125% TORQUE & 565 RPM

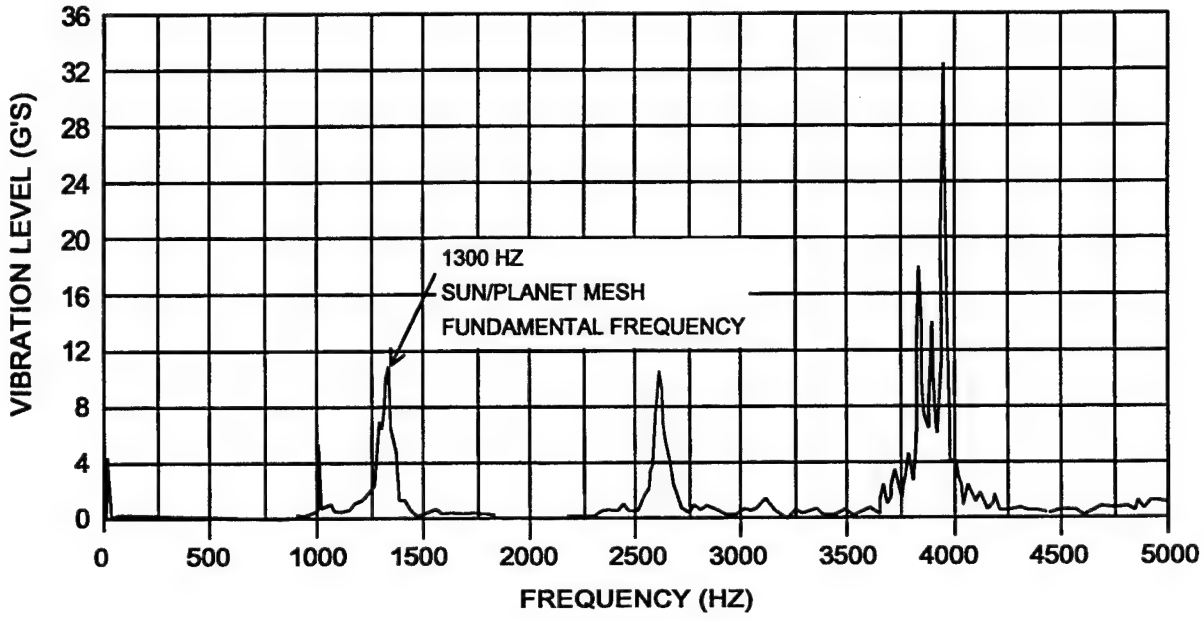

FIGURE 51: VIBRATION LEVELS OF ATCI STD PLANETARY @ 125% TORQUE & 565 RPM

Figures 52 thru 57 are plots of the noise levels at each test step measured with microphones located near the test section housing as shown in Figure 41. The plots presented are from the microphone in the horizontal orientation which measured the highest noise levels. The plots labeled (a) are data recorded within 10 minutes after the beginning of each step, and the plots labeled (b) are data recorded within 10 minutes before the end of each step. Figure 58 presents a summary of the changes in noise amplitude from step to step for the fundamental frequency of the sun/planet gear mesh. The fundamental frequency is 1240 Hz for steps 1 thru 3 and 1550 Hz for steps 4 thru 6.

Figure 59 is a plot comparing the sound pressure level of the sun/planet mesh fundamental frequency and 1st two harmonics for the ART HCR planetary with the HCR planetary and standard planetaries tested under the ATCI program [1]. The ATCI planetaries were designed to transmit 1460 HP at 565 RPM in helicopter mode with a fundamental frequency of the sun/planet mesh of 1300 Hz for both planetaries.

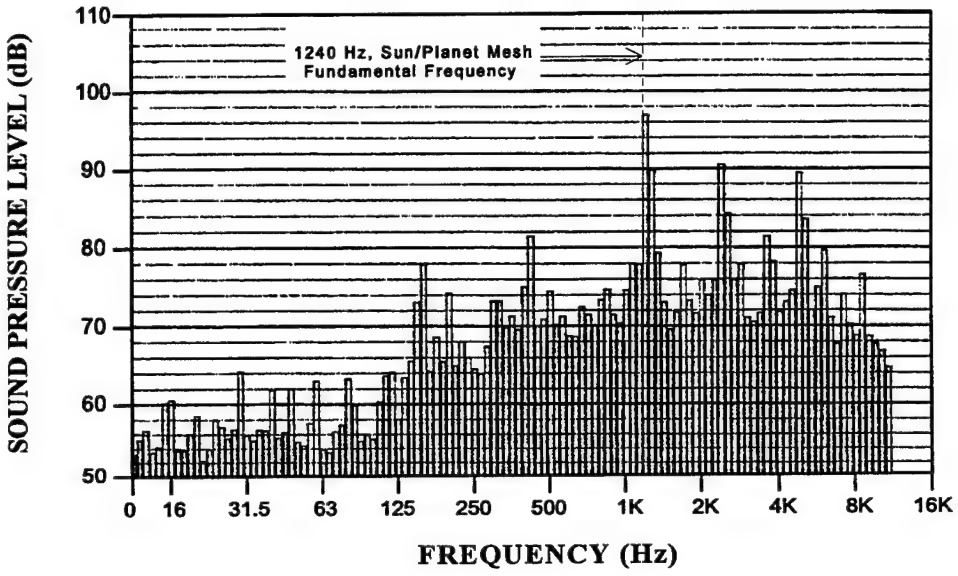

(a) Recorded approx. 10 min after start of step

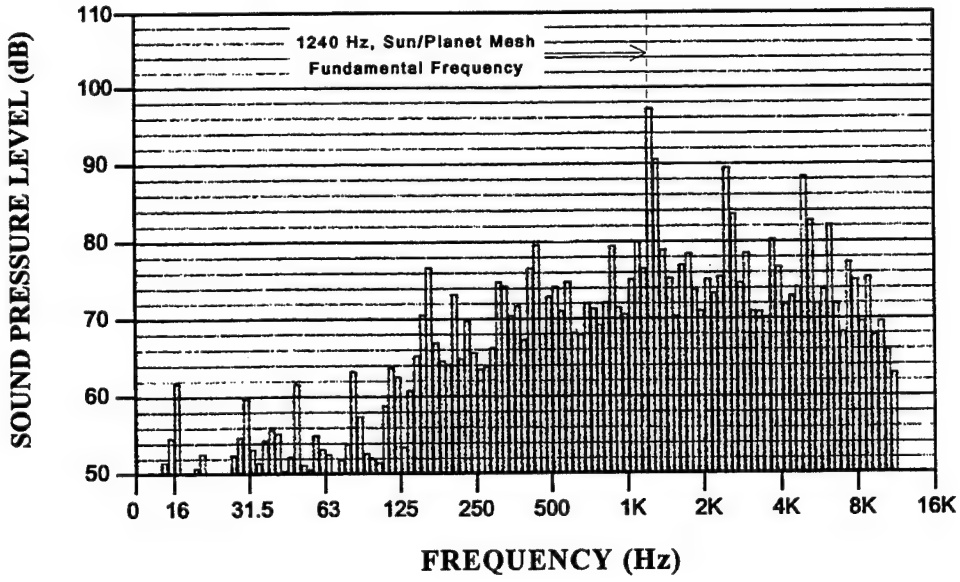

(b) Recorded approx. 10 min before end of step

FIGURE 52: ART HCR PLANETARY STEP 1 NOISE DATA - 75% TORQUE, 480 RPM

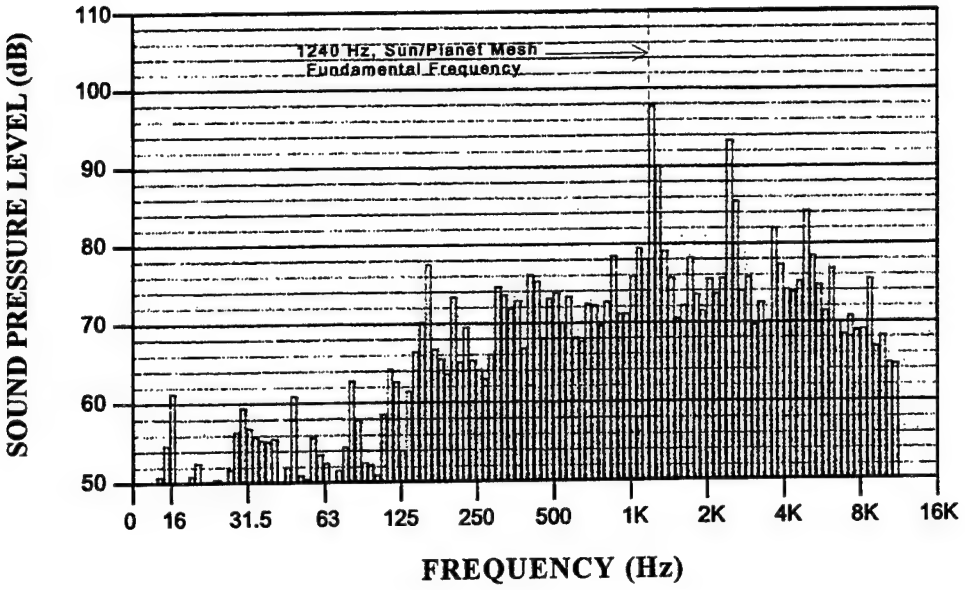

(a) Recorded approx. 10 min after start of step

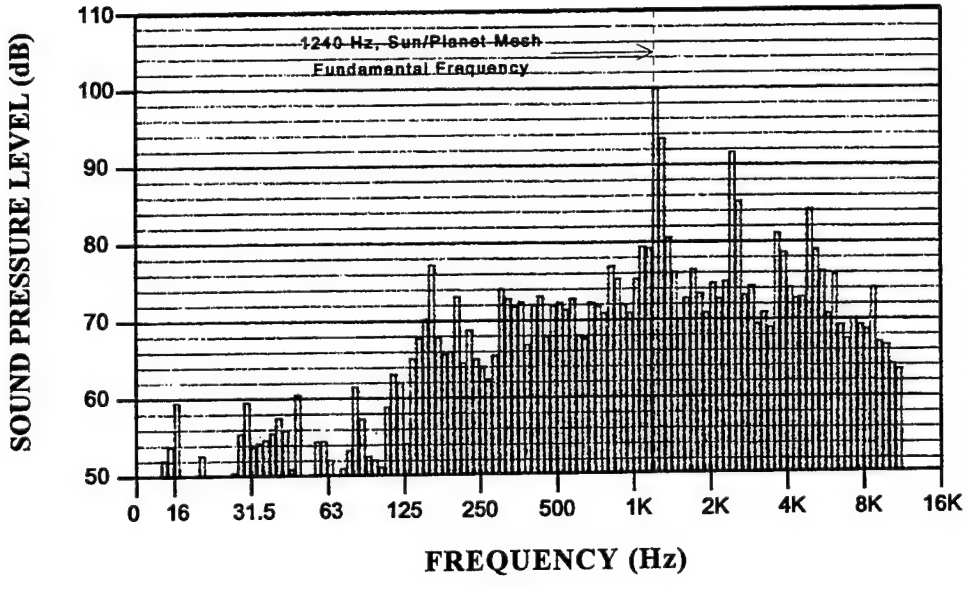

(b) Recorded approx. 10 min before end of step

FIGURE 53: ART HCR PLANETARY STEP 2 NOISE DATA - 100% TORQUE, 480 RPM

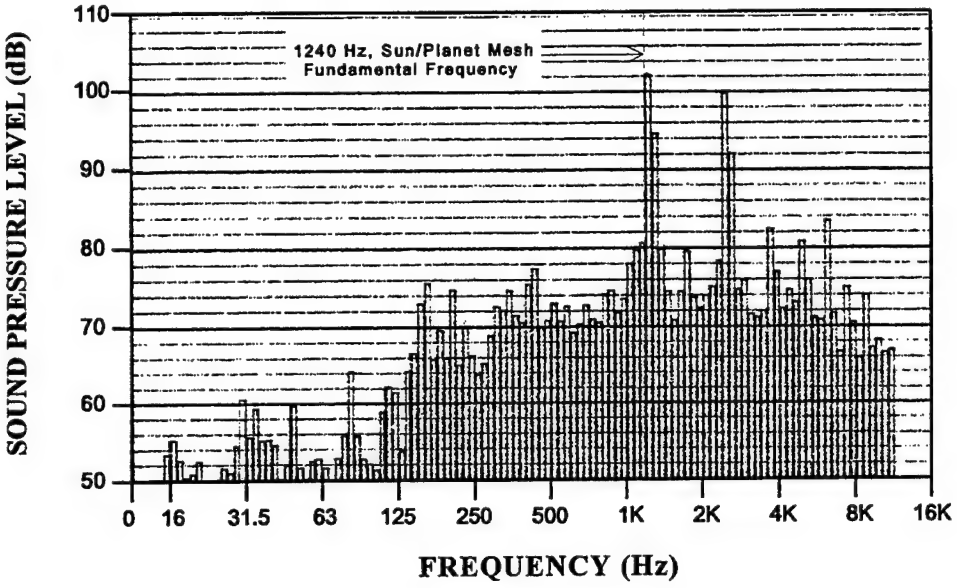

(a) Recorded approx. 10 min after start of step

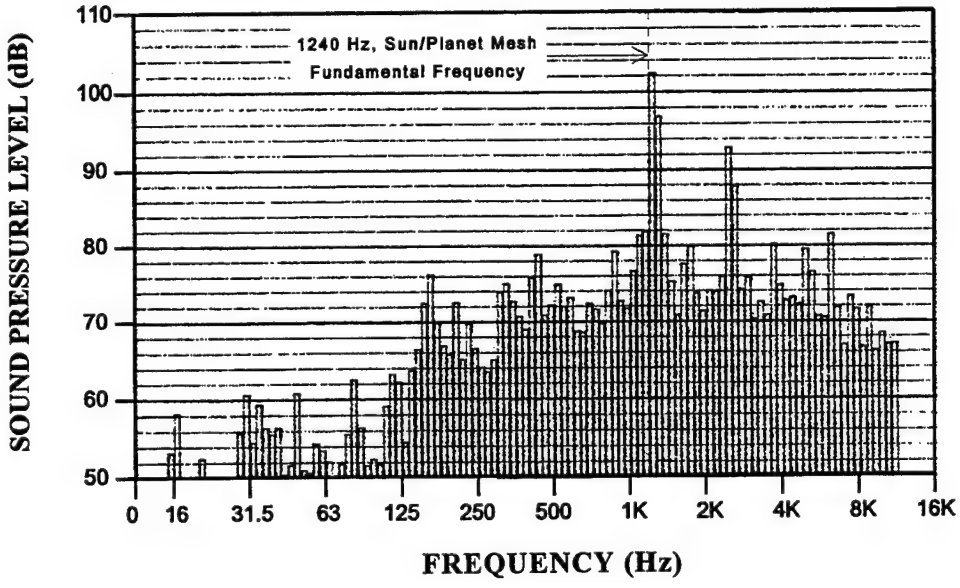

(b) Recorded approx. 10 min before end of step

FIGURE 54: ART HCR PLANETARY STEP 3 NOISE DATA - 125% TORQUE, 480 RPM

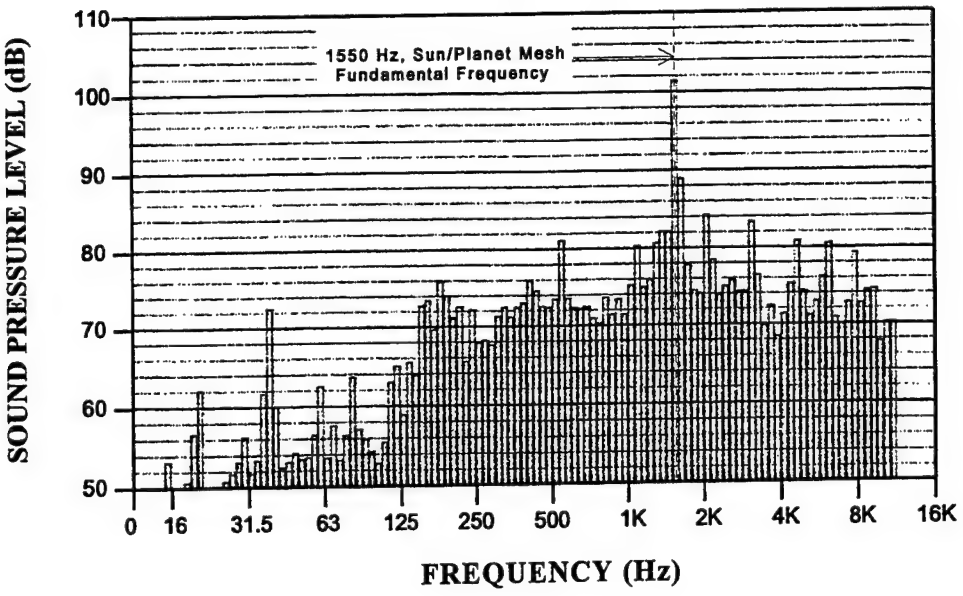

(a) Recorded approx. 10 min after start of step

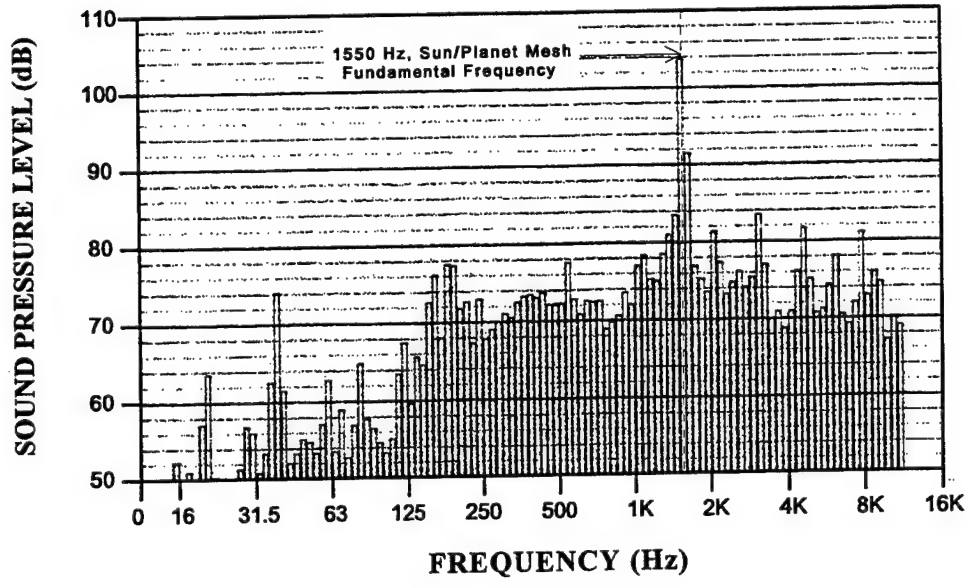

(b) Recorded approx. 10 min before end of step

FIGURE 55: ART HCR PLANETARY STEP 4 NOISE DATA - 75% TORQUE, 600 RPM

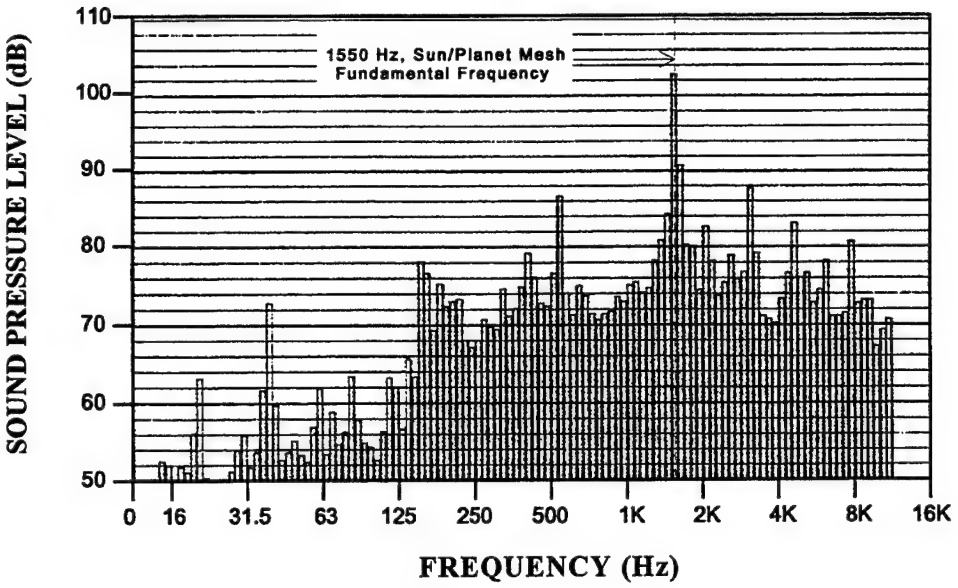

(a) Recorded approx. 10 min after start of step

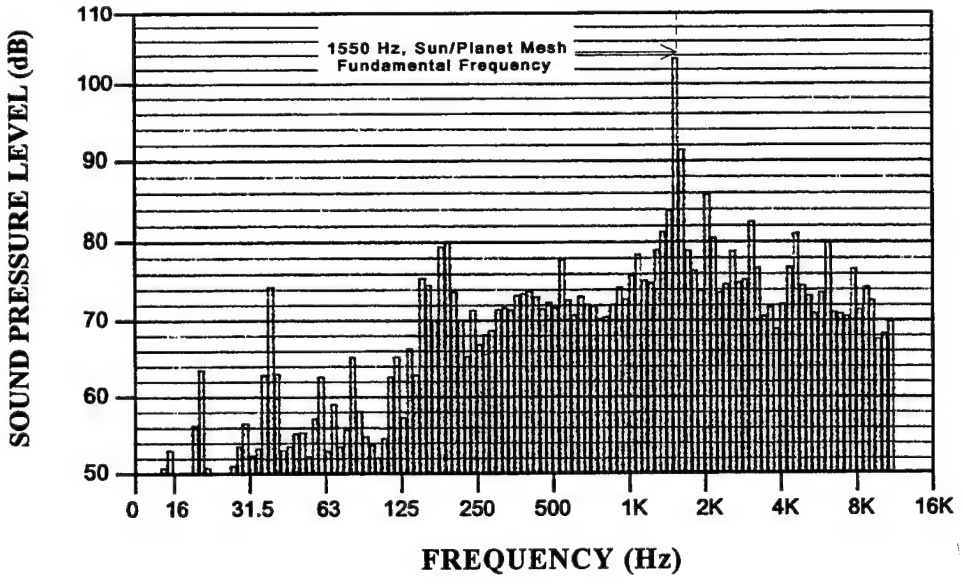

(b) Recorded approx. 10 min before end of step

FIGURE 56: ART HCR PLANETARY STEP 5 NOISE DATA - 100% TORQUE, 600 RPM

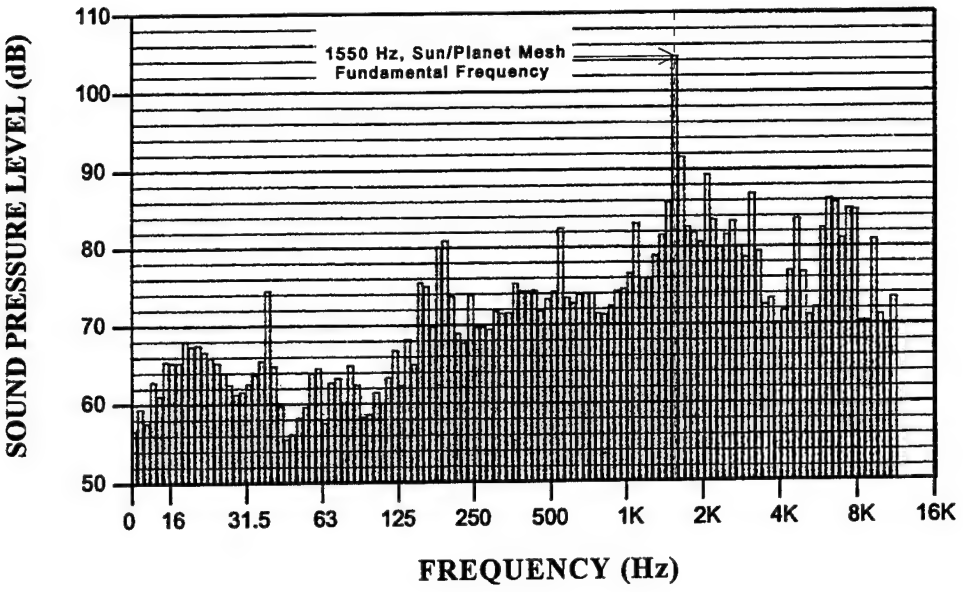

(a) Recorded approx. 10 min after start of step

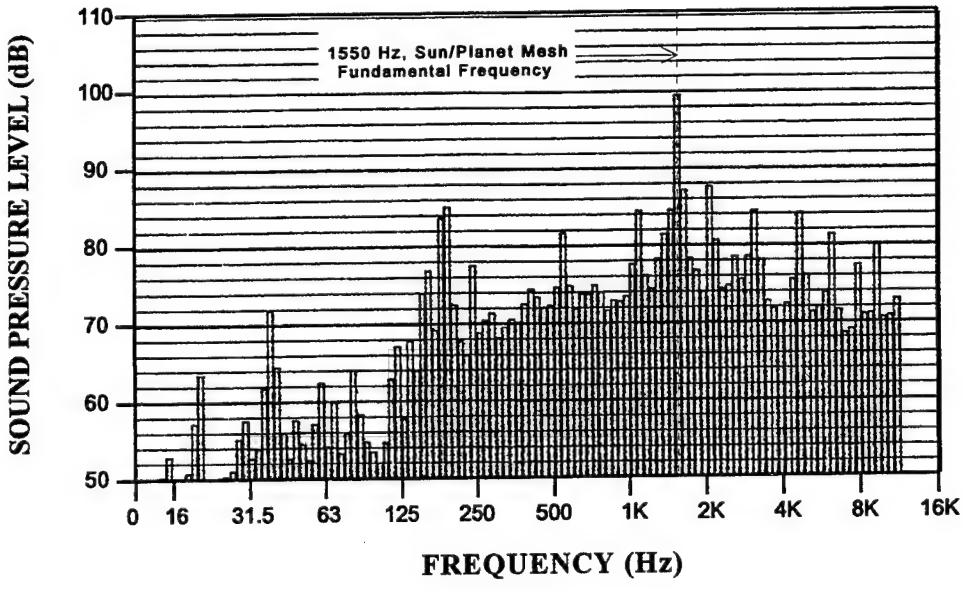

(b) Recorded approx. 10 min before end of step

FIGURE 57: ART HCR PLANETARY STEP 6 NOISE DATA - 125% TORQUE, 600 RPM

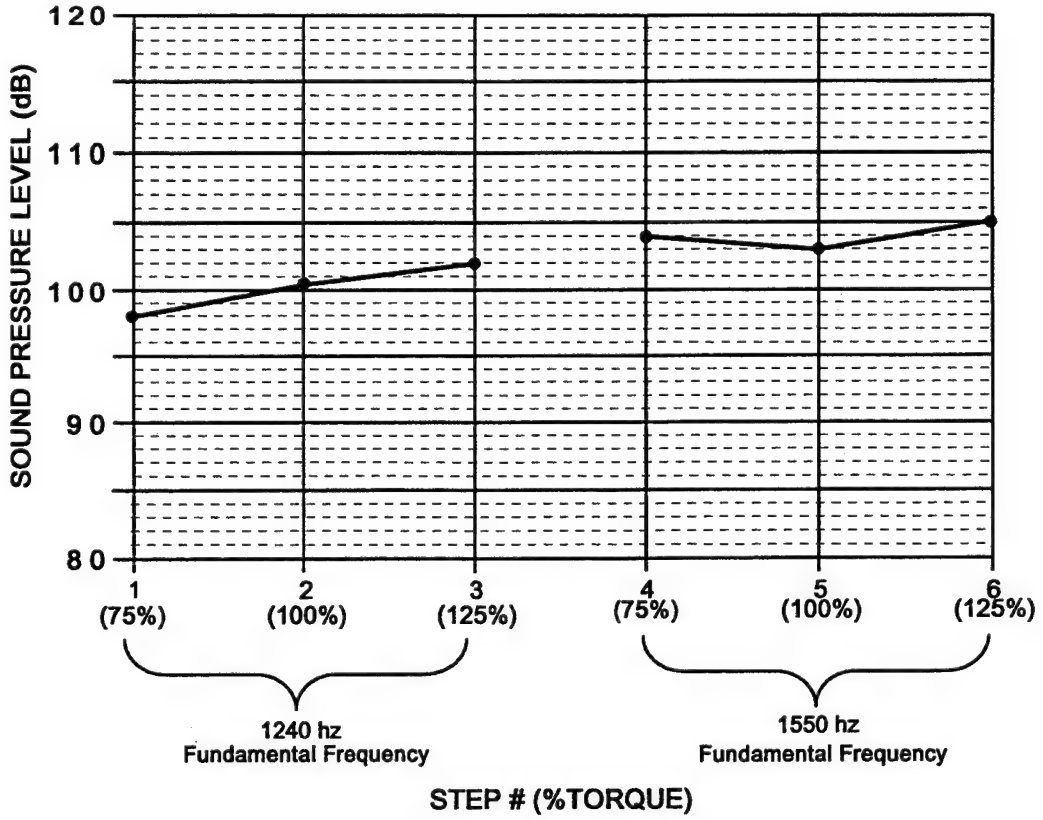

FIGURE 58: ART HCR SUN/PLANET FUNDAMENTAL FREQUENCY NOISE AMPLITUDE SUMMARY

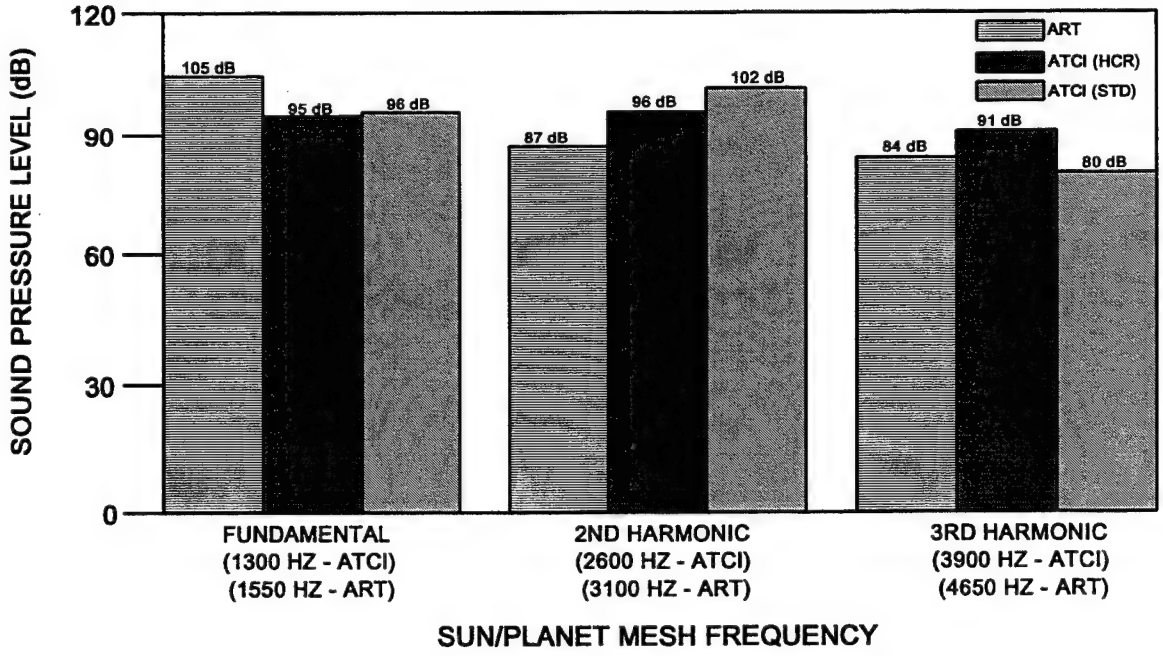

FIGURE 59: NOISE LEVELS OF ART VS. ATCI PLANETARIES (125% TORQUE, HELICOPTER SPEED)

6.1.2 PLANETARY EFFICIENCY MEASUREMENTS

Efficiency measurements were made simultaneously during the noise and vibration tests and immediately after completion of step 6 of Table 37 per the steps listed in Table 38. The efficiency of a HCR planetary is critical to its selection over a standard spur gear planetary because the actual weight savings gained may be more than offset by the effective weight saved due to the greater power loss for the HCR planetary. The comparison of the efficiencies of the standard (STD) and HCR planetaries determined during the ATCI program [1] were as follows:

TORQUE (%)	EFFICIENCY (%)	
	STD	HCR
50	99.77	99.73
100	99.7	99.67
125	99.67	99.64

Using the 100% torque level, the greater power loss for the HCR planetary translates into a 3 lb effective weight increase for the ART HCR planetary. There was a calculated 8 lb difference between the ART HCR planetary and a comparable ART STD planetary (see Section 4.1.5). Thus, real weight savings of the HCR planetary over the STD planetary is only 5 lb (8 lb - 3 lb = 5 lb).

The results of the efficiency measurements of the HCR planetary are shown graphically in Figure 60. Curves 1 and 2 were generated from data collected during the noise and vibration steps conducted per Table 37, and curves 3 and 4 were generated from data collected immediately after the completion of the last step of the noise and vibration test per Table 38. The oil-in temperature for all efficiency measurements was 260°± 5°F.

TABLE 38: HCR PLANETARY NOISE AND VIBRATION TEST SCHEDULE (ADDITIONAL TESTS)

STEP	PERCENT LOAD	INPUT SPEED (RPM)	INPUT TORQUE (IN-LB)	POWER (HP) REF	RUN TIME (MIN)
1	125	600	320,895	3,055	1.0
2	100	600	256,709	2,444	1.0
3	75	600	192,531	1,833	1.0
4	50	600	128,354	1,222	1.0
5	25	600	64,177	611	1.0
6	25	480	64,177	489	1.0
7	50	480	128,354	978	1.0
8	75	480	192,531	1,466	1.0
9	100	480	256,709	1,955	1.0
10	125	480	320,895	2,444	1.0

Curves 1 and 2 in Figure 60 shows the results of the efficiency measurements during steps 1 thru 3 and steps 4 thru 6 of Table 37, respectively. The efficiency plotted at each torque level for curves 1 and 2 is the average of the efficiency measurements collected over the one hour run time for each step. Curves 3 and 4 show the results of the steps listed in Table 38.

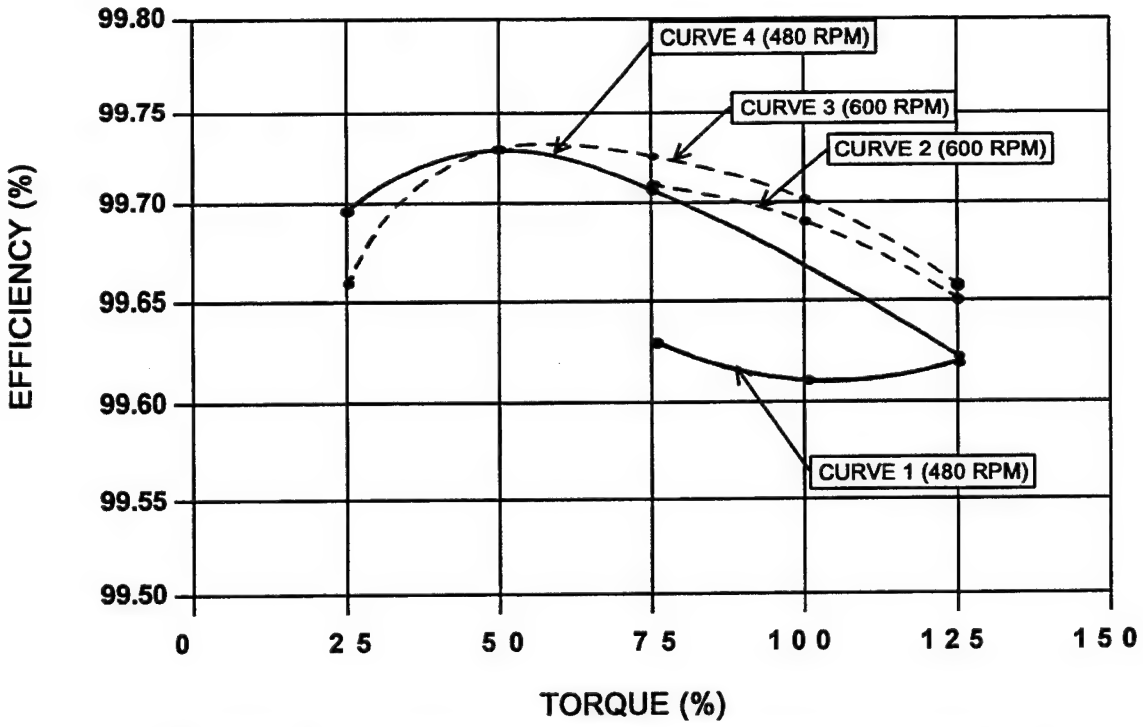

FIGURE 60: ART HCR PLANETARY - EFFICIENCY VS. TORQUE

The difference between curves 1 and 4 which were both taken at 480 rpm is most likely the result of the additional nine hours of run time accumulated between step 1 of Table 37 and step 1 of Table 38. The additional run time resulted in a reduction of the frictional losses of the assembly.

The efficiency calculations were made by measuring the total drag torque of the test rig on the instrumented drive shaft 'A' shown in Figure 41 and the input torque of the main torque shaft 'B'. The efficiency for each planetary is then calculated as:

$$\text{EFFICIENCY} = (1 - (\frac{\frac{TORQUE\ A}{2}}{TORQUE\ B})) \ X\ 100\%$$

Torque 'A' is divided by 2 to obtain a drag torque value for each of the planetary assemblies. The drag losses from the support bearings 'C' shown in Figure 41 are considered negligible.

The accuracy of the drag torque measured by shaft 'A' was verified by measuring the output from a load cell attached to a restraining arm located at a known distance from the center of the test assembly. The restraining arm is attached to the test rig frame and prevents the test assembly from rotating on bearings 'D' shown in Figure 41. The efficiency calculations for the drag torque measurements made at the restraining arm and on input shaft 'A' are shown in Figure 61. Curves 1a and 1b were generated from the data collected during steps 1 thru 3 of Table 37 and curves 2a and 2b from the data collected during steps 4 thru 6. The 'a' curves come from the drag torque measured by shaft 'A' and the 'b' curves from the restraining arm load cell output. The small difference between the 'a' and 'b' curves verifies the accuracy of the drag torque measurements and therefore the efficiency calculations for the planetary tests. The difference between curves 1a and 1b at the 75% torque level reflect only a 6% difference in the drag torque measurements between shaft 'A' and the restraining arm load cell. The drag torque measurements from shaft 'A' were used to generate all of the curves in Figure 60 because the variations in the measured output torque at each steady load condition were less than those measured at the restraining arm load cell.

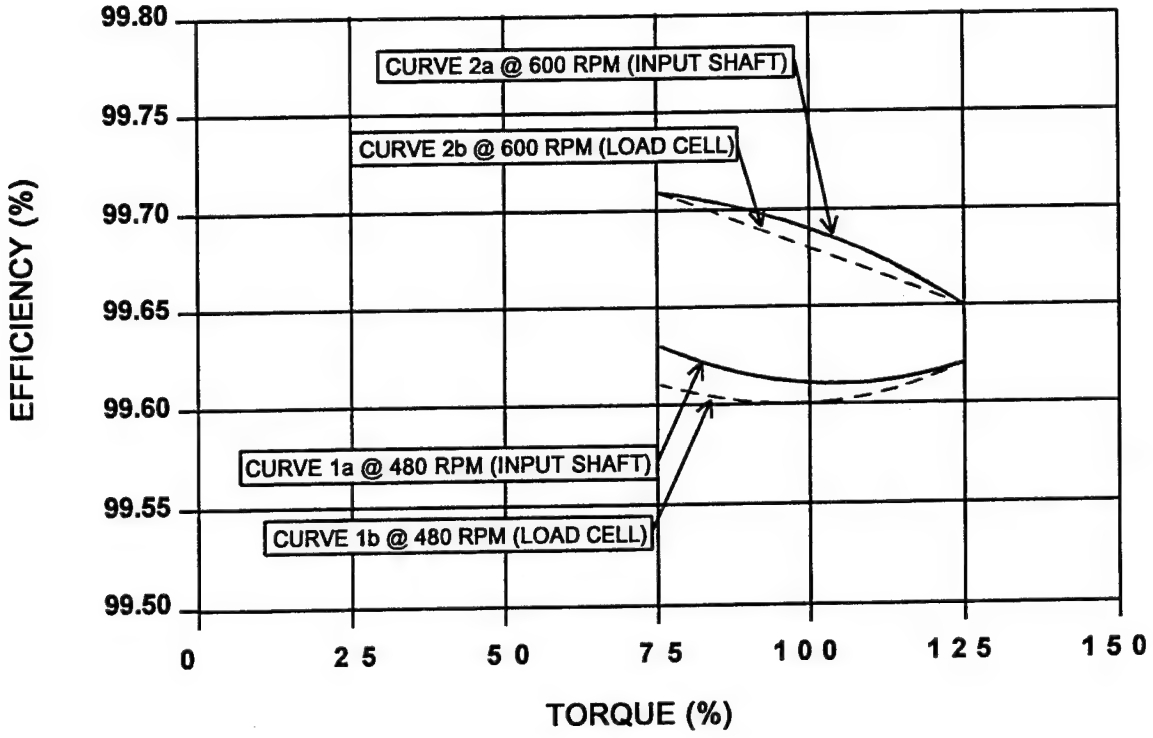

FIGURE 61: ART HCR PLANETARY - EFFICIENCY VS. TORQUE (DRAG TORQUE COMPARISON)

The results of the efficiency measurements show the ART HCR planetary to be as efficient if not more efficient than the ATCI HCR planetary eventhough the ART planetary uses less efficient spherical roller bearings.

6.1.3 PLANETARY SCORING TESTS

Scoring tests were conducted on the HCR planetary to determine the gear tooth scoring temperature. The scoring temperature is critical to the operation of a HCR planetary in a hot running transmission. The HCR planetaries were assembled as shown in Figure 41 with a separate lube system for the upper and lower sections of the test rig. The upper planetary was the test specimen. The lower planetary was not subjected to the high oil-in test temperatures for the upper planetary since its direction of rotation is opposite to that of the upper planetary. The oil-in temperature for the lower planetary was kept below 260° F.

The steps listed in Table 39 were run with no evidence of scoring observed after any of the steps. Further testing was suspended due to the excessive oil-in and oil-out temperatures which presented a potential fire hazard. The flash temperature of the DOD-L-85734 oil used in the test is 500° F and the auto-ignition temperature is 760° F. For each step the oil-out temperature was stabilized prior to the start of test time. After each step the gear teeth of the upper planetary were visually inspected.

TABLE 39: HCR PLANETARY SCORING TEST SCHEDULE

STEP	INPUT TORQUE (IN-LB)	CARRIER SPEED (RPM)	% TORQUE	POWER REF (HP)	MAX OIL-IN TEMP. (° F)	MAX OIL-OUT TEMP. (° F)	OIL FLOW TO GEAR MESHES (GPM)	RUN TIME (HR)	CALCULATED SCORING TEMP. (° F)
1	192,531	600	75	1,833	262	277	0.61	0.5	322
2	256,709	600	100	2,444	270	289	0.74	0.5	344.5
3	320,895	600	125	3,055	275	311	0.82	0.5	370
4	192,531	600	75	1,833	297	298	0.71	0.5	350
5	256,709	600	100	2,444	297	315	0.69	0.5	370.5
6	320,895	600	125	3,055	297	329	0.69	0.5	390
7	192,531	600	75	1,833	334	327	0.58	0.5	383
8	256,709	600	100	2,444	331	342	0.61	0.5	401
9	320,895	600	125	3,055	333	361	0.69	0.5	424
10	192,531	600	75	1,833	360	343	0.61	0.5	404
11	256,709	600	100	2,444	367	361	0.66	0.5	429
12	320,895	600	125	3,055	370	381	0.69	0.5	453
13	385,063	600	150	3,665	367	405	0.69	0.5	474
14	385,063	600	150	3,665	379	414	0.66	0.5	484.5
15	385,063	600	150	3,665	392	421	0.69	0.5	494.5
16	385,063	600	150	3,665	405	430	0.69	0.5	505
17	385,063	600	150	3,665	414	442	0.69	0.5	516
18	449,240	600	175	4,275	415	457	0.71	0.35	535
19	385,063	600	150	3,665	421	498	0.69	0.15	547.5
20	385,063	600	150	3,665	426	511	0.77	0.18	555.5
21	385,063	600	150	3,665	426	505	0.74	0.5	554
22	385,063	600	150	3,665	433	531	0.74	0.5	570
23	385,063	750	150	3,665	426	504	0.74	0.43	563
24	423,573	850	165	5,713	426	525	0.74	0.15	588
25	449,240	850	175	6,059	430	532	0.74	0.5	599
26	449,240	850	175	6,059	441	565	0.74	0.5	620
27	440,903	840	172	5,876	460	615	0.74	0.15	653

For steps 1 thru 18, the oil-out temperature was measured at the oil-out drain shown in Figure 41. Because the measured oil-out temperature was lower than the oil-in temperature for some steps (7, 10, and 11), it was decided to install a thermocouple just below the ring/planet mesh as shown in Figure 41 to measure the oil-out temperature for the remaining steps (19 thru 27). The measurement of the oil out temperature near the ring gear is a more accurate oil-out temperature, since the oil is just exiting the gear mesh with no opportunity to lose heat to the surrounding housing.

Based on previous scoring tests conducted on a HCR planetary at BHTI, it was anticipated that the planet teeth would score prior to Step 15. The inability to score the teeth even at the test conditions of Step 27 can be attributed to three factors or improvements over the HCR planetary which did score in previous tests. These improvements include designing the planetary for sequential meshing of the planet gears instead of simultaneous meshing (reduced dynamic factor), the use of spherical roller bearings for the planet pinions

instead of cylindrical rollers (reduced misalignment factor), and the incorporation of integral gear mesh oil jets optimized for maximum impingement depth (improved mesh lubrication and cooling).

6.1.4 PLANETARY GEAR TOOTH PITTING AND BEARING PITTING TEST

Two HCR planetaries were subjected to a 250 hour pitting test, one assembled with single row spherical roller planet bearings and the other with double row spherical roller planet bearings as shown in Figure 39. This test was conducted at 600 rpm, 100% load and 260° F oil-in temperature. The primary objective of this test was to demonstrate that the ART planetary, using either double or single row spherical roller bearings, is capable of operating at a 125% overstress (compressive stress) condition for 250 hours without a gear tooth or planet bearing pitting failure. The 100% compressive stress condition for the gear and bearing pitting mode of failure is assumed to occur at 64% operating power which is an assumed average operating power for the gearbox. The 125% overstress condition for the gear and bearing compressive stress occurs at 100% operating power since the compressive stress only increases by the square root of the increase in load.

$$125\%\ \text{stress} = 100\%\ \text{stress} \times (100\%\ \text{power}/64\%\ \text{power})^{1/2}$$

If no pitting failure occurs in the gears or bearings during the 250 hour test, then the reliability statement for the life limiting pitting mode of failure is: It can be said with 90% confidence that the probability of survival of the population of planetaries of that configuration operating at 64% power for 250 hours is .9470. The reliability of .9470 is based on 3 sigma = .30 X Mean.

Using the pitting life prediction methodology developed for the ART program, the L_2 lives for the planetary components are as follows:

Sun Gear	-	741,113 hours
Single Row Bearing	-	77,520 hours
Double Row Bearing	-	84,729 hours

Thus, no pitting failures were anticipated, and after the 250 hour pitting test no gear or bearing pitting failures were evident. There was however some minor flaking of the thin dense chrome from the inner races of two of the six single row spherical roller planetary bearings. No flaking was observed on any of the double row spherical roller planetary bearing inner races.

6.1.5 PLANETARY GEAR TOOTH BENDING FAILURE MODE & EFFECT TEST

Two HCR planetaries (upper and lower) were tested to determine the tooth bending fatigue strength of the planet pinions and to determine the failure mode and the effect of the failure. The planet pinions were expected to fail since they are subjected to reverse bending. The normal mode of gear tooth bending fatigue is when the tooth breaks off instead of the crack propagating through the rim and causing a catastrophic failure. A rim failure usually means that the ratio of the rim thickness to the tooth whole depth is too low. A secondary objective of this test was to evaluate the capability of the vibration monitoring system to detect a tooth crack before the tooth broke off and to detect the same tooth crack after the load had been reduced to the normal operating level.

The test was started with two HCR planetaries, test and slave, assembled with single row spherical roller planet bearings as shown in Figure 41 and was conducted at 600 rpm and 160° F oil-in temperature. The test schedule is shown in Table 40. Steps 1, 2, and 3 were successfully run for 8.6 hours each. A run time of 8.6 hours accumulates one million cycles of reverse bending on the gear teeth of each planet pinion. After

running for 7.3 hours at 200% load, Step 4, the rig was shutdown due to a chip alarm in the slave section of the assembly. After disassembly and inspection, it was discovered that the inner race of one of the slave planet bearing assemblies was severely pitted. This was not unexpected since the bearing inner race compressive stress level was 408 KSI at the 200% load level. The inner races of the remaining slave planet bearing assemblies and all of the slave planetary gear teeth exhibited evidence of secondary debris damage from the pitted inner race. Due to the secondary debris damage it was decided to replace the slave planetary assembly with the double row spherical roller planetary assembly tested during the pitting test.

TABLE 40: HCR PLANETARY GEAR TOOTH BENDING FATIGUE TEST SCHEDULE

STEP	RUN TIME (HR)	% TORQUE	POWER REF (HP)	INPUT TORQUE (IN-LB)	CALCULATED PLANET BENDING STRESS (KSI)
--	--	(100)	2,444	256,722	75,798
--	--	(80)	1,955	205,356	63,571
1	8.6	150	3,666	385,083	106,387
2	8.6	165	4,033	423,633	115,568
3	8.6	181	4,424	464,704	125,344
4	8.6	200	4,888	513,444	136,976
5	8.6	219	5,352	562,183	148,593
6	8.6	241	5,890	618,695	162,053
7	8.6	265	6,477	680,355	176,731
8	8.6	292	7,136	749,577	193,251
9	8.6	321	7,845	824,052	210,888

The test was resumed at 200% load and run for 1.3 hours to complete 8.6 hours on the test section planetary at Step 4. Step 5 was successfully run for 8.6 hours. After running for 4.6 hours at 241% load, Step 6, the rig was again shut down for a chip alarm in the slave section. Inspection of the chip detector revealed a considerable amount of metallic debris collected on the magnet. Some of the debris appeared to be fragments of gear teeth, indicating a possible tooth bending fatigue failure.

The test assembly was disassembled and the following component failures noted:

- 3/4 of one tooth on one slave planet pinion broke off at the root and the adjacent tooth was visibly cracked along 3/4 of its length. The broken tooth was not found intact. Only large amounts of smaller debris were found in the slave section.

- An adjacent pinion to the failed pinion had one tooth that had been chipped at the top of the tooth.

- All six slave planet pinions had scoring damage on the side of the teeth that mesh with the ring gear.

- The slave ring gear had approximately 5 teeth with large chips and areas of debris damage. Numerous other teeth displayed various amounts of debris damage.

- The slave sun gear showed some minor debris damage.

- No failures or damage were observed on any components of the test section planetary.

From the condition of the failed components, it appeared that one tooth from one planet pinion in the slave section broke off due to bending fatigue. The broken tooth was then caught in the mesh between the ring gear and adjacent planet pinion, causing the damage noted to the ring gear and adjacent planet pinion. The broken tooth itself was ground into smaller debris as it passed through the planet/ring mesh. The scoring noted on the ring gear meshing side of the slave planet pinions was probably initiated by the massive amount of debris damage. The ring gear damage and the excessive load level were also contributing factors to the scoring.

The slave section was flushed and cleaned of all debris and the test rig was reassembled for further testing of the components in their failed condition. The purpose of further testing was to collect additional vibration data and to evaluate the ability of the HCR planetary to function with broken teeth.

The original intent of the test plan was that at the first indication of a cracked or broken tooth, the load would be reduced to the 100% level and held at that level to gather vibration data. The load would then be reduced to the 80% level to collect additional vibration data. The test would then be stopped and the cracked or broken tooth verified. However, because of the large amount of debris generated by the initial failure, this portion of the test was not accomplished until the test rig was disassembled to determine which components failed. After collecting vibration data at the 80% and 100% torque levels, a 2 hour test would then be run at 100% load and 260° F oil-in temperature to demonstrate the capability of the ART planetary to operate at full power for 2 hours with a cracked or broken tooth.

If the 2 hour run at 100% load was successfully completed, the test torque would then be increased back to 241%, Step 6, where the cracked or broken tooth failure occurred and the remaining 4 hours at that step completed. The oil-in temperature would be lowered back to 160° F. If the planetaries were still operable, the load level would be increased to each next higher increment of load and the planetaries run for 8.6 hours at each step until failure or until the test stand drive reached its power limit.

After reassembly, the test assembly was brought up to 100% speed (600 rpm carrier speed) and minimum torque with no problems. Next, the torque was increased to 80% and maintained for approximately 6 minutes while vibration data was recorded. Again, the rig continued to run with no problems. The torque was then increased to 100% and run for approximately 5 minutes with no problems while recording vibration data. The oil heater was then turned up to increase the oil-in temperature from 160° F to 260° F, for the 2 hour run at 100% speed and load. Approximately one minute after turning up the oil heater, the stand locked up and automatically shutdown. Review of the data showed the drive motor speed went from 600 rpm to 0 rpm in less than 2 seconds.

The test rig was disassembled and the following component failures noted:

- Again no failures were observed on any of the test section planetary components.

- The slave section planetary was completely locked up and had to be removed from the test rig housing as a complete unit (sun gear, planet pinions and ring gear). A photograph of the failed planetary is shown in Figure 62. One planet pinion had rolled up onto a broken tooth from another planet pinion that had wedged itself into the ring gear. This effectively wedged the planet pinion between the sun gear and ring gear preventing any further rotation. The ring gear itself was

elongated (egg shaped), many broken teeth were observed on the planet pinions, and the sun gear teeth meshing with the planet pinions appeared to be bent over (yielded) in one direction.

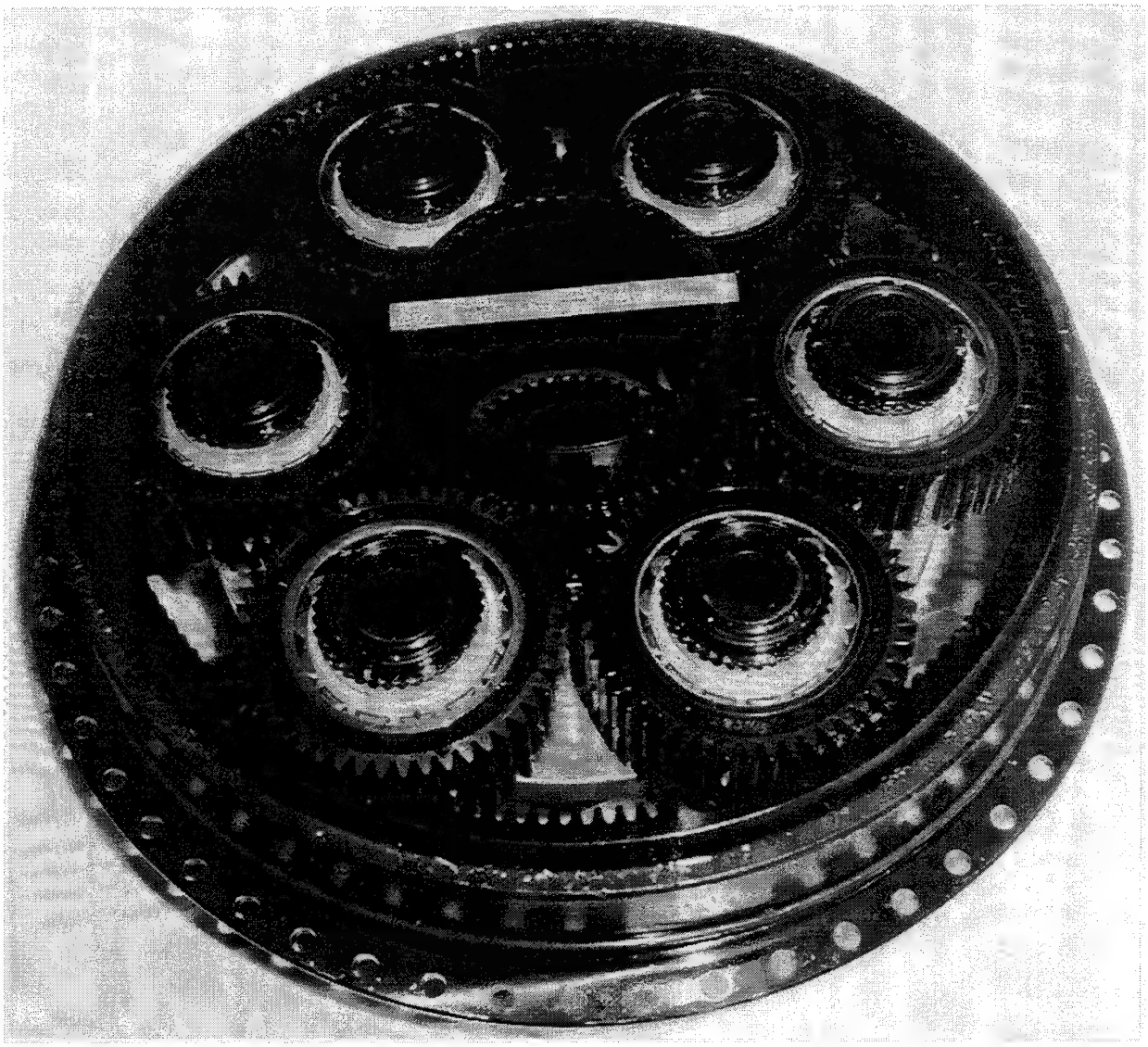

FIGURE 62: HCR PLANETARY - RESULTS OF FAILURE MODE TEST (LOCKED-UP)

This final failure was apparently caused when a tooth broke off from one planet pinion and remained wedged in the ring gear instead of falling out of mesh. The next planet pinion to roll through that portion of the ring gear rolled up onto the broken tooth which then effectively wedged the planet pinion between the sun gear and ring gear preventing further rotation. At 600 rpm, it takes .0167 seconds for a planet pinion to roll through the same location as the previous planet pinion. This would account for the sudden lock-up during the test. If the test rig drive motor had actually been driving the rig with 2444 HP instead of a maximum of 75 HP, the failure mode observed may have been much different. It is likely that with the driving torque at 2444 HP, the planetary would have continued to spin, shearing most of the teeth off of the planet pinions and sun gear without locking up the drive train. This is important to note since any rotorcraft auto-rotation maneuver is dependent upon freely spinning rotors. A locked up planetary would of course prevent the rotors from spinning. Figure 63 is a close-up photograph of the planet pinion teeth wedged on

top of the ring gear teeth. The vibration monitoring system was not able to predict the onset of failure prior to either planet gear tooth failures.

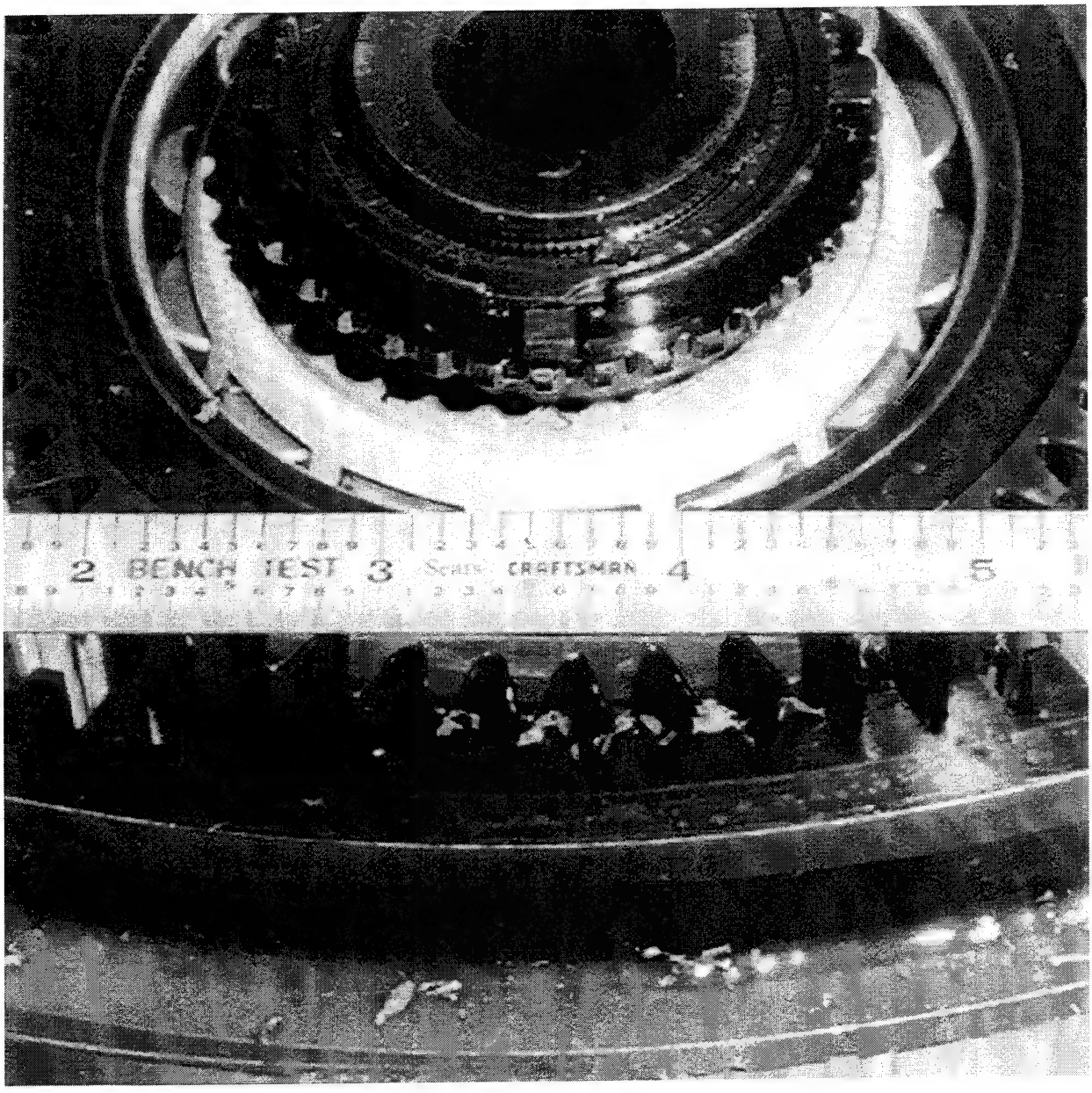

FIGURE 63: HCR PLANETARY - RESULTS OF FAILURE MODE TEST (PLANET TEETH WEDGED ON TOP OF RING GEAR TEETH)

6.1.6 HCR PLANETARY LOSS-OF-LUBE TESTS

Loss-of-Lube (LOL) tests were conducted on the ART high contact ratio planetary. The test rig was assembled as shown in Figure 41 with single row spherical roller bearings installed in the test planetary. The lube system was configured to allow the primary lube supply to the test section to be cut-off at the start of test time. The air/oil mist nozzle supplied continuous emergency lubrication to the test section planetary components during the one hour and four hour tests described below. The slave section was continuously supplied through the primary lube system. Prior to the start of each test, the test section planetary was operated at 100% power (2444 HP) and 100% speed (600 rpm of carrier) with full oil flow until the oil-in temperature had stabilized at 260°F ± 5°F.

The primary objective of the LOL test was to demonstrate that the ART planetary is capable of operating for 30 minutes after loss of the primary oil supply. The one hour test was conducted to substantiate 30 minutes of LOL operation. The one hour run was made up of an initial 2 minute step at 100% torque in helicopter mode (600 rpm), followed by a 45 second conversion and 54.5 minutes at 80% torque in airplane mode (480 rpm) and ending with another 45 second conversion and a final 2 minute step at 100% torque in helicopter mode (600 rpm) for a total of 60 minutes.

A secondary objective for the LOL test was to demonstrate that the ART planetary is capable of operating for 2 hours after loss of the primary oil supply. A 2 hour capability would allow a safe return of the aircraft from extended over-water operations. A two hour capability would be demonstrated by conducting a four hour test similar to the one hour test.

The first LOL test was successfully run for one hour with no component failures and no visible signs of distress other than some oil coking on the sun gear and planet pinions. The air supply pressure to the mist nozzle was set at 35 PSI which yielded an oil mist flow rate of approximately .0016 GPM. A plot of the ring gear blank temperature, input speed and input torque over the one hour test period is shown in Figure 64.

The same components used for the one hour test were used to conduct the second LOL test which was successfully run for four hours with no component failures and no visible signs of distress other than increased oil coking on the sun gear and planet pinions. The air supply pressure to the mist nozzle was set at 20 PSI which yielded an oil mist flow rate of approximately .0011 GPM. A plot of the ring gear blank temperature, input speed and input torque over the four hour test period is shown in Figure 65.

Due to the successful LOL runs completed with no failures, it was decided to run a LOL test on the same components with **no** emergency air/oil mist supply to the test section planetary. The test was conducted at the same speeds and powers as for the first one hour run but was suspended after 24 minutes of run time due to heavy scoring of the sun gear teeth. The increased friction of the sun/planet mesh overcame the power of the drive motor which stopped the rotation of the planetaries. A plot of the ring gear blank temperature, input speed and input torque over the 24 minute test period is shown in Figure 66.

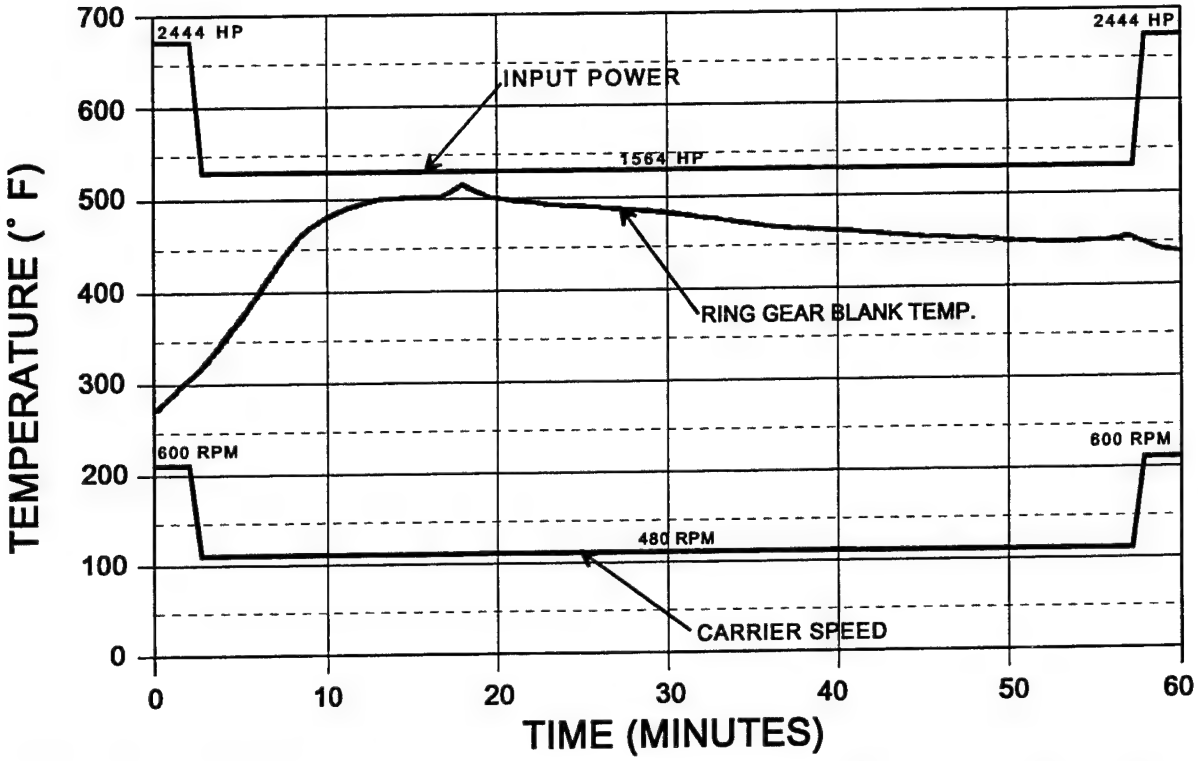

FIGURE 64: HCR PLANETARY ONE HOUR LOSS-OF-LUBE TEST - RING GEAR BLANK TEMP

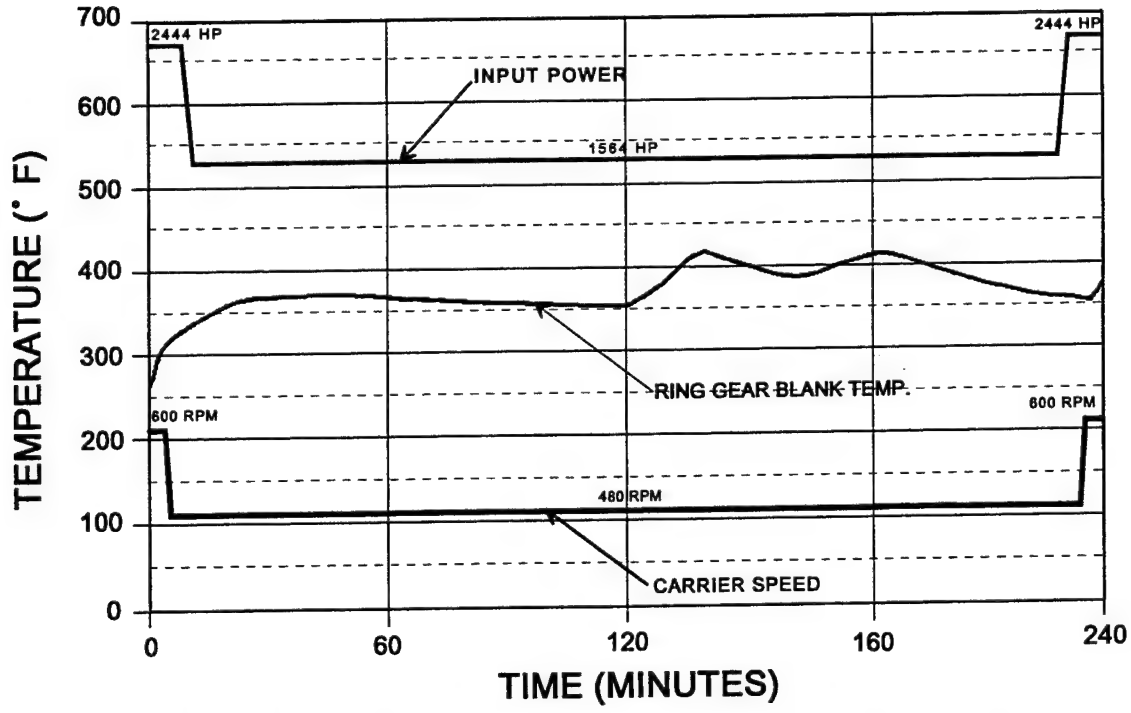

FIGURE 65: HCR PLANETARY 4 HOUR LOSS-OF-LUBE TEST - RING GEAR BLANK TEMP.

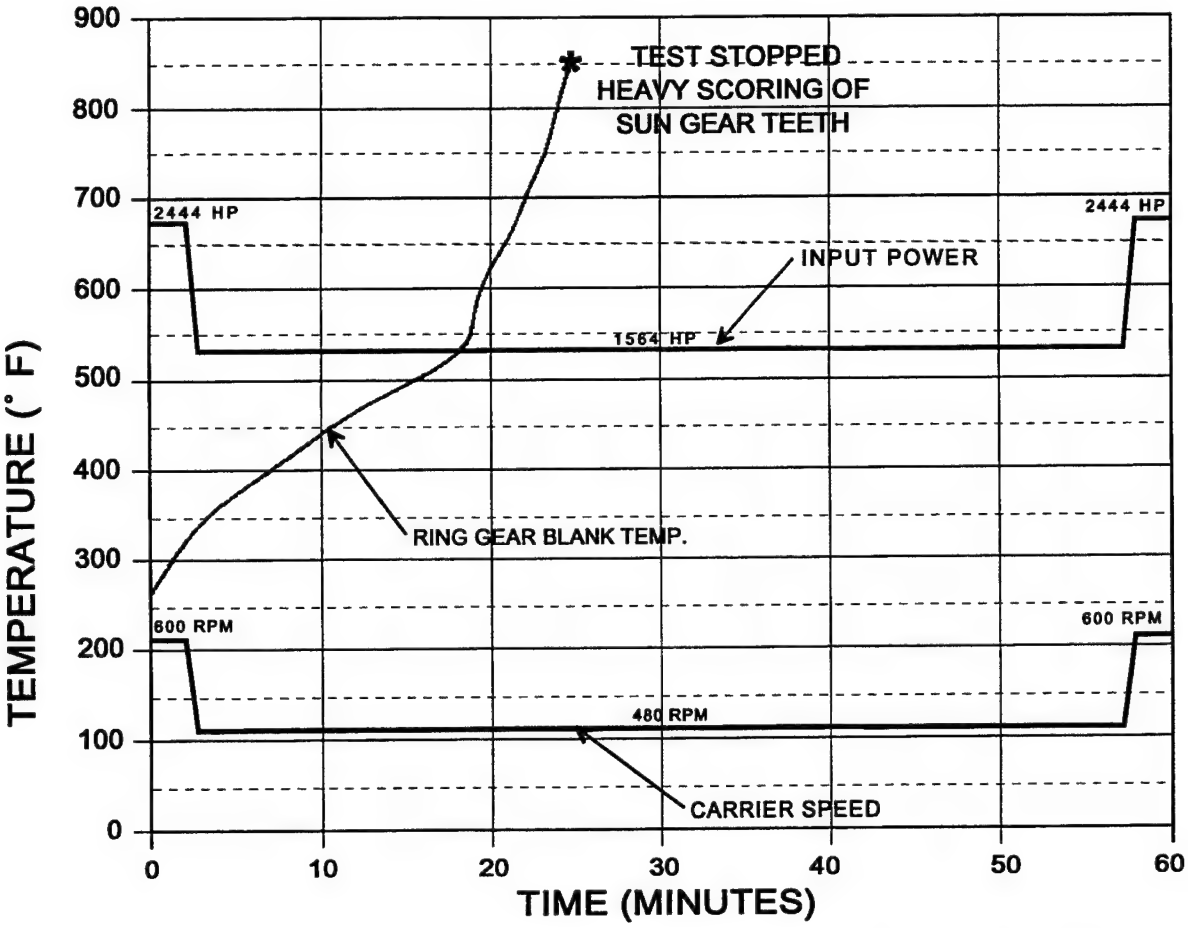

FIGURE 66.: HCR PLANETARY ONE HOUR LOSS-OF-LUBE TEST - RING GEAR BLANK TEMP (NO EMERGENCY AIR/OIL MIST LUBRICATION)

6.1.7 HCR PLANETARY TITANIUM CARRIER COATINGS EVALUATION

During the HCR planetary tests several base metal coatings applied to the test titanium carriers were also evaluated. The titanium carrier in the high contact ratio planetary assembly presents several areas of wear and fretting concern which are shown in Figure 67.

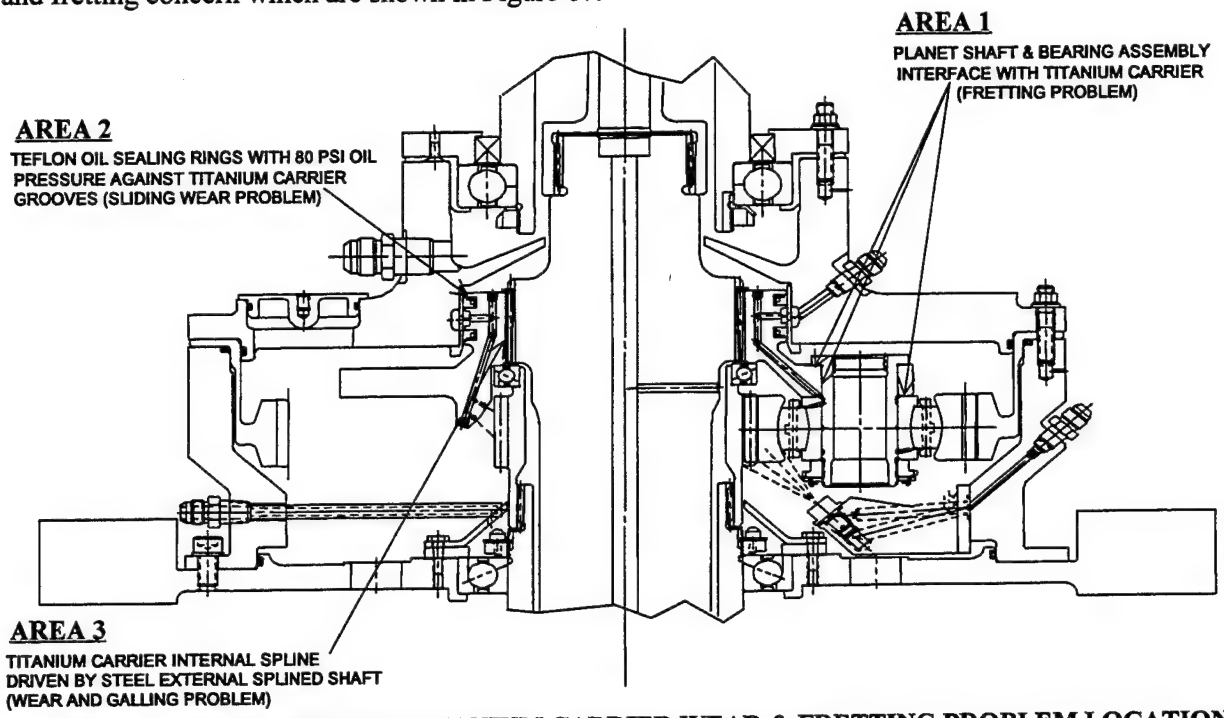

FIGURE 67: HCR PLANETARY TITANIUM CARRIER WEAR & FRETTING PROBLEM LOCATIONS

The following is a list of the coatings tested and the results:

COATING	AREA (SEE FIG 67)	RESULT
DICRONITE DL-5 - molecular bonding, solid film lubricant consisting of tungsten disulfide. Dimensional build-up less than .0001" on coated surface.	1	Minor fretting observed on I.D. and flange surfaces after noise and vibration tests. No galling observed when planet shafts pressed in and out of carrier.
	2	Excessive wear on groove sidewalls.
	3	Excessive spline wear on titanium carrier female spline.
Titanium nitride coated with a molybdenum disulfide solid film lubricant. Dimensional build-up less than .0001" on coated surface.	1	No fretting observed on I.D. or flange surfaces after 250 hour pitting test. No galling observed when planet shafts pressed in and out of carrier.
Titanium anodize with top coat of EM-6226 (proprietary solid bonded dry film lubricant). Dimensional build-up, .001" to .003" on coated surface.	2	No wear observed on groove sidewalls or on teflon sealing rings after 250 hour pitting test.
Titanium anodize with solid film lubrication.	3	Minimal wear on splines after 250 hour pitting test.

6.2 IMPROVED SPIRAL BEVEL GEARS

The ART drive system has two identical spiral bevel gear sets in the interconnect system which provide mechanical connection between the two proprotors. The duty cycle of these spiral bevel gears require that they operate at 100% torque only during single engine operation while for the majority of the time they will operate at less than 25% torque.

Proposed improvements to the spiral bevel gears were in two areas; noise level and tooth bending fatigue strength. The improvement in noise level was to be provided by reducing the kinematic error of the gear mesh [28] and the increased bending strength was to be provided by increasing the gear and pinion tooth fillet radii. Additionally, it was anticipated that both noise level and tooth bending fatigue strength would benefit from reduced spacing errors provided by spiral bevel gear grinding improvements made under U.S. Army Contract NAS3-25030 by the Gleason Works in Rochester, N.Y. with assistance from BHTI [29].

The bevel gear used for the ART component tests was the input spiral bevel set for the OH-58D helicopter developed for the Army in the Army's Helicopter Improvement Program (AHIP). Table 41 shows the design data for the OH-58D and the ART bevel gears. Although the reduction ratio and speeds are somewhat different, much of the data are similar, especially the diametral pitch and face width. Thus, the OH-58D bevel gears are considered to be representative of not only the ART bevel gears but most of those used in medium to high speed applications.

TABLE 41: DESIGN DATA FOR ART AND OH-58D SPIRAL BEVEL GEARS

	ART		OH-58D	
	PINION	GEAR	PINION	GEAR
NO. OF TEETH	37	59	19	62
DIAMETRAL PITCH (IN^{-1})	6.500		6.092	
PRESSURE ANGLE	20°		20°	
SPIRAL ANGLE	35°		35°	
SHAFT ANGLE	93.5°		95°	
PITCH DIAMETER	5.692 in.	9.077 in.	3.119 in.	10.177 in.
FACE WIDTH	1.360		1.450	
CONTACT RATIO	2.642		2.605	
RPM	10,175	6,381	6,016	1,844
PITCH LINE VELOCITY	15,162 ft/min		4,912 ft/min	

Three configurations of spiral bevel gears were designed, manufactured and tested to evaluate the benefits of increased tooth fillet radii and reduced kinematic error tooth geometry.

The configurations were:

Configuration #1 - Baseline OH-58D input spiral bevel set except made from X-53 alloy steel instead of 9310.

Configuration #2 - Same as #1 except for increased tooth fillet radii

Configuration #3 - Same as #2 except tooth geometry to provide reduced kinematic error. The machine settings and tooth contact analysis to produce the reduced kinematic error spiral bevel gear sets were provided by Dr. Faydor Litvin of the University of Illinois at Chicago. Four iterations were submitted for analysis and three were manufactured for kinematic error tests and loaded tooth contact tests. Based on the results of the analysis and the tests, Configuration #3C was selected for further verification tests as described below.

The OH-58D input spiral bevel set is designed to transmit 464 HP at 6016 RPM of the pinion. A cross section of the OH-58D main transmission is shown in Figure 68.

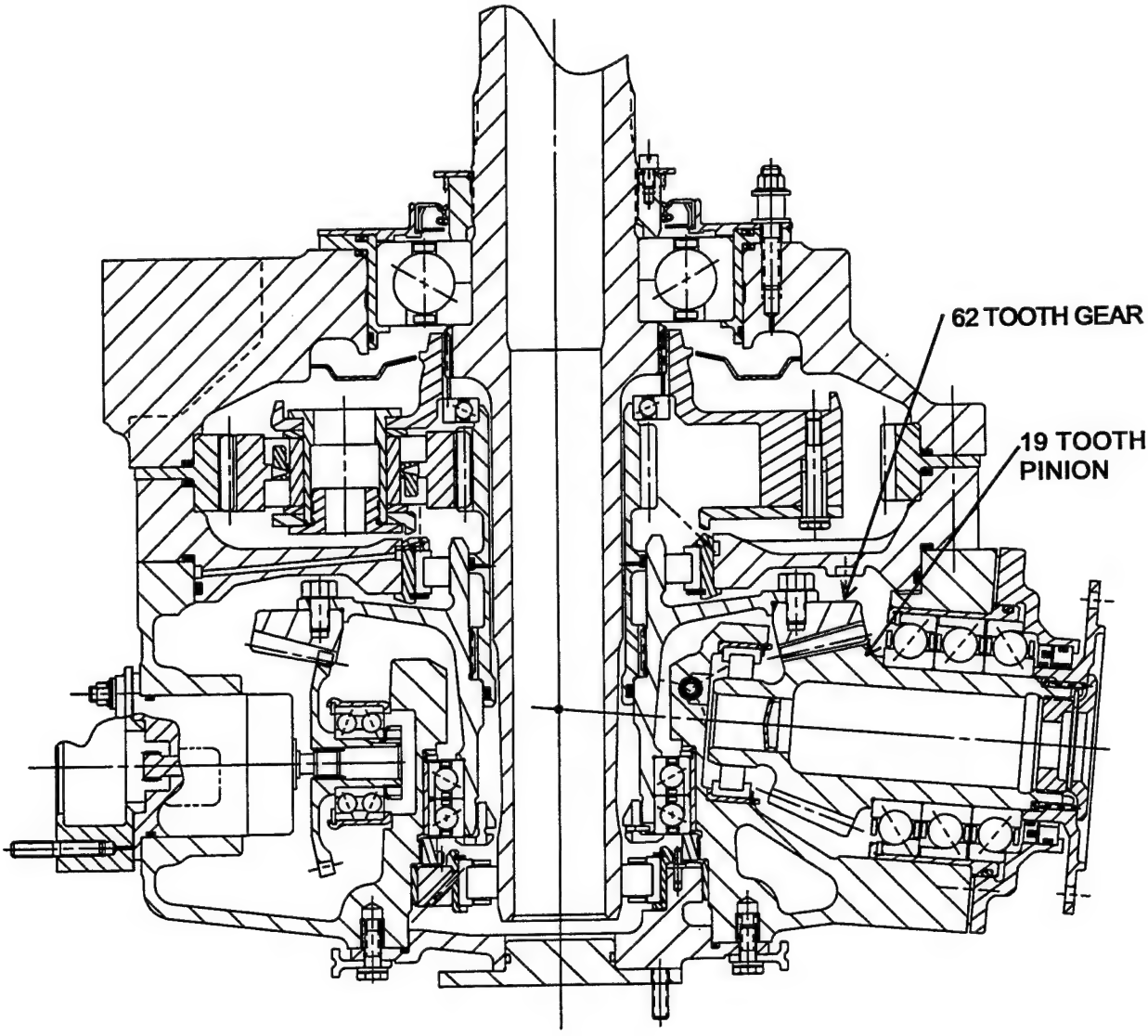

FIGURE 68: CROSS SECTION OF OH-58D MAIN TRANSMISSION

6.2.1 SPIRAL BEVEL GEAR ANALYSIS

A complete analysis of each configuration was performed by The Gleason Works of Rochester, N.Y. This analysis included Tooth Contact Analysis (TCA), Loaded Tooth Contact Analysis (LTCA), and Finite Element Analysis (FEA). The input for the analysis included tooth geometry, torque, and predicted housing deflections. Table 42 below presents a summary of the predicted maximum stresses and kinematic error levels for all of the spiral bevel gear set configurations.

TABLE 42: SUMMARY OF PREDICTED SPIRAL BEVEL MAXIMUM STRESSES & KINEMATIC ERRORS

CONFIGURATION	TOOTH BENDING[1] STRESS (KSI)		TOOTH[1] COMPRESSIVE STRESS (KSI)	TRANSMISSION ERROR (ARCSEC)			
	GEAR	PINION		@ NO[2] LOAD	@ 63%[3] LOAD	@94%[3] LOAD	@ 125%[3] LOAD
#1 BASELINE	140.7	145.7	275.1	19.6	15.3	10.7	7.3
#2 (INC. FILLET)	142.7	116.5	299.5	19.6	14.5	12.3	10.0
#3A (LITVIN #1)	111.5	116.8	271.4	5.6	3.9	5.6	4.5
#3B (LITVIN #2)	119.0	124.5	309.0	6.8	2.3	5.1	6.8
#3C (LITVIN #3)	118.9	120.5	292.8	10.0	3.3	5.0	7.8
#3D (LITVIN #4)	107.7	117.5	281.0	6.7	3.4	6.7	7.4

[1]FEA @125% LOAD
[2]TCA
[3]LTCA

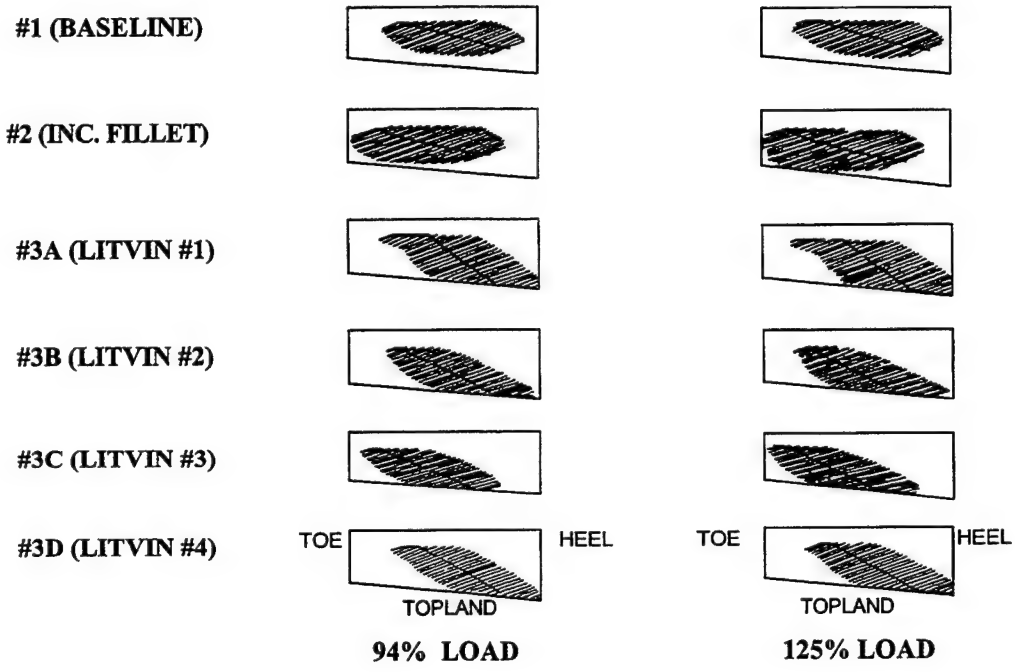

FIGURE 69: LTCA PREDICTED SPIRAL BEVEL GEAR MEMBER TOOTH CONTACT

The gear member tooth contact patterns under load, predicted by Gleason's LTCA program are presented in Figure 69 for each configuration gear mesh.

The contact patterns shown for Configurations #1 and #2 are typical BHTI spiral bevel patterns with the contact pattern remaining within the perimeter of the tooth surface even at high loads. The tooth contact pattern for Configuration #3A shows a much different pattern shape and orientation with the lines of contact running off the tooth topland and ending abruptly at the root indicating tip interference on both the gear and pinion members. Configuration #3B was an attempt to maintain the very low transmission errors predicted for Configuration #3A while trying to replicate the pattern for Configuration #1. Configuration #3C was designed to shift the pattern for #3B to the toe of the tooth to reduce tooth mesh entrance interference at the heel. Configuration #3D was designed to move the pattern back towards the heel of the tooth after observing the actual loaded tooth contact patterns for Configuration #3C which showed no contact on a portion of the heel even at 125% load. Configuration #3C was selected for further testing as described below and therefore, Configuration #3D was analyzed for reference only.

6.2.2 SPIRAL BEVEL KINEMATIC ERROR TESTS

A kinematic error test was completed on two Configuration #1 spiral bevel gear sets, two Configuration #2 gear sets and on one set each of Configurations #3A, #3B, and #3C. Transmission error data was collected for each gear set run with minimum load at 100 RPM of pinion speed. Evaluations of the gear set transmission error were made at the proper mounting distance, at varied mounting locations (sensitivity study), and at the deflection locations predicted for 125% load. A summary of the data for each gear set is presented in Tables 43 through 49. The mounting location terminology (P =, G =, E =) used for the kinematic error tests is shown in Figure 70. At the "deflected" location in Tables 43 through 49, E = -.002", P = +.014", G = -.002", and α= 94° 58'.

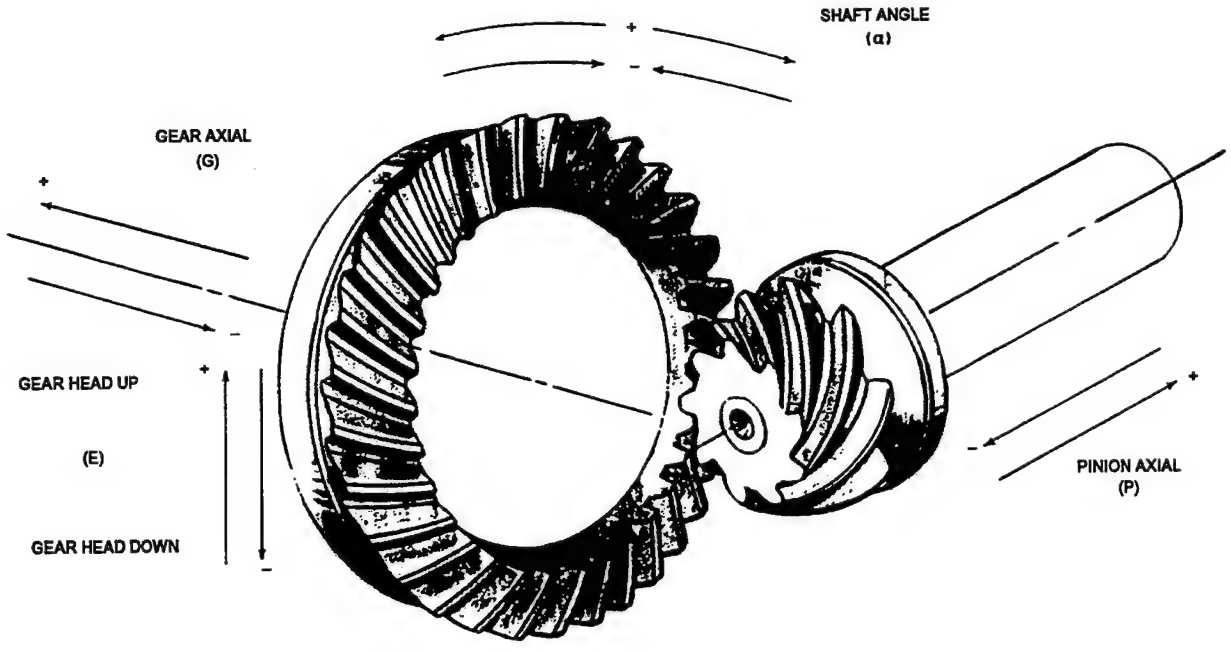

FIGURE 70: MOUNTING LOCATION OFFSET TERMINOLOGY FOR KINEMATIC ERROR TESTS

TABLE 43: TRANSMISSION ERROR SUMMARY FOR CONFIGURATION #1 SPIRAL BEVEL GEAR SET (PINION SERIAL NO. A-22, GEAR SERIAL NO. A-15)

MOUNTING LOCATION	TOTAL ACCUMULATED PITCH VARIATION (ARCSEC)	AVERAGE PROFILE ERROR (ARCSEC)	TOTAL TRANSMISSION ERROR (ARCSEC)	1ST MESH HARMONIC (ARCSEC)
NO OFFSETS	142	25	166	20
P = +.002"	138	26	166	20
P = - .002"	138	24	162	19
G = +.002"	138	24	166	20
G = - .002"	138	25	166	20
E = +.002"	134	26	162	21
E = -.002"	138	24	162	19
DEFLECTED	142	27	170	22

TABLE 44: TRANSMISSION ERROR SUMMARY FOR CONFIGURATION #1 SPIRAL BEVEL GEAR SET (PINION SERIAL NO. A-30, GEAR SERIAL NO. A-4)

MOUNTING LOCATION	TOTAL ACCUMULATED PITCH VARIATION (ARCSEC)	AVERAGE PROFILE ERROR (ARCSEC)	TOTAL TRANSMISSION ERROR (ARCSEC)	1ST MESH HARMONIC (ARCSEC)
NO OFFSETS	61	24	85	19
P = +.002"	61	24	85	20
P = - .002"	61	23	85	19
G = +.002"	65	23	85	19
G = - .002"	65	23	85	20
E = +.002"	61	24	85	20
E = -.002"	65	23	85	19
DEFLECTED	142	25	170	21

TABLE 45: TRANSMISSION ERROR SUMMARY FOR CONFIGURATION #2 SPIRAL BEVEL GEAR SET (PINION SERIAL NO. A-93, GEAR SERIAL NO. A-35)

MOUNTING LOCATION	TOTAL ACCUMULATED PITCH VARIATION (ARCSEC)	AVERAGE PROFILE ERROR (ARCSEC)	TOTAL TRANSMISSION ERROR (ARCSEC)	1ST MESH HARMONIC (ARCSEC)
NO OFFSETS	65	22	81	18
P = +.002"	65	23	81	18
P = - .002"	65	23	85	18
G = +.002"	65	23	81	18
G = - .002"	61	23	81	18
E = +.002"	65	24	85	18
E = -.002"	65	23	85	18
DEFLECTED	65	26	89	21

TABLE 46: TRANSMISSION ERROR SUMMARY FOR CONFIGURATION #2 SPIRAL BEVEL GEAR SET (PINION SERIAL NO. A-73, GEAR SERIAL NO. A-33)

MOUNTING LOCATION	TOTAL ACCUMULATED PITCH VARIATION (ARCSEC)	AVERAGE PROFILE ERROR (ARCSEC)	TOTAL TRANSMISSION ERROR (ARCSEC)	1ST MESH HARMONIC (ARCSEC)
NO OFFSETS	61	23	85	19
P = +.002"	65	24	85	19
P = - .002"	61	22	85	18
G = +.002"	57	23	81	19
G = - .002"	61	23	85	19
E = +.002"	61	23	85	19
E = -.002"	61	22	85	18
DEFLECTED	65	26	89	21

TABLE 47: TRANSMISSION ERROR SUMMARY FOR CONFIGURATION #3A SPIRAL BEVEL GEAR SET (PINION SERIAL NO. A-111 GEAR SERIAL NO. A-19)

MOUNTING LOCATION	TOTAL ACCUMULATED PITCH VARIATION (ARCSEC)	AVERAGE PROFILE ERROR (ARCSEC)	TOTAL TRANSMISSION ERROR (ARCSEC)	1ST MESH HARMONIC (ARCSEC)
NO OFFSETS	41	7	49	4
P = +.002"	45	7	49	4
P = - .002"	41	10	49	7
G = +.002"	41	9	49	5
G = - .002"	45	8	49	5
E = +.002"	41	7	49	5
E = -.002"	41	9	49	6
DEFLECTED	41	12	57	9

TABLE 48: TRANSMISSION ERROR SUMMARY FOR CONFIGURATION #3B SPIRAL BEVEL GEAR SET (PINION SERIAL NO. A-116 GEAR SERIAL NO. A-6)

MOUNTING LOCATION	TOTAL ACCUMULATED PITCH VARIATION (ARCSEC)	AVERAGE PROFILE ERROR (ARCSEC)	TOTAL TRANSMISSION ERROR (ARCSEC)	1ST MESH HARMONIC (ARCSEC)
NO OFFSETS	41	11	53	9
P = +.002"	41	11	49	9
P = - .002"	45	11	53	9
G = +.002"	45	12	53	9
G = - .002"	45	12	57	9
E = +.002"	45	11	53	9
E = -.002"	45	12	53	9
DEFLECTED	45	9	53	6

TABLE 49: TRANSMISSION ERROR SUMMARY FOR CONFIGURATION #3C SPIRAL BEVEL GEAR SET (PINION SERIAL NO. A-65 GEAR SERIAL NO. A-45)

MOUNTING LOCATION	TOTAL ACCUMULATED PITCH VARIATION (ARCSEC)	AVERAGE PROFILE ERROR (ARCSEC)	TOTAL TRANSMISSION ERROR (ARCSEC)	1ST MESH HARMONIC (ARCSEC)
NO OFFSETS	61	15	73	11
P = +.002"	57	14	69	11
P = - .002"	57	15	69	11
G = +.002"	57	15	69	11
G = - .002"	57	15	69	11
E = +.002"	57	16	69	12
E = -.002"	57	15	69	11
DEFLECTED	57	11	69	8

For the data in each table, the total accumulated pitch variation provides a measurement of the indexing accuracy of the gear teeth and the amount of runout relative to the gear mounting axis, and the average profile error provides a measurement of the tooth to tooth meshing accuracy of the gear set. The minor variations of the average profile error measured for all of the gear sets and among the various mounting locations, demonstrate the ability of the tooth geometry to accommodate typical installation and housing deflections for rotorcraft spiral bevel gear sets.

Table 50 presents a summary of the predicted and measured kinematic error levels at no load for each configuration. The results of the kinematic error tests clearly demonstrate the accuracy of the LTCA predicted transmission error levels.

TABLE 50: SUMMARY OF PREDICTED SPIRAL BEVEL KINEMATIC ERROR LEVELS VS. MEASURED LEVELS

CONFIGURATION	1ST MESH HARMONIC TRANSMISSION ERROR (ARCSEC)	
	LTCA PREDICTED	MEASURED
#1	20	19 - 20
#2	18	18 - 19
#3A	6	4
#3B	7	9
#3C	10	11

6.2.3 SPIRAL BEVEL LOADED TOOTH CONTACT PATTERN EVALUATION

A loaded tooth contact pattern development test was conducted on one set of each configuration of spiral bevel gears at The Gleason Works in Rochester, N.Y. Each set was assembled in the OH-58D main transmission housing and rolled through mesh at 5 RPM of the pinion at loads from 0 to 125% torque in 25% increments. A schematic of the test rig is shown in Figure 71. Photographs were taken of the tooth contact pattern on the gear member after each load step. Sketches of the photos are shown in Figure 72. The similarity of the actual tooth contact patterns to those predicted by LTCA, shown in Figure 69, verify the accuracy of the LTCA program for predicting tooth contact patterns.

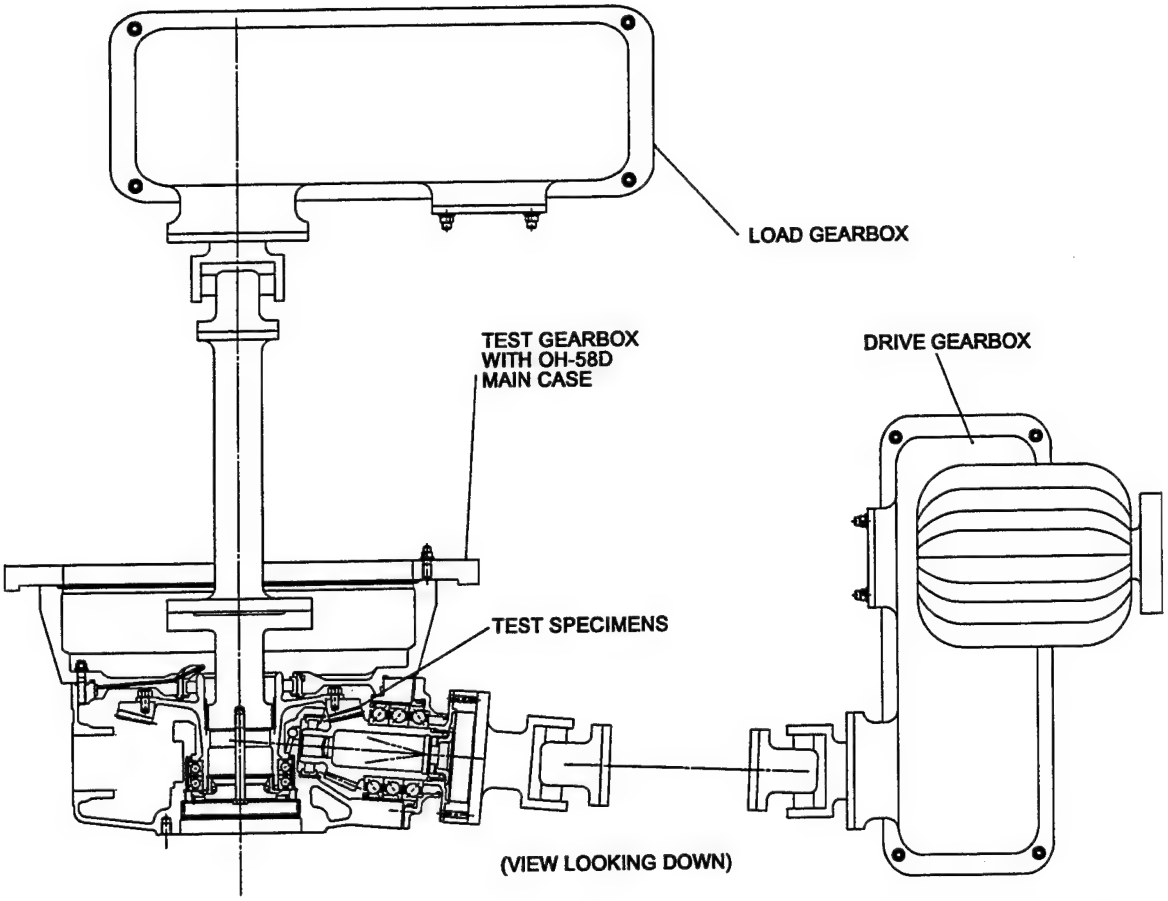

FIGURE 71: SCHEMATIC OF SPIRAL BEVEL LOADED TOOTH CONTACT TEST RIG

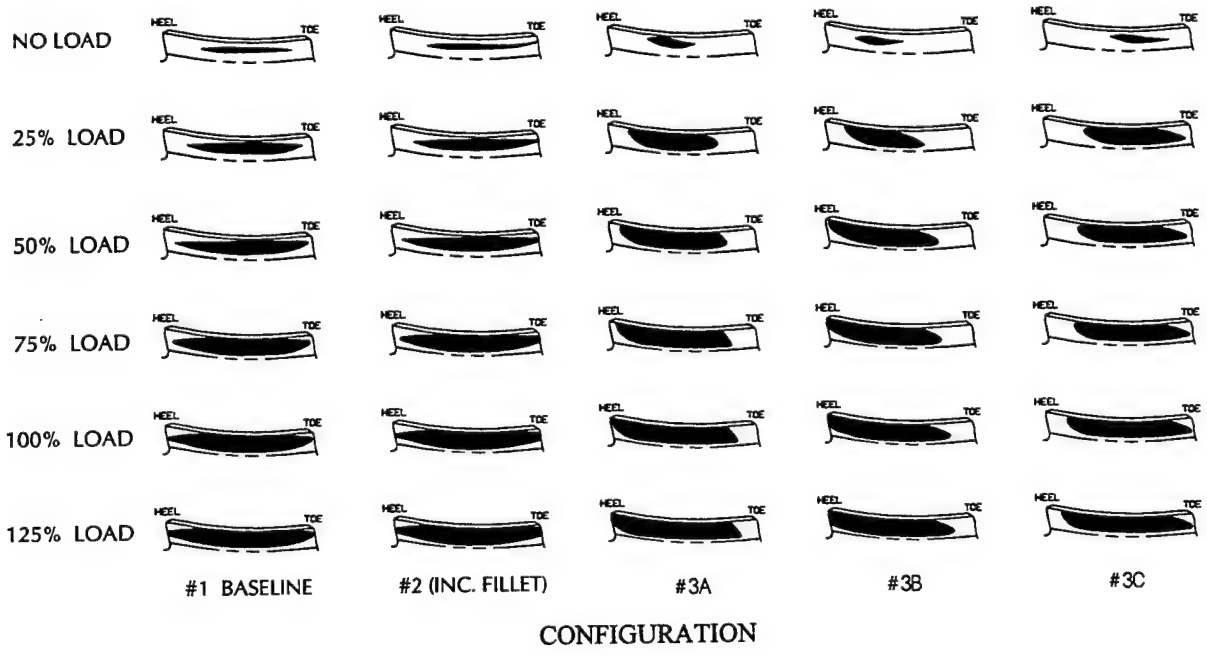

FIGURE 72: GEAR TOOTH CONTACT PATTERNS FROM LOADED TOOTH CONTACT TESTS

Based on the data listed in Table 42 and the results of the loaded tooth contact tests, Configuration #3C was selected for further tests (tooth bending, tooth pitting, tooth scoring, noise and vibration, and tooth strain survey) for comparison with Configurations #1 and #2. Configuration #3C was selected because its tooth contact pattern was the closest to the pattern for the baseline spiral bevel set while the measured gear mesh transmission error was 40% to 60% lower.

6.2.4 SPIRAL BEVEL NOISE AND VIBRATION TESTS

Noise and vibration measurements were made for two sets of each configuration gear set (#1, #2, and #3C) assembled in a complete OH-58D main transmission as shown in Figure 68. The tests were conducted in the 500 hp helicopter transmission test stand at NASA Lewis Research Center in Cleveland, Ohio [31]. A schematic of the test stand is shown in Figure 73.

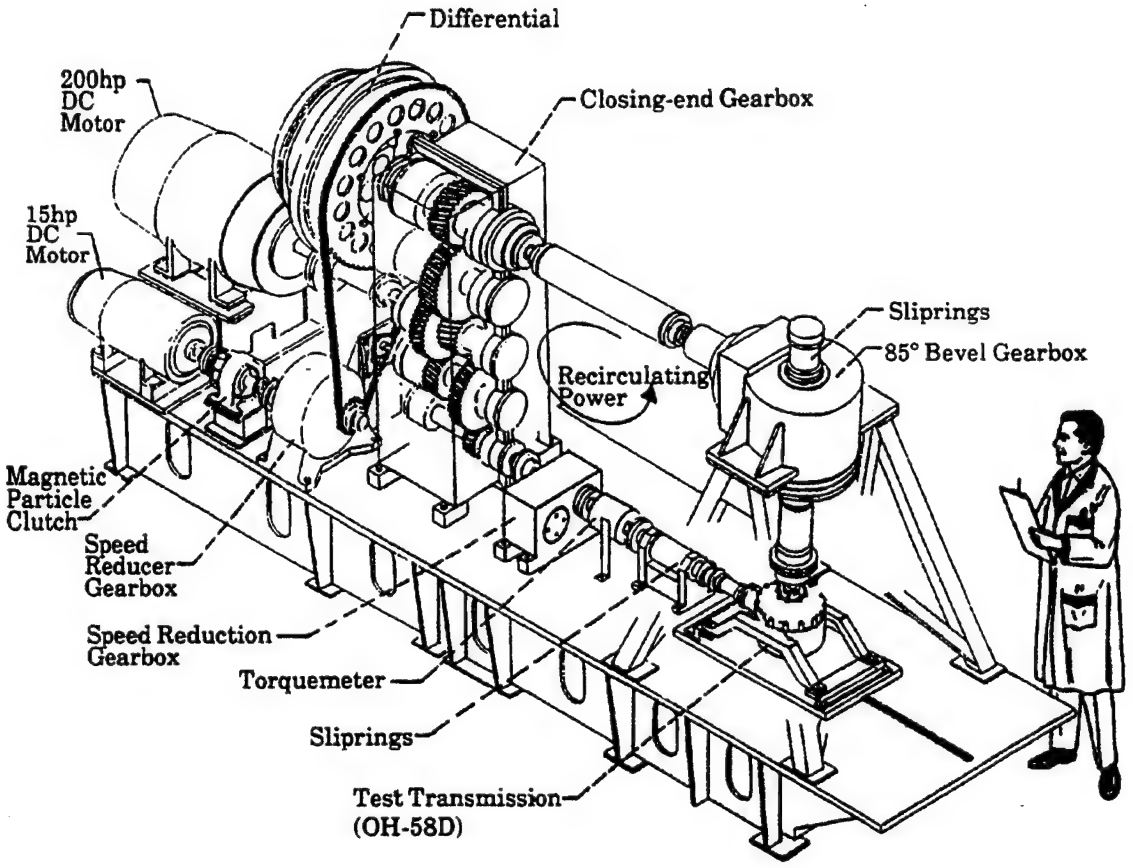

FIGURE 73: NASA 500 HP TEST STAND WITH OH-58D TRANSMISSION INSTALLED

The noise and vibration measurements were made concurrently for each set of gears tested. Each set of gears was installed in the OH-58D transmission and tested at 6016 RPM input speed (100%) and 210° ± 5°F oil-in temperature. The test lubricant was DOD-L-85734. Noise and vibration measurements were made at 50%, 75%, 100% and 125% torque levels after the transmission oil outlet temperature had stabilized.

For the noise tests, acoustic intensity measurements were made using the two microphone technique. The microphones were connected to a spectrum analyzer which computed the acoustic intensity from the imaginary

part of the cross-power spectrum. Near the input region of the test transmission, a grid was installed which divided the region into sixteen areas as shown in Figure 74. The acoustic intensity was measured at the center of each of the sixteen areas. Only positive acoustic intensities (noise flowing out of the area) were considered. The acoustic intensities were then added together and multiplied by the total area of the grids to obtain the sound power of the transmission input region. For each acoustic intensity spectrum at a grid point, 100 frequency-domain averages were collected and the sound power spectrum computed.

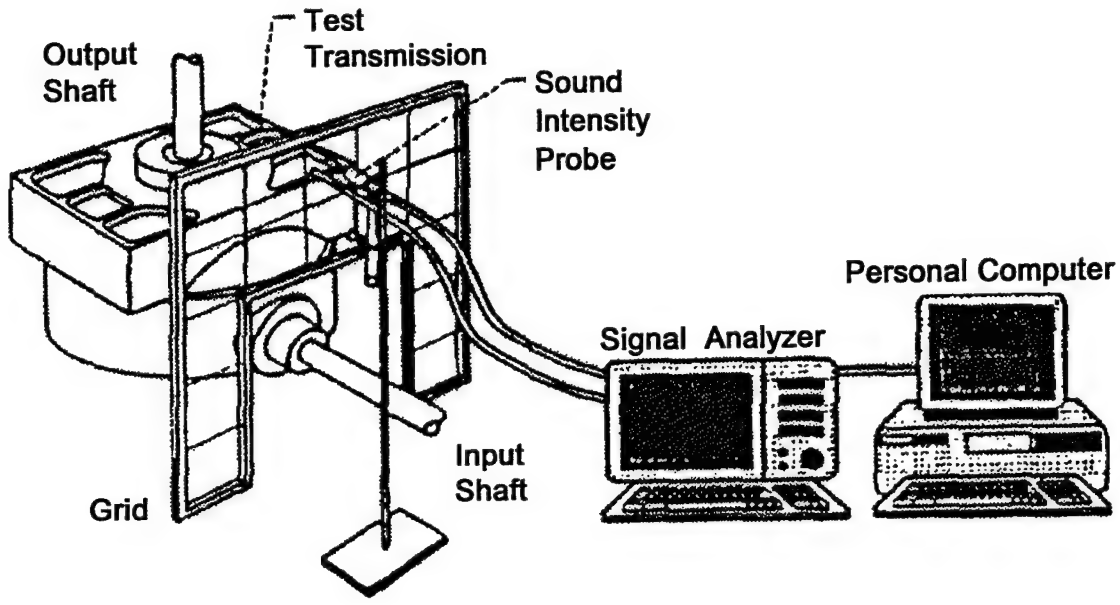

FIGURE 74: SPIRAL BEVEL NOISE TEST - SOUND INTENSITY MEASUREMENT SYSTEM

For the vibration measurements, ten accelerometers were mounted at the various locations on the OH-58D transmission shown in Figure 75. Accelerometers 1, 2, and 10 measured vibrations radially to the input shaft, 3, 4, and 9 measured radially to the planetary, and 5 and 8 measured vertically.

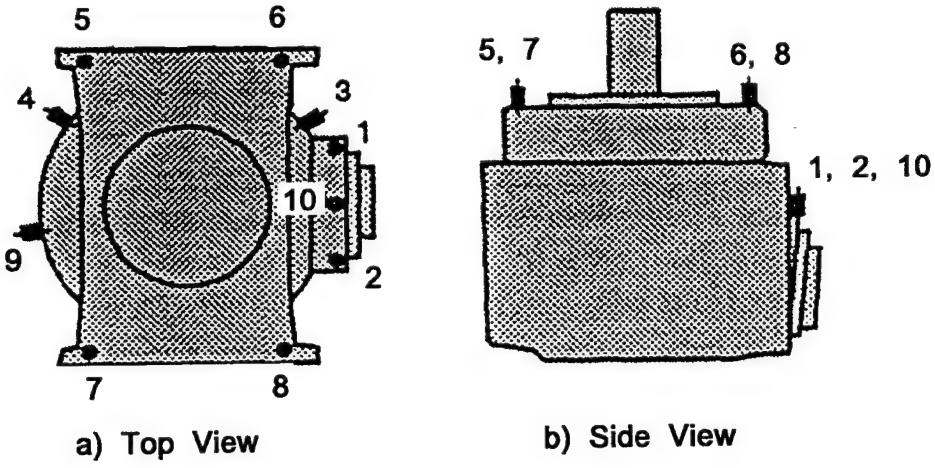

FIGURE 75: SPIRAL BEVEL VIBRATION TEST - ACCELEROMETER LOCATIONS

The vibration data for each test was recorded on tape and was subsequently analyzed using time averaging. The vibration data was input into a signal analyzer along with a tach pulse from the transmission input shaft. The signal analyzer was triggered from the tach pulse to read the vibration data when the transmission input shaft was at the same position. The vibration signal was then averaged in the time domain using 100 averages which removed all the vibration which was not synchronous to the input shaft. This allowed a clear comparison of the vibration data for each spiral bevel set tested.

The results of the noise measurements are shown in Figure 76 with the combined sound power of the 1st (1905 Hz) and 2nd (3810 Hz) harmonics of the spiral bevel meshing frequency plotted against the input torque levels.

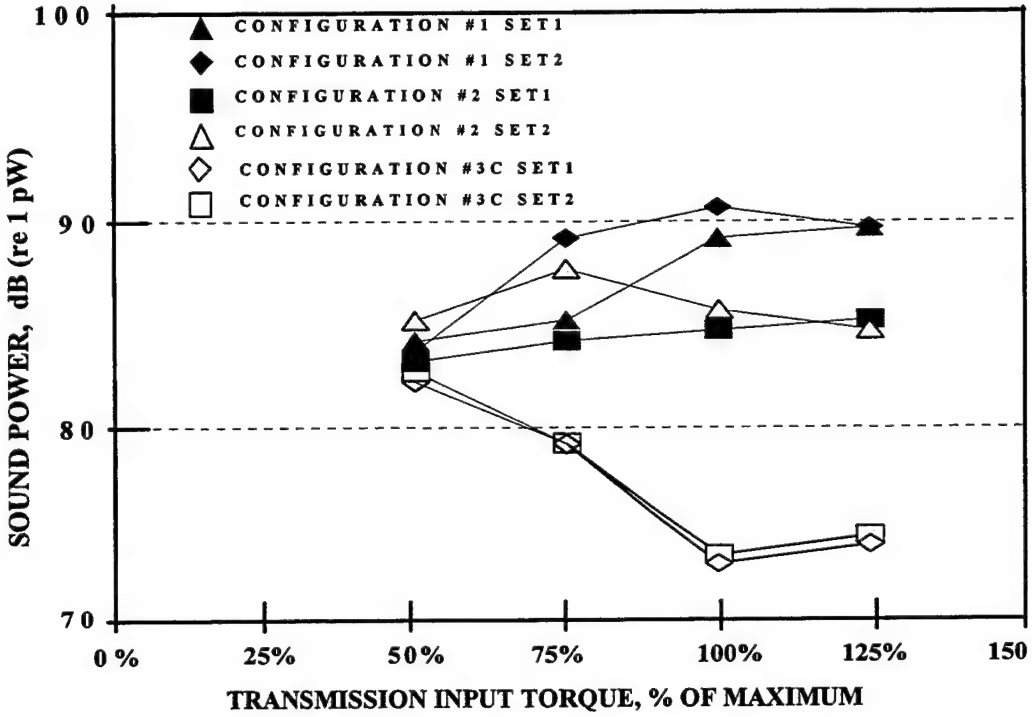

FIGURE 76: RESULTS OF SPIRAL BEVEL NOISE MEASUREMENTS

While there is some scatter among the baseline (Conf. #1) and increased fillet (Conf. #2) gear sets, the reduced transmission error sets (Conf. #3C) produced a significant reduction in the sound power level. At 100% torque, the sound power level is 11 to 18 dB lower than for the baseline and increased fillet sets. No noise level reduction was expected for the increased fillet gear sets since the gear tooth profile surface is identical to the baseline geometry. Differences in noise levels between the baseline and increased fillet sets can be attributed to differences in tooth stiffnesses, manufacturing tolerances, and assembly tolerances.

To further investigate the effect of assembly tolerances on the measured noise levels, the tests on set one of the Configuration #3C gears was repeated twice. Prior to each repetition, the gear and pinion were removed from and then reinstalled into the main transmission. The results were repeatable for all three tests conducted on the same gear mesh within about 2 dB at each torque level.

The results of the vibration measurements are shown in Figure 77 with the time averaged acceleration response from accelerometer #1, mounted near the input spiral bevel mesh, plotted against the input torque levels. As with the noise measurements, the reduced kinematic error Configuration #3C gear produced a significant

reduction in the vibration levels. The vibration response from the other 9 accelerometers mounted at the various locations showed similar results. On the average, at the 100% torque level, the vibration levels for the Configuration #3C gear sets were 5 to 10 g's lower than the Configuration #1 and #2 sets.

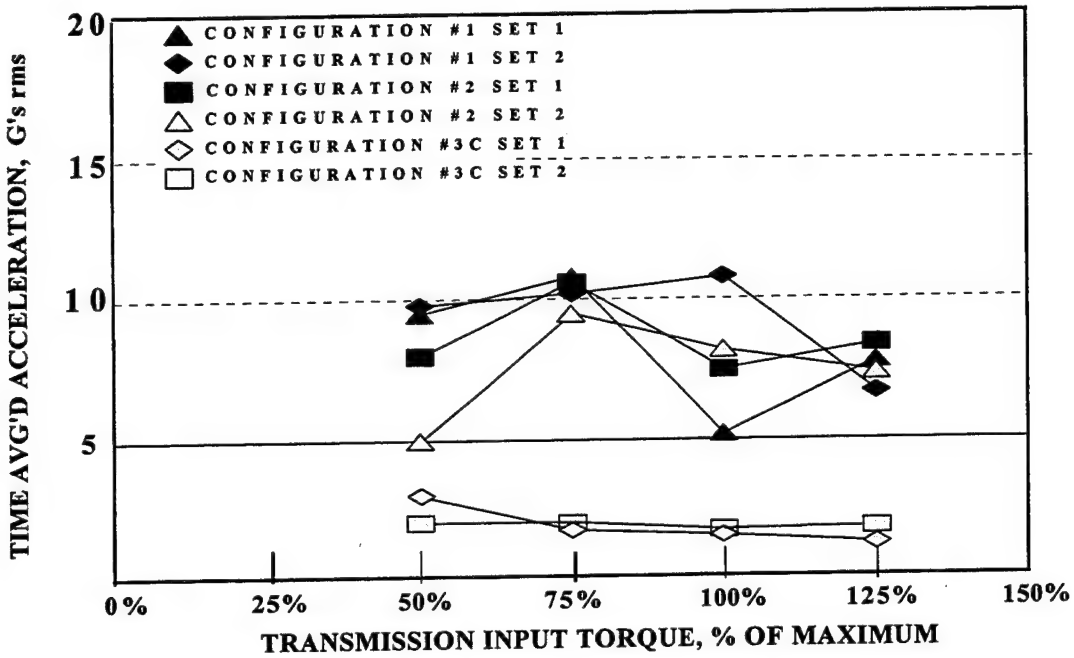

FIGURE 77: RESULTS OF SPIRAL BEVEL VIBRATION MEASUREMENTS (ACCELEROMETER #1)

6.2.5 SPIRAL BEVEL DYNAMIC & STATIC TOOTH BENDING STRAIN SURVEY

In addition to the noise and vibration tests, a dynamic and static tooth bending strain survey was conducted on one set of each configuration spiral bevel gear set at the NASA Lewis Research Center [31]. These tests were also conducted in the OH-58D transmission installed in the 500 Hp transmission test stand shown in Figure 73.

Twenty-six strain gages were mounted on each gear member. Seven gages were located in the tooth fillet on the drive side (highest tensile strain) at a line 45° to the tooth centerline as shown in Figure 78. Five of the fillet gages were evenly distributed from toe to heel and the two additional gages were clustered around the gage located nearest the point of highest strain predicted by Gleason's FEA program. Five gages were located in the tooth root as shown in Figure 78 evenly distributed from toe to heel and one gage was located in the tooth root centered over the attaching bolt hole for the gear. This arrangement of 13 gages was repeated on adjacent teeth for a total of 26 gages located as shown in Figure 79(b). Twenty gages were mounted on each pinion member in locations similar for the gages on the gear member as shown in Figure 79(a).

The fillet gages were located at the 45° location to avoid any tooth meshing damage. A 30° location may have been optimum for maximum tooth bending strain measurements [32] but would have located the gages higher on the gear tooth profile presenting possible interference with the mating teeth. The root gages were mounted to measure root stresses which can be significant in thin-rimmed aerospace gear applications [33]. The grid length of the gages was .015", and the nominal resistance was 120 Ω.

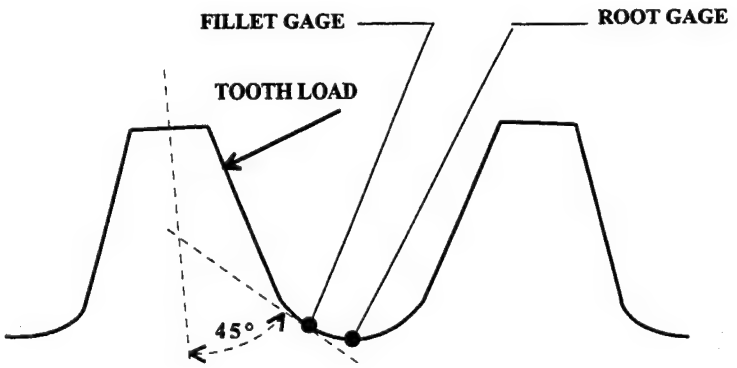

FIGURE 78: SPIRAL BEVEL FILLET & ROOT STRAIN GAGE LOCATIONS

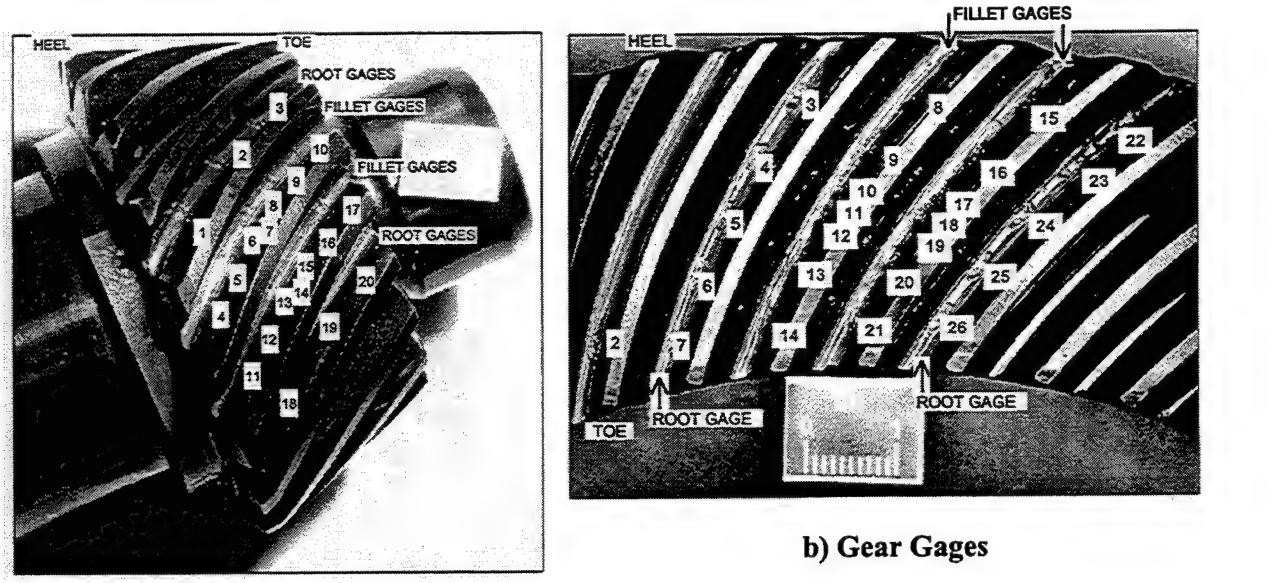

a) Pinion Gages

b) Gear Gages

FIGURE 79: STRAIN GAGE LOCATIONS ON SPIRAL BEVEL PINION AND GEAR

The static strain measurements were made on both the gear and pinion members of each configuration (#1, #2, & #3C) at room temperature and at 50%, 75%, 100%, and 125% torque levels. A handcrank was installed on the input shaft to manually rotate the pinion and gear through mesh as shown in Figure 80. A sensor was installed on the transmission output shaft to measure input shaft position. At the start of each test, the transmission was completely unloaded and the strain gage conditioners zeroed. The transmission was then loaded to the test torque level, the shaft positioned and the strain measurements recorded. This was repeated over a range of shaft positions to obtain the tooth strain as a function of shaft position for the pinion and gear gages. After each strain measurement at each shaft position and torque level, the transmission was completely unloaded and the gage conditioner zeroes checked for drift.

The dynamic strain measurements were made on the pinion members only of each configuration at 6016 RPM of the input pinion and at 50%, 75%, 100%, and 125% torque levels. The oil-inlet temperature was maintained at 210° ± 5° F throughout the tests. The pinion gages were connected to slip rings mounted on the input shaft as shown in Figure 80.

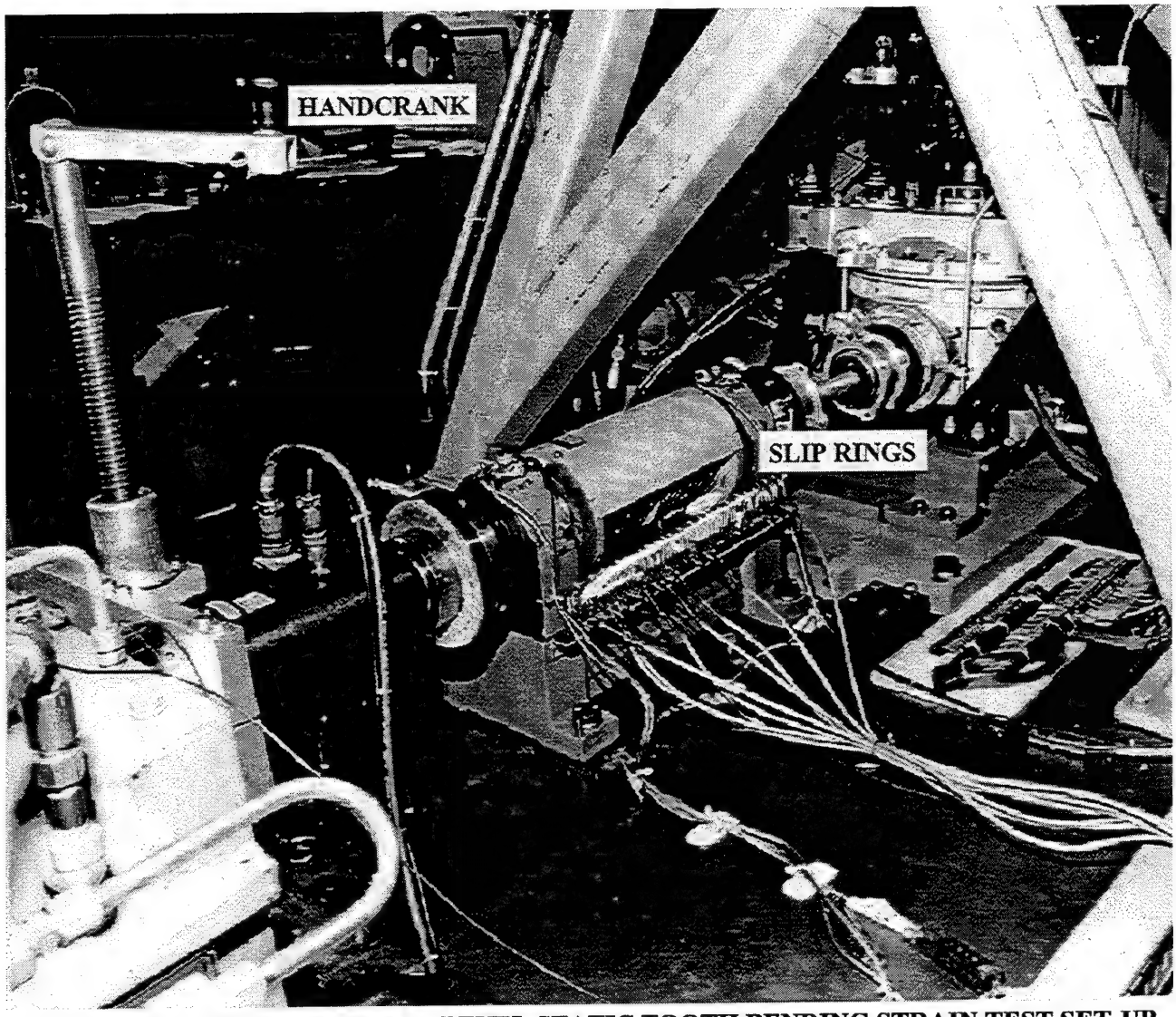

FIGURE 80: IMPROVED SPIRAL BEVEL STATIC TOOTH BENDING STRAIN TEST SET-UP

The results of the static tests at 125% torque for each configuration gear and pinion are presented in Figure 81. Figures 81(a) and 81(b) show the maximum tensile and compressive stress distribution across the pinion and gear face widths for the fillet gages at 125% torque, and Figures 81(c) and 81(d) show the maximum tensile and compressive stress distribution across the pinion and gear face widths for the root gages at 125% torque. The stresses plotted for each location are the maximum tensile and compressive stresses measured over a range of input shaft positions covering a complete meshing cycle of the gear and pinion. The results clearly show the benefit of increasing the tooth fillet radius on both the gear and pinion. While Gleason's analysis had predicted a 20% reduction in the pinion tensile stress (145.7 KSI reduced to 116.5 KSI) between the baseline and increased fillet geometry, the measured tensile stress on the increased fillet pinion was actually 24% lower than the baseline pinion (143.5 KSI reduced to 108.4 KSI). For the gear tensile stress, Gleason's analysis had predicted a slight increase in the bending tensile stress (140.7 KSI increased to 142.7 KSI) for the increased fillet geometry over the baseline gear, but the measured tensile stress was actually 10% lower for the increased fillet geometry (98.2 KSI reduced to 88.4 KSI).

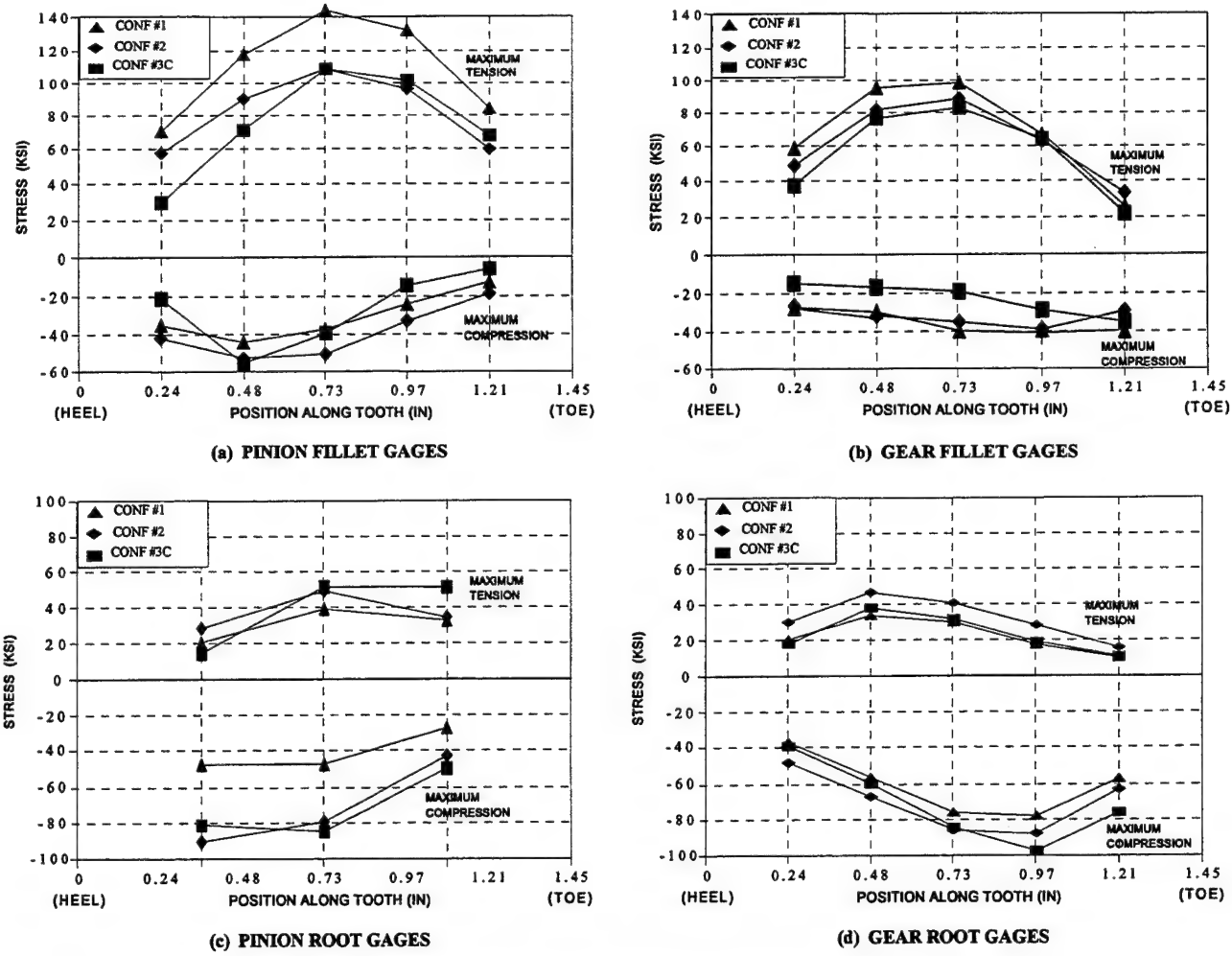

FIGURE 81: SPIRAL BEVEL STATIC STRAIN TEST RESULTS AT 125% TORQUE

For the low noise geometry spiral bevel set (Conf. #3C) Gleason's analysis had predicted an 18% reduction in the maximum pinion tensile stress (145.7 KSI reduced to 118.9 KSI) between the baseline and low noise geometry, while the measured stress on the low noise pinion was also 24% lower than the baseline pinion (143.5 KSI reduced to 108.5 KSI). For the gear stress, Gleason's analysis had predicted a 14% reduction in the maximum bending stress (140.7 KSI reduced to 120.5 KSI) between the low noise and baseline geometry, while the measured stress was actually 16% lower for the low noise geometry (98.2 KSI reduced to 82.8 KSI).

The gear stresses predicted by Gleason's analysis are substantially higher than those measured because the Gleason analysis included thermal growth deflections for the gearbox at normal operating temperatures. The static strain survey was conducted at room temperature.

Figure 82 shows the stress cycles for the highest stressed location of each gear and pinion tooth for each configuration. While the increased fillet geometry of Configuration #2 clearly reduced the maximum tensile stress on both the gear and pinion, it also caused an increase in the maximum compressive stress on the pinion. The Configuration #3C geometry significantly reduced the maximum tensile stress of both the gear and pinion without increasing the maximum compressive stress.

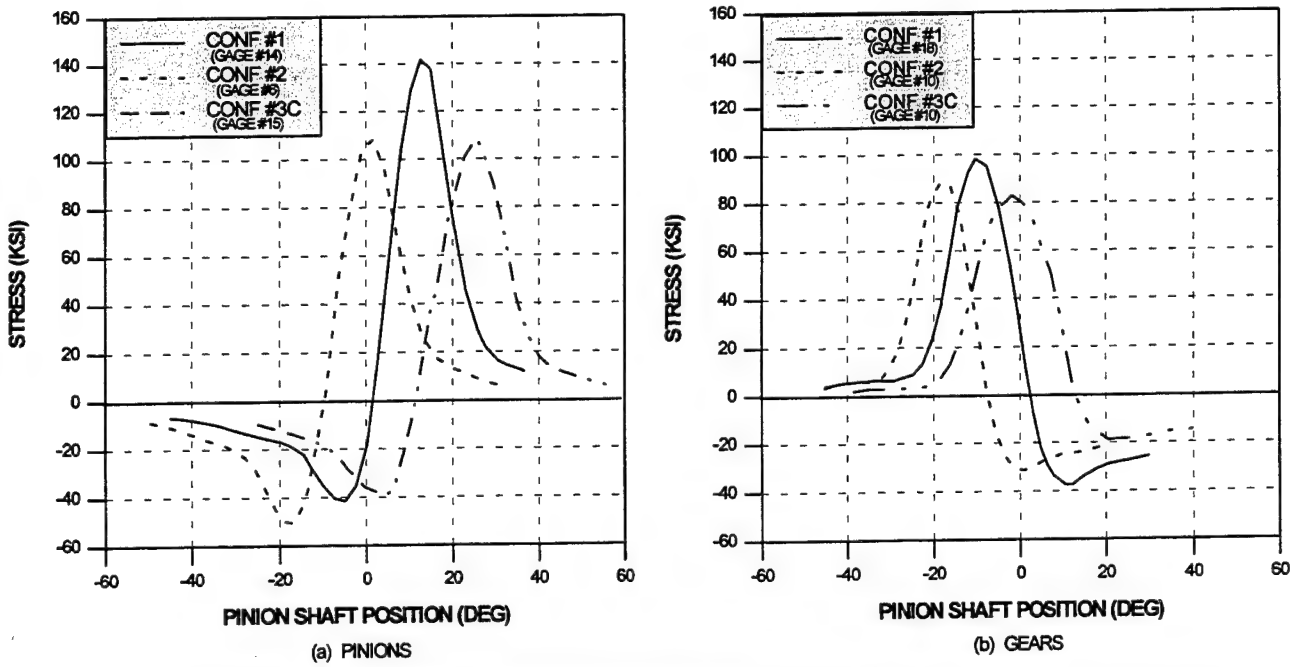

FIGURE 82: MAXIMUM MEASURED STRESS CYCLE AT TOOTH FILLET GAGES - SPIRAL BEVEL STATIC STRAIN SURVEY AT 125% TORQUE

To quantify the benefits of Configurations #2 and #3C over the baseline Configuration #1, the data from Figure 82 has been plotted on the Modified Goodman Diagrams in Figure 83. The line plotted for the perfect specimen is the fatigue fracture line established by the results of the flexure fatigue tests conducted on gas carburized, notched X-53 flexure specimens (see section 6.3). Two data points were established by the flexure fatigue tests. The first at 100 ± 100 KSI is the mean - 3 sigma endurance limit for the specimens and the Y-intercept at 140 KSI oscillatory stress is equal to 70% of the unidirectional endurance limit [10] of 200 KSI (100 ± 100 KSI).

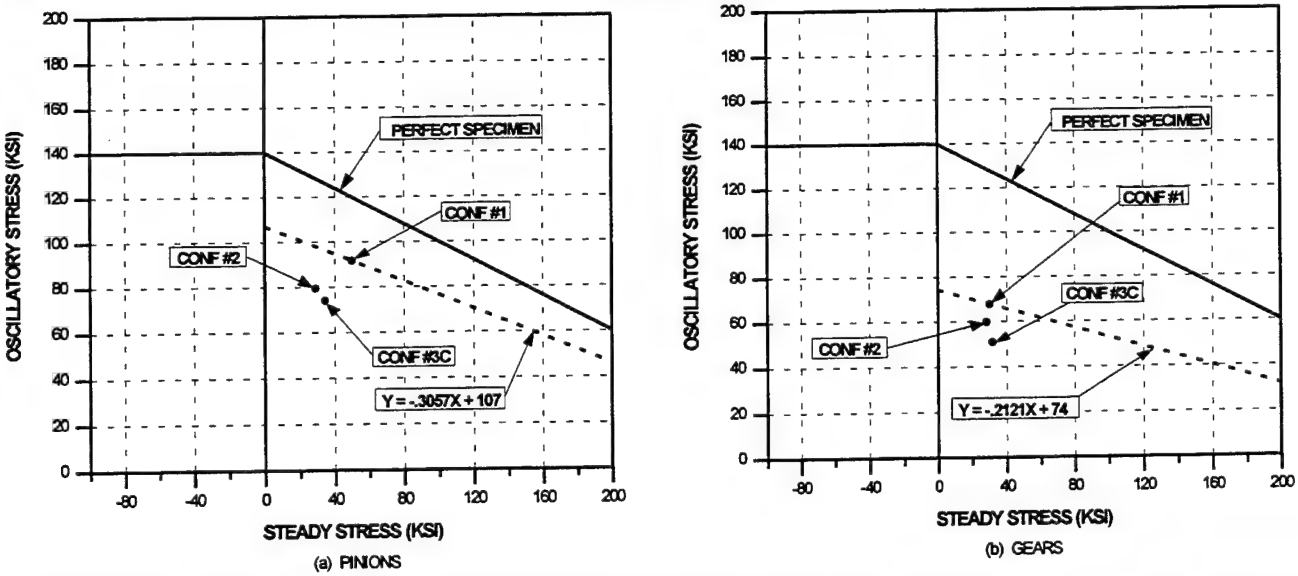

FIGURE 83: MODIFIED GOODMAN DIAGRAMS FOR SPIRAL BEVEL GEAR & PINION COMPARISON

For the pinions, the line plotted through the Configuration #1 data point of 50.2 ± 91.7 KSI extends to the same x-intercept as for the perfect specimen. This becomes the baseline allowable fracture fatigue line represented by the linear equation:

$$Y = -.3057X + 107$$

Where Y = oscillatory stress (KSI) and X = steady stress (KSI).

The allowable increase in torque for the Configuration #2 pinion is calculated by substituting the measured stress level (29 ± 79.4 KSI) into the linear equation for the Configuration #1 pinion.

$$(79.4) \times F = [(-.3057)(29) \times F] + 107; \quad \text{Where F = torque increase factor}$$

Solving for 'F', the allowable increase in torque for the Configuration #2 pinion over the torque level for Configuration #1 is 21%. Similarly the allowable torque level increase for the Configuration #3C pinion (34.6 ± 74 KSI measured stress level) is 27%.

For the gears, the line plotted through the Configuration #1 data point of 30.4 ± 67.8 KSI extends to the same x-intercept as for the perfect specimen. This becomes the baseline allowable fracture fatigue line represented by the linear equation:

$$Y = -.2121X + 74$$

Where Y = oscillatory stress (KSI) and X = steady stress (KSI).

The allowable increase in torque for the Configuration #2 gear is calculated by substituting the measured stress level (28.5 ± 59.9 KSI) into the linear equation for the Configuration #1 gear.

$$(59.9) \times F = [(-.2121)(28.5) \times F] + 74; \quad \text{Where F = torque increase factor}$$

Solving for 'F', the allowable increase in torque for the Configuration #2 gear over the torque level for Configuration #1 is 12%. Similarly the allowable torque level increase for the Configuration #3C gear (32 ± 50.9 KSI measured stress level) is 28%.

Figure 84 shows the increase in the measured stress level for the maximum stress cycle locations for each gear and pinion as the torque level is increased from 50% to 125% during the static strain tests. As expected the stress level increases linearly with the increase in torque level.

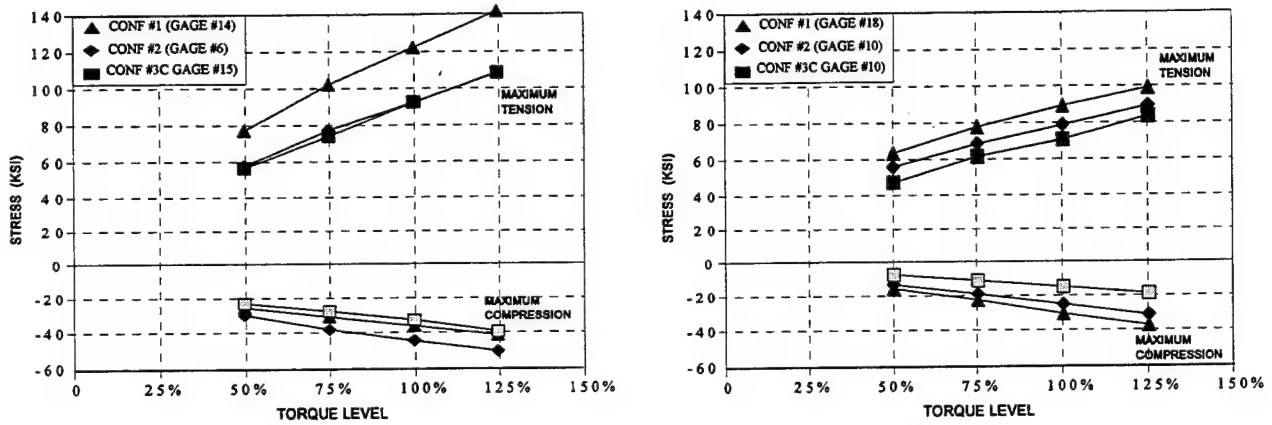

(a) PINION FILLET GAGES

(b) GEAR FILLET GAGES

FIGURE 84: MEASURED STRESS LEVEL VS. TORQUE LEVEL (SPIRAL BEVEL STATIC STRAIN TEST)

The results of the dynamic strain survey conducted on the instrumented spiral bevel pinions, did not show any increase in the measured stress levels as compared to the stresses measured for the static tests. A 5% increase is typically assumed as a dynamic factor but the stress levels were actually lower for the dynamic strain measurements. Table 51 presents a comparison of the maximum and minimum stress levels measured during the static and dynamic tests at 125% torque for the Configuration #2 and #3C pinions. No comparison data is available for the Configuration #1 pinion since the strain gages at the high stress locations had failed prior to the 125% dynamic test.

TABLE 51: COMAPRISON OF MEASURED STRESS LEVELS FROM SPIRAL BEVEL STATIC AND DYNAMIC STRAIN TESTS AT 125% TORQUE

	CONFIGURATION #2		CONFIGURATION #3C	
	STATIC	DYNAMIC	STATIC	DYNAMIC
MAXIMUM STRESS (KSI)	108.4	101.8	108.5	104.1
MINIMUM STRESS (KSI)	-50.5	-54.1	-39.4	-43.1

6.2.6 SPIRAL BEVEL GEAR TOOTH PITTING FATIGUE TESTS

Gear tooth pitting fatigue tests were conducted on two sets of each configuration gear set at the Gleason Works in Rochester, N.Y. The tests were conducted in Gleason's four-square test rig shown in Figure 85. The test transmission was an OH-58D main transmission with the planetary removed, also shown in Figure 85. The speed of the test rig was limited to 3000 RPM for continuous operation, therefore the 6016 input RPM for the spiral bevel pinion was reduced to 3000 RPM for these tests. Each pitting test on each set of spiral bevel gears was conducted for 180 hours with the oil-in temperature maintained at 230° ± 10° F. For Configurations #1 and #2 the tests were conducted at 100% torque but for Configuration #3C the tests were conducted at 125% torque combining the pitting test for this configuration with the tooth bending fatigue test described in Section 6.2.7. The test time of 180 hours was selected to subject the gear member of each set to 10 million fatigue cycles.

The objective of these tests was to demonstrate the capability of each configuration to pass a qualification type pitting overstress test. No pitting failures were expected. After each test the gears were removed from the gearbox for close visual inspection and magnetic particle inspection. No pitting failures were observed on any of the test gears, however, a hardline, polished line of black oxide removal, (see Figure 86) was observed in the flank of each Configuration #3C pinion and on the corresponding tip of each mating gear. A close visual examination under a microscope revealed a line of black oxide removal in the flank of the pinions and a corresponding line of black oxide removal on the tips of the mating gear teeth. No evidence of micropitting was observed, and a surface profile trace through the hardline on the pinion showed a depth of approximately .000050". The width of the hardline on the pinion flank was approximately .020".

A subsequent close visual inspection of the Configuration #3C spiral bevel set tested at NASA LeRC revealed the same type of polished hardline. The bevel set at NASA had been run for less than 20 hours at various load levels from 50% to 125% torque whereas the bevel sets at Gleason had been run for 180 hours at 125% torque and yet the size and appearance of the hardline was nearly identical for all three sets. This suggests that the hardline occurs early in the gear set meshing, probably at the higher load levels, but does not progress beyond the initial black oxide removal.The hardline is most likely the result of gear tip/pinion flank mesh interference caused by tooth deflections at higher loads. A separate modification and test program was undertaken to eliminate the hardline without affecting the low noise characteristics for this gear set. This effort is described in Section 6.2.9.

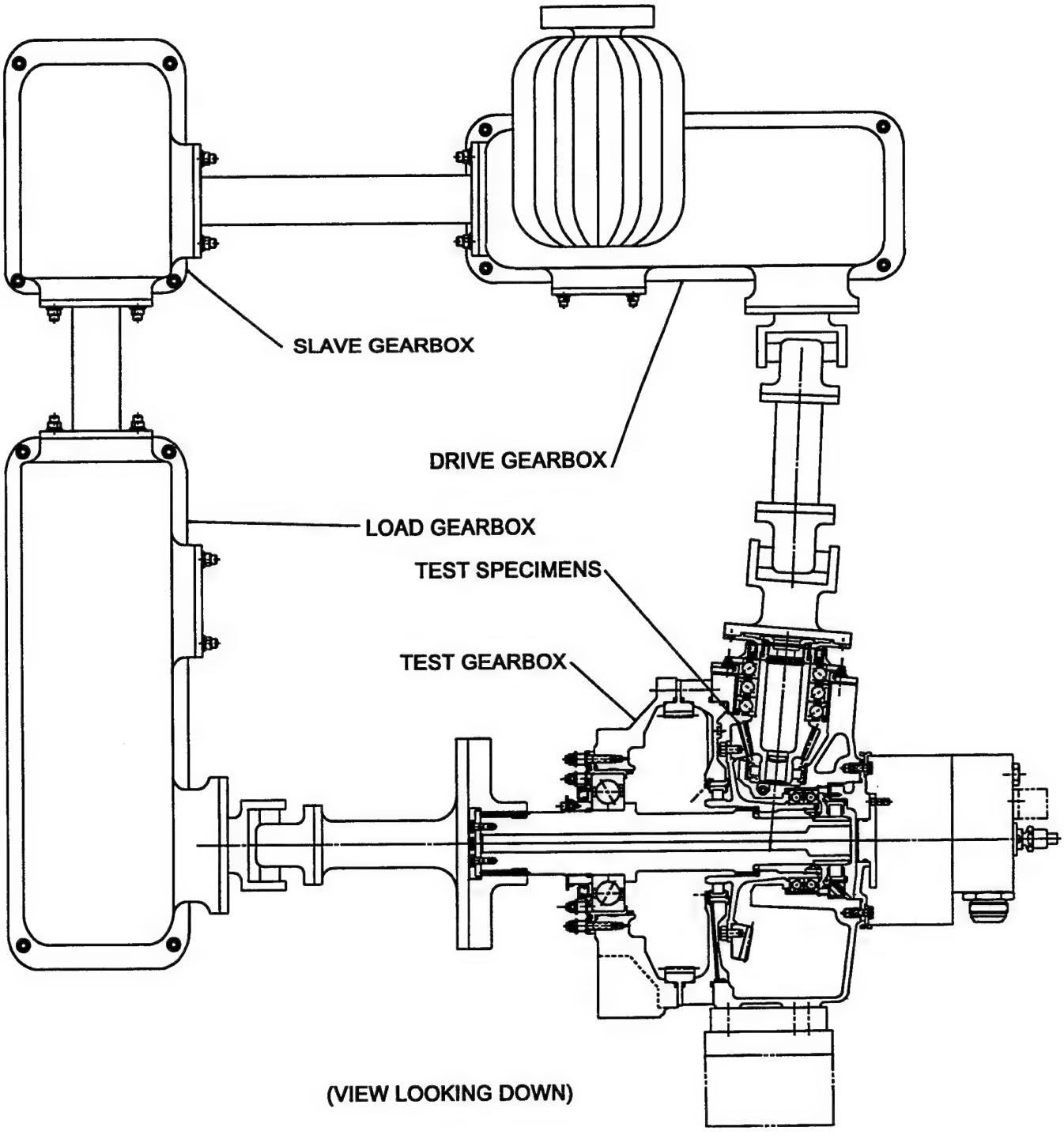

FIGURE 85: SCHEMATIC OF SPIRAL BEVEL DYNAMIC TEST RIG

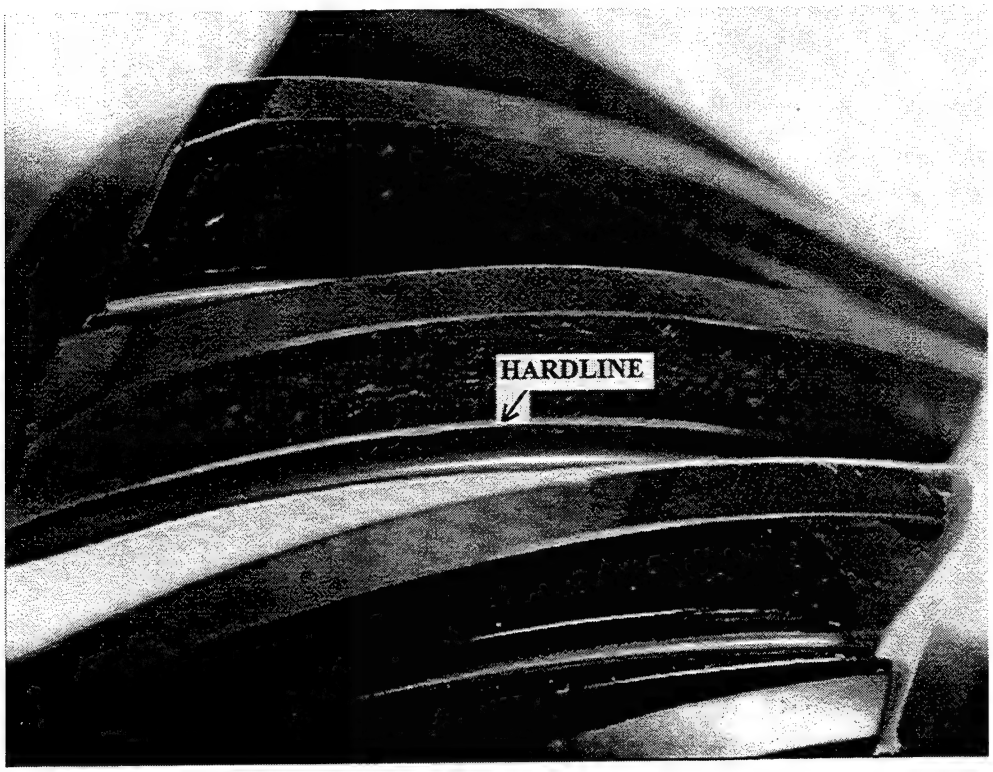

FIGURE 86: HARDLINE IN FLANK OF CONF. #3C SPIRAL BEVEL PINION AFTER 180 HR PITTING/BENDING TEST

6.2.7 SPIRAL BEVEL GEAR TOOTH BENDING FATIGUE TESTS

Gear tooth bending fatigue tests were conducted on two sets of each configuration gear set at the Gleason Works in Rochester, N.Y. These tests were conducted in the same test rig as for the tooth pitting tests. Each test on each set of spiral bevel gears was conducted for 180 hours at 125% torque. For Configurations #1 and #2, the oil-in temperature was maintained at 160° ± 10° F , but for Configuration #3C the tests were conducted at 230° ± 10° F oil-in combining the bending test for this configuration with the tooth pitting fatigue test described in Section 6.2.6. The test time of 180 hours was selected to subject the gear member of each set to 10 million fatigue cycles.

The objective of these tests was to demonstrate the capability of each configuration to pass a qualification type bending fatigue overtorque test. No bending failures were expected. After each test the gears were removed from the gearbox for close visual inspection and magnetic particle inspection. No bending failures or cracks were observed on any of the test gears.

6.2.8 SPIRAL BEVEL GEAR TOOTH SCORING TESTS

Gear tooth scoring tests were conducted on two sets of each configuration gear set at the Gleason Works in Rochester, N.Y. These tests were conducted in the same test rig as for the bending and pitting tests (see Figure 85). The objective of the scoring test was to determine the effects of the larger tooth fillet radius (Conf. #2) and the reduced kinematic error (Conf. #3C) on the capability of the spiral bevel gears to resist scoring. It was

anticipated that the larger fillet radius would have little effect, but the reduced kinematic error could significantly increase the scoring resistance.

One set of each configuration gear set was tested as described in Table 52 using DOD-L-85734 oil. No scoring was observed on any of the gear sets after any of the test steps. Each test was conducted as follows. The test gears were run for 30 minutes at the load level specified after the oil-out temperature had stabilized. After completing the 30 minute run, the gearbox was shut down and the gears visually inspected for scoring. If no scoring had occurred, the next test step was run until all 18 test steps had been completed. A thermocouple was located in the air-oil mist within .25 inches of the heel of the bevel gear mesh for each set to get an indication of the onset of scoring.

The inability to score any of the gear sets can be attributed to the high load carrying capacity of the test lubricant, DOD-L-85734 oil. The scoring test was designed to compare the relative scoring resistance of the three spiral bevel gear configurations, however the inability to score the test gears prevented any comparison. Therefore, the test lubricant was changed to MIL-L-7808 for the remaining scoring tests conducted on one of each configuration. MIL-L-7808 oil has a much lower load carrying capacity than DOD-L-85734 oil which would increase the chances of scoring the test gears during one of the 18 test steps.

One set of each configuration gear set was tested as described in Table 52 using the MIL-L-7808 oil. Again, no scoring was observed on any of the gear sets after any of the test steps. Although the results of the scoring test prevent any comparison of the 3 configurations tested, they do substantiate the durability and more than acceptable scoring resistance of each configuration.

TABLE 52: SPIRAL BEVEL GEAR TOOTH SCORING TEST SCHEDULE

STEP	PERCENT LOAD	OIL-IN TEMP. (°F)	INPUT TORQUE (IN-LB)	CALCULATED SCORING TEMP. (°F)
1	100	265	4,861	493
2	110	265	5,347	504
3	120	265	5,833	515
4	130	265	6,319	525
5	140	265	6,805	535
6	150	265	7,291	545
7	100	327	4,861	555
8	110	327	5,347	566
9	120	327	5,833	577
10	130	327	6,319	587
11	140	327	6,805	597
12	150	327	7,291	607
13	100	389	4,861	617
14	110	389	5,347	628
15	120	389	5,833	639
16	130	389	6,319	649
17	140	389	6,805	659
18	150	389	7,291	669

6.2.9 CONFIGURATION #3C MODIFICATION TO ELIMINATE HARDLINE

An attempt was made to eliminate the hardline of black oxide removal observed on the Configuration #3C spiral bevel gear sets after tests conducted at NASALeRC and Gleason. The hardline occurred at the tip of the gear tooth and the corresponding flank of each pinion and was the result of tooth meshing interference caused by tooth deflections at the higher load levels. To eliminate the tooth interference, TOPREM was added to the finish grinding summary of the pinion member only. TOPREM is a protuberance added to the finish grinding wheel which provides a relief in the flank of the pinion at a selected distance above the root line. No other changes were made and the rest of the tooth surface geometry was identical to the tooth geometry without TOPREM.

For the modification effort, a protuberance was selected which produced a 0.001" flank relief 0.050" above the pinion root line. An LTCA of the modified geometry was performed by Gleason. The results are shown in Figure 87 along with the results for the original Configuration #3C gear set for comparison.

As shown in Figure 87, the addition of TOPREM to the pinion member has the desired effect of pulling the contact pattern off the top of the gear tooth (corresponding pinion flank) as compared to the original Configuration #3C contact patterns.

Several of the Configuration #3C pinions were reground with the TOPREM modified geometry. The noise and vibration tests and a kinematic error test were conducted with the modified pinions using an original Configuration #3C gear. The results of the noise and vibration tests on the modified gear set were nearly identical to the results for the Configuration #3C gear set as shown in Figures 88 and 89. The results of the kinematic error tests are shown in Table 53 along with those for the Configuration #3C gear set and show some minor improvement.

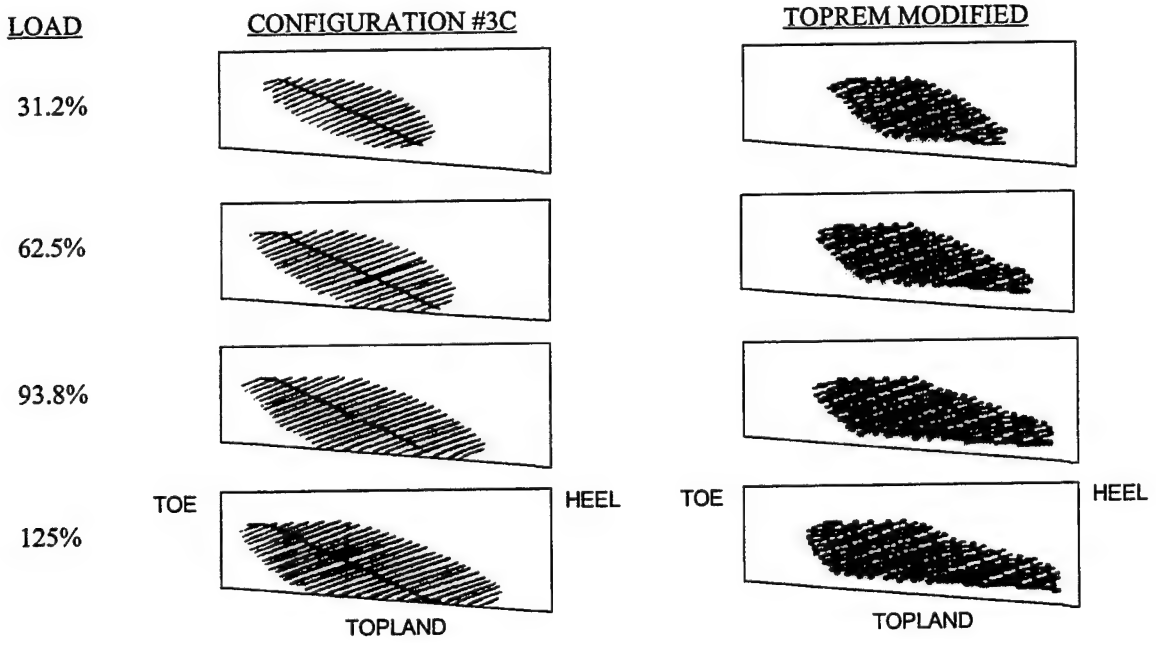

FIGURE 87: COMPARISON OF LTCA PREDICTED SPIRAL BEVEL GEAR TOOTH CONTACT PATTERNS

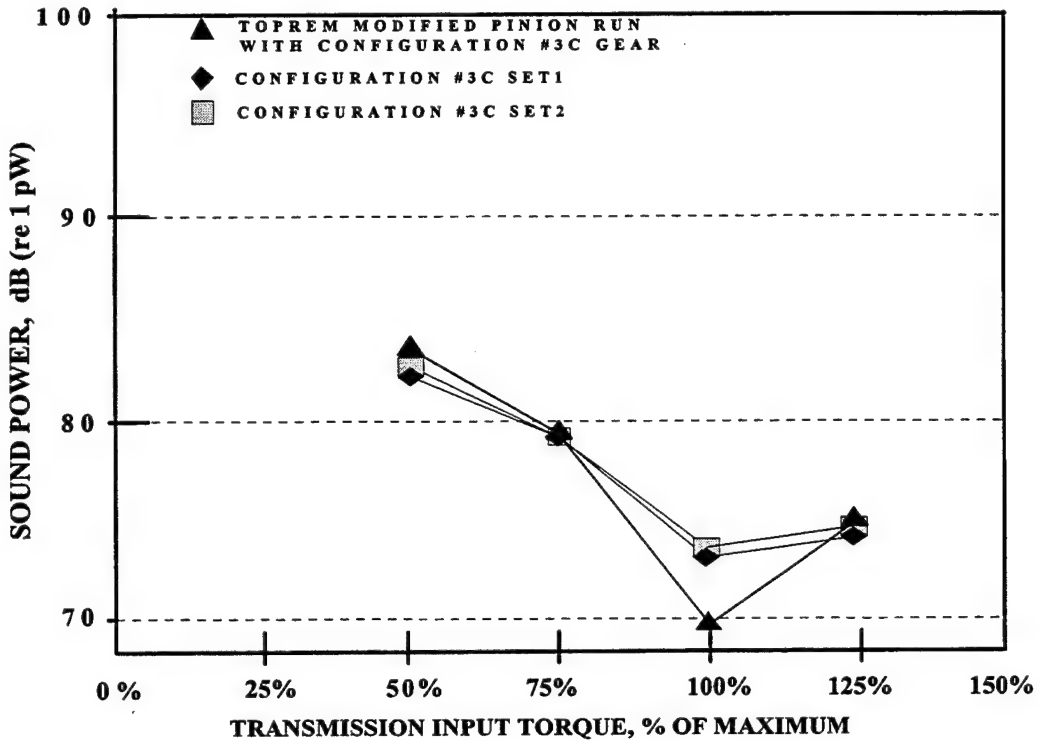

FIGURE 88: RESULTS OF NOISE TEST CONDUCTED ON TOPREM MODIFIED SPIRAL BEVEL PINION

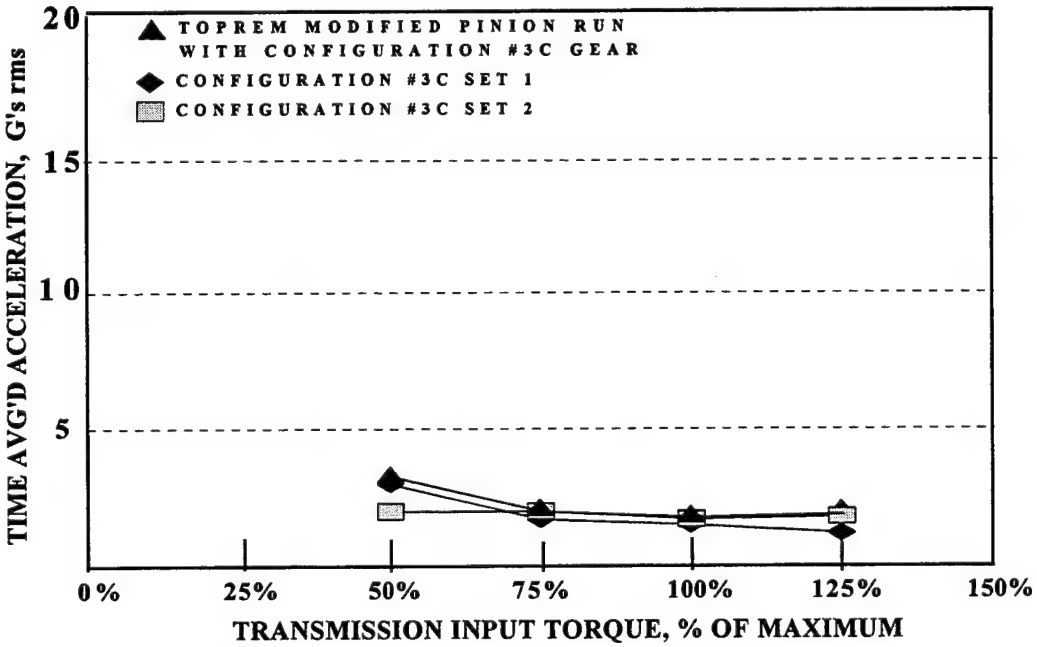

FIGURE 89: RESULTS OF VIBRATION TESTS CONDUCTED ON TOPREM MODIFIED SPIRAL BEVEL PINION

TABLE 53: TRANSMISSION ERROR SUMMARY FOR TOPREM MODIFIED PINION & ORIGINAL CONF. #3C SPIRAL BEVEL GEAR SET

MOUNTING LOCATION	TOTAL ACCUMULATED PITCH VARIATION (ARCSEC)		AVERAGE PROFILE ERROR (ARCSEC)		TOTAL TRANSMISSION ERROR (ARCSEC)		1ST MESH HARMONIC (ARCSEC)	
	CONF #3C	TOPREM MODIFIED	CONF #3C	TOPREM MODIFIED	CONF #3C	TOPREM MODIFIED	CONF #3C	TOPREM MODIFIED
NO OFFSETS	61	49	15	12	73	57	11	10
P = +.002"	57	49	14	12	69	57	11	10
P = - .002"	57	53	15	12	69	61	11	10
G = +.002"	57	49	15	12	69	57	11	10
G = - .002"	57	53	15	12	69	61	11	10
E = +.002"	57	53	16	12	69	61	12	10
E = -.002"	57	57	15	12	69	57	11	10
DEFLECTED	57	57	11	11	69	61	8	10

After completing the noise and vibration test, a hardline was still evident on the flank of the modified pinion as shown in Figure 90. This hardline is approximately 50% shorter in length than the hardline observed on the Configuration #3C pinion. Therefore, the TOPREM did reduce the hardline without effecting the reduced noise and vibration levels. Based on the results of this modification, it appears that an increase in the TOPREM from .050 to approximately .080 would eliminate the hardline without effecting the reduced noise and vibration levels provided by the reduced kinematic error geometry.

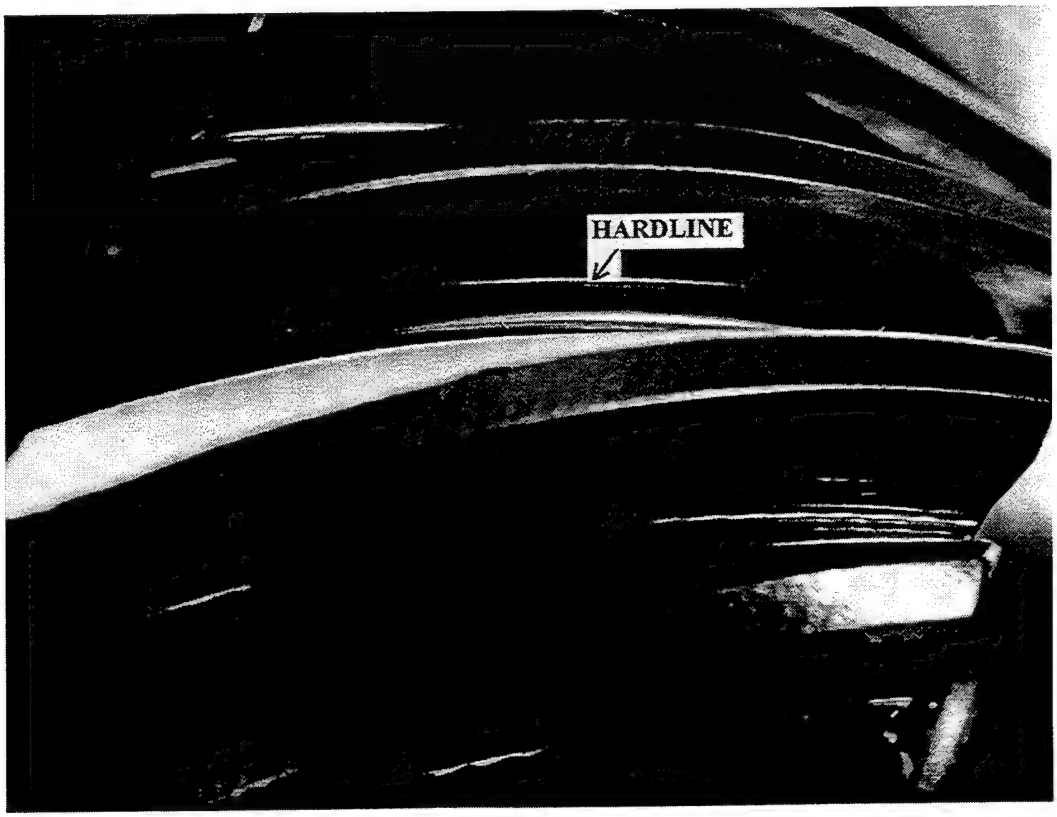

FIGURE 90: HARDLINE ON FLANK OF TOPREM MODIFIED SPIRAL BEVEL PINION

6.3 FLEXURE FATIGUE TESTS

Flexure fatigue tests were conducted on six groups of notched flexure specimens to evaluate possible improvements in bending fatigue strength provided by plasma carburizing, precision forging, and ceramic shot peening. The material and processing combinations tested include:

Configuration #1 - Gas carburized and steel shot peened Pyrowear 53 (X-53) alloy steel specimens machined from bar stock (Baseline)

Configuration #2 - Plasma carburized and steel shot peened X-53 alloy steel specimens machined from bar stock

Configuration #3 - Plasma carburized and ceramic shot peened X-53 alloy steel specimens machined from bar stock

Configuration #4 - Gas carburized and steel shot peened X-53 alloy steel specimens with the notch precision forged parallel (longitudinal) to the grain flow of the starting bar stock

Configuration #5 - Gas carburized and steel shot peened X-53 alloy steel specimens with the notch precision forged perpendicular (transverse) to the grain flow of the starting bar stock

Configuration #6 - Plasma carburized and steel shot peened X-53 alloy steel specimens with the notch precision forged parallel (longitudinal) to the grain flow of the starting bar stock

6.3.1 MATERIAL AND PROCESS IMPROVEMENTS

X-53 alloy steel is a second generation modification of AISI 9310 alloy steel and has the following advantages over 9310 without any loss in bending fatigue strength:

(1) The tempering temperature for X-53 is 150° to 200° F higher than for 9310 which allows higher operating temperature capability for the X-53 and improved scoring resistance.

(2) X-53 has approximately a 235% better B_1 pitting life than 9310 based on spur gear pitting tests conducted at NASA Lewis Research Center [14].

(3) The toughness of X-53 is equivalent to 9310.

Ceramic shot peening has the potential for introducing a deeper compressive stress layer than conventional cast steel shot peening with a larger compressive stress at the surface. This should improve the bending fatigue strength of the peened base metal; however, the resultant increased roughness of the surface finish due to the harder ceramic shot may offset any benefits of the improved surface compressive stresses.

The benefits of plasma carburizing and precision forging were previously discussed in Sections 4.12.1 and 4.12.2.

6.3.2 FLEXURE FATIGUE TEST SPECIMEN

Figure 91 shows the design of the notched flexure specimens machined from bar stock and Figure 92 shows the design of the specimens made from precision forgings. The specimens were designed with the 0.045" notch fillet radius to simulate a typical gear tooth fillet radius. All of the specimens were made from the same heat of VIM-VAR X-53 and were shot peened with .007" diameter shot to .007A - .009A intensity, 100% coverage after finish grinding. All specimens were peened with cast steel shot, except Configuration # 3 which were peened with ceramic shot.

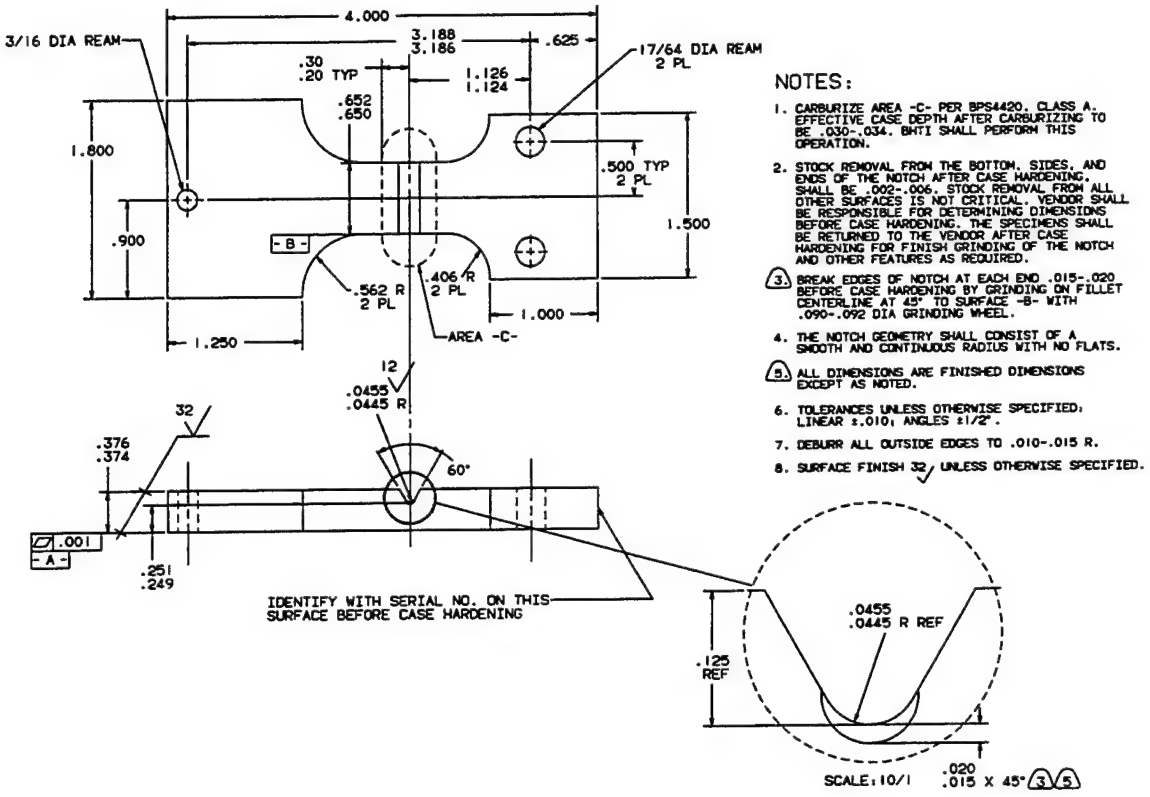

FIGURE 91: NOTCHED FLEXURE FATIGUE SPECIMEN MACHINED FROM BAR STOCK

6.3.3 FLEXURE FATIGUE TEST PROCEDURE

The specimens were tested at a constant stress ratio of approximately zero with the mean load set at 20 to 25 lbs greater than the oscillatory load to maintain a minimum tension load at the specimen notch. This test load cycle simulated unidirectional bending of a gear tooth. Tests were conducted on a Sonntag fatigue test machine with the test load applied at a frequency of 30 cycles per second. The specimens were subjected to unidirectional bending at various load levels until failure or until 10 million cycles of bending were accumulated. Ten million cycles was considered as a runout data point for these tests. The loads were varied as required to generate the necessary failures and runouts to establish the bending fatigue strength and S-N curve shapes for each group of specimens. A sketch of the test apparatus is shown in Figure 93.

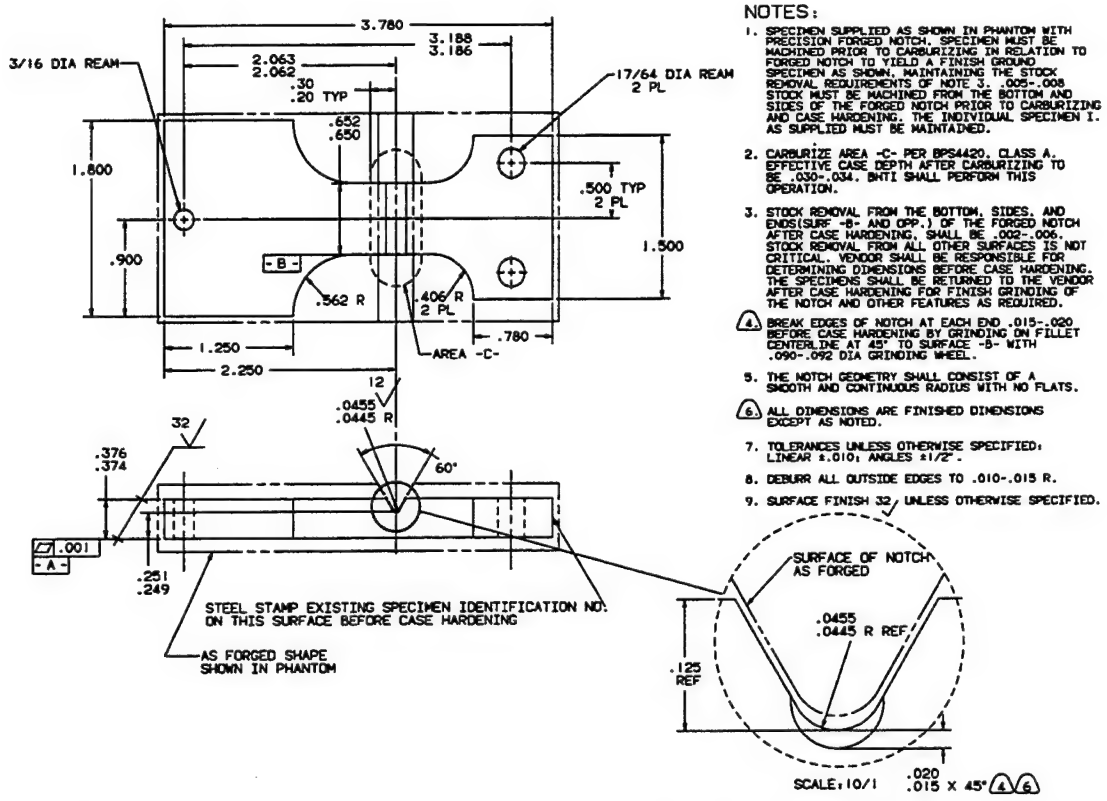

FIGURE 92: NOTCHED FLEXURE FATIGUE SPECIMEN (PRECISION FORGING)

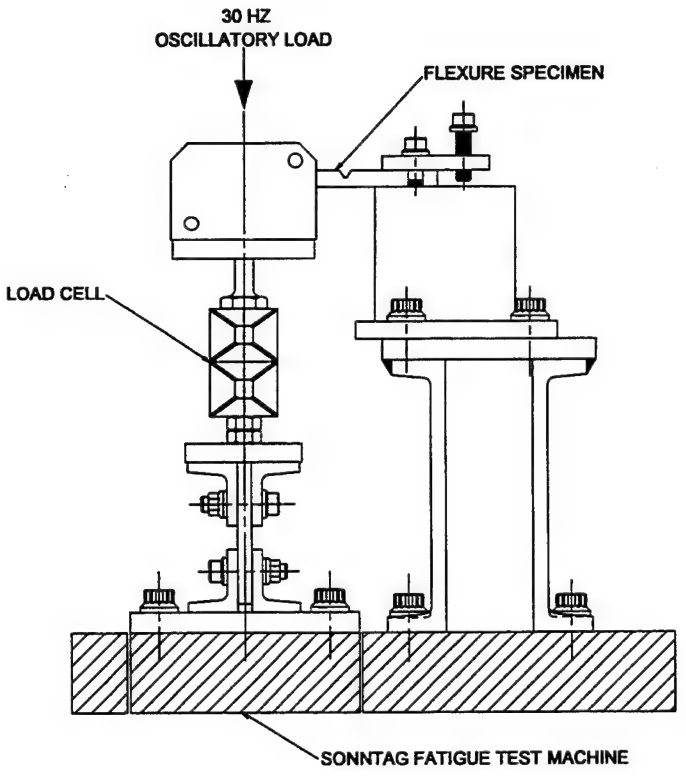

FIGURE 93: FLEXURE FATIGUE TEST FIXTURE

6.3.4 FLEXURE FATIGUE TEST RESULTS

The results of the fatigue tests are presented in Tables 54 through 59. S-N curves for each specimen configuration are shown in Figures 94 through 99. One set of curve shape factors was used for the specimens machined from bar stock and a different set for the precision forged specimens. The curve shape factors for theses two groups were determined from the combined data within each group.

TABLE 54: CONFIGURATION #1 - BASELINE NOTCHED FLEXURE FATIGUE DATA (MACHINED FROM BAR STOCK, GAS CARBURIZED, STEEL SHOT PEENED)

SPECIMEN NO.	MAXIMUM STRESS (KSI)	CYCLES TO FAILURE (IN MILLIONS)
B2	230	10.006
B5	230	0.590
B7	240	0.545
B8	230	5.202
B9	240	5.007
B11	220	4.095
B12	220	2.892
B13	250	3.237
B14	260	0.063
B15	250	0.839
B16	240	5.315
B19	260	0.128
B20	260	1.146
B21	220	10.005
B22	215	4.725
B24	230	3.992
B25	250	2.101
B26	230	3.992
B29	240	3.576
B30	230	13.125

TABLE 55: CONFIGURATION #2 NOTCHED FLEXURE FATIGUE DATA (MACHINED FROM BAR STOCK, PLASMA CARBURIZED, STEEL SHOT PEENED)

SPECIMEN NO.	MAXIMUM STRESS (KSI)	CYCLES TO FAILURE (IN MILLIONS)
B41	210	10.000
B42	210	10.000
B44	230	0.185
B45	230	1.050
B46	230	3.250
B48	220	3.350
B49	230	8.100
B50	210	9.300
B51	215	0.760
B52	210	10.000
B53	220	1.650
B54	220	1.150
B55	220	1.500
B56	215	2.200
B57	220	10.000
B58	220	0.870
B59	240	1.900
B60	240	6.800
B61	250	0.475
B62	250	0.410
B63	240	0.650
B64	240	0.295
B65	230	0.195
B66	210	10.000
B67	210	2.650
B68	210	0.950
B69	230	1.350
B70	230	4.350
B75	220	0.730
B76	250	0.165
B77	230	2.200

TABLE 56: CONFIGURATION #3 NOTCHED FLEXURE FATIGUE DATA (MACHINED FROM BAR STOCK, PLASMA CARBURIZED, CERAMIC SHOT PEENED)

SPECIMEN NO.	MAXIMUM STRESS (KSI)	CYCLES TO FAILURE (IN MILLIONS)
B71	250	0.390
B72	240	2.300
B73	230	4.650
B78	230	4.250
B79	210	10.000
B80	210	10.000
B81	210	10.000
B82	215	1.800
B83	220	7.800
B84	230	0.590
B85	220	5.300
B86	230	0.365
B87	210	10.000
B88	220	0.165
B89	215	0.149
B90	250	0.028
B91	250	0.520
B92	220	5.300
B93	240	0.280
B95	210	4.150
B96	250	1.050
B97	240	1.300
B98	230	9.900
B99	240	2.200
B100	210	2.050

TABLE 57: CONFIGURATION #4 NOTCHED FLEXURE FATIGUE DATA (PREC. FORGED, GAS CARB., STL SHOT PEENED, NOTCH PARALLEL TO GRAIN FLOW OF STARTING BAR STOCK)

SPECIMEN NO.	MAXIMUM STRESS (KSI)	CYCLES TO FAILURE (IN MILLIONS)
C27	260	7.520
C28	270	10.000
C29	280	1.361
C34	270	10.000
C35	260	10.000
C36	290	0.104
C39	260	10.000
C41	260	10.000
C42	270	10.000
C43	280	2.760
C46	290	0.105
C47	270	10.000

TABLE 58: CONFIGURATION #5 NOTCHED FLEXURE FATIGUE DATA (PREC. FORGED, GAS CARB., STL SHOT PEENED, NOTCH TRANSVERSE TO GRAIN FLOW OF STARTING BAR STOCK)

SPECIMEN NO.	MAXIMUM STRESS (KSI)	CYCLES TO FAILURE (IN MILLIONS)
D17	260	8.500
D18	260	10.000
D20	270	10.000
D21	280	7.300
D22	290	3.450
D27	300	1.460
D29	280	10.000
D40	270	10.000

TABLE 59: CONF. #6 NOTCHED FLEXURE FATIGUE DATA (PREC. FORGED, PLASMA CARB., STL SHOT PEENED, NOTCH PARALLEL TO GRAIN FLOW OF STARTING BAR STOCK)

SPECIMEN NO.	MAXIMUM STRESS (KSI)	CYCLES TO FAILURE (IN MILLIONS)
C52	270	0.041
C55	270	2.900
C59	250	3.350
C60	250	10.000
C62	260	7.200
C63	260	0.690
C64	280	0.075
C65	280	1.500
C66	290	0.017
C67	290	0.011
C68	290	0.075
C69	250	1.750
C70	250	10.000
C71	280	0.040
C72	270	10,000
C73	260	10.000
C74	260	10.000
C75	270	10.000
C76	270	10.000
C77	270	9.300
C78	280	0.020
C79	280	2.900
C80	270	10.000
C81	260	0.020
C82	250	6.300
C83	250	10.000
C84	260	10.000
C85	260	0.075

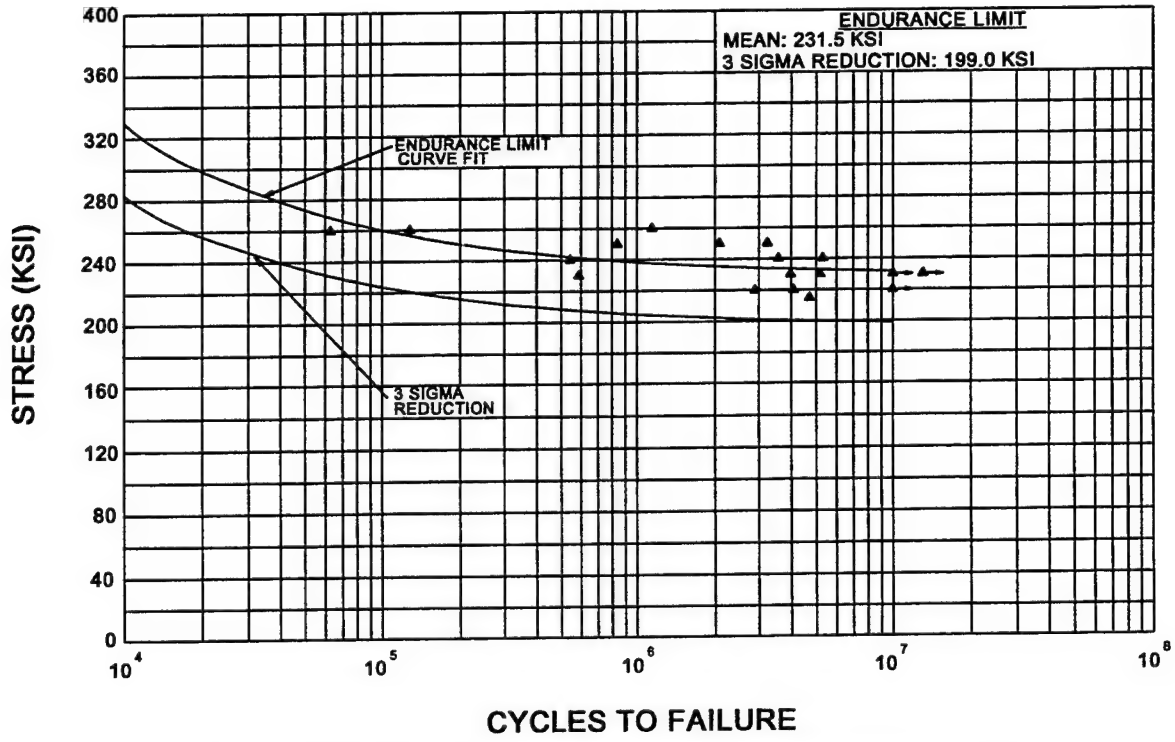

FIGURE 94: FATIGUE LIFE OF GAS CARBURIZED & STEEL SHOT PEENED, X-53, NOTCHED FLEXURE FATIGUE SPECIMENS MACHINED FROM BAR STOCK (CONF. #1)

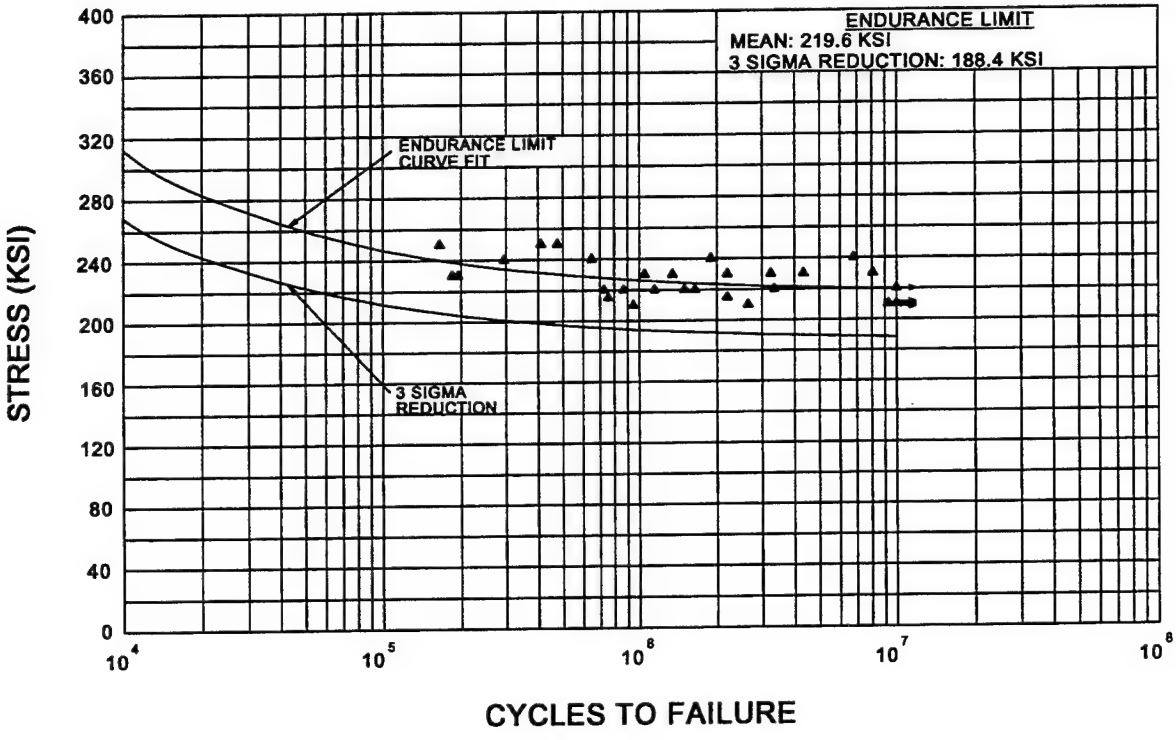

FIGURE 95: FATIGUE LIFE OF PLASMA CARBURIZED & STEEL SHOT PEENED, X-53, NOTCHED FLEXURE FATIGUE SPECIMENS MACHINED FROM BAR STOCK (CONF. #2)

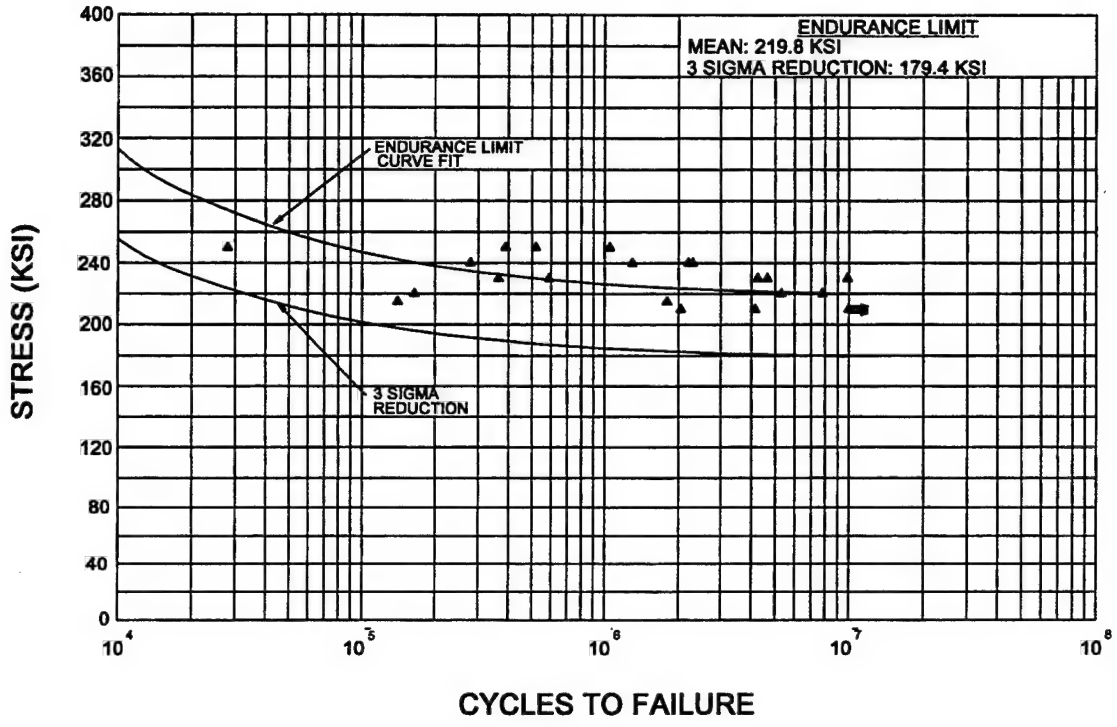

FIGURE 96: FATIGUE LIFE OF PLASMA CARB., & CERAMIC SHOT PEENED, X-53, NOTCHED FLEXURE FATIGUE SPECIMEN MACHINED FROM BAR STOCK (CONF. #3)

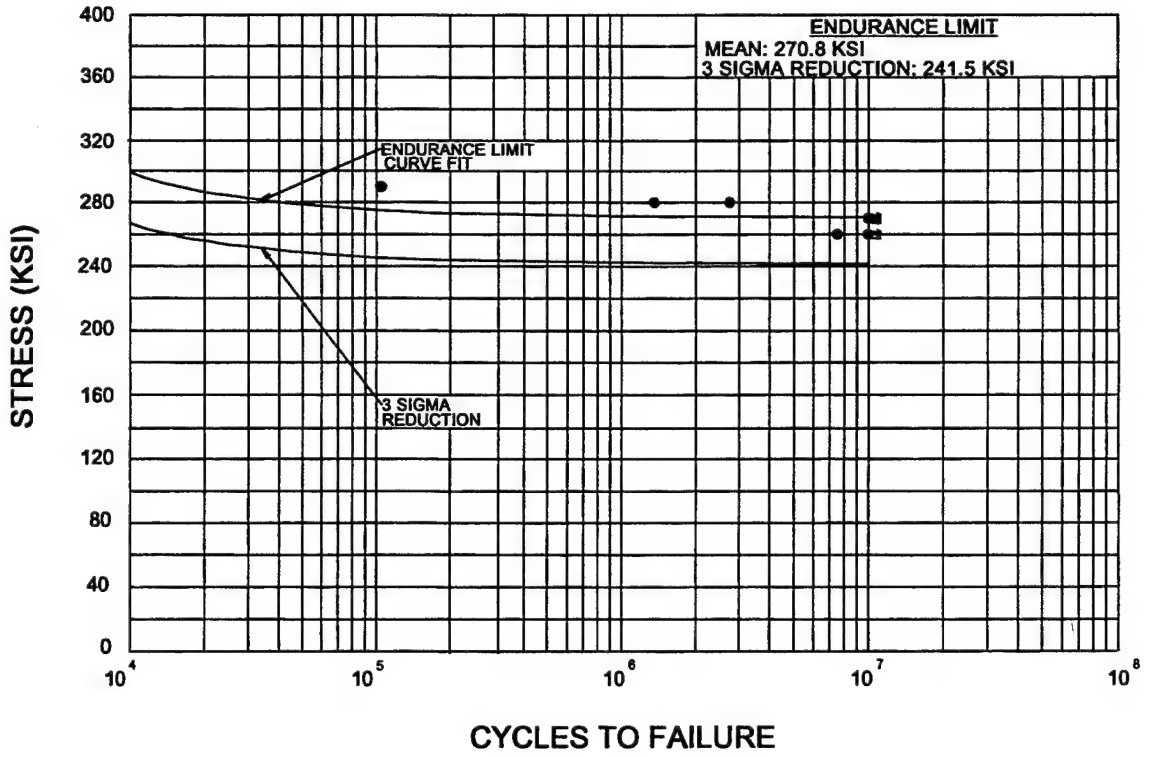

FIGURE 97: FATIGUE LIFE OF GAS CARB., & STL SHOT PEENED, X-53, NOTCHED FLEXURE FATIGUE SPECIMENS - NOTCH PRECISION FORGED PARALLEL (LONGITUDINAL) TO STARTING BAR STOCK GRAIN FLOW (CONF. #4)

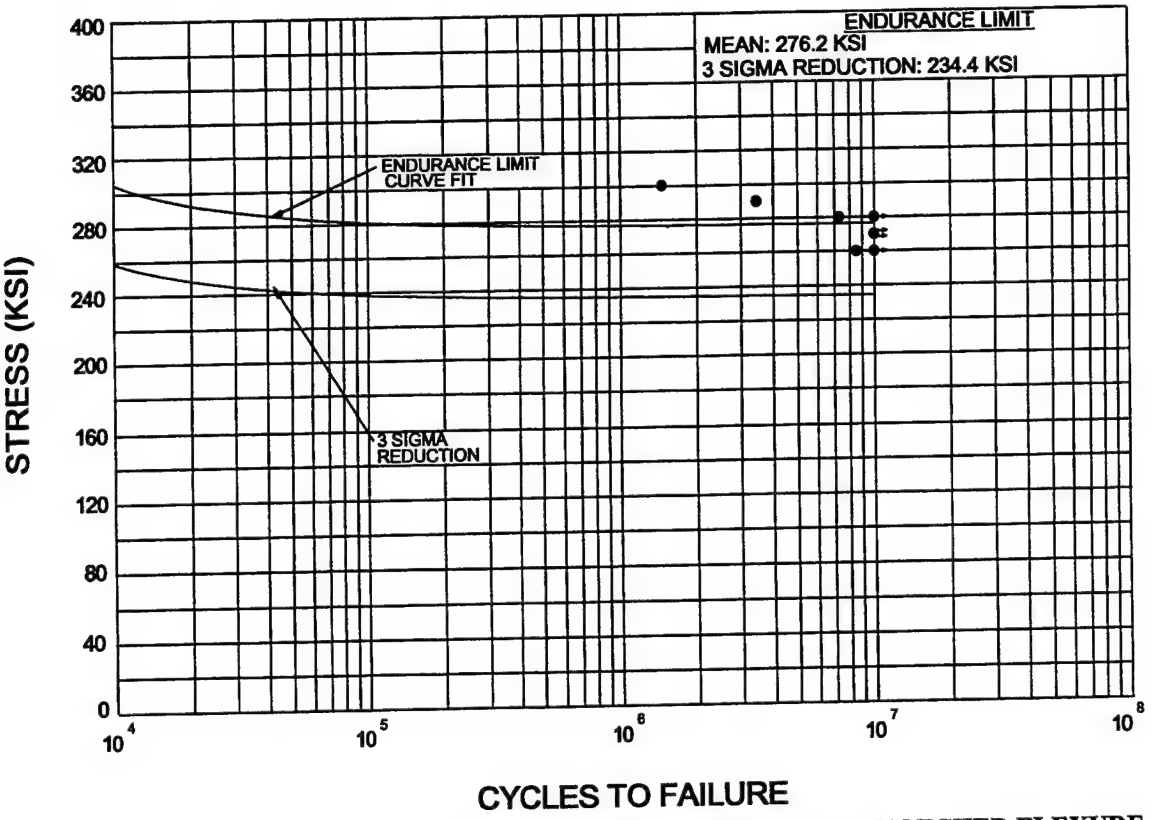

FIGURE 98: FATIGUE LIFE OF GAS CARB., & STL SHOT PEENED, X-53, NOTCHED FLEXURE FATIGUE SPECIMENS - NOTCH PRECISION FORGED PERPENDICULAR (TRANSVERSE) TO STARTING BAR STOCK GRAIN FLOW (CONF. #5)

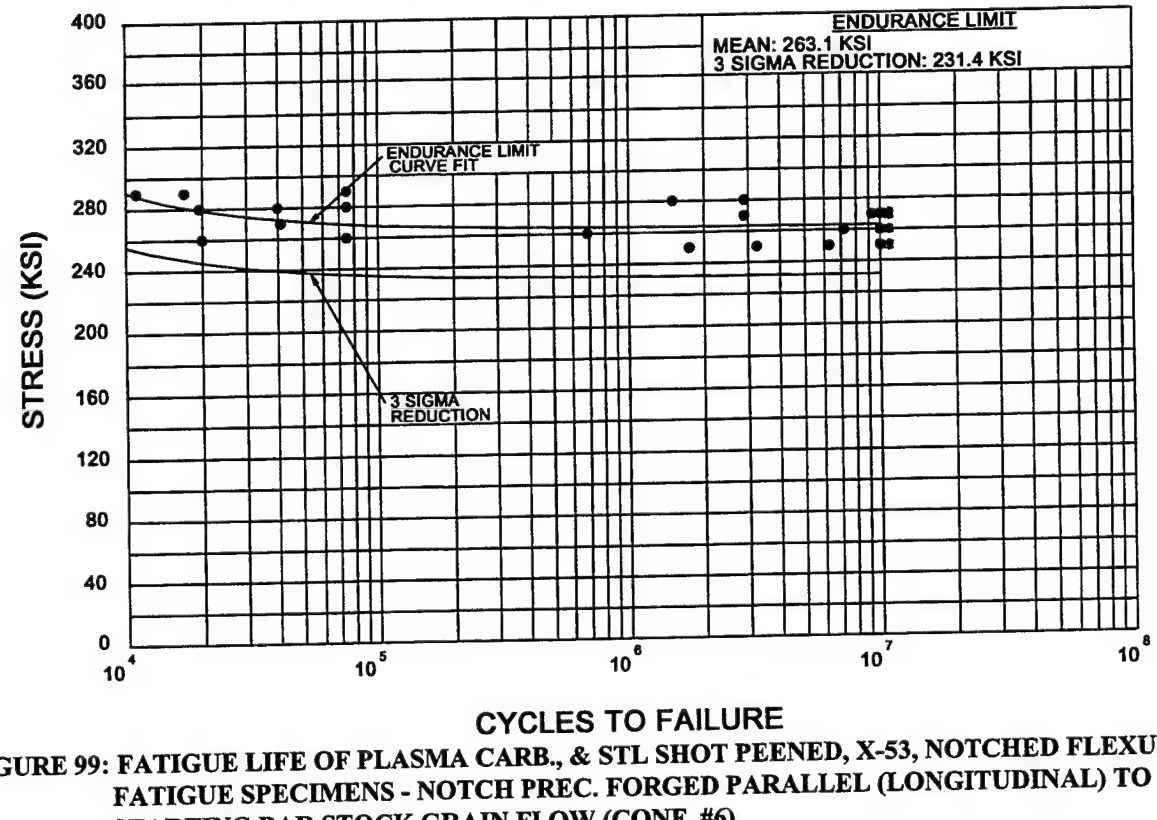

FIGURE 99: FATIGUE LIFE OF PLASMA CARB., & STL SHOT PEENED, X-53, NOTCHED FLEXURE FATIGUE SPECIMENS - NOTCH PREC. FORGED PARALLEL (LONGITUDINAL) TO STARTING BAR STOCK GRAIN FLOW (CONF. #6)

A summary of the test results is shown in Table 60. The tests show that precision forging provides approximately a 20% increase in the bending fatigue strength of the flexure specimens demonstrating the benefits of conformal grain flow, even for super clean VIM-VAR X-53. Comparing the results for Configurations #2 and #3, peening the specimens with ceramic shot instead of cast steel shot does not increase the bending fatigue strength. A comparison of gas carburizing versus plasma carburizing shows the plasma carburizing process to have a slightly detrimental effect (3% to 5% reduction) on the bending fatigue strength. Overplots of the S-N curves for Configurations #2 and #6 are shown in Figure 100 and clearly show the significant improvement in bending fatigue strength provided by the precision forging process as well as the curve shape differences between the specimens machined from bar stock and the precision forged specimens.

TABLE 60: SUMMARY OF FLEXURE FATIGUE TEST RESULTS

SPECIMEN TYPE	ENDURANCE LIMIT (KSI)		RANK BY MEAN - 3SIGMA
	MEAN	MEAN - 3SIGMA	
#1 BAR STOCK, GAS CARB, STEEL SHOT	231.5	199.0	4
#2 BAR STOCK, PLASMA CARB, STEEL SHOT	219.6	188.4	5
#3 BAR STOCK, PLASMA CARB, CERAMIC SHOT	219.8	179.4	6
#4 PREC. FORGED, LONG. NOTCH, GAS CARB, STEEL SHOT	270.8	241.5	1
#5 PREC. FORGED, TRAN. NOTCH, GAS CARB, STEEL SHOT	276.2	234.3	2
#6 PREC. FORGED, LONG. NOTCH, PLASMA CARB, STEEL SHOT	263.1	231.4	3

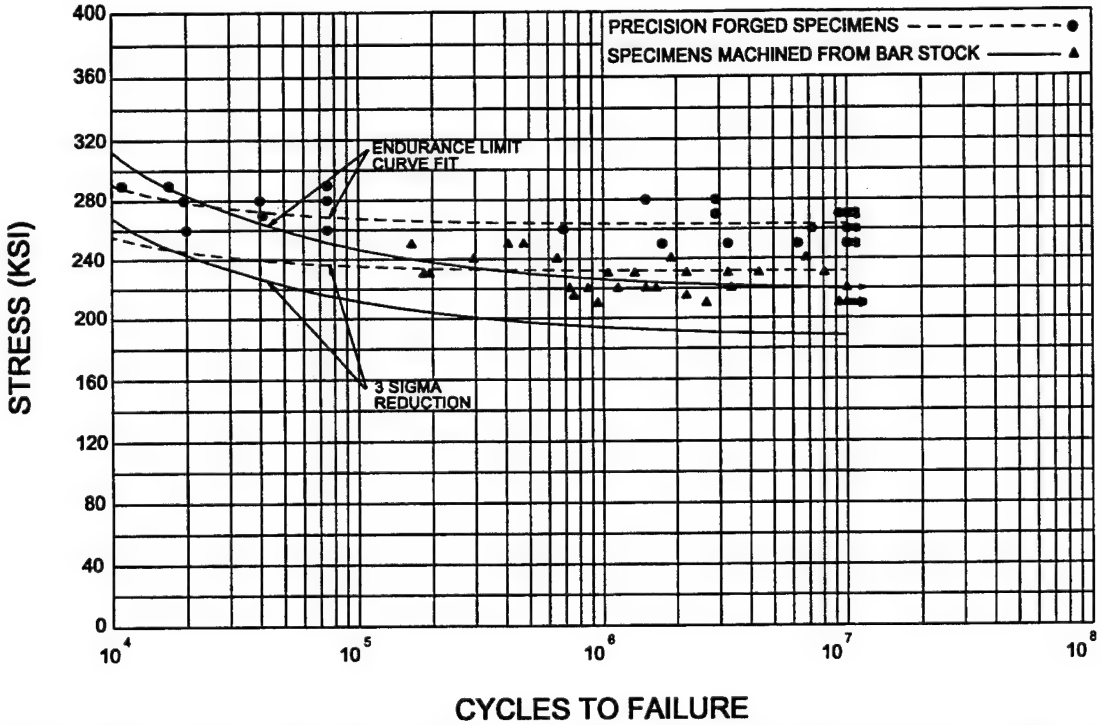

FIGURE 100: FATIGUE LIFE OF PLASMA CARB., & STL SHOT PEENED, X-53, NOTCHED FLEXURE FATIGUE SPECIMENS MACHINED FROM BAR STOCK VS. SPECIMENS WITH NOTCH PREC. FORGED PARALLEL (LONGITUDINAL) TO STARTING BAR STOCK GRAIN FLOW (CONF. #2 VS. #6)

6.4 HIGH TEMPERATURE WE43 MAGNESIUM EVALUATION

One of the major factors contributing to the ART weighing 29% less than the SOAT was the substitution of WE43 magnesium for A357 aluminum alloy as the main housing material. Magnesium is 40% lighter than aluminum, and the WE43 magnesium alloy is reported to have excellent corrosion resistance and mechanical properties at elevated temperatures similar to cast aluminum alloys [Magnesium Elektron Ltd. Data Sheet 467]. To use WE43 magnesium as the housing material for the ART, a protective coating scheme is required which will prevent any corrosion (general or galvanic) on the assembled magnesium housing.

6.4.1 MAGNESIUM FLAT PANEL CORROSION TESTS

To evaluate the corrosion resistance of the WE43 magnesium and to develop an effective coating scheme, corrosion tests were conducted on ZE41 magnesium and WE43 magnesium flat panels coated with the various protection schemes listed in Table 61. ZE41 magnesium alloy was chosen for comparison purposes as a baseline since it is currently used as the material for the transmission main case on the OH-58D helicopter. In addition to the sealing system evaluation, three bare specimens were also corrosion tested. The specimens were WE43 Mag alloy, ZE41 Mag alloy, and A357 aluminum alloy.

TABLE 61: MAGNESIUM FLAT PANEL SPECIMEN PROTECTION SCHEMES

SPECIMEN S/N	MATERIAL	PRE-TREATMENT	RESIN COATING
A-1	WE43	CHROME MANGANESE	MIL-R-3043
A-2	WE43	CHROME MANGANESE	SERMETEL BD-O
A-3	WE43	CHROME MANGANESE	DTD5562
A-4	WE43	DOW 17	MIL-R-3043
A-5	WE43	DOW 17	SERMETEL BD-O
A-6	WE43	DOW 17	DTD5562
B-1	ZE41	DOW 7	MIL-R-3043
B-2	ZE41	DOW 7	SERMETEL BD-O
B-3	ZE41	DOW 7	DTD5562
B-4	ZE41	DOW 17	MIL-R-3043
B-5	ZE41	DOW 17	SERMETEL BD-O
B-6	ZE41	DOW 17	DTD5562
C-1	ZE41	DOW 7	SERMETEL XP871083

After the specimens were pre-treated and sealed as shown in Table 61, all except specimen C-1 were primed with two coats of MIL-P-23377 primer. The hardware shown in Figure 101 was then installed on each specimen and sealed with a bead of MIL-S-8802 (except specimen C-1) on both sides. Finally, the specimens (except C-1) were painted with two coats of MIL-C-22750 paint. The hardware shown in Figure 100 was chosen to represent various galvanic potentials. Photographs of typical specimen assemblies prior to corrosion testing are shown in Figure 102. (Photograph of specimen C-1 not available.)

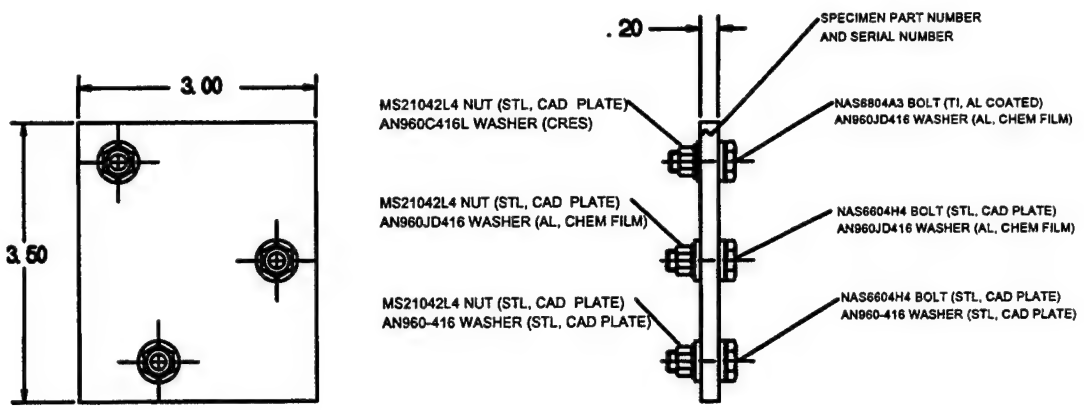

FIGURE 101: MAGNESIUM CORROSION TEST PANEL ASSEMBLY HARDWARE

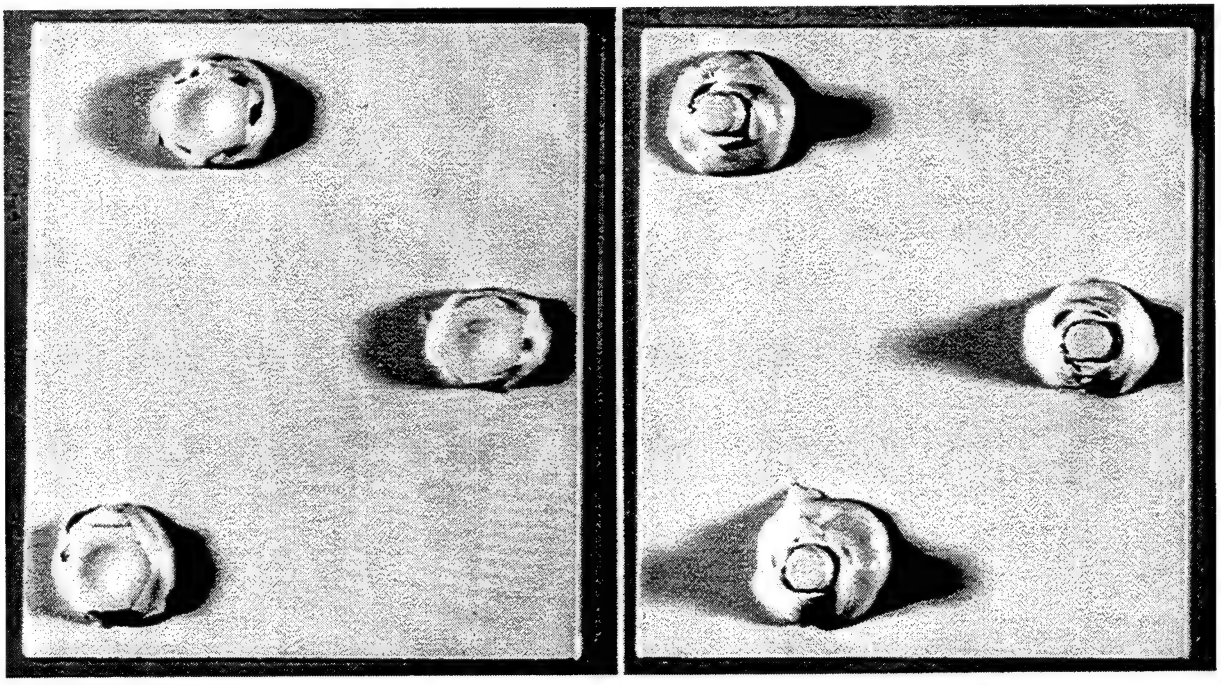

a) Typical Front Side (Specimen A-1)

b) Typical Back Side (Specimen B-1)

FIGURE 102: MAGNESIUM FLAT PANELS PRIOR TO CORROSION TESTS

The 12 specimens were then concurrently subjected to twenty, 24 hr cyclic environmental atmospheres, each consisting of 4 hrs of salt spray (fog) per ASTM-B-117 and 20 hrs of cyclic humidity per MIL-STD-810C Method 570.1. This 24 hr cycle is shown in Figure 103. After exposure to ten of the 24 hour cycles (246 hours actual test time), small blisters were observed on the edges of specimens B-4, B-5, and B-6, and specimen B-2 exhibited some larger areas of blistering along the edges. No corrosion was observed on the remaining specimens. Photographs of typical specimen assemblies after the 246 hour test are shown in Figures 104 and 105.

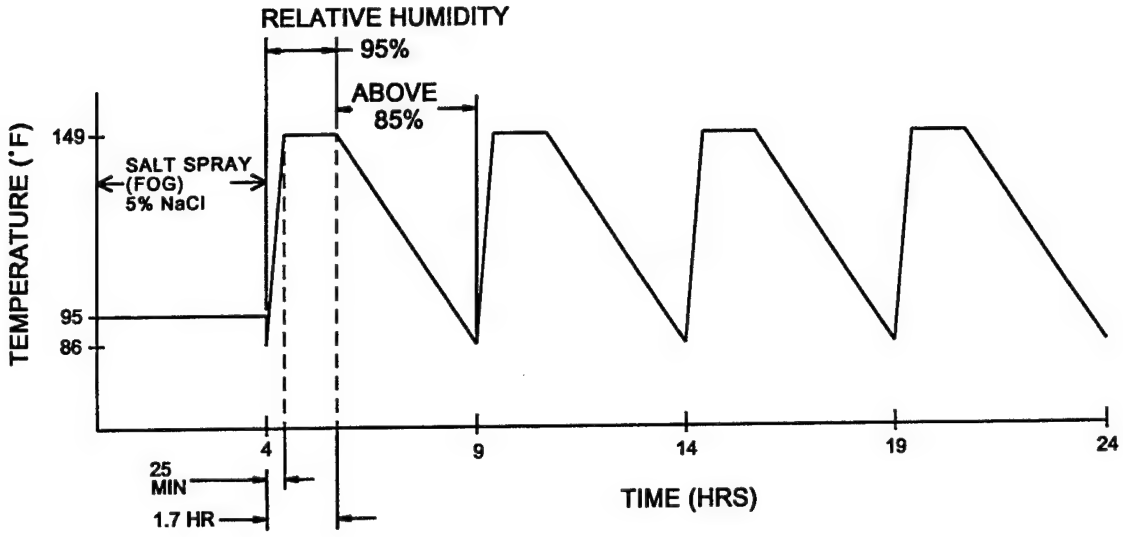

FIGURE 103: CORROSION TEST CYCLE

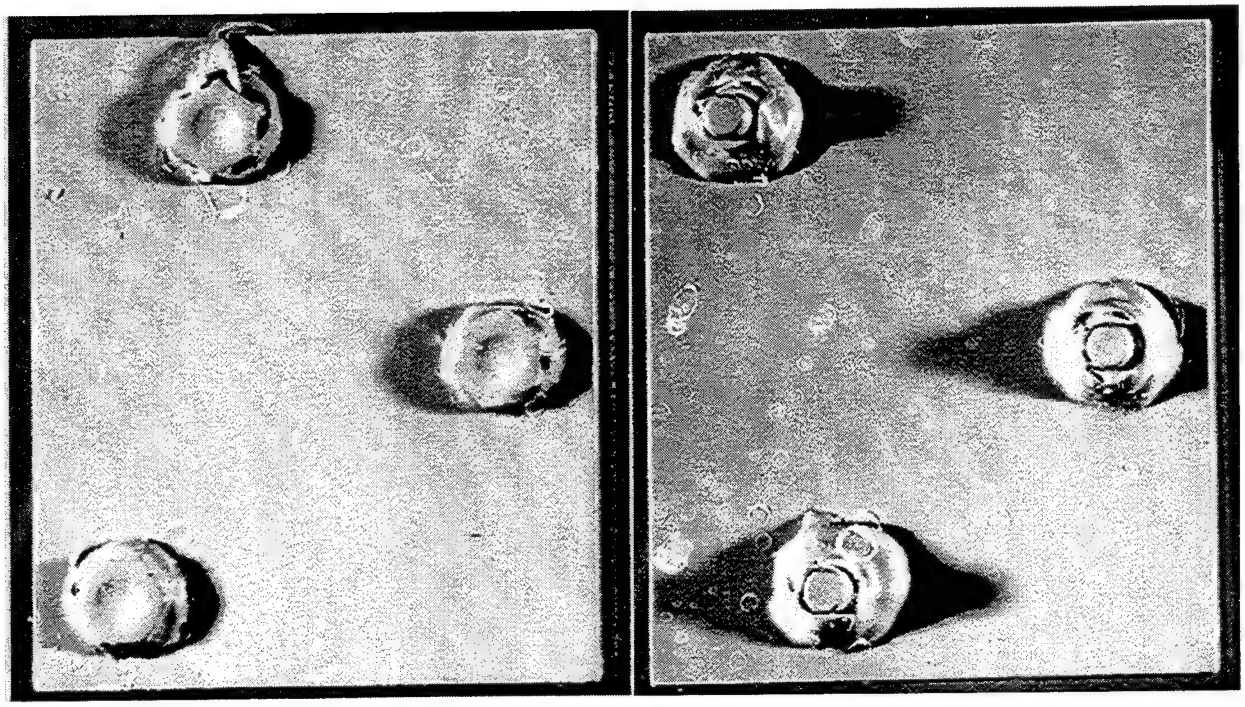

a) Typical Front Side
(Specimen A-1)

b) Typical Back Side
(Specimen B-1)

FIGURE 104: MAGNESIUM FLAT PANELS AFTER 246 HR CORROSION TEST

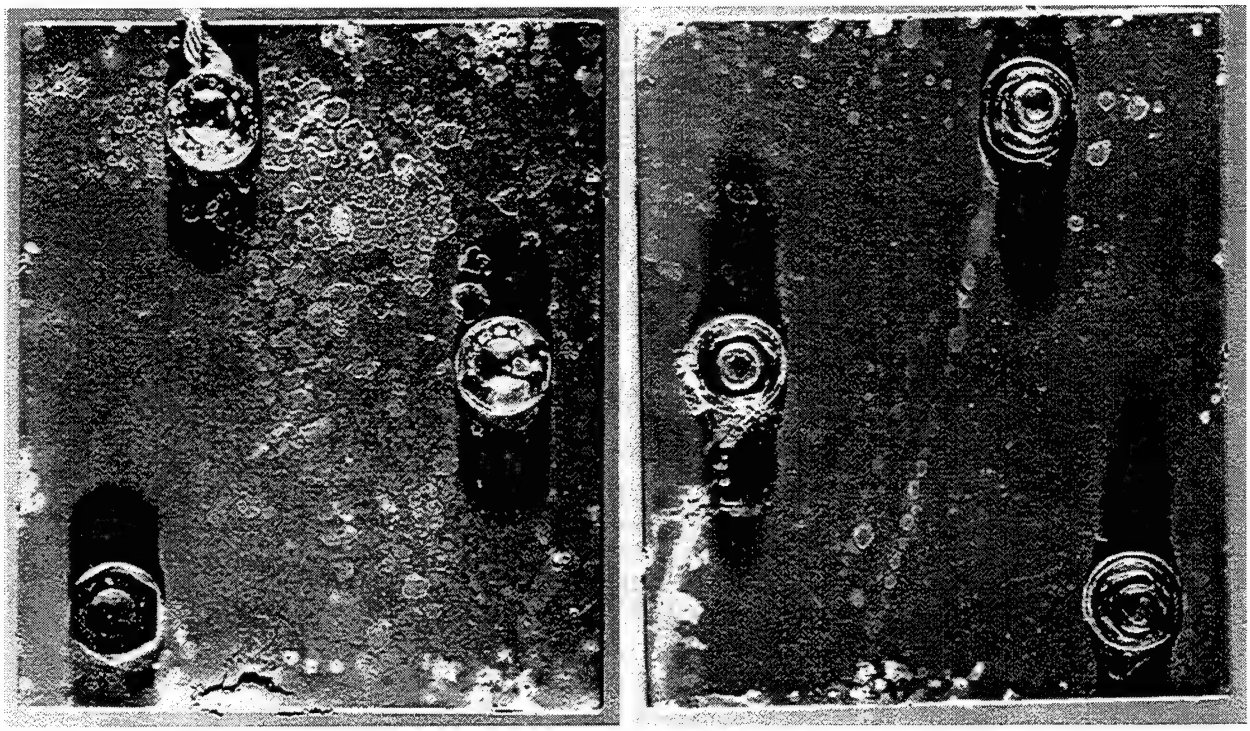

a) Specimen C-1, Front Side b) Specimen C-1, Back Side

FIGURE 105: MAGNESIUM FLAT PANELS AFTER 246 HR CORROSION TEST

To evaluate the ability of each sealing system to resist corrosion or prevent corrosion propagation when damaged, the specimens were subjected to impact damage and were also scribed with an "X" to expose the bare metal beneath the seal. The impact damage was made with a .625" diameter steel ball with 25 in-lbs of impact force which cracked the coating on each specimen on the side opposite the impact impression. The base metal was not exposed on the impact side of the specimen. The impact impression was approximately .010 deep and 5/32" diameter. The scribed "X" was approximately one inch square and was made on the side opposite the crack resulting from the impact damage. Figure 106 shows a photograph of a typical scribed 'X' on each specimen. The 12 specimens (A-1 thru A-6 and B-1 thru B-6) were then subjected to ten additional 24 hour test cycles (244 hours actual test time).

Visual inspection revealed varying degrees of corrosion on each of the specimens, and a brief description of the corrosion observed on each specimen is provided in Table 62. The rank listed in Table 62 is based on the sealing system performance only with 1 for the best protection against corrosion propagation and 5 for the worst protection. Specimen B-2 exhibited the most corrosion (severe) and specimen A-6 the least (very minor). The corrosion observed on specimen B-2 had severely blistered approximately 30% of the sealed surface area. Large areas of corrosion deposits were evident, and the corrosion had propagated not only from the controlled damage areas but also from the initial corrosion around the edges. The corrosion on specimen A-6 was limited to the bare metal areas exposed by the controlled damage with no indications of propagation. Minute corrosion deposits were observed on the edge of the exposed areas but were limited to the surface (no pitting). The corrosion appears to have been arrested since this minor corrosion was observed in the early portions of the second 244 hours of exposure with

no change in appearance by the end of the test. Photographs of some of the typical corrosion observed are shown in Figures 107 and 108.

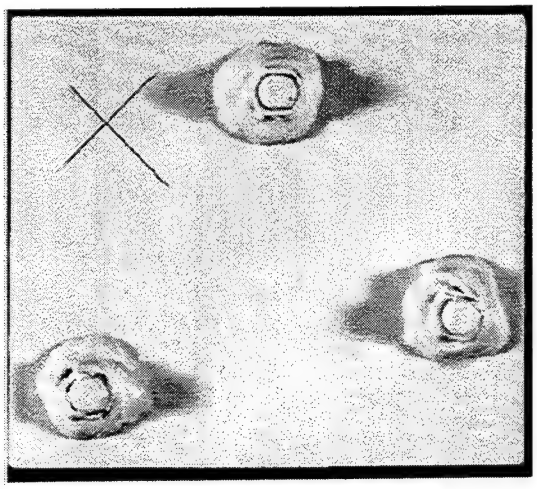

FIGURE 106: TYPICAL SCRIBED DAMAGE - MAGNESIUM FLAT PANEL ASSEMBLY B-2

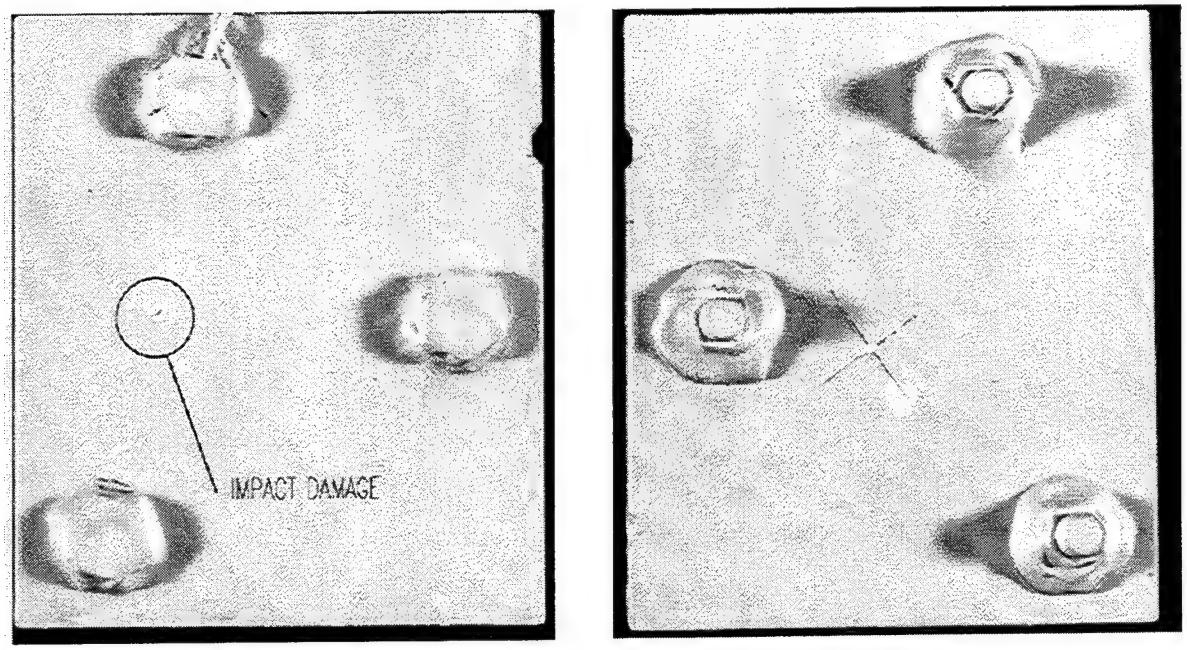

a) Front Side

b) Back Side

FIGURE 107: MAGNESIUM FLAT PANEL AFTER ADDITIONAL 244 HR CORROSION TEST (490 HOURS TOTAL) - SPECIMEN A-6

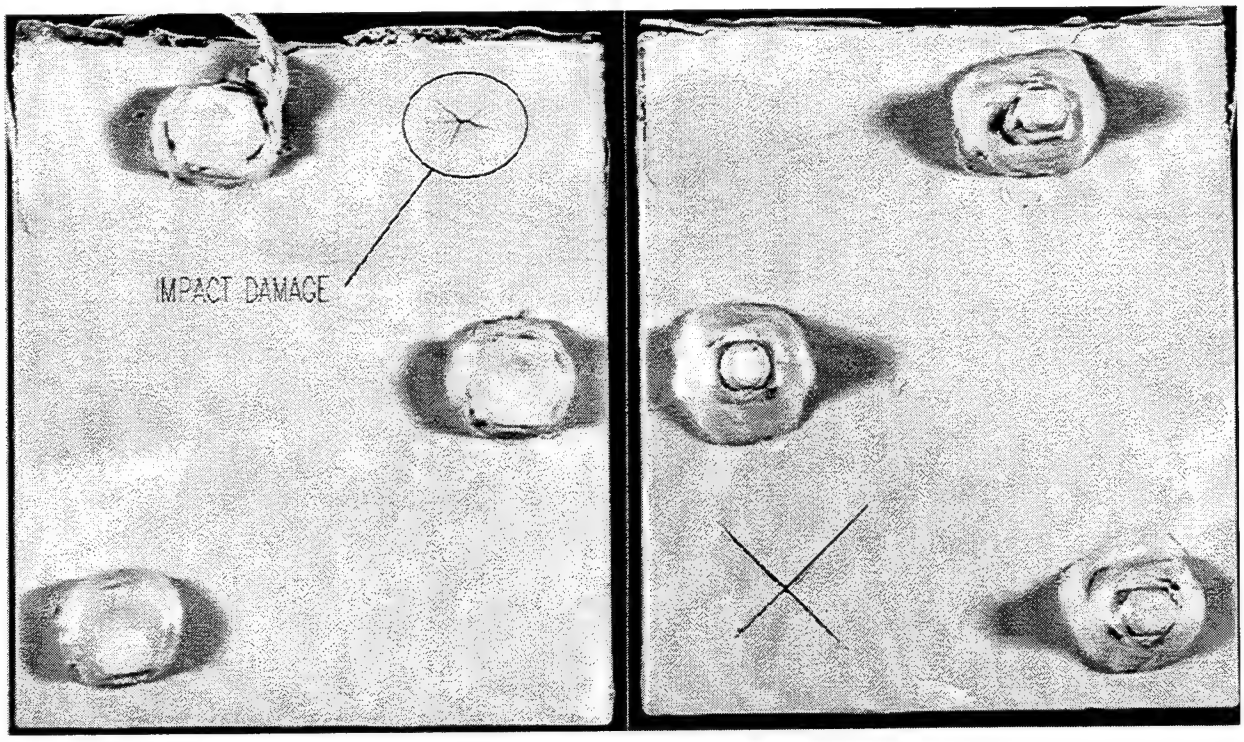

a) Front Side b) Back Side

FIGURE 108: MAGNESIUM FLAT PANEL AFTER ADDITIONAL 244 HR CORROSION TEST (490 HOURS TOTAL) - SPECIMEN B-2

Based on the visual examination of each of the 12 specimens the following conclusions can be made:

- WE43 is a much better corrosion resistant magnesium alloy than ZE41, limiting corrosion to the surface of any exposed areas, whereas ZE41 exhibits deep corrosion pits

- DOW 17 is a better pre-treatment than DOW 7 or chrome-manganese since it works with the subsequently applied sealing system to prevent corrosion propagation

- The DTD5562 resin and the MIL-R-3043 resin are better corrosion resistant sealers than the SERMETEL 1083 since they were able to greatly retard corrosion on the DOW 7 treated ZE41 specimens which the SERMETEL did not.

- The DTD5562 resin is a slightly better corrosion resistant sealer than MIL-R-3043 resin as observed in the comparison of specimen A-6 to A-4.

TABLE 62: MAGNESIUM FLAT PANEL CORROSION TEST RESULTS

SPECIMEN	COMMENTS	RANK
A-1	Minor surface corrosion and some peeling away of seal around controlled damage areas, no corrosion propagation underneath	3
A-2	Minor surface corrosion around controlled damage areas, some propagation around impact damage area	4
A-3	Minor surface corrosion and some peeling away of seal around controlled damage areas, no corrosion propagation underneath	2
A-4	Minor surface corrosion in controlled damage areas, no corrosion propagation underneath sealing system	1
A-5	Minor surface corrosion in controlled damage areas with minimal corrosion propagation underneath sealing system	2
A-6	Minor surface corrosion in controlled damage areas, no corrosion propagation underneath sealing system	1
B-1	Corrosion around corners and edges, deep pitting in impact damage area, corrosion propagation under sealing system	4
B-2	Severe corrosion on 30% of surface, controlled damage areas completely corroded, corrosion propagation unimpeded by sealing	5
B-3	Deep corrosion pits in controlled damage areas, minimal corrosion propagation	4
B-4	Deep corrosion pits in controlled damage areas, minimal corrosion propagation	3
B-5	Some corrosion in controlled damage areas but no propagation, several small corrosion blisters on edge of part	2
B-6	Deep corrosion pits in controlled damage areas, minimal corrosion propagation, several small corrosion blisters on edge of part	2

For comparison, three bare specimens were also corrosion tested. The specimens shown in Figure 109 were WE43 Mag alloy, ZE41 Mag alloy, and A357 aluminum alloy. Each was subjected to ten, 24 hr cyclic environmental atmospheres (247 hours actual) as shown in Figure 103. The results of the corrosion test are shown in Figures 110 and 111. Figure 110 shows the specimens as removed from the corrosion chamber and Figure 111 shows the specimens after washing away the corrosion debris. The following visual observations were made.

SPECIMEN	COMMENTS
ZE41 MAG	Most severe corrosion, deep pitting and exfoliation (flakes and scales)
WE43 MAG	Light non-progressive surface corrosion (shallow pitting), initial corrosion occurred at beginning of exposure to corrosion atmosphere with little progression
A357 Al	Minimal surface corrosion limited to small pits with evidence of intergranular attack

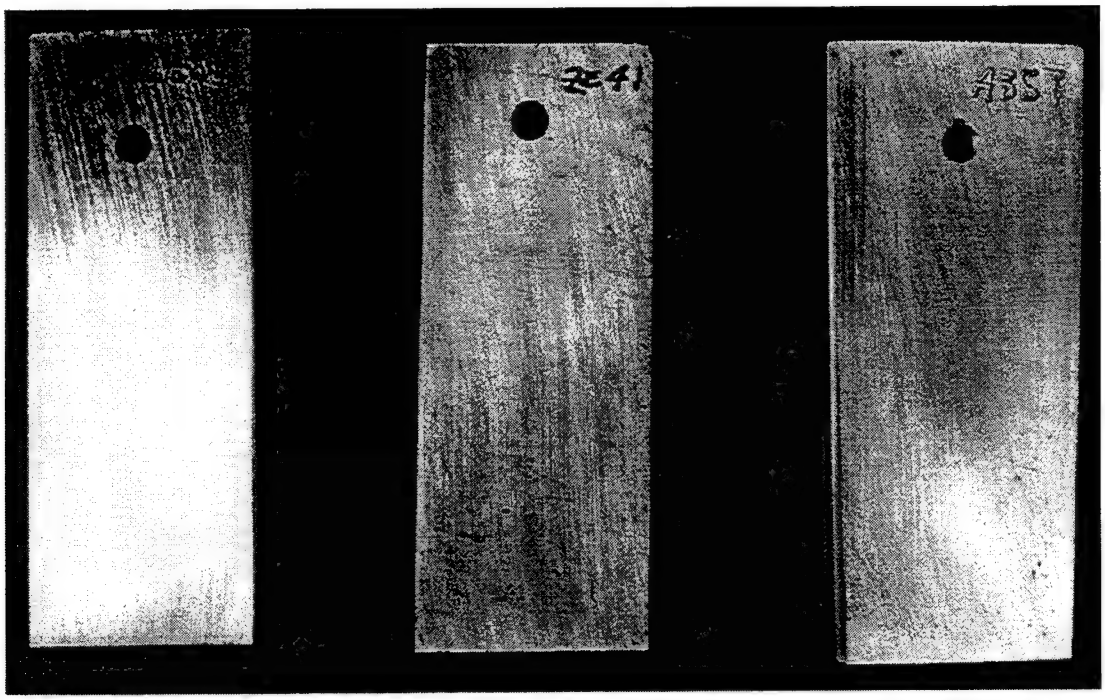

a) WE43 MAG b) ZE41 MAG c) A357 AL

FIGURE 109: BARE PANELS PRIOR TO CORROSION TEST

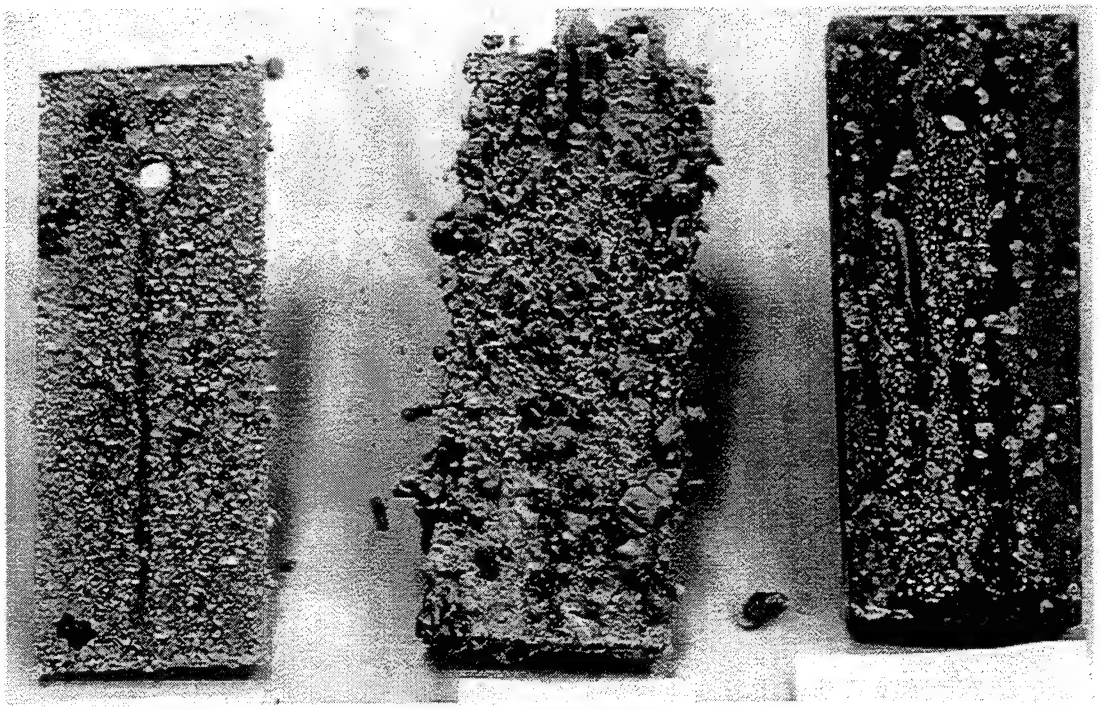

a) WE43 MAG b) ZE41 MAG c) A357 AL

FIGURE 110: BARE PANELS AFTER 247 HOUR CORROSION TEST

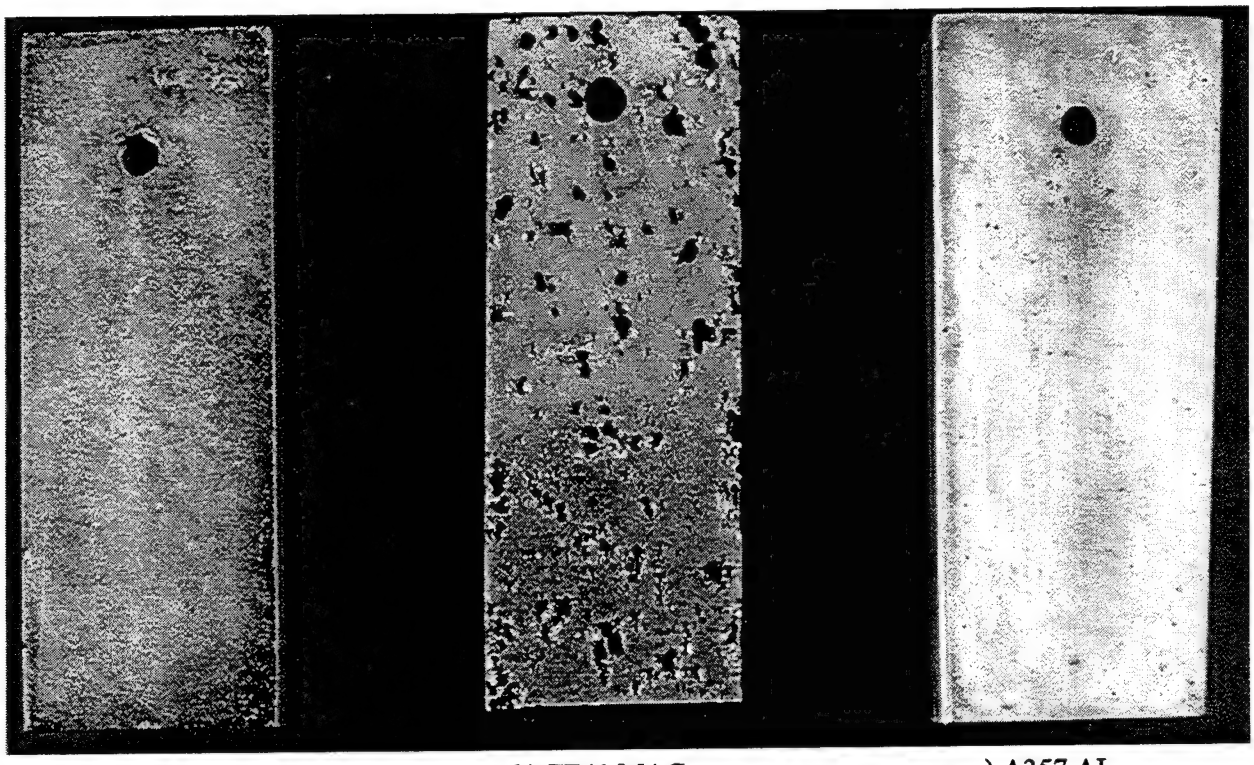

a) WE43 MAG b) ZE41 MAG c) A357 AL

FIGURE 111: BARE PANELS AFTER 247 HR CORROSION TEST - CORROSION DEBRIS REMOVED

6.4.2 MAGNESIUM HOUSING CORROSION TESTS

The purpose of this test was to evaluate the corrosion resistance of a used WE43 magnesium housing with that of a used ZE41 magnesium housing assembly. Based on the results of the flat panel tests described in Section 6.4.1, one ZE41 and one WE43 housing were sealed with the following corrosion protection scheme:

- Anodic treat casting per BPS 4509 Type II, Class D (DOW 17)
- Apply two coats of MIL-R-3043* resin by dipping (.0004 - .0007 total thickness)
- Machine casting
- Chrome Manganese treat per BPS 4003
- Install housing hardware (studs etc.)
- Apply third coat of MIL-R-3043 resin by spraying (.0002 - .00035 thick)
- Apply two coats of MIL-P-23377 Type II epoxy polyamide primer per BPS 4451 to all external non-machined surfaces
- Apply two coats of MIL-C-22750 epoxy paint per BPS 4427 to all external non-machined surfaces

*MIL-R-3043 was used instead of the DTD5562 resin, because MIL-R-3043 is the primary resin used at BHTI, and the performance of the DTD5562 resin was only slightly better than the MIL-R-3043 during the flat panel corrosion tests.

Each housing was subsequently used during the improved spiral bevel tests described in Section 6.2.6 through 6.2.8. Both housings were subjected to hundreds of hours of run time at high load and high operating temperatures and numerous assemblies and disassemblies. Any wear or assembly/disassembly damage to the housing sealing system was left unrepaired.

For the corrosion tests, the housings were assembled with the various hardware, covers, plates and plugs shown in Figures 112 through 114. Table 63 shows the material and coating configurations of the plates, covers, plugs and hardware. The mating surfaces between the magnesium housing and each cover or plate was coated with a thin film of MIL-S-8874 sealant prior to assembly. All nuts, bolts, screws and washers were wet installed with MIL-S-8802 Class B2 sealant. After complete assembly, a bead of MIL-S-8802 Class B2 sealant was applied to each mating joint including all covers, plates, plugs, screws, nuts, and bolts. The studs shown in Figure 119 were left exposed, no bead of sealant, to demonstrate the detrimental effect of an unsealed galvanic potential on a magnesium housing. The final housing assembly was painted with two coats of MIL-P-22750 epoxy paint per BPS 4427 (gray color no. 16440 per FED STD 595). Photographs of the WE43 housing assembly prior to corrosion testing are shown in Figures 116 through 121. The ZE41 housing assembly was identical in appearance.

Both housings were then concurrently subjected to twenty-four, 24 hour cyclic environmental atmospheres shown in Figure 115 (same cycle used for flat panel corrosion tests). Each housing was re-oriented in the test chamber after each complete 24 hour cycle so that each side of the housing assembly was exposed to six different orientations twice. The housings were placed in the environmental chamber in the six different orientations shown in Figures 116 through 121 so that the surface shown was the top surface.

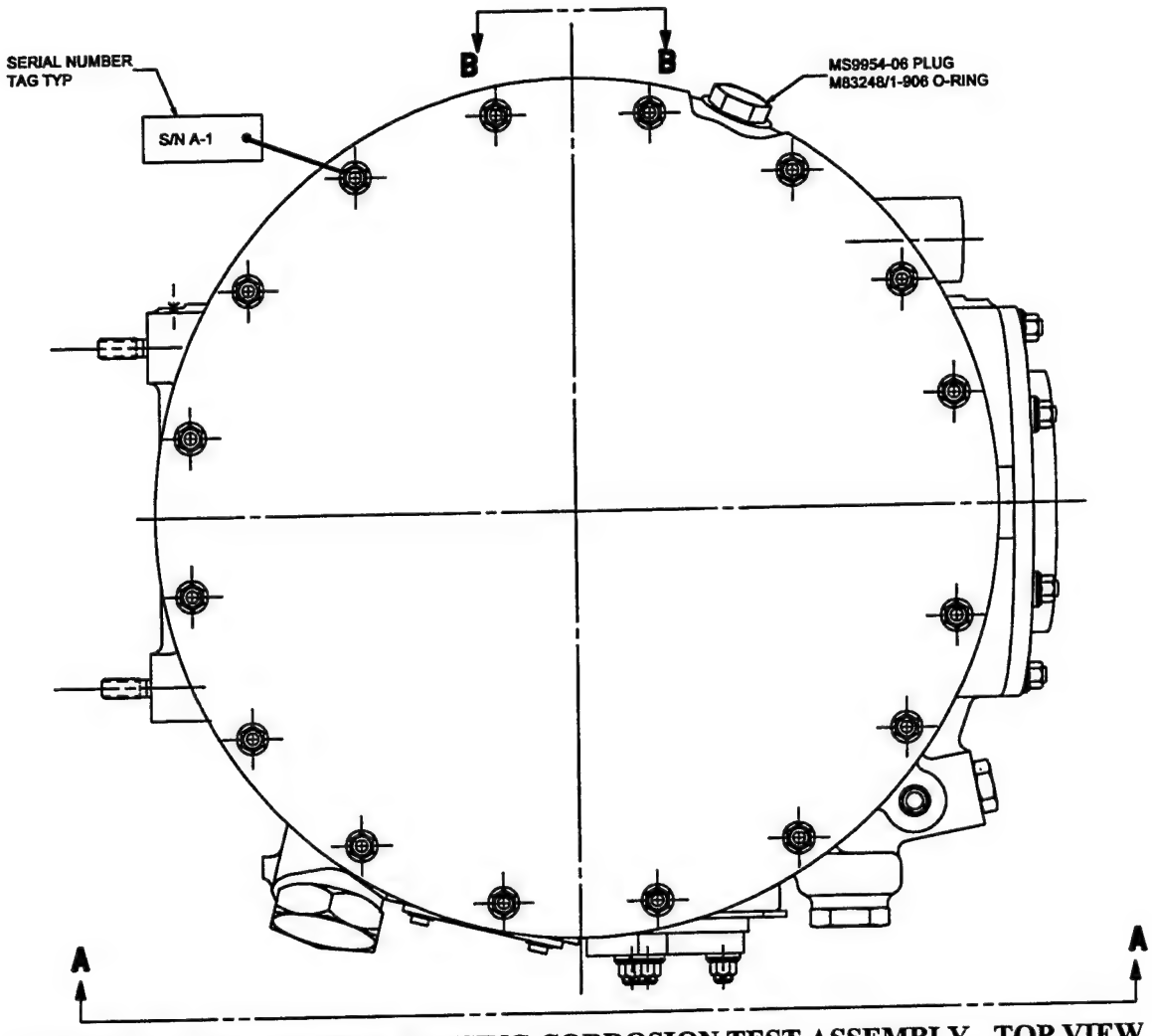

FIGURE 112: MAGNESIUM HOUSING CORROSION TEST ASSEMBLY - TOP VIEW

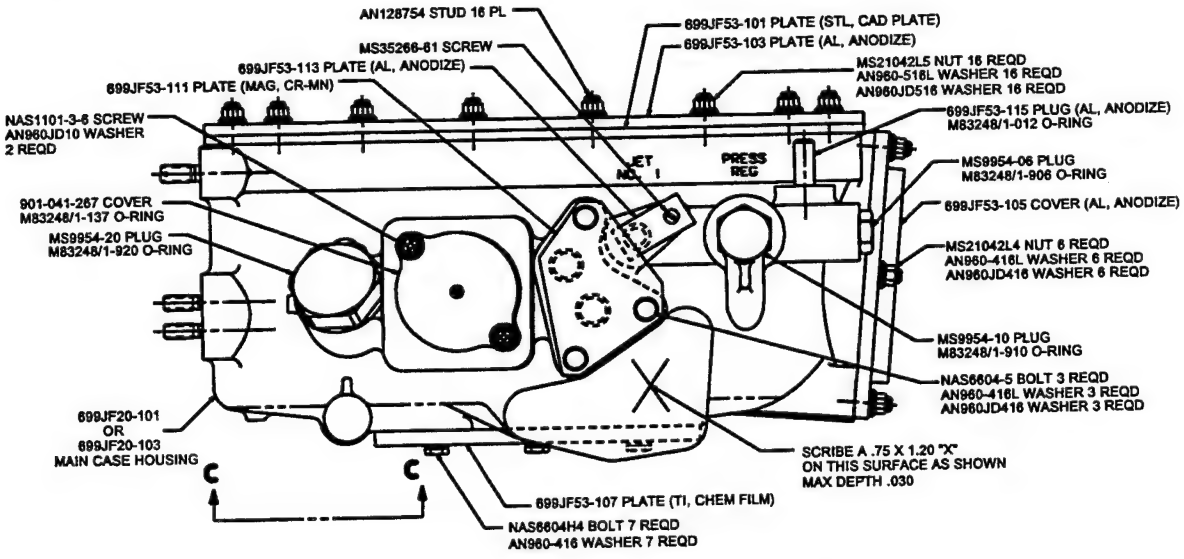

NOTE: AN960JD WASHERS SHALL BE IN CONTACT WITH 699JF53 COVERS AND PLATES

FIGURE 113: MAGNESIUM HOUSING CORROSION TEST ASSEMBLY - SIDE VIEW A-A

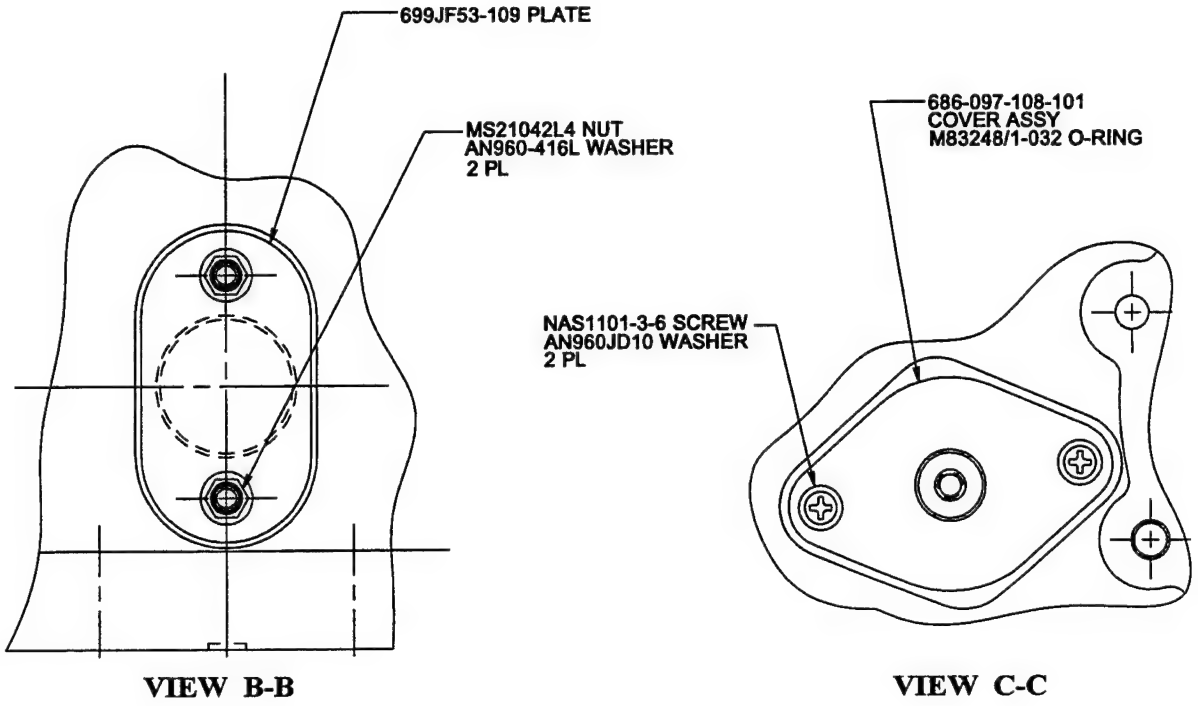

FIGURE 114: MAGNESIUM HOUSING CORROSION TEST ASSY - VIEWS B-B & C-C

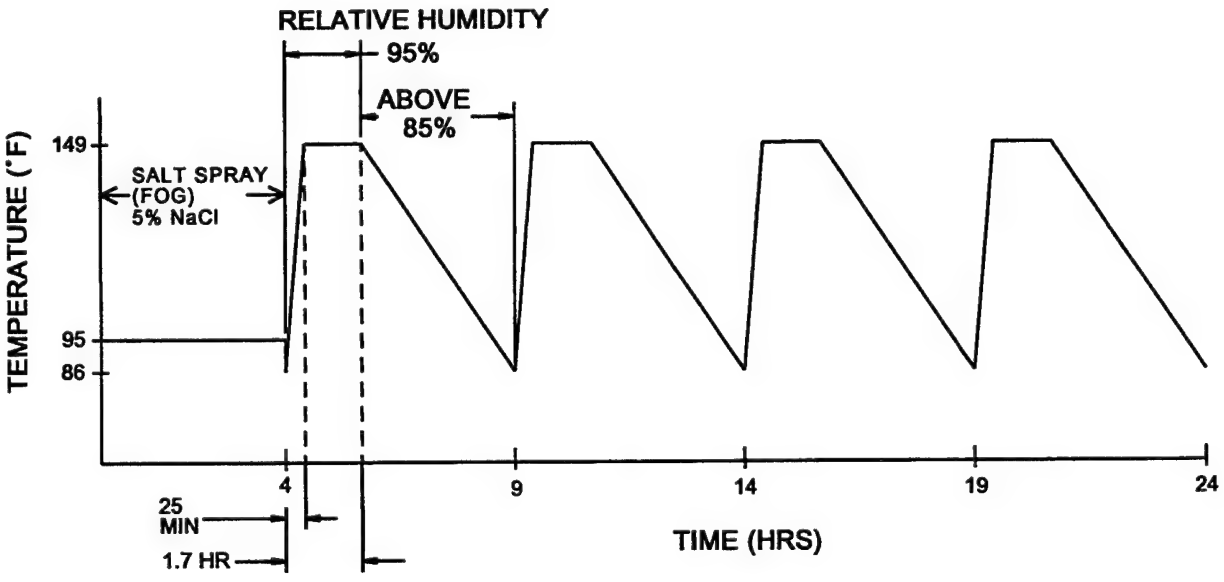

FIGURE 115: MAGNESIUM HOUSING CORROSION TEST CYCLE

The results of the 576 hour corrosion test on each housing are shown in Figures 122 through 133. For the ZE41 housing, corrosion was observed around the 901-041-267 cover as shown in Figure 125. The mating surface on the main housing had been previously machined, chrome manganese treated and then sprayed with one coat of resin. Some chipping and flaking of the resin coating was observed prior to assembling the housing for the corrosion test. The corrosion appears to have started in a non-galvanic area and spread underneath the resin coating leading to galvanic corrosion between the 901-041-267 cover and the ZE41 housing. This type of corrosion is consistent with the results of the panel tests which showed that chrome manganese is inferior to Dow 17 as a base metal coating for subsequent resin coating. The chrome manganese was used for all machined surfaces since it yields little dimensional build-up and is a non-anodic coating which can be applied after installation of steel liners and studs. No corrosion was observed at the same location for the WE43 housing as seen in Figure 131. This demonstrates the superior resistance of the WE43 magnesium to non-galvanic corrosion as both housings had identical anti-corrosion treatments. Chips and flakes were also observed in the resin coating on this area of the WE43 housing prior to assembly for the corrosion test.

Heavy galvanic corrosion was observed on both housings around the exposed studs as shown in Figure 126 and 132. This was expected since no attempt was made to inactivate the galvanic potential between the steel studs and the magnesium housings. The heavy corrosion points up the effectiveness of the sealing system used for other stud locations on the magnesium housings shown in Figures 122, 123, 124, 127, 128, 129, 130, and 133. No corrosion occurred around these studs which were sealed to prevent any moisture from activating the galvanic potential.

The scribed 'X' on the ZE41 housing shown in Figure 125 had the same results as for the flat panel tests, some corrosion at the surface of the exposed metal with no propagation underneath the sealing system. The scribed 'X' on the WE43 housing shown in Figure 131 also had the same results as for the flat panel tests, minute corrosion at the surface of the exposed metal with no propagation underneath the sealing system. Some peeling of the paint also occurred but with no effect on the WE43 magnesium housing.

Prior to disassembly and cleaning, the only other corrosion observed was on the WE43 housing as shown in Figure 131. Galvanic corrosion was observed between the 699JF53-111 plate (WE43 mag) and the AN960JD416 washer on one of the bolts where the MIL-S-8802 sealant had been peeled away during the corrosion tests due to rough handling. The corrosion was limited to the 699JF53-111 plate and did not progress to the main WE43 housing.

After disassembling each housing, the only additional corrosion found was around the 901-041-267 cover on the ZE41 housing as shown in Figure 134. The corrosion consisted of deep corrosion pits and evidence of severe galvanic corrosion between the ZE41 magnesium housing and the aluminum cover. No additional corrosion was observed on the WE43 housing after disassembly.

TABLE 63: MAG HOUSING ASSY COMPONENTS & HARDWARE MATERIAL & FINISH

PART NO.	NOMENCLATURE	MATERIAL	FINISH	HARDWARE: MATL, FINISH
699JF53-101	TOP RING	4340 ALLOY STL	CAD PLATE, PRIME	STUD: STL, CAD PLATE NUT: STL, CAD PLATE WASHER: STL, CAD PLATE WASHER: AL, CHEM FILM
699JF53-103	TOP PLATE	2024 AL ALLOY	ANODIZE, PRIME	STUD: STL, CAD PLATE NUT: STL, CAD PLATE WASHER: STL, CAD PLATE WASHER: AL, CHEM FILM
699JF53-105	INPUT PLATE	2024 AL ALLOY	ANODIZE, PRIME	STUD: STL, CAD PLATE NUT: STL, CAD PLATE WASHER: STL, CAD PLATE WASHER: AL, CHEM FILM
699JF53-107	BOTTOM PLATE	6AI-4V TI ALLOY	CHEM FILM, PRIME	BOLT: STL, CAD PLATE WASHER: STL, CAD PLATE
699JF53-109	OVAL PLATE	4340 ALLOY STL	CAD PLATE, PRIME	STUD: STL, CAD PLATE NUT: STL, CAD PLATE WASHER: STL, CAD PLATE
699JF53-111	FILTER PLATE	WE43 MAG ALLOY	CR MANG., PRIME	BOLT: STL, CAD PLATE WASHER: STL, CAD PLATE WASHER: AL, CHEM FILM
699JF53-113	JET PLATE	2024 AL ALLOY	ANODIZE, PRIME	SCREW: STL, CAD PLATE
699JF53-115	PLUG	2024 AL ALLOY	ANODIZE, PRIME	N/A
686-097-108-101	COVER ASSY	2024 AL ALLOY	ANODIZE	SCREW: STL, CAD PLATE WASHER: AL, CHEM FILM
901-041-267-101	COVER	2024 AL ALLOY	ANODIZE, PRIME	SCREW: STL, CAD PLATE WASHER: AL, CHEM FILM

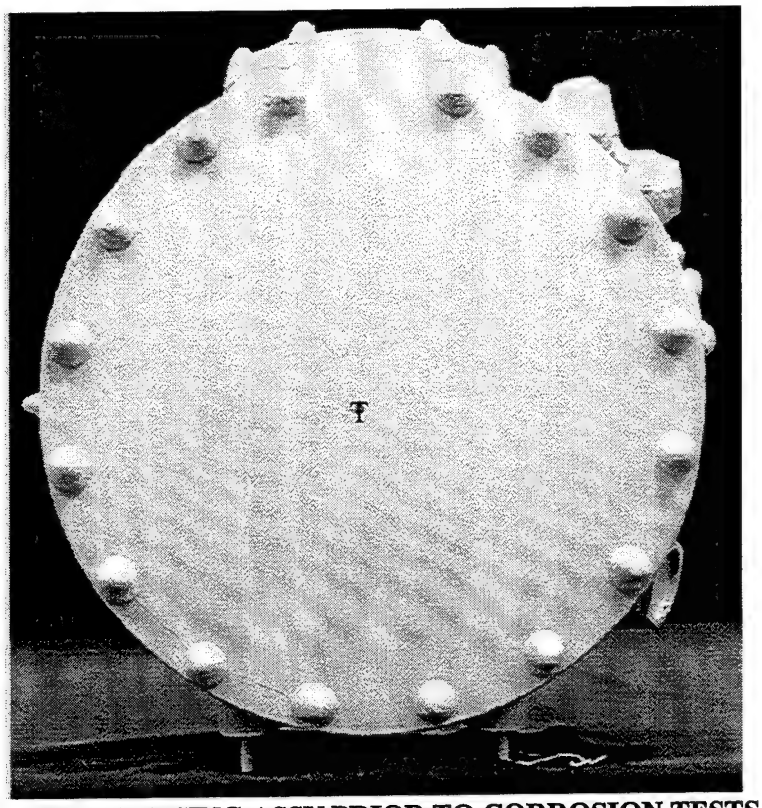

FIGURE 116: WE43 HOUSING ASSY PRIOR TO CORROSION TESTS - TOP VIEW

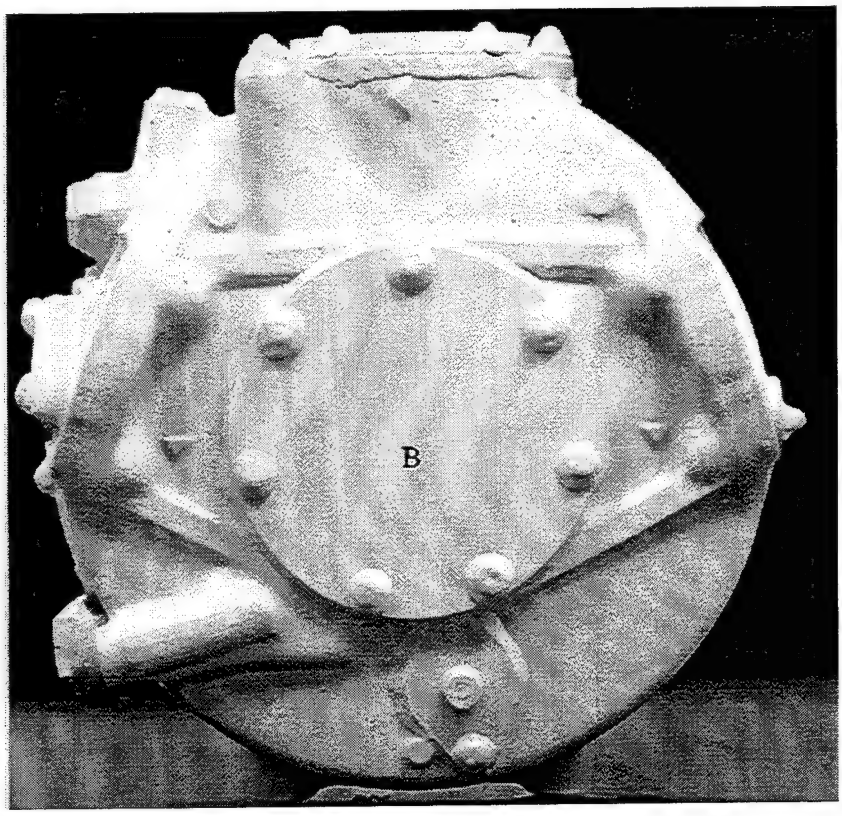

FIGURE 117: WE43 HOUSING ASSY PRIOR TO CORROSION TESTS - BOTTOM VIEW

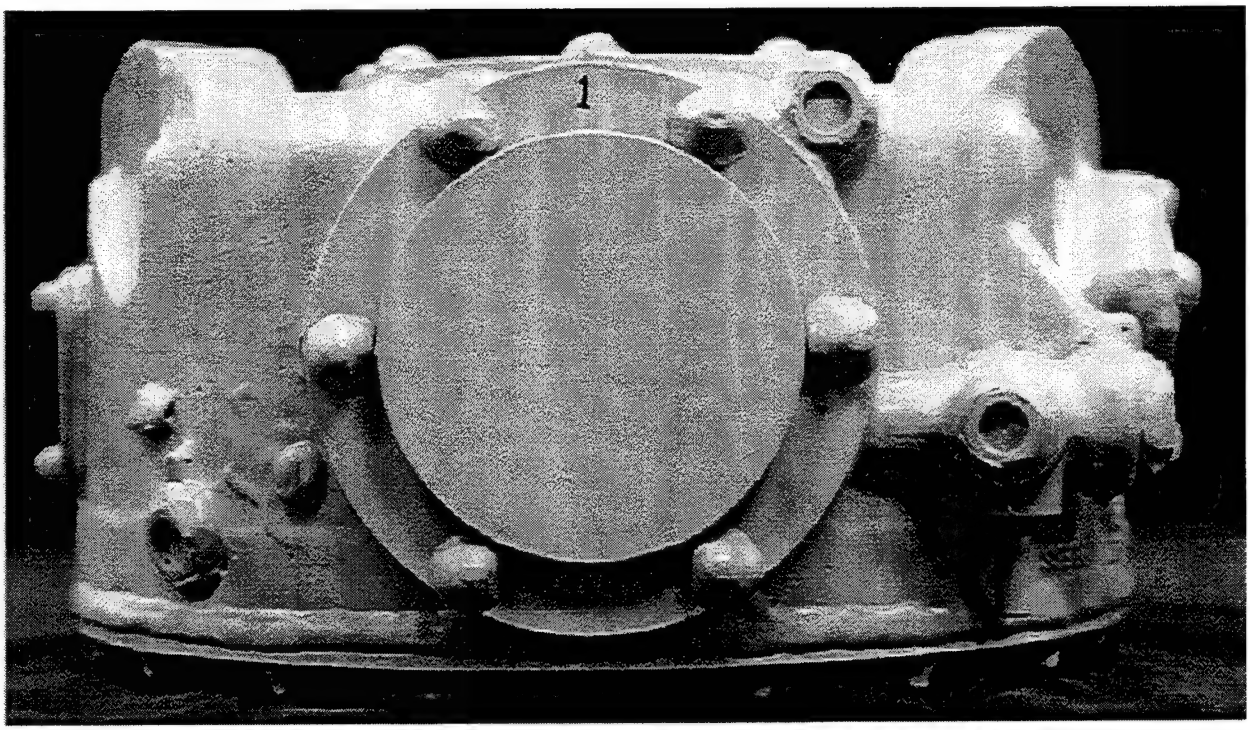

FIGURE 118: WE43 HOUSING ASSY PRIOR TO CORROSION TESTS - SIDE VIEW 1

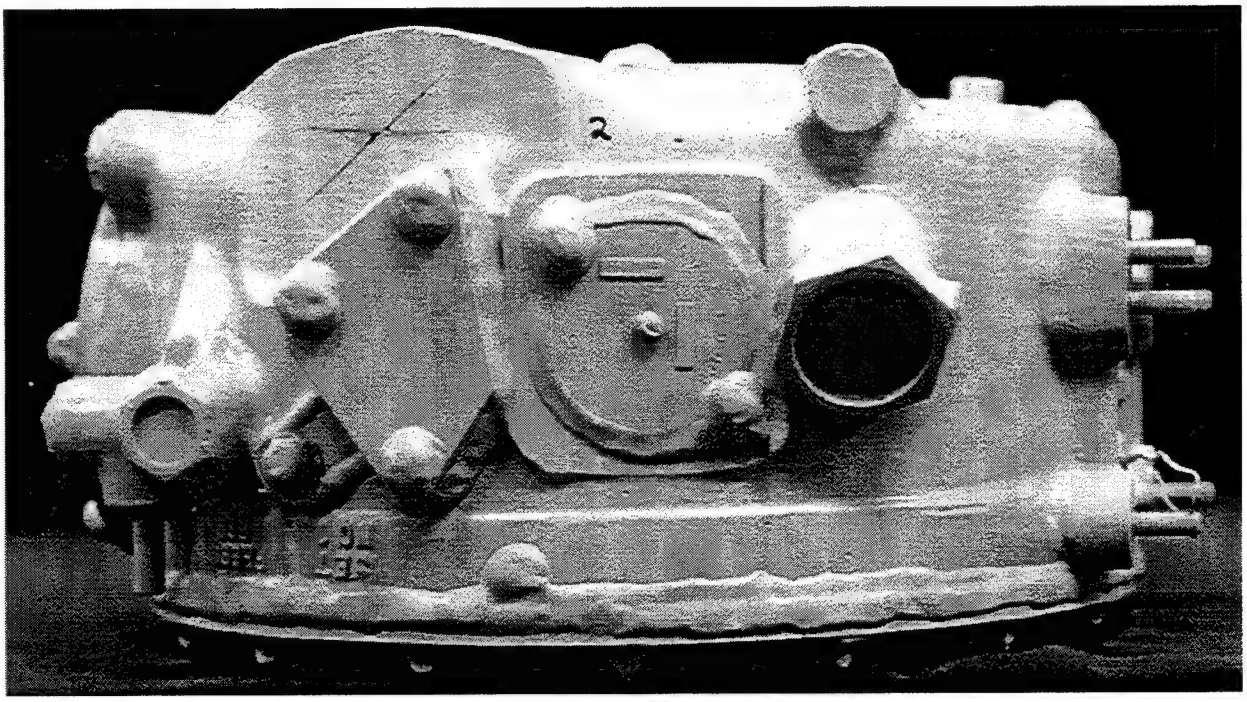

FIGURE 119: WE43 HOUSING ASSY PRIOR TO CORROSION TESTS - SIDE VIEW 2

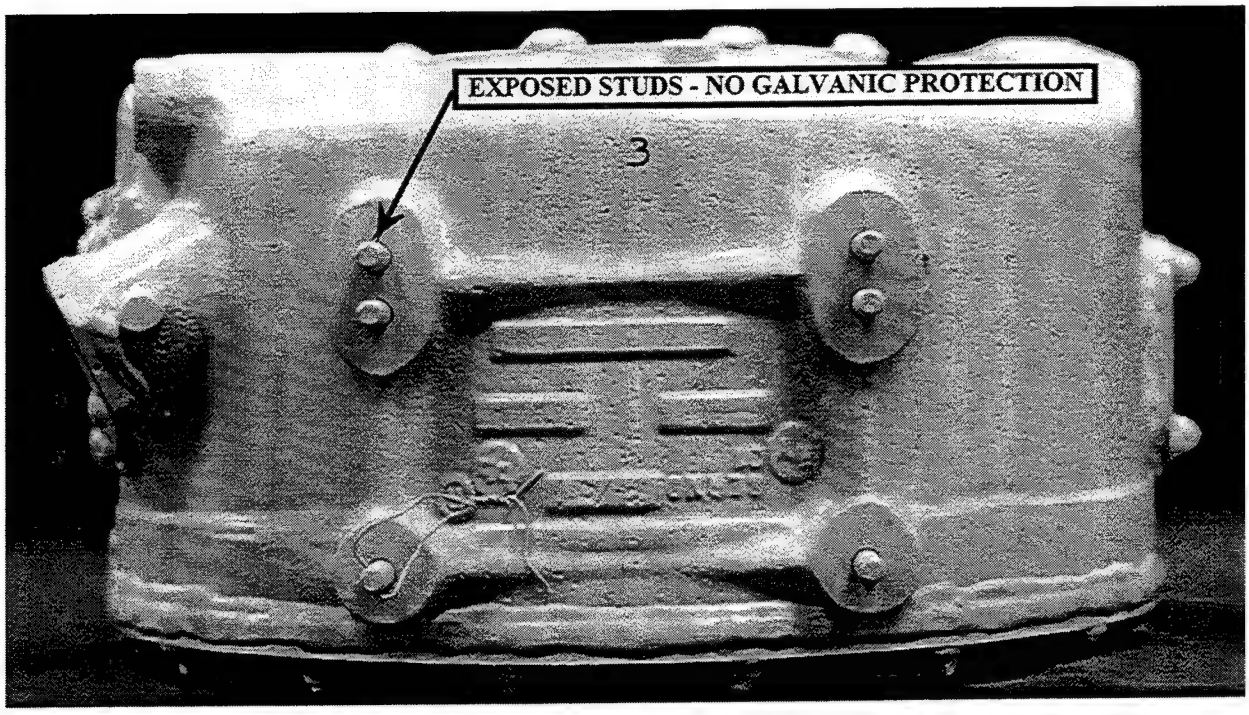

FIGURE 120: WE43 HOUSING ASSY PRIOR TO CORROSION TESTS - SIDE VIEW 3

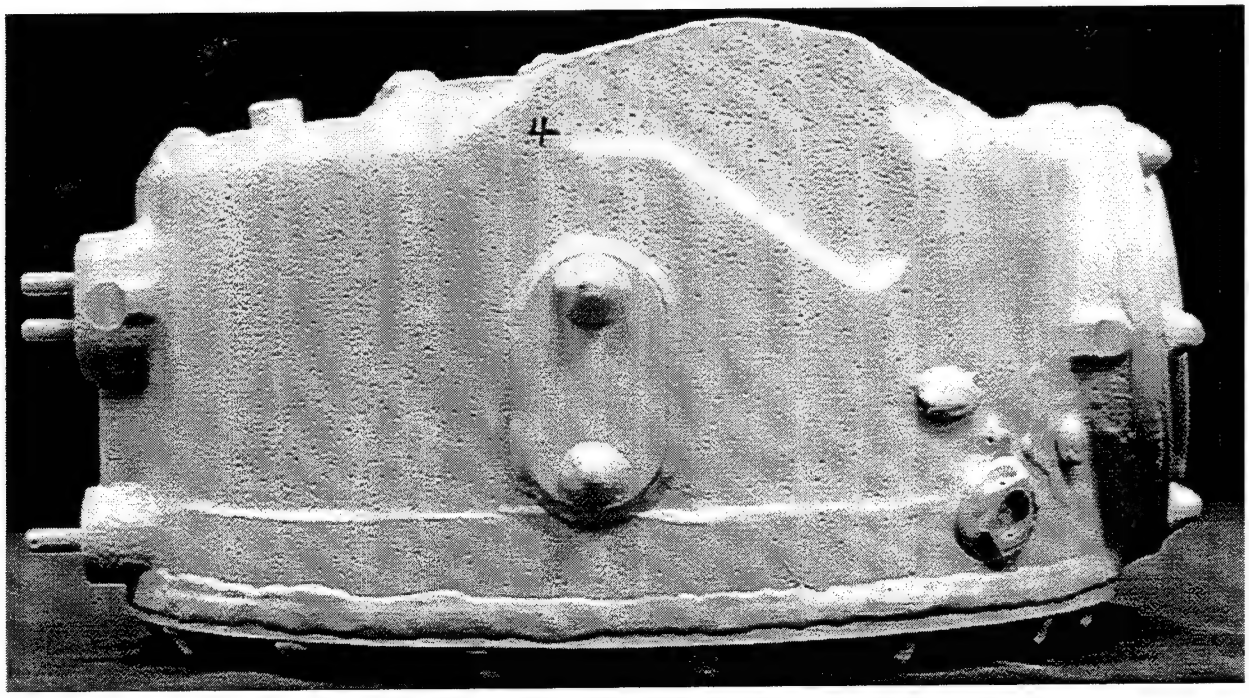

FIGURE 121: WE43 HOUSING ASSY PRIOR TO CORROSION TESTS - SIDE VIEW 4

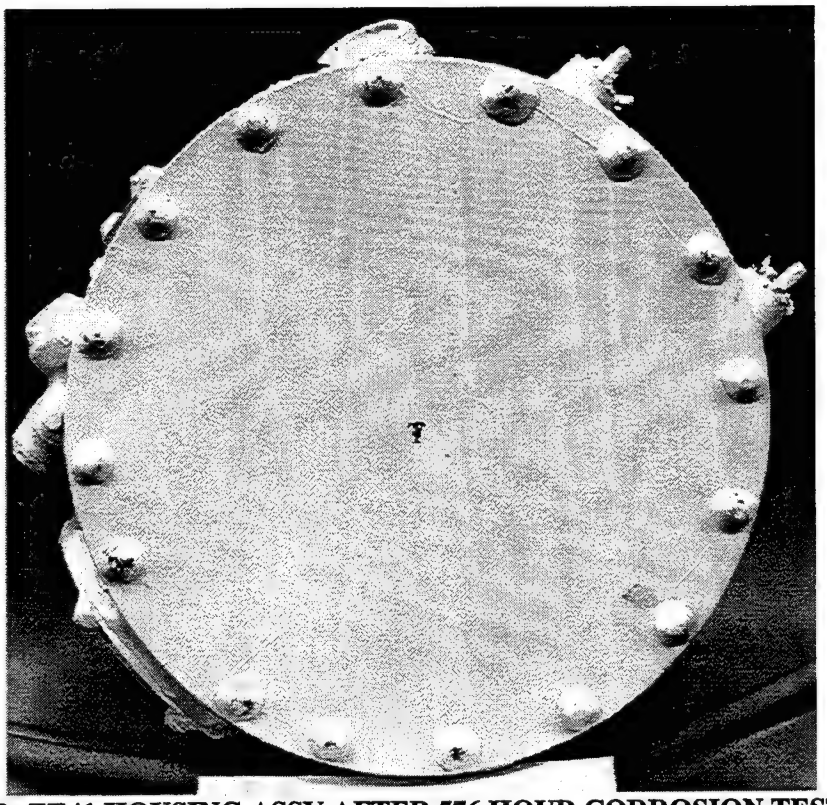

FIGURE 122: ZE41 HOUSING ASSY AFTER 576 HOUR CORROSION TEST - TOP VIEW

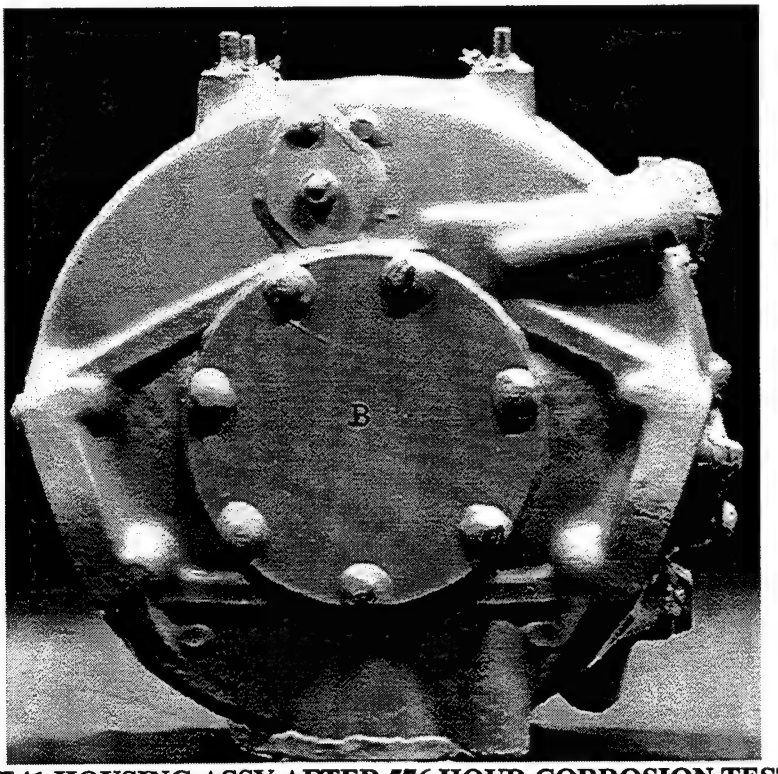

FIGURE 123: ZE41 HOUSING ASSY AFTER 576 HOUR CORROSION TEST - BOTTOM VIEW

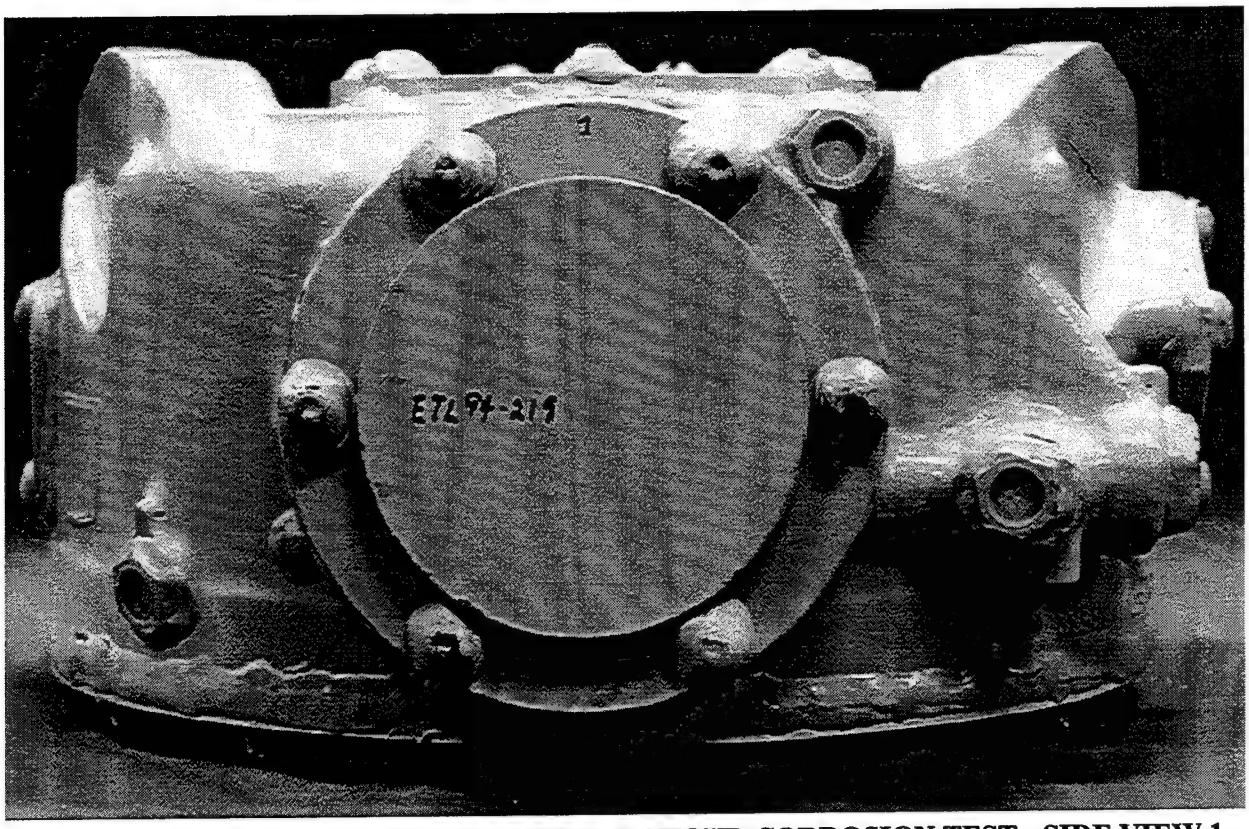

FIGURE 124: ZE41 HOUSING ASSY AFTER 576 HOUR CORROSION TEST - SIDE VIEW 1

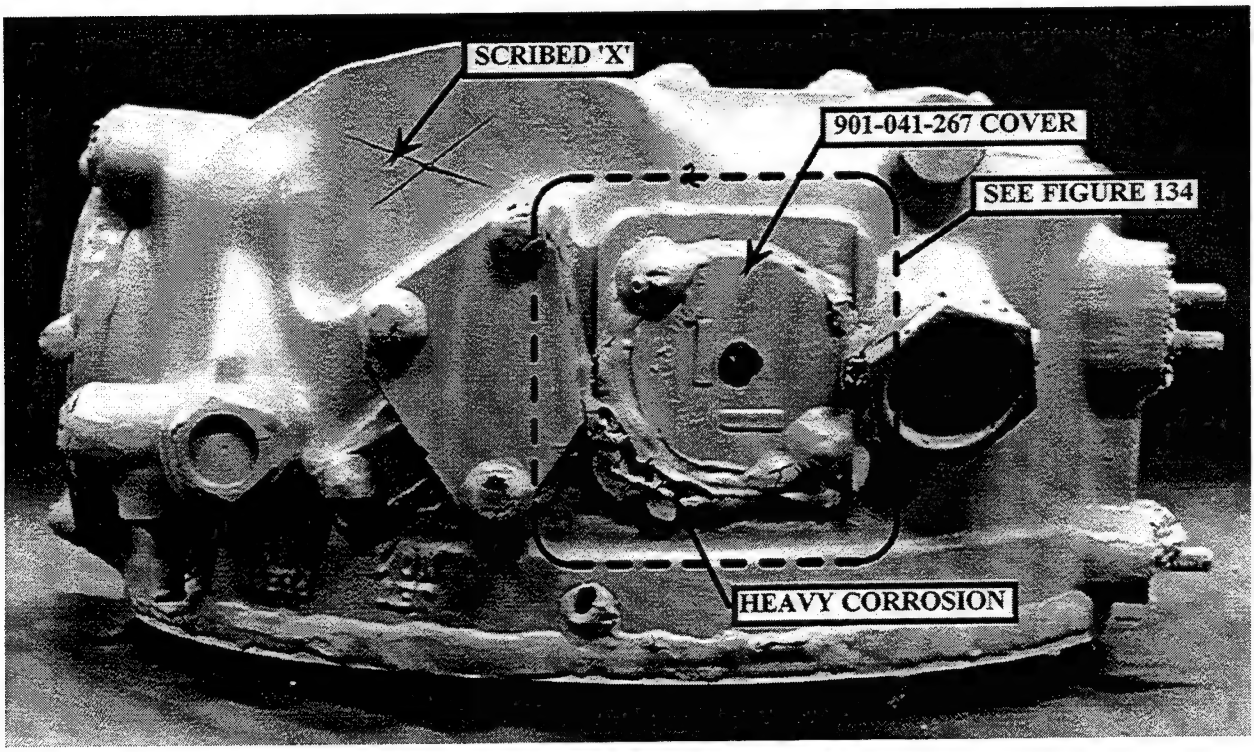

FIGURE 125: ZE41 HOUSING ASSY AFTER 576 HOUR CORROSION TEST - SIDE VIEW 2

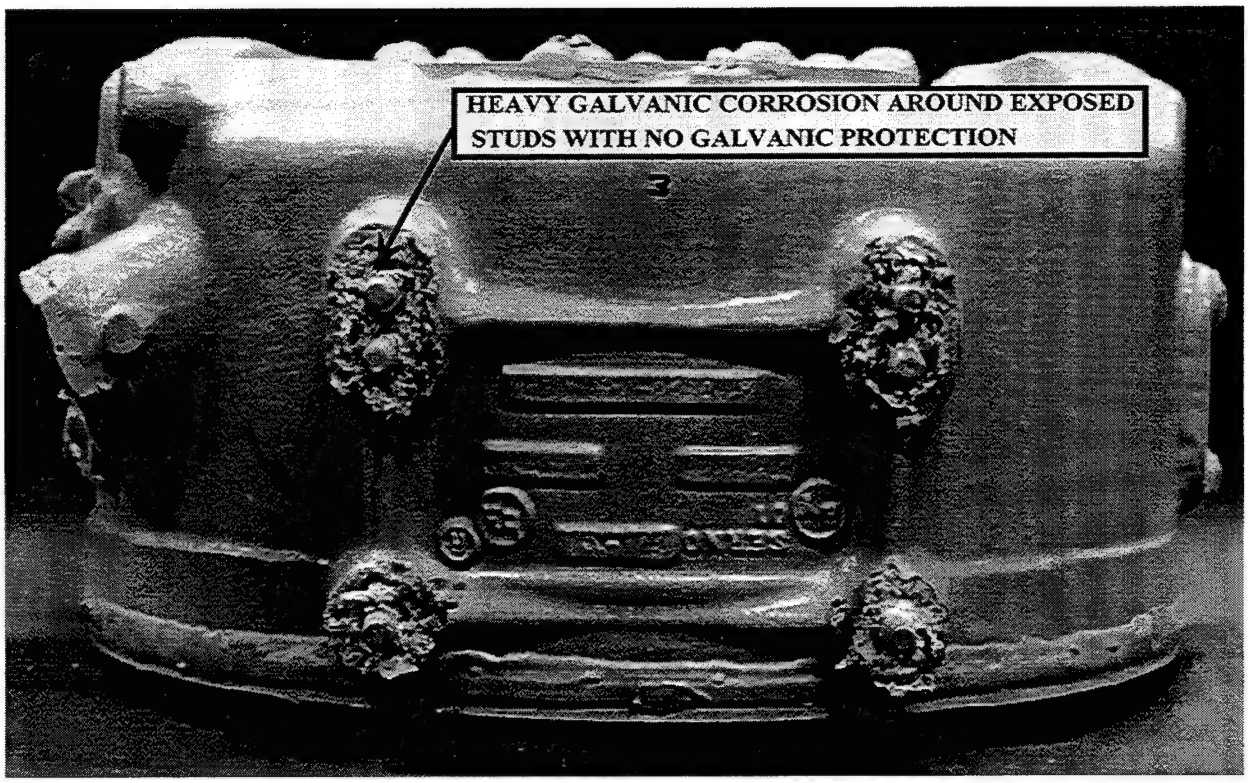

FIGURE 126: ZE41 HOUSING ASSY AFTER 576 HOUR CORROSION TEST - SIDE VIEW 3

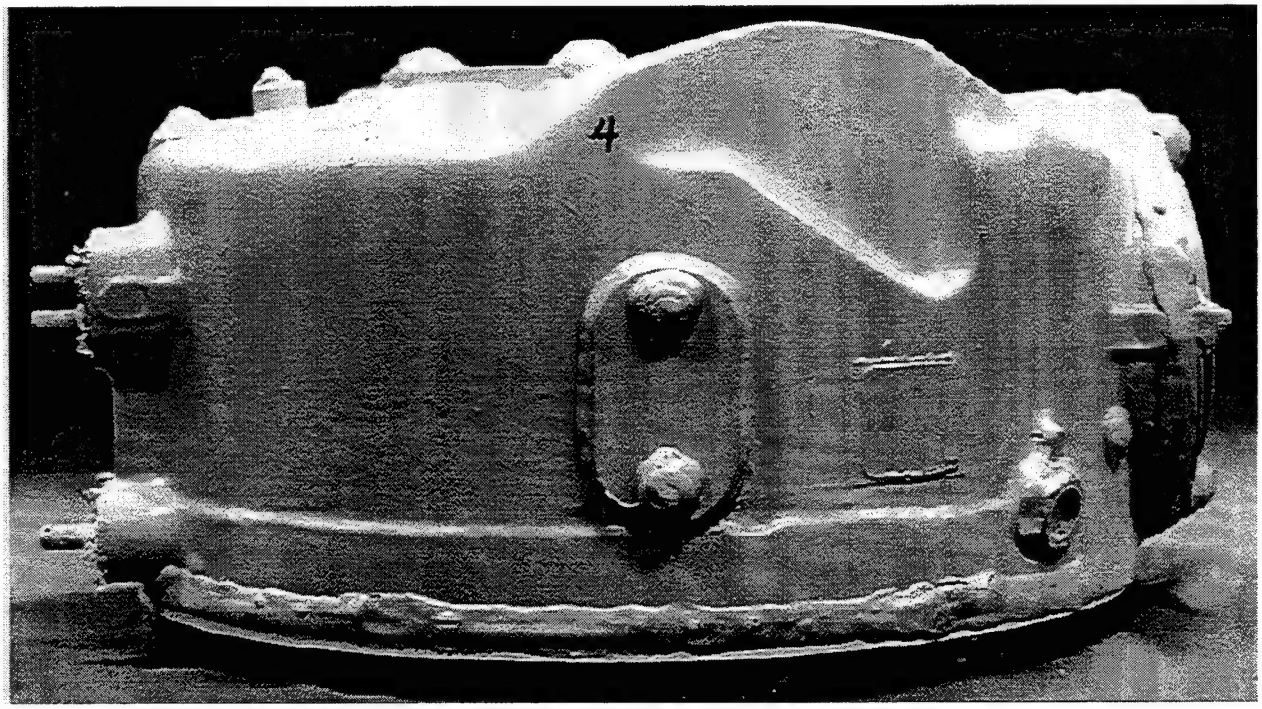

FIGURE 127: ZE41 HOUSING ASSY AFTER 576 HOUR CORROSION TEST - SIDE VIEW 4

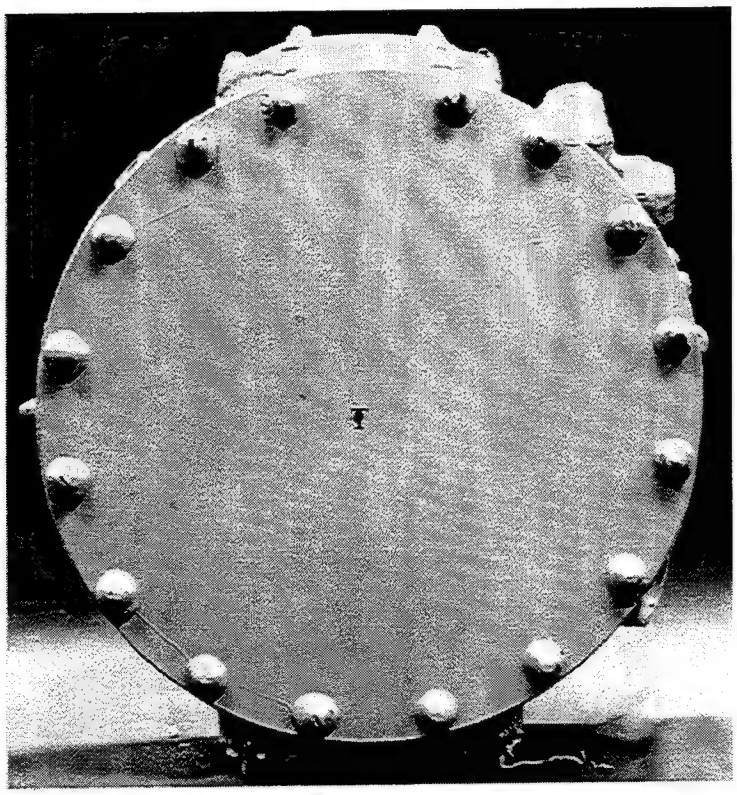

FIGURE 128: WE43 HOUSING ASSY AFTER 576 HOUR CORROSION TEST - TOP VIEW

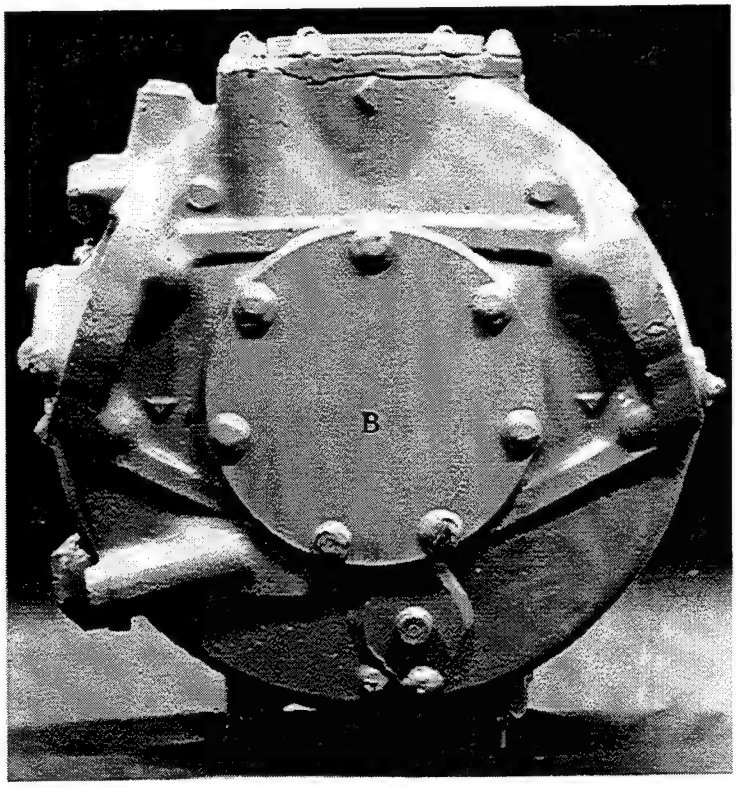

FIGURE 129: WE43 HOUSING ASSY AFTER 576 HOUR CORROSION TEST - BOTTOM VIEW

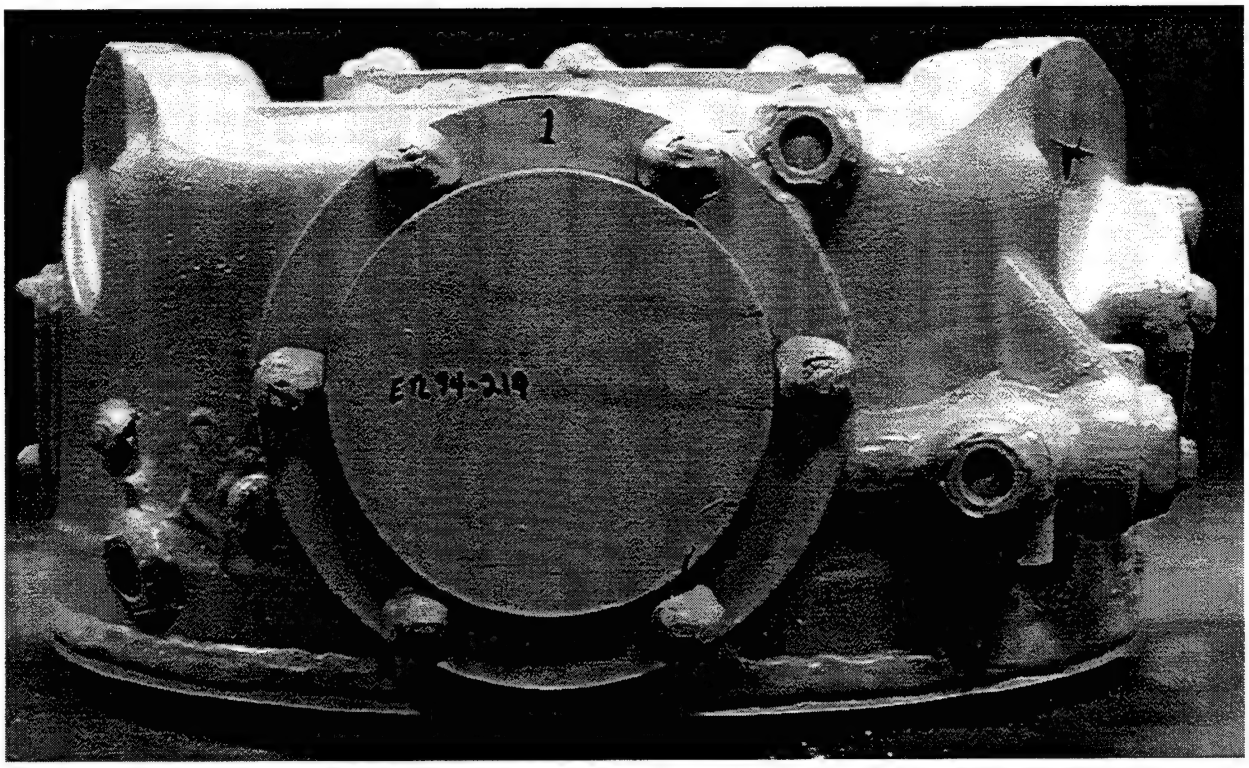

FIGURE 130: WE43 HOUSING ASSY AFTER 576 HOUR CORROSION TEST - SIDE VIEW 1

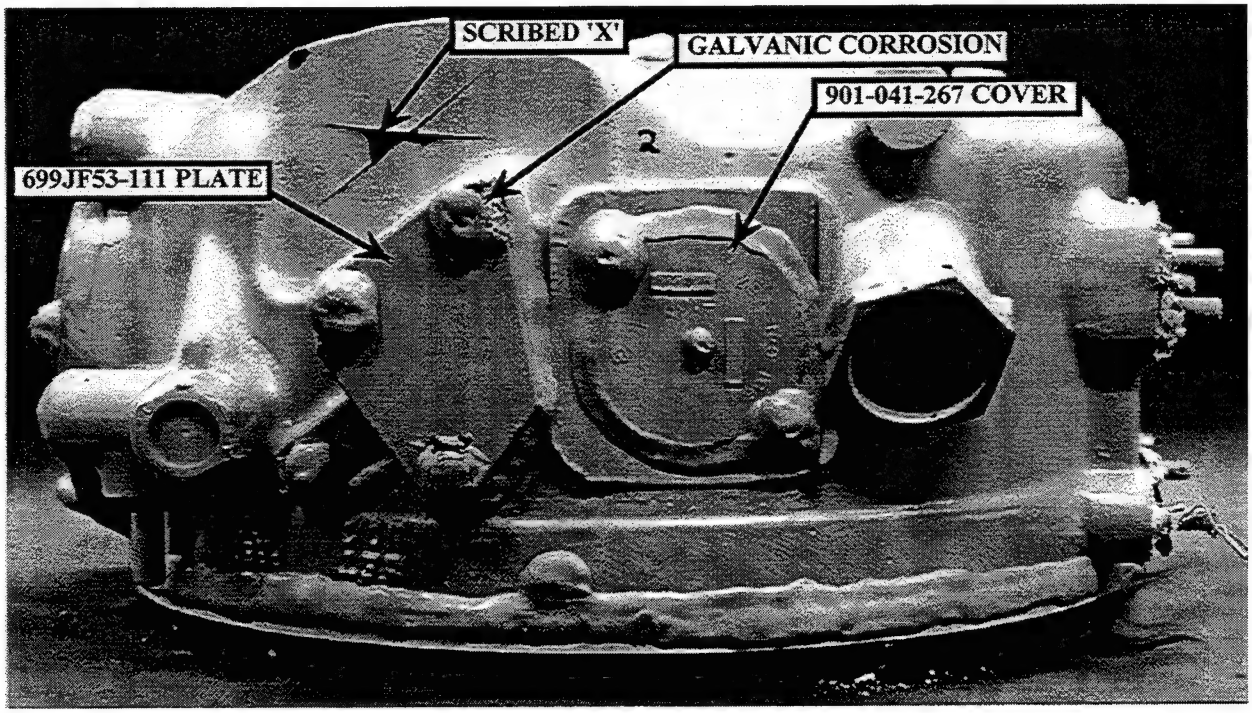

FIGURE 131: WE43 HOUSING ASSY AFTER 576 HOUR CORROSION TEST - SIDE VIEW 2

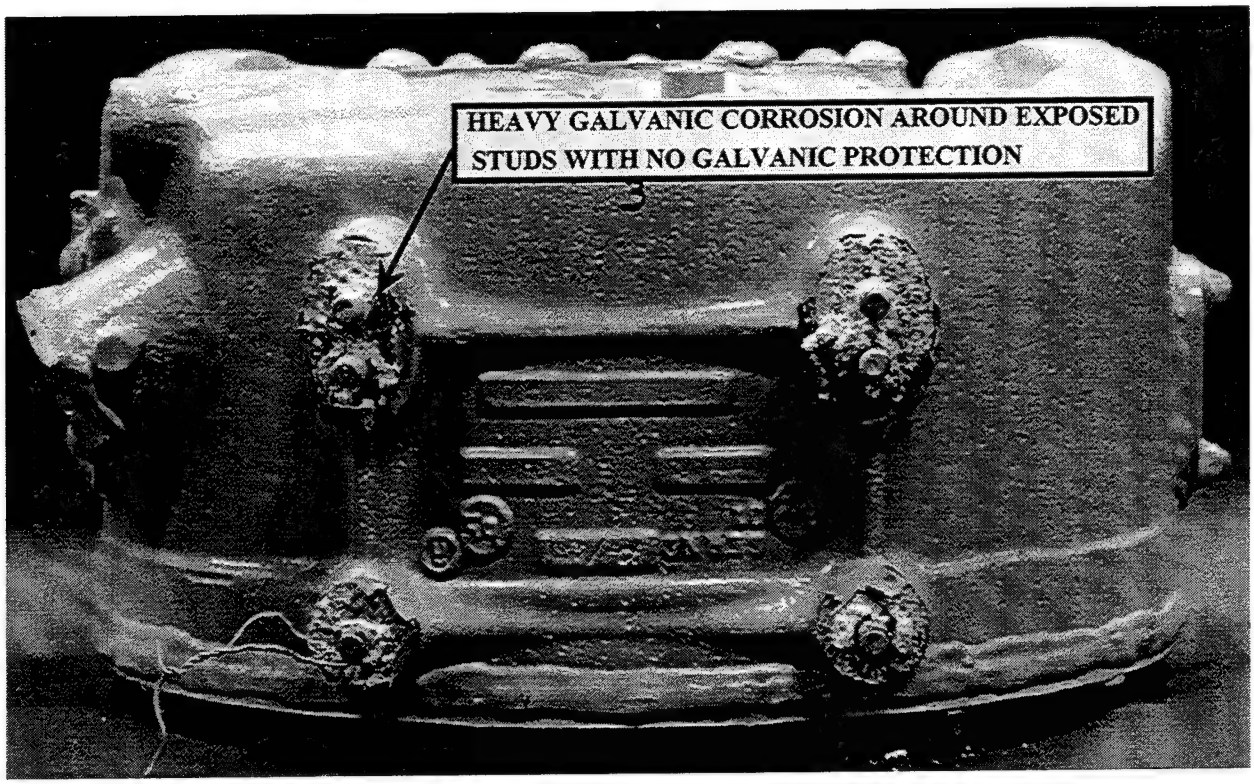

FIGURE 132: WE43 HOUSING ASSY AFTER 576 HOUR CORROSION TEST - SIDE VIEW 3

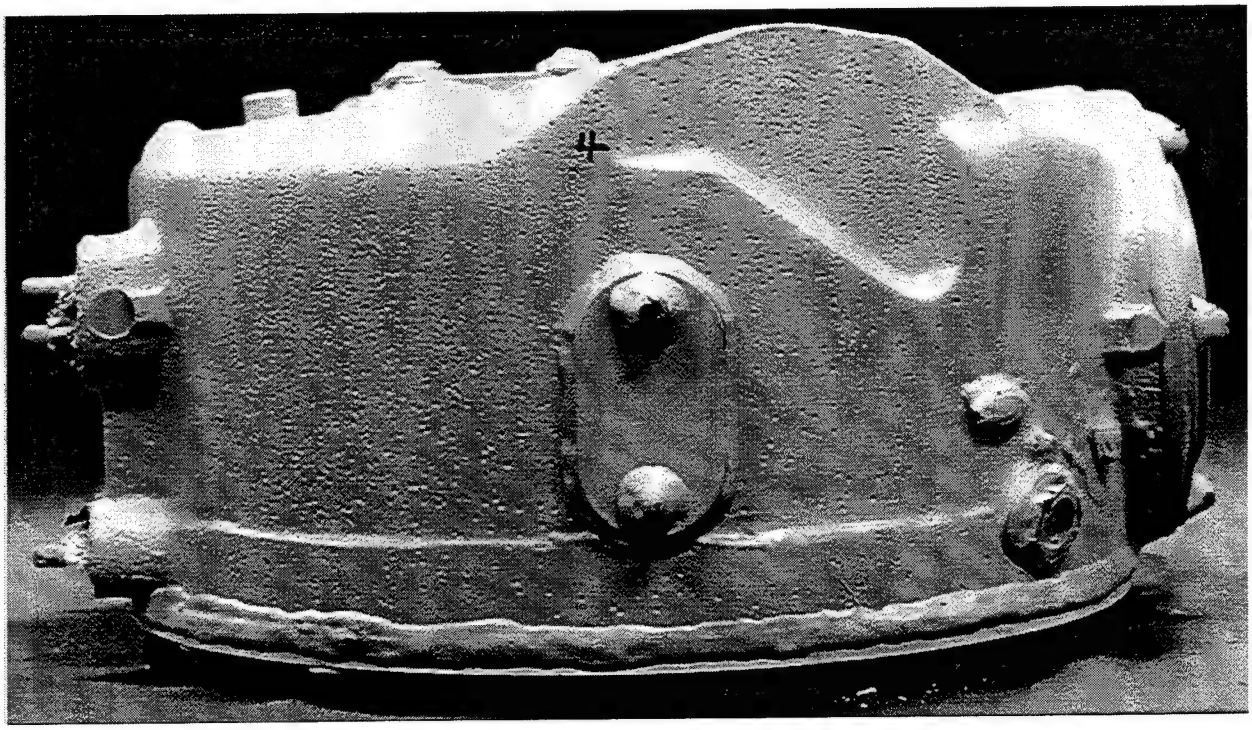

FIGURE 133: WE43 HOUSING ASSY AFTER 576 HOUR CORROSION TEST - SIDE VIEW 4

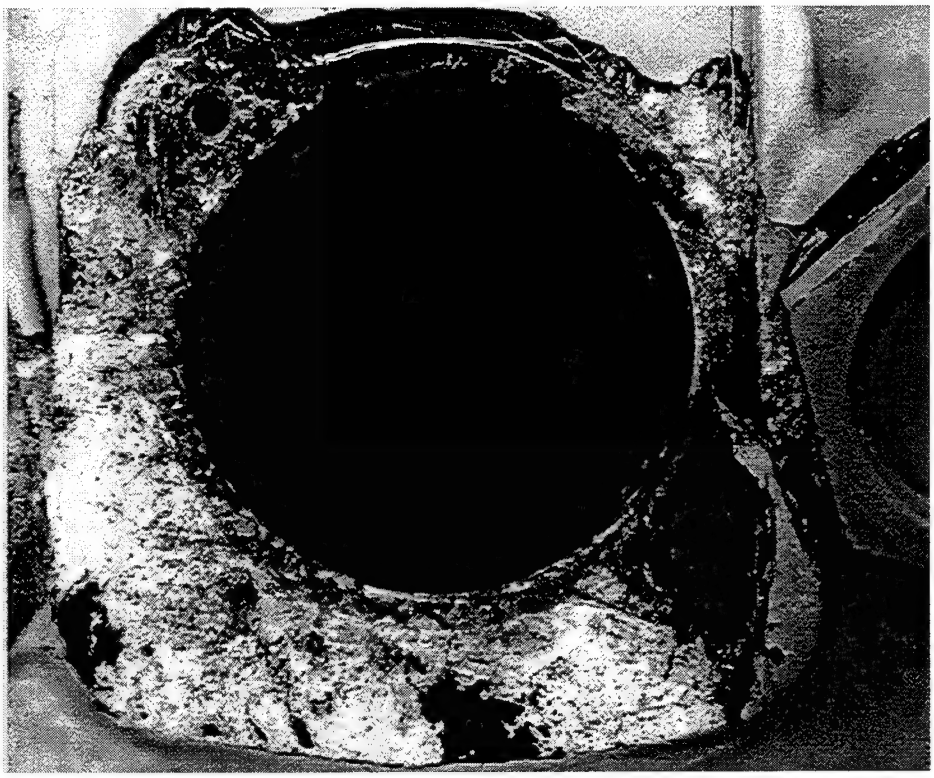

FIGURE 134: ZE41 MAGNESIUM HOUSING ASSEMBLY - CLOSE-UP OF CORROSION AFTER DISASSEMBLY (SEE FIGURE 125)

7.0 SUMMARY OF RESULTS

1. Based on the results of the tradeoff studies and component verification tests, the proposed ART will meet or exceed the 3 stated goals of the program:

    - 25% weight reduction relative to SOAT
    - 5000 hour MTBR
    - 10 dB noise level reduction relative to SOAT

2. For the reduction ratio and HP requirements of the ART, the SABP planetary was at least 28% heavier and larger in size than a two stage simple planetary with standard tooth contact ratios.

3. The HCR planetary was selected for the ART over the standard, split power, SABP, and compound planetaries because it yielded the optimum combination of low weight, noise, cost, and risk, minimum spatial envelope, and high life, survivability, and efficiency.

4. The input sprag clutch was selected for the ART over the spring and roller ramp clutches because it yielded the optimum combination of low weight, cost, and risk, minimum spatial envelope, and high life and survivability.

5. The ART configuration, optimized for low weight, noise, cost, and risk, minimum spatial envelope, and high life, survivability, and efficiency is a two stage input helical reduction with a single stage HCR planetary reduction to the mast and the overrunning clutch located on the engine input shaft.

6. Increasing the allowable oil-out temperature for the ART from 240° F to 334° F will decrease the weight of the transmission lube system by 40 lb without reducing any component lives.

7. For the FAAV interconnect cross-shafting system, no appreciable benefits are gained by designing the system to be supercritical.

8. Geometry restrictions and load requirements prevent the design of a fail-safe steel/composite mast for the ART which is weight competitive with the all steel ART mast.

9. For cast housings with simple geometry, investment cast titanium will yield parts at least 1/3 lighter than investment cast aluminum.

10. The ART yields reduced acquisition, direct operating, and life cycle costs and additional airframe weight reductions as compared to the SOAT.

11. Successful completion of all the tests conducted on the ART HCR planetary demonstrate the sound design and reliability of the planetary. The planetary as designed is qualified for production.

12. The inability to score the HCR planet gear teeth at extreme load, speed, and temperature conditions, and the gear tooth fatigue failure at 241% torque provide support data to reduce the gear face widths, further reducing the weight of the planetary assembly.

13. The efficiency of a planetary tested in a back-to-back test rig, as used for the ART HCR planetary tests, can be reliably calculated based on the measured drag torque and input torque. It is not

necessary to determine the efficiency by measuring the oil-in and oil-out temperatures for a completely insulated test assembly.

14. The ART HCR planetary demonstrated an extremely high gear tooth scoring temperature resistance due to sequential meshing of the planet gears and the use of spherical roller planet bearings, DOD-L-85734 oil, and oil jets optimized for maximum impingement depth.

15. The ART HCR planetary with emergency air/oil mist nozzles, will continue to transmit torque at normal operating conditions for 4 hours after loss of the primary oil supply.

16. Without an emergency air/oil mist system, the ART HCR planetary will not transmit torque at normal operating conditions for more than 30 minutes after loss of the primary oil supply.

17. Titanium nitride coating on the ART HCR titanium planetary carrier effectively eliminates fretting and galling with the planet bearing shafts.

18. The reduced kinematic error geometry OH-58D spiral bevel gears reduced the measured noise level by up to 18 dB as compared to the baseline gear set.

19. The reduced kinematic error geometry OH-58D spiral bevel gears reduced the measured vibration levels by up to 50% as compared to the baseline gear set.

20. Increasing the tooth root fillet radii on the OH-58D input spiral bevel pinion reduced the maximum gear tooth tensile stress by 24%.

21. Considering the entire gear tooth stress cycle (tensile to compressive) on the OH-58D input spiral bevel gears as they go through mesh: increasing the tooth root fillet radii on the gear and pinion would allow a 12% and 21% increase, respectively, in the allowable torque level. Incorporating the reduced kinematic error geometry with the increased tooth root fillet radii would allow a 27% increase in the allowable torque level of the pinion and 28% increase for the gear.

22. X-53 gear steel enhances the scoring resistance of the OH-58D spiral bevel gears.

23. The reduced kinematic error geometry OH-58D spiral bevel gear set produced an undesirable hardline in the flank of the driving pinion. Adding some flank relief (TOPREM) to the pinion reduced the hardline without affecting the reduced noise level of the gear set. Additional flank relief is required to completely eliminate the hardline. The effect this will have on the reduced noise level is unknown.

24. Precision forging increases the bending fatigue strength of X-53 flexure specimens by 20%, demonstrating the benefits of conformal grain flow.

25. Shot peening X-53 flexure specimens with ceramic shot, instead of steel shot, does not increase the bending fatigue strength.

26. Plasma carburizing X-53 flexure specimens, instead of gas carburizing, produces a slight reduction (3% to 5%) in the bending fatigue strength.

27. WE43 magnesium is a much better corrosion resistant magnesium alloy than ZE41, limiting corrosion to the surface of any exposed areas, whereas ZE41 exhibits deep corrosion pits.

28. DOW 17 is a better pre-treatment for magnesium than DOW 7 or chrome-manganese since it works with the subsequently applied resin sealing system to prevent corrosion propagation.

29. DTD5562 resin and MIL-R-3043 resin are better corrosion resistant sealers for magnesium than SERMETEL 1083 since they were able to greatly retard corrosion on DOW 7 treated ZE41 specimens which the SERMETEL did not.

30. DTD5562 resin is a slightly better corrosion resistant sealer for magnesium than MIL-R-3043 resin.

31. The non-galvanic corrosion resistance of WE43 magnesium is comparable to A357 aluminum.

32. A detailed corrosion resistant sealing system significantly improved the corrosion resistance of a ZE41 magnesium housing assembly and prevented any corrosion on a WE43 magnesium housing assembly.

REFERENCES

1. Braddock, C.E., Richardson, D.J., Battles, R.A., *Advanced Transmission Components Investigation*, Bell Helicopter Textron, Inc., USAAVRADCOM TR-83-D-31A & B, Applied Technology Laboratory, U.S. Army Research and Technology Laboratories (AVSCOM), Fort Eustis, Virginia, June 1984.

2. Schmidt, A.H., *A Method for Estimating the Weight of Aircraft Transmissions,* Society of Allied Weight Engineers, Technical Paper No. 1120, 1976.

3. Folenta, D., *Design Study of a Self-Aligning Bearingless Planetary Gear (SABP),* NASA Contractor Report NAS3-21604, NASA-CP-2210, Advanced Power Transmission Technology, June 9-11, 1982, pp. 151-160.

4. Kish, J.G., *30,000 RPM/800 SHP Overrunning Clutch Program*, Sikorsky Aircraft, USAAVSCOM-TR-88-D-19, Aviation Applied Technology Directorate, U.S. Army Aviation Research & Technology Activity (AVSCOM), Fort Eustis, VA, January, 1989.

5. Kish, J.G., *Helicopter Freewheel Unit Design Guide*, USAAMRDL-TR-77-18, Applied Technology Laboratory, U.S. Army Research and Technology Laboratories (AVRADCOM), Fort Eustis, VA, October, 1977.

6. Bowen, C.W., *The Practical Significance Of Designing To Gear Pitting Fatigue Life Criteria,* ASME Publication 77-DET-122, 1977.

7. Dudley, D.W., *Handbook Of Practical Gear Design*, McGraw-Hill Book Co., New York, 1984.

8. Bowen, C.W., *Analysis Of Transmission Failure Modes*, SAE Publication 710454, 1971.

9. Townsend, D.P., Coy, J.J., Zaretsky, E.V., *Experimental And Analytical Load-Life Relation For AISI 9310 Steel Spur Gears*, NASA TM X-73590, 1977.

10. AGMA Standard 218.01, *Rating The Pitting Resistance And Bending Strength Of Spur And Helical Involute Teeth*, American Gear Manufacturers Association, Arlington, Va., 1982.

11. Lynwander, P., *Gear Drive Systems*, Marcel Dekker, Inc., New York, 1983.

12. Harris, T.A., *Roller Bearing Analysis,* John Wiley & Sons, New York, 1984.

13. Walker, H., *Helical Gears*, The Engineer, July 12, 1946.

14. Townsend, D.P., *Surface Fatigue Life & Failure Characteristics Of EX-53, CBS1000M, & 9310*, NASA TP-E-2578, 1985.

15. Townsend, D.P., Zaretsky, E.V., *Effect Of Five Lubricants On Life Of AISI 9310 Spur Gears*, NASA TP 2419, 1985.

16. Tauber, T., Hudgins, W.A., Lee, R.S., *Full-Flow Debris Monitoring And Fine Filtration For Helicopter Propulsion Systems*, American Helicopter Society RWP-24, Nov. 1982.

REFERENCES (Cont'd)

17. Sayles, R.S., Macpherson, P.B., *Influence Of Wear Debris On Rolling Contact Fatigue,* Special Technical Publication 771, American Society for Testing and Materials, Philadelphia, PA 1982.

18. Townsend, D.P., Zaretsky, E.V., *Effect Of Shot Peening On Surface Fatigue Life Of Carburized And Hardened AISI 9310 Spur Gears,* NASA TP 2047, 1982.

19. Bhattacharyya, S., Howes, M.A.H., Bock, F.C., Parikh, N.N., *ASME Report On Chemical Effects Of Lubrication In Contact Fatigue*, Report No. ASME/RCL/1975-1, 1975.

20. Palmgren, A., *Ball And Roller Bearing Engineering*, S.H. Burbank and Co., Inc., Philadelphia, Pa. 1959.

21. Coy, J.J., Townsend, D.P., Zaretsky, E.V., *Dynamic Capacity And Subsurface Fatigue Life For Spur And Helical Gears*, ASME Publication 75-LUB-19, 1975.

22. Johnson, L.G., *The Statistical Treatment Of Fatigue Experiments*, Elsevier Publishing Co., New York, 1964.

23. Bowen, C.W., Dyson, L.L., Walker, R.D., *Mode Of Failure Investigations Of Helicopter Transmissions,* Bell Helicopter Company, USAAVLABS TR 70-66, Eustis Directorate Laboratory, Fort Eustis, Virginia, January 1971.

24. Bamberger, E.N., Harris, T.A., Kaemarsky, W.M., Moyer, C.A., Parker, R.J., Sherlock, J.J., Zaretsky, E.V., *Life Adjustment Factors For Ball And Roller Bearings,* New York, ASME, September 1971.

25. Zwirlein, O., Schlicht, H., *Rolling Contact Fatigue Mechanisms - Accelerated Testing Versus Field Performance*, ASTM Special Technical Publication 771, 1982.

26. Unpublished paper titled, *"A Practical Method Of Calculating The Attainable Life In Aerospace Applications"*, FAG Aerospace Bearings, MAR/SON19B, Schweinfurt, West Germany, March 1988.

27. Burroughs, L., Fitzgerald, G., *Evaluation Of Advanced Gear Forging Techniques*, Sikorsky Aircraft, USAAVLABS TR 69-11, 1969.

28. Litvin, F.L., Tsung, W.J., Coy, J.J, Heine, C., *Generation of Spiral Bevel Gears With Zero Kinematical Errors & Computer Aided Tooth Contact Analysis,* NASA TM-87273, USAAVSCOM TR-86-C-2, NASA Lewis Research Center and Propulsion Directorate, U.S. Army Aviation Research and Technology Activity (AVSCOM), Cleveland, Ohio, March 1986.

29. Scott, H.W., *Computer Numerical Control Grinding Of Spiral Bevel Gears,* NASA CR-187175,1991.

30. Opitz, H., Zumbroich, H., Timmers, J., *Production Studies Of Noise Behavior Of Modern High-Load Gear Drives,* Industrie-Anzeiger, No. 96, Part 1, Nov. 1965, Essen, W. Germany.

31. Lewicki, D.G., Handschuh, R.F., Henry, Z.S., Litvin, F.L., *Low-Noise, High -Strength, Spiral Bevel Gears For Helicopter Transmissions,* NASA TM-106613, ARL-TR-459, 1994.

REFERENCES (Cont'd)

32. Hirt, M.C.O., *Stress In Spur Gear Teeth And Their Strength As Influenced By Fillet Radius,* Ph.D. Dissertation, Technische Universitat Munchen, 1976, translated by the American Gear Manufacturers Association.

33. Drago, R.J., *Design Guidelines For High-Capacity Bevel Gear Systems,* AE-15 Gear Design, Manufacturing and Inspection Manual, Society of Automotive Engineers, 1990, pp. 105-121.

REPORT DOCUMENTATION PAGE

Form Approved
OMB No. 0704-0188

1. AGENCY USE ONLY (*Leave blank*)	2. REPORT DATE	3. REPORT TYPE AND DATES COVERED
	June 1995	Final Contractor Report

4. TITLE AND SUBTITLE

Bell Helicopter Advanced Rotorcraft Transmission (ART) Program

5. FUNDING NUMBERS

WU–505–62–36
1L162211A47A

6. AUTHOR(S)

Zachary S. Henry

7. PERFORMING ORGANIZATION NAME(S) AND ADDRESS(ES)

Bell Helicopter Textron, Inc.
P.O. Box 482
Fort Worth, Texas 76101

8. PERFORMING ORGANIZATION REPORT NUMBER

E–9708

9. SPONSORING/MONITORING AGENCY NAME(S) AND ADDRESS(ES)

Vehicle Propulsion Directorate
U.S. Army Research Laboratory
Cleveland, Ohio 44135–3191
and
NASA Lewis Research Center
Cleveland, Ohio 44135–3191

10. SPONSORING/MONITORING AGENCY REPORT NUMBER

NASA CR–195479
ARL–CR–238

11. SUPPLEMENTARY NOTES

Project Manager, Robert F. Handschuh, Propulsion Systems Division, NASA Lewis Research Center, organization code 2730, (216) 433–3969.

12a. DISTRIBUTION/AVAILABILITY STATEMENT

Unclassified - Unlimited
Subject Category 37

This publication is available from the NASA Center for Aerospace Information, (301) 621–0390.

12b. DISTRIBUTION CODE

13. ABSTRACT (*Maximum 200 words*)

Future rotorcraft transmissions require key emerging material and component technologies using advanced and innovative design practices in order to meet the requirements for a reduced weight to power ratio, a decreased noise level, and a substantially increased reliability. The specific goals for the future rotorcraft transmission when compared with a current state-of-the-art transmission (SOAT) are: (1) a 25% weight reduction, (2) a 10 dB reduction in the transmitted noise level, and (3) a system reliability of 5000 hours mean-time-between-removal (MTBR) for the transmission. This report summarizes the work conducted by Bell Helicopter Textron, Inc. to achieve these goals under the Advanced Rotorcraft Transmission (ART) program from 1988 to 1995. The reference aircraft selected by BHTI for the ART program was the Tactical Tiltrotor which is a 17,000 lb gross weight aircraft. A tradeoff study was conducted comparing the ART with a Selected SOAT. The results showed the ART to be 29% lighter and up to 13 dB quieter with a calculated MTBR in excess of 5000 hours. The results of the following high risk component and material tests are also presented: (i) sequential meshing high contact ratio planetary with cantilevered support posts, (ii) thin dense chrome plated M50 NiL double row spherical roller planetary bearings, (iii) reduced kinematic error and increased bending strength spiral bevel gears, (iv) high temperature WE43 magnesium housing evaluation and coupon corrosion tests, (v) flexure fatigue tests of precision forged coupons simulating precision forged gear teeth, and (vi) flexure fatigue tests of plasma carburized coupons simulating plasma carburized gear teeth.

14. SUBJECT TERMS

Transmissions; Mechanical drives; Gear; Helicopters

15. NUMBER OF PAGES

221

16. PRICE CODE

A10

17. SECURITY CLASSIFICATION OF REPORT	18. SECURITY CLASSIFICATION OF THIS PAGE	19. SECURITY CLASSIFICATION OF ABSTRACT	20. LIMITATION OF ABSTRACT
Unclassified	Unclassified		

National Aeronautics and
Space Administration

Lewis Research Center
21000 Brookpark Rd.
Cleveland, OH 44135-3191